AD-A070 827 ILLINOIS UNIV AT URBANA-CHAMPAIGN ELECTROMAGNETICS LAB F/G 20/3
SOURCE RADIATION IN THE PRESENCE OF CONVEX BODIES.(U)
JUN 79 S SAFAVI-NAINI, R MITTRA N00014-75-C-0293
UNCLASSIFIED UIEM-79-9 NL

1 OF 3
AD A070827

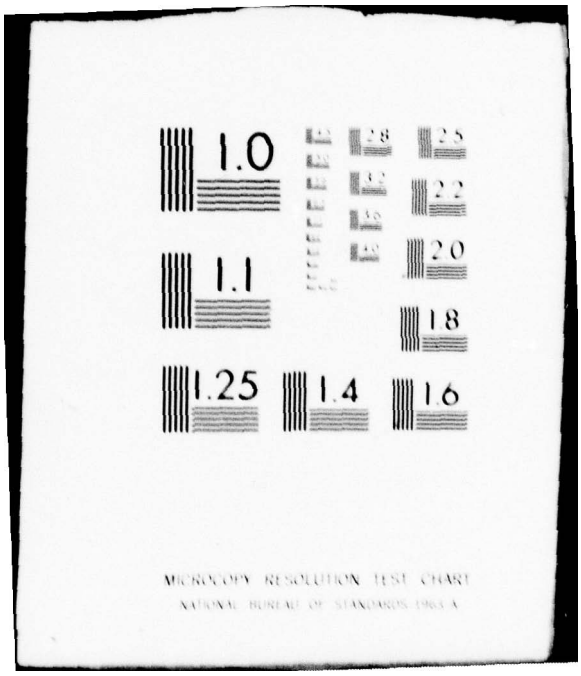
1.0
1.1
1.25
1.4
1.6
2.2
2.0
1.8
MICROCOPY RESOLUTION TEST CHART
NATIONAL BUREAU OF STANDARDS 1963-A

LEVEL II

ELECTROMAGNETICS LABORATORY
TECHNICAL REPORT NO. 79-9

June 1979

AD A070827

DDC FILE COPY

SOURCE RADIATION IN THE PRESENCE OF CONVEX BODIES

S. Safavi-Naini

R. Mittra

ELECTROMAGNETICS LABORATORY
DEPARTMENT OF ELECTRICAL ENGINEERING
ENGINEERING EXPERIMENT STATION
UNIVERSITY OF ILLINOIS AT URBANA-CHAMPAIGN
URBANA, ILLINOIS 61801

Supported by
Contract No. N00014-75-C-0293
Office of Naval Research
Department of the Navy
Arlington, Virginia 22217

Unclassified

SECURITY CLASSIFICATION OF THIS PAGE (When Data Entered)

REPORT DOCUMENTATION PAGE

READ INSTRUCTIONS BEFORE COMPLETING FORM

1. REPORT NUMBER

2. GOVT ACCESSION NO.

3. RECIPIENT'S CATALOG NUMBER

4. TITLE (and Subtitle)
SOURCE RADIATION IN THE PRESENCE OF CONVEX BODIES

5. TYPE OF REPORT & PERIOD COVERED
Technical Report

6. PERFORMING ORG. REPORT NUMBER
EM-79-9; UILU-ENG-79-2552

7. AUTHOR(s)
Safieddin Safavi-Naini
Raj Mittra

8. CONTRACT OR GRANT NUMBER(s)
N00014-75-C-0293

9. PERFORMING ORGANIZATION NAME AND ADDRESS
Electromagnetics Laboratory, Dept. of Elect. Eng.
University of Illinois at Urbana-Champaign
Urbana, Illinois 61801

10. PROGRAM ELEMENT, PROJECT, TASK AREA & WORK UNIT NUMBERS

11. CONTROLLING OFFICE NAME AND ADDRESS
Office of Naval Research
Department of the Navy
Arlington, VA 22217

12. REPORT DATE
June 1979

13. NUMBER OF PAGES
247

14. MONITORING AGENCY NAME & ADDRESS (if different from Controlling Office)
228p.

15. SECURITY CLASS. (of this report)

15a. DECLASSIFICATION/DOWNGRADING SCHEDULE

16. DISTRIBUTION STATEMENT (of this Report)

Distribution unlimited. Reproduction in whole or in part is permitted for any purpose of the United States Government.

17. DISTRIBUTION STATEMENT (of the abstract entered in Block 20, if different from Report)

18. SUPPLEMENTARY NOTES

19. KEY WORDS (Continue on reverse side if necessary and identify by block number)
Electromagnetic radiation and scattering; Geometrical theory of diffraction; Spectral domain approach; Asymptotic techniques for high frequencies; Fock's Theory; Stationary phase methods; Diffraction by finite cylinder; Equivalent edge current; Paraxial region; Caustic region; Diffraction by smooth surface

20. ABSTRACT (Continue on reverse side if necessary and identify by block number)
The first part of this work ~~(Chapters 2 and 3)~~ considers the problem of radiation from sources in the presence of smooth, convex, impenetrable objects and presents a brief survey of various high-frequency techniques. A generalization of the geometrical theory of diffraction and two new techniques -- based on the spectral domain approach and an asymptotic evaluation of the radiation integral for the surface current -- also are discussed. Some numerical results derived from the spectral domain formulas are presented, and a comparison with available theoretical and experimental data is included. (Over)

DD FORM 1 JAN 73 1473 EDITION OF 1 NOV 65 IS OBSOLETE

408 192

Unclassified

SECURITY CLASSIFICATION OF THIS PAGE (When Data Entered)

The second part of this work ~~(Chapters 4 through 10)~~ describes a new technique for analyzing the radiation from a point electromagnetic source located on an infinitely conducting solid cylinder with a finite length. The method presented in this work is based upon a generalization of STD to the case of curved surfaces.

UILU-ENG-79-2552

Electromagnetics Laboratory Report No. 79-9

SOURCE RADIATION IN THE PRESENCE OF CONVEX BODIES

Technical Report

S. Safavi-Naini

R. Mittra

June 1979

Office of Naval Research
Department of the Navy
Arlington, Virginia 22217

Contract No. N00014-75-C-0293

Electromagnetics Laboratory
Department of Electrical Engineering
Engineering Experiment Station
University of Illinois at Urbana-Champaign
Urbana, Illinois 61801

ABSTRACT

The first part of this work (Chapters 2 and 3) considers the problem of radiation from sources in the presence of smooth, convex, impenetrable objects and presents a brief survey of various high-frequency techniques. A generalization of the geometrical theory of diffraction and two new techniques -- based on the spectral domain approach and an asymptotic evaluation of the radiation integral for the surface current -- also are discussed. Some numerical results derived from the spectral domain formulas are presented, and a comparison with available theoretical and experimental data is included.

The second part of this work (Chapters 4 through 10) describes a new technique for analyzing the radiation from a point electromagnetic source located on an infinitely conducting solid cylinder with a finite length. The method presented in this work is based upon a generalization of STD to the case of curved surfaces.

TABLE OF CONTENTS

LIST OF FIGURES

Figure

LIST OF TABLES

1. INTRODUCTION

The problems of radiation from sources in the presence of impenetrable smooth convex objects and the diffraction of a plane wave by such objects are of great practical interest in the design of antennas on structures, e.g., conformal arrays. Unfortunately, the exact analytical solutions to these problems, based on the methods of "separation of variables" or "function-theoretic" procedures (Wiener-Hopf technique, residue calculus, etc.), exist only for a very limited number of scattering geometries. Furthermore, the exact solutions are typically highly complex in nature; hence, the process of extracting numerical results from them can be very time-consuming and is by no means trivial. This situation has motivated many researchers to explore approaches to the problems of radiation and scattering from smooth convex structures.

In the low and resonant frequency ranges, several reliable numerical procedures, e.g., the moment method, are available for solving the radiation and scattering problems. However, in the high frequency domain, numerical techniques based on matrix methods become unwieldy, if not impractical, prompting one to employ asymptotic techniques suitable for large $k(=2\pi/\lambda)$, where λ is the wavelength of the illuminating wave.

In this work, we begin by presenting, in Chapter 2, a survey of various high frequency asymptotic techniques for the problem stated above. The survey will be necessarily brief, and will cover only the highlights of a number of important approaches to the problem at hand, viz., Fock's theory, the geometrical theory of diffraction (GTD), and the direct integral equation approach. The reader interested in further details may choose to consult the works of Bowman, et al. [1], Uslenghi [2], and Kouyoumjian [3].

In Chapter, 3, we consider the generalization of GTD and present some new approaches to the curved surface radiation and scattering problems. Some numerical results based on one of these new approaches are presented in Chapter 3, and a comparison with other available methods is included.

Throughout the rest of the work, we apply the results of the new approach combined with STD interpretation of wedge diffraction to some special case of great theoretical and practical interest. The high frequency radiation of an electromagnetic point source on the surface of conducting circular cylinder with finite length is analyzed by a new technique combining the main features of different asymptotic theories. Chapter 4 is concerned with the general formulation of the problem. Chapters 5, 6, and 7 describe the methods used in calculating different "constituents" of the total radiated field, namely, surface and wedge diffracted rays. Chapter 8 is concerned with analyzing the effect of the finiteness of the cylinder. Field evaluation in paraxial region is explained in Chapter 9. Numerical results are discussed in Chapter 10, and finally, a brief conclusion is given in Chapter 11.

2. SURVEY OF AVAILABLE HIGH-FREQUENCY ASYMPTOTIC TECHNIQUES

2.1 Watson Transformation and Physical Optics

One of the first successful attempts to derive an asymptotic expansion for the far-field generated by a point source located in the proximity of a conducting surface was made by G. N. Watson in 1918 [4]. His method, essentially, consisted of two steps: 1) transforming the original infinite series solution into a contour integral (by Cauchy's residue theorem); 2) deforming the contour of integration so as to capture a set of complex poles of the integrand. The original integral is then expressed in terms of an infinite series which converges very rapidly, provided the observation point is in the shadow region. The first few terms of this series were later interpreted as "creeping waves." The method was first applied to a sphere and circular cylinder, and later to some other geometries as well. The mathematical rigor of the method was the subject of further investigations by other researchers ([5], [6], and [7]). Although the Watson transformation can only be applied to a few simple geometries, e.g., the sphere, cylinder, cone, spheroid, etc., it is still regarded as one of the cornerstones of the general high frequency techniques because of its mathematical rigor. The Watson transformation is especially powerful in the shadow region of the geometric optics field. In the lit region, the above-mentioned contour integral is evaluated using the "stationary phase" method and yields the reflected field from the surface. In this region, the most significant contribution to the total scattered field typically comes from the surface current induced on the smooth convex part of the object; the so-called "Physical Optics" approximation can be applied ([8], [9], and [10]) to derive the reflected field. The Physical Optics method is based upon approximating the induced surface current in the lit region of the object by the current that would be

induced on the local tangent plane, and by assuming that the surface current is zero in the shadow region. The far field is constructed by substituting the above estimate for the induced surface current in the integral representation of the scattered field, and evaluating the same in an asymptotic sense. The dominant term of the asymptotic expansion of this integral can be shown to be identical to the first term of the Luneberg-Kline expansion of the geometrical optics far field ([11] and [12]). However, the higher-order terms derived from the physical optics approach do not provide us with correct results in the shadow or transition regions where the diffracted field contributes the most.

In the next subsection, we discuss Fock's theory, which can fill the gap between the Physical Optics in the lit region and the "creeping wave" representation in the shadow region.

2.2 Fock's Theory

The region between the lit and the shadow part on a surface is called "penumbra region." The angular width of this region is approximately given by $(\lambda r_o^2/\pi)^{1/3}$ where λ is the wavelength of the illumination and r_o is the radius of curvature of the surface of the object in this region in the incident plane (Fig. 1). Fock's theory invokes the principle of *local* character of the field in the penumbra region [13] and is based on the conjecture that all bodies with a smoothly varying curvature have the same current distribution in the penumbra region, provided that the curvature and the incident wave are the same near the point under consideration. This principle allows one to locally replace the surface of the object by a portion of a paraboloid of revolution. A unique feature of the expressions for Fock currents is that they provide a convenient transformation of the geometric optics currents

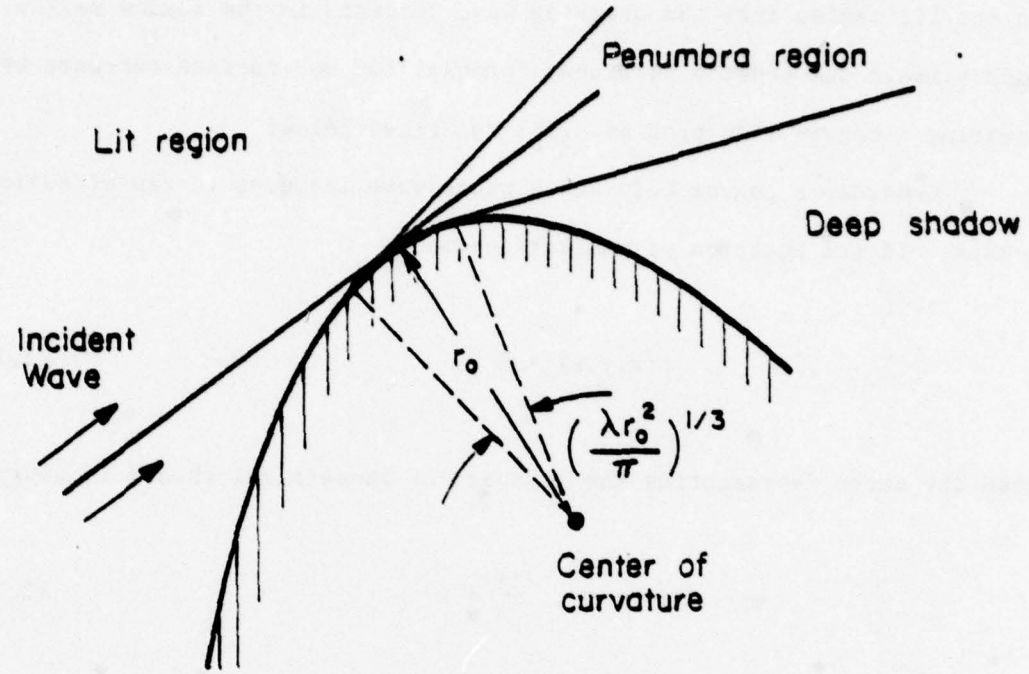

Figure 1: Section of the body in the plane of incidence.

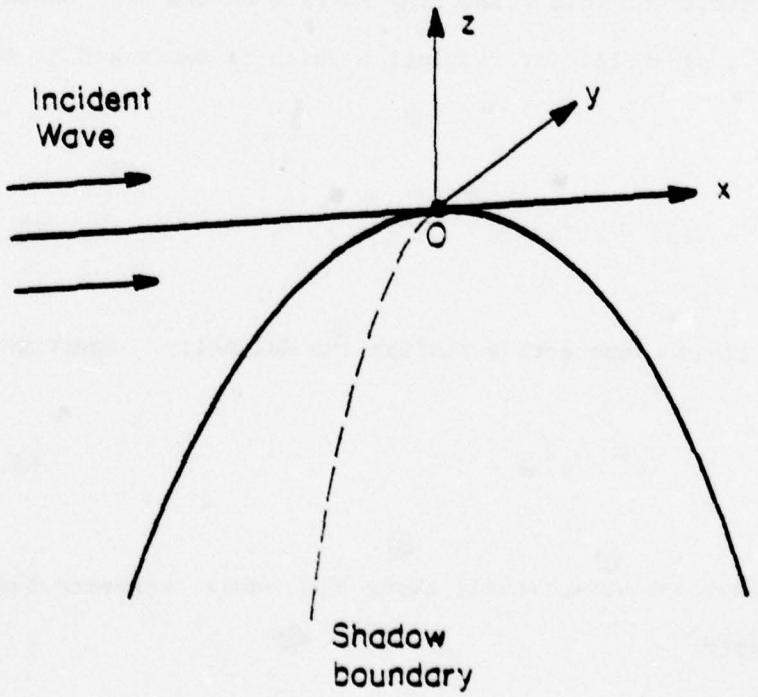

Figure 2: Plane wave incident upon a smooth convex body.

in the lit region into the creeping wave currents in the shadow region. Fock himself deduced the pertinent formulas for the surface currents by treating a convex body problem [14] described below:

Consider a convex body and a plane wave incident in the direction of the x-axis. If the equation of the surface is

$$f(x,y,z) = 0 \tag{2.1}$$

then the curve representing the boundary of geometrical shadow is given by

$$f(\vec{r}) = 0 \ , \quad \frac{\partial f}{\partial x} = 0 \tag{2.2}$$

Consider a point 0 on the boundary of a shadow region where we set up a rectangular coordinate system as shown in Fig. 2 ($\hat{z}$: normal to the surface, $\hat{x}$: in the direction of propagation, and $\hat{y}$ is the tangent to the boundary of shadow). In the vicinity of this point, the surface of the body could be locally replaced by a paraboloid of revolution which is expressed by the equation.

$$z + 1/2\ (ax^2 + 2bxy + cy^2) = 0 \tag{2.3}$$

Each of the field components satisfies the Helmholtz equation

$$(\nabla^2 + k^2)\Psi = 0 \tag{2.4}$$

The fact that the incident wave travels along the x-axis, suggests that Ψ be written in the form

$$\Psi = \tilde{\Psi} e^{-jkx} \tag{2.5}$$

where an $\exp(j\omega t)$ time dependence has been assumed. Substituting (5) in (4) gives

$$\nabla^2 \tilde{\Psi} - 2jk \frac{\partial}{\partial x} \tilde{\Psi} = 0 \tag{2.6}$$

At this point, two basic assumptions are introduced in Fock's theory, viz.

i) $\tilde{\Psi}$'s are relatively slowly varying function of coordinates

ii) $\tilde{\Psi}$ varies more rapidly in the z-direction than in x and y, i.e.,

$$\frac{\partial \tilde{\Psi}}{\partial z} = O(\frac{k}{m} \tilde{\Psi}), \quad \frac{\partial \tilde{\Psi}}{\partial x} = O(\frac{k}{m}, \tilde{\Psi}), \quad \frac{\partial \tilde{\Psi}}{\partial y} = O(\frac{k}{m}, \tilde{\Psi}) \tag{2.7}$$

Based upon (2.7), we can write (2.6) as

$$\frac{\partial^2 \tilde{\Psi}}{\partial z^2} - 2jk \frac{\partial \tilde{\Psi}}{\partial x} = 0 \tag{2.8}$$

and consequently $m' = m^2$ (m is very large), where the terms of relative order $1/m^2$ have been omitted.

Inserting these estimates and assumptions into the Maxwell's equations, we can find some simple expressions for all the field components in terms of H_y and H_z. If we write H_y as

$$H_y = H_y^0 e^{-jkx} \tilde{\Psi} \tag{2.9}$$

where H_y^0 is the magnitude of the incident wave at infinity, then Ψ must satisfy

$$\frac{\partial^2 \tilde{\Psi}}{\partial z^2} - 2jk \frac{\partial \tilde{\Psi}}{\partial x} = 0 \qquad (2.10)$$

with boundary condition

$$\frac{\partial \tilde{\Psi}}{\partial z} - jk \left(ax + by + \frac{1}{\sqrt{\eta}}\right) \tilde{\Psi} = 0 \qquad (2.11)$$

on the surface of the body. Equation (2.11) is the simplified version of the Leontovich boundary condition where

$$\eta = \varepsilon - j \frac{\sigma}{\omega}$$

The final solution for H_y on the surface of the body, which satisfies the boundary condition and the condition at infinity, may be written in the form

$$H_y = H_y^{ex} \, G(\xi, q) \qquad (2.12)$$

where H_y^{ex} = external field

$G(\xi,q) = e^{-(j/3)\,\xi^3} V_1(\xi,q)$

$V_1(\xi,q)$ = Fock function defined in the Appendix A.

$\xi = m(ax + by)$ = reduced distance from the shadow boundary = ℓ/d.

$m = (kr_o/2)^{1/3}$, m^{-1} is the angular width of penumbra region.

d = the width of penumbra region = $(2r_o^2/k)^{1/3}$.

ℓ = distance between the observation point and the shadow boundary along the incident ray (Fig. 3).

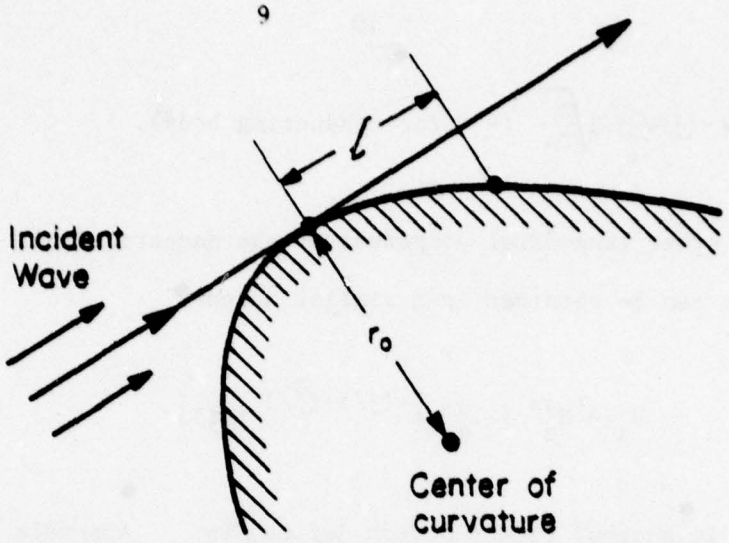

Figure 3: Geometric meaning of the quantity ℓ in (2.12).

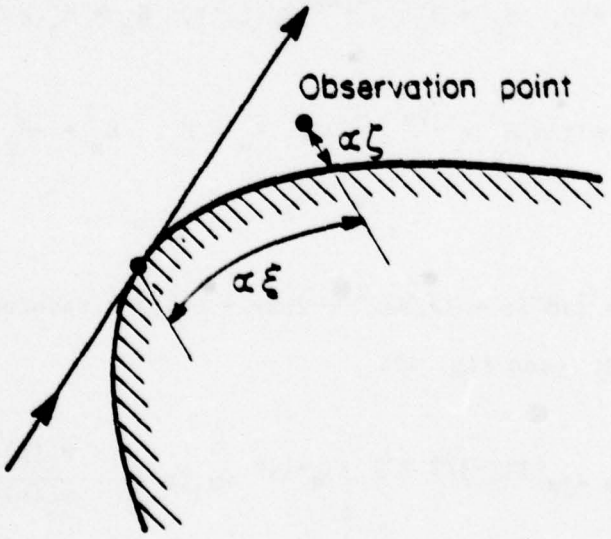

Figure 4: Coordinates of observation point in terms of ξ and ζ.

$q = -jm/\sqrt{n} = -(j/\sqrt{n})\, 3\sqrt{\frac{k}{2a}}$ (= 0 for conducting body).

The other tangential component of the magnetic field H_x on the surface of the body can be obtained in a similar manner

$$H_x = H_z^{ex}\left[-\frac{j}{m}\, e^{-(j/3)\xi^3/3}\, f(\xi)\right] \tag{2.13}$$

where $f(\xi)$ is another Fock function defined in Appendix A. Fock's formulas not only give the surface value of the field, but also can be utilized to find the field in the proximity of the object. For a plane wave incidence, the first order, i.e., $0(1/m)$ terms for the scattered field within a certain layer around the object, can be written as

$$H_x = 0,\quad H_y = H_y^0\, e^{-jkx}\,\tilde{\Psi}(\xi,\zeta),\quad H_z = H_z^0\, e^{-jkx}\,\tilde{\Phi}(\xi,\zeta)$$

$$E_x = (j/m)H_y^o\, e^{-jkx}\,\partial\tilde{\Psi}/\partial\zeta,\quad E_y = H_z,\quad E_z = -H_y \tag{2.14}$$

where

$\zeta = 2am^2[z + (1/2)(ax^2 + 2bxy + cy^2)]$ = reduced height from the surface of the body (see Fig. 4).

$$\tilde{\Psi} = -je^{(j\xi\zeta - j/3\,\xi^3)} \int_c e^{-j\xi t}\left[w_1(t-\zeta) - \frac{w_1'(t)-qw_1(t)}{w_2'(t)-qw_2(t)}\, w_2(t-\zeta)\right] dt$$

$$\tilde{\Phi} = \frac{-je}{2\sqrt{\pi}}^{j\xi\zeta-(j/3)\xi^3} \int_c e^{-j\xi t}\left[w_1(t-\zeta) - \frac{w_1(t)}{w_2(t)}\, w_2(t-\zeta)\right] dt \tag{2.15}$$

The path of integration for $\tilde{\Phi}$ and $\tilde{\Psi}$ is shown in Fig. 5 .

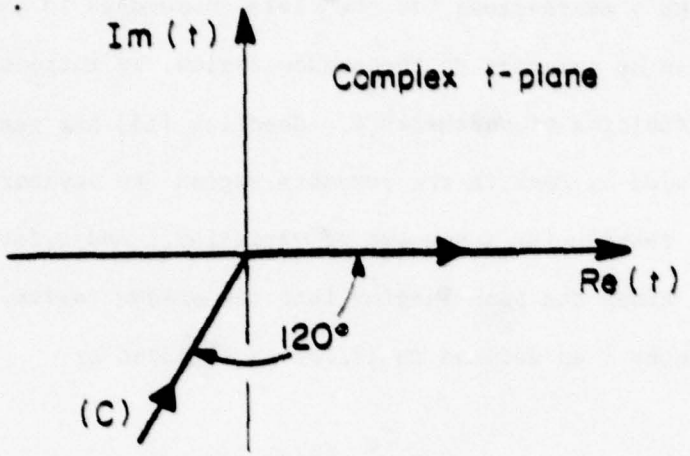

Figure 5: Path of integration for (2.15) in the complex t-plane.

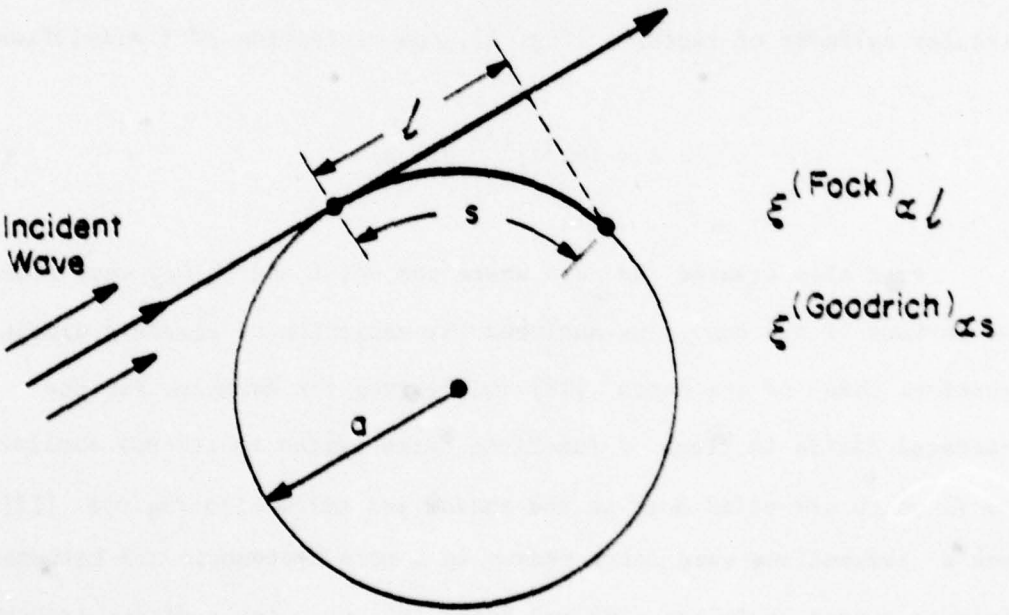

Figure 6: Comparison between the various definitions of parameter ξ for the case of a circular cylinder.

Fock's expressions for the field components in the penumbra region ($\xi \simeq 0$) can be extended to the shadow region, by introducing some modifications in the definition of parameter ξ. Goodrich [15] has generalized the argument used by Fock in the penumbra region to anywhere in the shadow region by introducing a new set of variables, ξ and ζ, for the incremental distances along the path leading into the shadow region. In this generalization, the parameter ξ as defined in (2.12) is replaced by

$$\xi = \int_o^s \left(\frac{kR(s)}{2}\right)^{1/3} \frac{ds}{R(s)} \tag{2.16}$$

where s is the arc length along the geodesics which originate from the shadow boundary and go into the shadow region along the surface, and R(s) is the radius of curvature of the surface along the geodesics. For the case of a circular cylinder of radius a (Fig. 6), the expression of ξ simplifies to

$$\xi = (ka/2)^{1/3}\,\theta = s/d \tag{2.17}$$

Fock also treated the case where the point source was very close to the surface of the body. He analyzed the radiation of electric dipoles near a spherical model of the earth [16] and derived the formulas for the scattered fields in terms of functions (attenuation functions) similar to $\tilde{\phi}$ and $\tilde{\Psi}$, which are valid both in the shadow and transition regions [17]. Fock's assumptions were later proven in a more systematic and mathematically rigorous manner by Cullen [18] and Hong [19] by using a direct integral equation approach. This method is described in the next section.

2.3 Direct Integral Equation Approaches

This method, which is closely related to Fock's theory, can be illustrated by analyzing the diffraction of a plane electromagnetic wave by an arbitrary conducting body (large compared with λ). Cullen [18] obtained a first-order asymptotic solution to the integral equation for the induced surface current

$$\vec{J}(\vec{r}) = 2\vec{n}(\vec{r}) \times \vec{H}^{inc}(\vec{r}) - (1/2\pi)\vec{n}(\vec{r}) \times \int_S \int ds' \frac{1+jkR}{R^3} \{\vec{J}(\vec{r}') \times \vec{R} e^{-jkR}\} \tag{2.18}$$

where $\vec{n}(\vec{r})$ is the outward unit normal to the surface at $\vec{r}$, $\vec{H}^{inc}(\vec{r})$ is the incident magnetic field on the surface (S) of the body, and $R = \vec{r} - \vec{r}'$ ($\vec{r}'$ is a variable point on the surface).

Fock used this integral equation to deduce the important principle of local character of the field in the penumbra region. Cullen derived a first-order asymptotic solution to (2.18) which agreed with Fock's results given in (2.12) and (2.13). Cullen's method consists of transforming the two-dimensional integral equation (2.18), in the penumbra region, to a one-dimensional, Volterra-type equation. This is accomplished by applying the stationary phase technique to the original integral while integrating with respect to one of the variables. The resulting one-dimensional Volterra equation is then solved in Cullen's method by the Fourier transform technique. A similar procedure was used by Hong [19] to analyze, asymptotically, the diffraction of electromagnetic and acoustic plane waves by smooth convex bodies. We will now proceed to explain Hong's method in a little more detail by referring back, once again, to the integral equation (2.18). The surface is parametrized

by the geodesic coordinate system (σ,v) such that the shadow boundary for the incident plane wave traveling along the tangent $\hat{\sigma}(0,v)$ to the $v = 0$ curve is the $\sigma = 0$ curve. The quantities $\hat{\sigma}(\sigma,v)$, $\hat{b}(\sigma,v)$ and $\hat{n}(\sigma,v)$ form a right-hand local orthonormal basis ($\hat{n} = \hat{\sigma} \times \hat{b}$) as shown in Fig. 7.

Since the incident field has a phase factor $e^{-jk\hat{\sigma}(0,0)\cdot\hat{r}(\sigma,0)}$, we write the surface current in the form

$$\vec{J}(\vec{r}) = [I_\sigma(\vec{r})\ \hat{\sigma}(\vec{r}) + I_b(\vec{r})\ \hat{b}(\vec{r})]\ e^{-jk\sigma} \tag{2.19}$$

where σ is the arc length along the geodesic. Substituting (2.19) back into (2.18) and restricting the resulting equation to the points on the geodesic v=0, we obtain two coupled, two-dimensional integral equations for $I_\sigma(\sigma,0)$ and $I_b(\sigma,0)$. It can be shown that these integrals have saddle points at v=0 (for the v-integration). Applying the "steepest descent path" method to v-integration, and keeping the terms up to the order $1/M_0^2$, where $M_0 = (k\rho_\sigma(\sigma,0))^{1/3}$, we obtain the following decoupled one-dimensional, Volterra-type integral equations for $I_b(\xi,0)$ and $I_\sigma(\xi,0)$

$$\begin{aligned} I_\sigma(\xi,0) &= 2\ I_\sigma^{inc}(\xi,0) - \int_{-\infty}^{\xi} d\tau\ I_\sigma(\xi,0)\ K_\sigma(\xi-\tau) + 0(M_0^{-3}) \\ I_b(\xi,0) &= 2\ I_b^{inc}(\xi,0) - \int_{-\infty}^{\xi} d\tau\ I_b(\xi,0)\ K_b(\xi-\tau) + 0(M_0^{-3}) \end{aligned} \tag{2.20}$$

$\rho_\sigma(\sigma,v)$ is the radius of curvature of the surface along geodesics (v = constant curves) at point (σ,v).

Solving (2.20) by Fourier transforms, we obtain the expression for the induced currents in the penumbra and shadow regions, and the first-order solutions

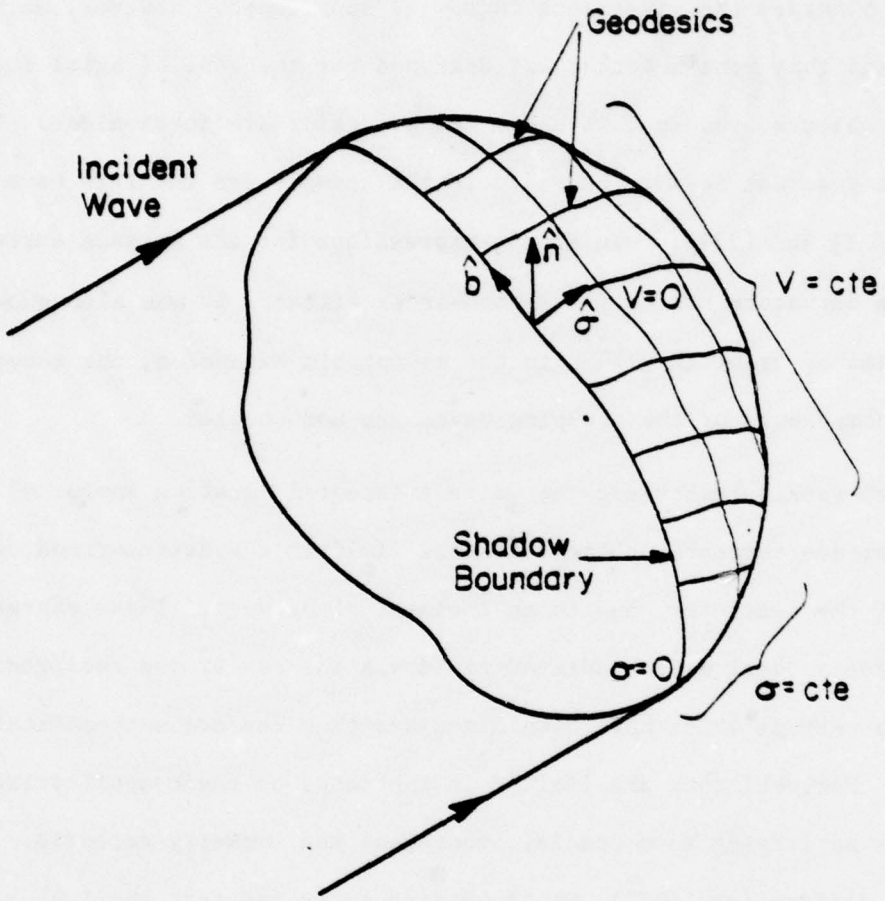

Figure 7: Geodetic coordinate system on a smooth convex body.

are found to be the same as those of Fock and Keller's GTD [20]. One of the important conclusions drawn from Hong's solution is that the leading term in the asymptotic expansion, which is the same for the acoustic and electromagnetic problems, is independent of curvature in the direction transverse to the geodesic, provided the divergence factor is suppressed. However, we should bear in mind that Hong's method was designed for the case of axial incidence on symmetric objects, and in this case, the geodesics are torsionless. The above conclusion does not seem to be valid in the cases where the rays have nonzero torsion ([21] and [22]). In Hong's expressions for the surface current, the transverse curvature has only a second-order effect. It was also shown that up to the terms of order $(k\rho_\sigma)^{-2/3}$ in the asymptotic expansion, the tangential and binormal components of the creeping waves are not coupled.

Both Fock's theory and the "direct integral equation approach" give the induced surface current, or the scattered field in the neighborhood of the surface of the scatterer, due to an incident plane wave. These expressions can also be used to derive the radiated field via the use of the reciprocity theorem.

The methods which have been discussed thus far are mathematically rigorous. However, they are limited in the scope of their application to geometries satisfying some special smoothness and symmetry criteria. "Geometrical theory of diffraction" (GTD), which we discuss in the next section, has a broader scope, although it does lack the mathematical rigor of approaches described until now.

2.4 Geometrical Theory of Diffraction (GTD)

Geometrical theory of diffraction (GTD), developed by J. B. Keller ([20], [23], [24], [25], and [26]) is a generalization of geometrical optics.

It is based upon the assumption that fields propagate along rays. Keller's major contribution was to introduce the new kinds of rays called the "diffracted rays," which together with the geometrical optics rays, constitute the total field. In our problem, viz., source radiating in the proximity of the smooth object, the diffracted rays travel along the curves on the surface of the scatterer. By applying Fermat's principle to these surface rays, we conclude that the above-mentioned curves should be geodesics on the surface of the body. In the GTD procedure, one assigns a value to the field along each of these surface rays.The total field at any point in the space is the sum of the fields due to various rays (incident, reflected and diffracted) passing through that point. An important advantage of the GTD approach is that it can be applied to both scalar (acoustic) and vector (electromagnetic) problems and to smooth convex objects of an arbitrary shape.

Consider the problem of determining the radiated field of a scalar point source located on the surface of a smooth convex opaque body. If the observation point is in the shadow region, the ray paths originating at Q and reaching P (observation point) are comprised of two sections. One of the sections follows straight line path P_1P, while the other travels along a geodesic on the surface (Fig. 8). Let us consider the propagation of the field along each section.

a) Rays in free space: Behavior of the fields along these rays can be determined by obtaining a high-frequency asymptotic solution to Maxwell's equation in a source-free homogeneous isotropic medium. We begin with the Luneberg-Kline asymptotic expansion of the electric field ([11] and [12]):

$$\vec{E}(\vec{r}) \sim k^{\tau} e^{-jk_o S(\vec{r})} \sum_{m=0}^{\infty} (jk)^{-m} \vec{e}_m(\vec{r}) \qquad (2.21)$$

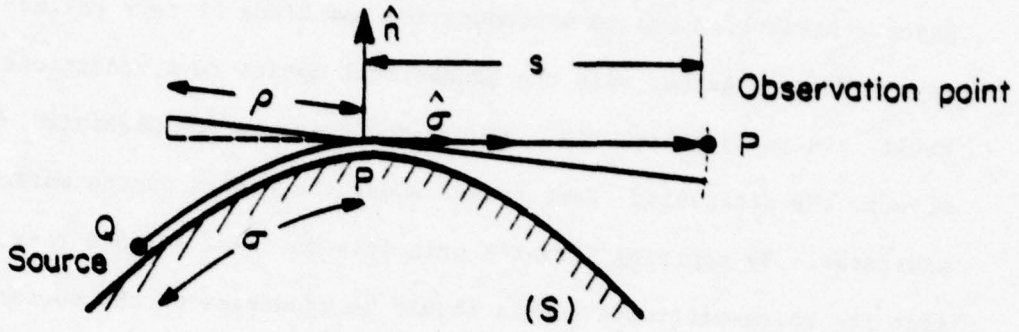

Figure 8: Diffraction by a smooth convex body when the observation point is in the shadow region of the source Q.

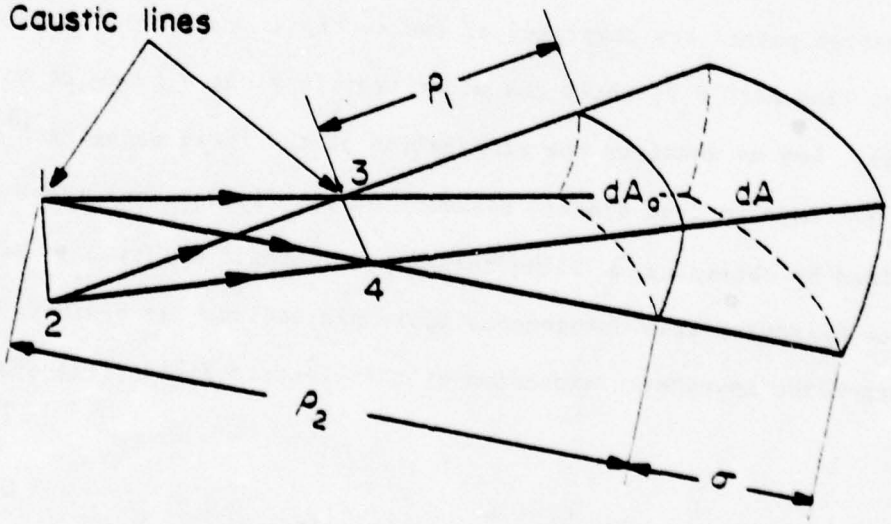

Figure 9: Diverging pencil of rays in free space.

and insert it into the Maxwell's equations. This results in the following equations governing the propagation of electromagnetic fields along the rays.

$$[\nabla S(\vec{r})]^2 = 1 \qquad \text{(Eikonal equation)} \tag{2.22}$$

$$2(\nabla S\cdot\nabla)\vec{e}_m + (\nabla^2 S)\vec{e}_m = -\nabla^2 \vec{e}_{m-1} \quad \text{(Transport equation)} \tag{2.23}$$

$$\nabla S\cdot\vec{e}_m = -\nabla\cdot\vec{e}_{m-1} \qquad \text{(Gauss's Law)} \tag{2.24}$$

$$\vec{e}_{-1} = 0, \quad m = 0, 1, 2, \ldots$$

The zeroth-order solution to the above system of equations, which turns out to be in agreement with what one would obtain by geometric optics, may be written as

$$\vec{E}(\sigma) \sim \vec{E}_0(0)e^{-jk_0 S(0)} \cdot \sqrt{\frac{\rho_1\rho_2}{(\rho_1+\sigma)(\rho_2+\sigma)}}\; e^{-jk_0\sigma} \tag{2.25}$$

where σ is the distance traveled along the ray from the reference point $0(\sigma=0)$ on the ray path (Fig. 9). ρ_1 and ρ_2 are the principal radii of curvature of the wavefront at $\sigma=0$. It is apparent that the expression fails when $\sigma=-\rho_1$ or $\sigma = -\rho_2$, i.e., at the caustic lines (Fig. 9). In the cases where it is convenient to choose the point of diffraction on the surface of a body as the reference point 0, the formula (2.25) should be modified as follows:

$$\vec{E}(\sigma) \sim \vec{\delta}_0 \cdot \sqrt{\frac{\rho}{\sigma(\rho+\sigma)}}\; e^{-jk\sigma} \tag{2.26}$$

In these cases, the point of diffraction itself is a caustic, and ρ is the distance between this point and the second caustic.

b) Surface Rays: These rays follow the surface S along the geodesics into the shadow region, and shed off energy tangentially as they propagate. In order to study the behavior of the field along these rays, we introduce a special ray-fixed coordinate system, $\hat{\sigma}, \hat{n}, \hat{b}$.

$\hat{\sigma}$: Unit vector tangent to the ray; $\hat{n}$: outward unit normal to the surface; and $\hat{b} = \hat{t} \times \hat{n}$ or binormal direction; a vector field can be decomposed into its components along these unit vectors as

$$\vec{E} = E_\sigma \hat{\sigma} + E_n \hat{n} + E_b \hat{b} \tag{2.27}$$

At this point, several important assumptions are introduced in the GTD approach [Levy and Keller, 1959]:

i) $\vec{E}$ and $\vec{H}$ are orthogonal to each other and to the ray.

ii) Variation of the phase of the field along the ray is the same for both fields.

iii) E_n and E_b propagate independently, and $E_\sigma = 0$.

iv) E_b satisfies the scalar wave equation $(\nabla^2+k^2)\, u=0$ with the boundary condition $u=0$ on the surface S, while E_n satisfies the same equation with the boundary condition $\frac{\partial u}{\partial n} = 0$.

The next step in the GTD approach is to conjecture, on the basis of the solution to some canonical problems, that the surface field propagating along each ray is comprised of an infinite set of "modes." Along a ray-fixed path GTD assigns a complex value to each component of the field associated with the individual modes. The propagation of this modal field is described by the equation

$$a(\sigma) = A(\sigma)\, e^{j(\phi_0 - k\sigma)} \tag{2.28}$$

where σ is the distance between an arbitrary point along the ray and the source Q and ϕ_0 is the phase of the field at the source point. Next, invoking the principle of conservation of energy between two adjacent rays, and using the fact that the surface rays shed energy off tangentially, we can arrive at the following expression for $a(\sigma)$

$$a(\sigma) = K\sqrt{\frac{d\Psi_1}{\rho d\Psi_2}}\ \exp\left[-jk\sigma - \int_0^{\sigma} \alpha\,(\sigma')d\sigma'\right] \tag{2.29}$$

where $\alpha(\sigma)$ is the "attenuation constant," K is proportional to the strength of the source, and $d\Psi_1$, $d\Psi_2$ and ρ are shown in Fig. 10. The quantity $[d\Psi_1/(\rho d\Psi_2)]^{1/2}$ indicates the "spreading of the surface ray tube" as it travels along the surface. Equations (2.26) and (2.29) describe the laws of propagation for the rays which originate from the source point Q, are diffracted at P_1, and reach the observation point P. To complete the solution, we need to determine the actual values of the fields from these equations. These require the knowledge of $\vec{\delta}_0$ and K, which, in turn, are related to the initial values of the rays QP_1 and P_1P as well as the attenuation constant $\alpha(\sigma)$. The initial value of the field at Q is related to the strength of the source by L(Q), the so-called "launching coefficient," while the initial value of the field at P_1 is related to the actual field on the surface at P_1 through the "diffraction coefficient" $D(P_1)$. If we now sum up the contributions of all the modes, we obtain the final solution [25] for the field radiated in the shadow region by an infinitesimal magnetic dipole of strength $\vec{M}$ located on a smooth convex conducting body

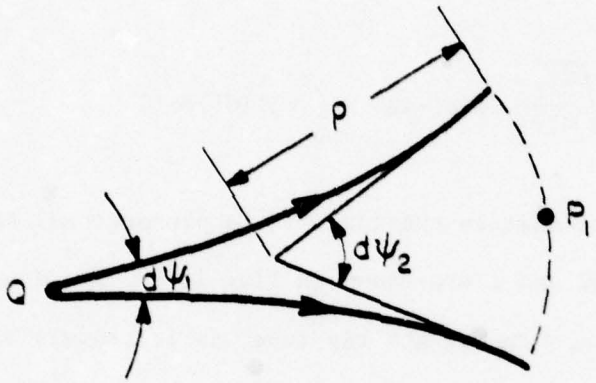

Figure 10: Divergence of surface rays.

$$\vec{E}^d(P) = \vec{M} \cdot [\hat{b}(Q)\hat{n}(P_1)F + \hat{\sigma}(Q)\hat{b}(P_1)G] \sqrt{\frac{\rho}{s(\rho+s)}}\, e^{-jks} \qquad (2.30a)$$

where

$$F = \frac{-jke}{4\pi}^{-jk\sigma} \sqrt{\frac{d\Psi_1}{\sigma d\Psi_2}} \sum_{p=1}^{\infty} L_p^h(Q) D_p^h(P_1) \exp\left[-\int_o^\sigma \alpha_p^h(\sigma')d\sigma'\right] \qquad (2.30b)$$

and the expression for G is obtained by replacing the superscript "h" by "s" in (2.30b), where h and s stand for hard and soft boundary conditions, viz., u=0 and $\partial u/\partial n = 0$, respectively. The quantities $L_p^{h,s}$, $D_p^{h,s}$ and $\alpha_p^{h,s}$, appearing in (2.30b), in general, depend upon the local geometry and the electromagnetic characteristic of the surface, frequency k, and the mode of propagation. They are determined by studying the asymptotic expansions of the exact solutions of some special canonical problems. Keller and Levy ([20] and [27]), have derived the first few terms of the asymptotic expansions for D and α by considering the canonical problems of scalar diffraction by a circular cylinder, sphere, elliptical and parabolic cylinder. A study of the above-mentioned asymptotic expansions and the works of Franz and Klante [28] and Voltmer [29], who have also investigated the same problem, as well as a comparison with the results of the "direct integral equation approach," reveals the following characteristics of the solution: i) the first-order terms in the asymptotic expansion of D and α are independent of whether the problem under consideration is scalar or vector; ii) the first-order approximation of D and α are dependent only on ρ_σ, the radius of curvature of the surface along the ray; iii) the second-order terms are functions not only of ρ_σ, but also of $\frac{d\rho_\sigma}{d\sigma}$, $\frac{d^2\rho_\sigma}{d\sigma^2}$, and $\rho_{\sigma n}$ (the radius of the curvature of the surface transverse to the ray). Finally, the higher-order terms are different for scalar and vector problems.

The leading terms in the asymptotic expansion of "diffraction coefficient" D, "attentuation constant" α and "launching coefficient" L are presented below:

"Soft" polarization:

$$[D_p^s]^2 = \frac{\pi^{1/2} \cdot 2^{-5/6} \cdot \rho_\sigma^{1/3} \cdot e^{-j\pi/12}}{k^{1/6} \cdot [Ai'(-r_p)]^2} \tag{2.31}$$

$$\alpha_p^s = \frac{r_p \cdot e^{j\pi/6}}{\rho_\sigma} \left(\frac{k\rho_\sigma}{2}\right)^{1/3} \tag{2.32}$$

$$L_p^s = e^{-j\pi/12} (2\pi k)^{1/2} \left(\frac{2}{k\rho_\sigma}\right)^{2/3} \cdot Ai'(-r_p) \cdot D_p^s \tag{2.33}$$

"Hard" polarization:

$$[D_p^h]^2 = \frac{\pi^{1/2} \cdot 2^{-5/6} \cdot \rho_\sigma^{1/3} \cdot e^{-j\pi/12}}{k^{1/6} \cdot r'_p \cdot [Ai(-r'_p)]^2} \tag{2.34}$$

$$\alpha_p^h = \frac{r'_p \cdot e^{j\pi/6}}{\rho_\sigma} \left(\frac{k\rho_\sigma}{2}\right)^{1/3} \tag{2.35}$$

$$L_p^h = e^{j\pi/12} \cdot (2\pi k)^{1/2} \left(\frac{2}{k\rho_\sigma}\right)^{1/3} \cdot Ai(-r'_p) \cdot D_p^h \tag{2.36a}$$

where Ai(x) is the Airy function:

$$Ai(x) = \frac{1}{\pi} \int_0^\infty \cos\left(\frac{t^3}{3} + xt\right) dt \quad (x \text{ real}) \tag{2.36b}$$

and $Ai(-r_p) = 0$, $Ai'(-r_p') = 0$, (Ai' is the derivative of Ai with respect to its argument). Higher-order terms in the expansion of D, α and L have been given in [25] and [30] and in some of the other works on GTD mentioned earlier.

The expression (2.30) is convenient to use in the shadow region. However, in the shadow part of the transition region, since the exponential decay of the terms in (2.30) is weak, the convergence of the series representation is very slow. Furthermore, the series diverges in the lit part of the transition region. Consequently, in these regions, it is more reasonable to use an integral representation for the surface ray field, which, in our case, can be expressed in terms of Fock functions [25].

Attempts have been made to establish the mathematical validity of GTD and to minimize its "nondeductive parts" (parts which are based upon physical intuition or the study of the asymptotic solution of some simple problem geometrical concepts of different kinds of rays, diffraction coefficients, attenuation constants, etc.). Kravtsov [31] and Ludwig [32] have analyzed the field near the caustic surface (smooth envelope of a family of rays),and have developed a "uniform asymptotic solution" in the sense that it is finite at the caustic and reduces to geometrical optics away from the caustic.

3. GENERALIZATION OF GTD AND INVESTIGATION OF ALTERNATE METHODS

3.1 Generalization of GTD to Arbitrary Surfaces

Keller's generalization of GTD for the analysis of the field diffracted from a smooth convex object is closely related to what is known as the "boundary layer technique" in the theory of differential equations [43]. On the other hand, the "uniform asymptotic theory" is analogous to the method used by R. E. Langer [34] and F. J. Olver [35] to find the asymptotic solutions of the second-order differential equations near their "turning points," which are counterparts of the transition regions in our case [33], [34] and [35].

The second prodecure is based upon the generalization of the G.O. interpretation of the circular cylinder problem. The solution obtained by this method involves some functions with unknown phase and amplitude, similar to Bessel and Hankel functions. Since the surface of a smooth object is actually the caustic surface of diffracted rays, the above-mentioned formulation is applicable in this case, too. Lewis et al. [36] have modified this solution to make it satisfy the boundary condition on a convex body. Using ray formalism, they have obtained an asymptotic solution in a complicated form, which they call "creeping wave" and satisfies the boundary condition on and is uniformly valid near and away from the surface. It should be mentioned that the method has been developed primarily for scalar diffraction problems.

Creeping waves that travel on the surface of the body generate other kinds of diffracted rays in the presence of any irregularities in the geometric or electromagnetic characteristics of the surface. The effects of discontinuity in the surface curvature, its higher-order derivatives, or the surface impedance have been studied by many authors [37], [38], [39] and [40].

An exhaustive study of various diffraction mechanisms and corresponding diffraction coefficients, and constants associated with the propagation of creeping waves, has been carried out by Albertsen [41].

At this point, let us examine the most important features of the GTD and its various modifications. GTD formulation is essentially scalar in nature and is heuristic in some parts. Thus, when GTD is applied to a vector problem, it is not surprising that the coupling between various components of the fields are neglected, and each one of them is treated as an uncoupled scalar wave. The other assumptions in GTD are concerned with the directions of these field components and the kind of boundary conditions they satisfy (see Sec. 2.4). As mentioned earlier, non-deductive parts of GTD are based on asymptotic expansions of known solutions to some selected "canonical" problems. Quite often these canonical problems are not general enough to fully and accurately describe the local behavior of the field for an arbitrary structure. Finally, most of the canonical problems investigated are two-dimensional in nature. The only exception to this is the sphere. However, insofar as the geometric properties of the surface are concerned, the sphere is a very special case since its radius of curvature is the same in all directions and, consequently, the surface rays are torsionless. Finally, GTD fails when the observation point is located in the transition regions, shadow boundaries or in the neighborhood of a caustic. In each of these regions, one needs to carefully modify the GTD formulas and often such a modification is not too simple. Nevertheless, in spite of these difficulties, GTD is recognized to be a powerful high-frequency technique for computing the leading terms of the asymptotic solution. Two of the principal attributes of GTD are its simplicity and wide scope of application.

3.2 Spectral Domain Approach

We now examine an approach different from GTD which uses the spectrum of the induced current, or the expression for the radiated field, as a starting point. In order to gain a better insight into the curved-surface radiation and scattering problem and to verify the basic assumptionsof GTD, it is worthwhile to consider such alternative approaches, particularly if they apply to canonical problems which are more general in nature than those employed to derive the GTD results. An example of such a study would be to consider the case of surface ray propagation with non-zero torsion, a situation that occurs when a magnetic dipole source radiates from a location on the surface of a circular cylinder.

The geometry of the problem is shown in Fig. 11. The radius of the cylinder is a and the source,which is an infinitesimal magnetic dipole with density $\vec{M}$,is located at the point Q described by the spherical polar coordinates ($r=a$, $\theta=90°$, $\phi=0°$). Each point P on the surface of the cylinder is defined by a "geodetical polar coordinate" system (σ,β), where σ is the arclength of the geodesic connecting Q to P and β is the angle between $\hat{\phi}$ (at point Q) and geodesic QP. The local orthonormal basis vectors $(\hat{\sigma},\hat{\beta})$ are also associated with these two parameters. The observation point in the far field is specified by its spherical polar coordinates (r,θ,ϕ). The radiated field at an arbitrary point can be expressed in terms of two potentials, Φ and Ψ, which, in cylindrical coordinates, can be written as:

$$\Phi = \frac{1}{2\pi} \sum_{n=-\infty}^{\infty} e^{-jn\phi} \int_{-\infty}^{\infty} f_n(k_z) \cdot H_n^{(2)}(k_t\rho)\, e^{-jk_z z}\, dk_z \qquad (3.1)$$

$$\Psi = \frac{1}{2\pi} \sum_{n=-\infty}^{\infty} e^{-jn\phi} \int_{-\infty}^{\infty} g_n(k_z) \cdot H_n^{(2)}(k_t\rho) \cdot e^{-jk_z z}\, dk_z \qquad (3.2)$$

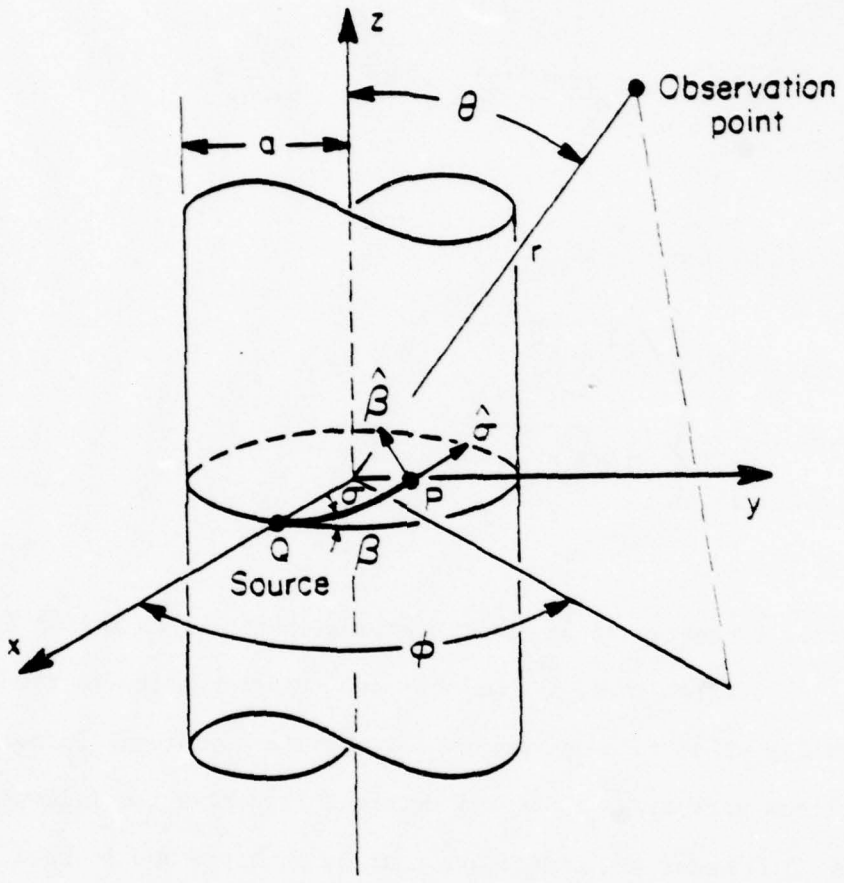

Figure 11: Geometry of the cylinder problem.

For the problem under consideration, we can express the spectral weight coefficients as

$$f_n(k_z) = \frac{-j\omega\varepsilon M_\phi}{2\pi k_t^2 H_n^{(2)}(k_t a) \cdot a} \tag{3.3}$$

$$g_n(k_z) = \frac{1}{k_t H_n^{(2)'}(k_t a) \cdot a} \left[\frac{-M_z}{2\pi} + \frac{n k_z M_\phi}{2\pi k_t^2 a}\right] \tag{3.4}$$

where

$$k_t = \begin{cases} \sqrt{k^2 - k_z^2}, & k > k_z \\ -j\sqrt{k_z^2 - k^2}, & k < k_z \end{cases} \tag{3.5}$$

In order to derive an asymptotic expansion of (3.1) and (3.2), we proceed as follows. As a first step, we apply Watson's transformation to the infinite summation with respect to n and employ appropriate asymptotic formulas for Hankel functions with large order and argument to derive the following expressions for (3.1) and (3.2) under the conditions that ka is large and ϕ small compared to π:

$$\Phi \sim \frac{\omega\varepsilon M_\phi}{(2\pi)^2 \cdot a} \sqrt{\frac{2\pi}{\rho}}\, e^{j\pi/4} \int_{-\infty}^{\infty} dk_z\, e^{-j\Omega} \cdot \frac{m^2}{k^{5/2}} \cdot f_0(\xi_1) \tag{3.6}$$

$$\Psi \sim \frac{jM_\phi}{(2\pi)^2 \cdot a} \sqrt{\frac{2\pi}{\rho}} \cdot \frac{e^{j\pi/4}}{2} \cdot \int_{-\infty}^{\infty} dk_z \cdot e^{-j\Omega} \cdot \frac{k_z}{k_t^{5/2}} [jm\, g_1(\xi_1) + 2m^3 g_0(\xi_1)]$$

$$-j\frac{M_z}{(2\pi)^2} \cdot \sqrt{\frac{2\pi}{\rho}} \cdot \frac{e^{j\pi/4}}{2} \cdot \int_{-\infty}^{\infty} dk_z \cdot \frac{e^{-j\Omega}}{k_t^{1/2}} \cdot g_0(\xi_1) \qquad (3.7)$$

where

$$\Omega = k_z z + k_t[\rho + a(\phi - \pi/2)]$$

$$m = (k_t a/2)^{1/3}$$

$$\xi_1 = m(\phi - \pi/2)$$

f_0, g_0, g_1 = Fock's functions defined in Appendix A.

M_ϕ and M_z = components of $\vec{M}$, $(\vec{M}\cdot\hat{n}=0)$

Next, applying the "saddle-point" technique to (42) and (43) and keeping only the first-order terms, the far field can be written in terms of its components along the normal and tangent to the surface at the "stationary point" P_1 as

$$E_{n_2} = (\vec{M}\cdot\hat{\beta}_1)\left(\frac{jke^{-jk\sigma}}{4\pi}\right) \cdot g_o(\xi_{1s}) \cdot \frac{e^{-jkR}}{R}$$

$$- \frac{(\vec{M}\cdot\hat{\phi}_1)(\hat{\phi}_1\cdot\hat{\beta}_1)}{4\pi a} \cdot e^{-jk\sigma} \cdot \left(\frac{k\rho_\sigma}{2}\right)^{1/3} \cdot g_1(\xi_{1s}) \cdot \frac{e^{-jkR}}{R} \qquad (3.8)$$

$$E_{\beta_2} = \frac{(\vec{M}\cdot\hat{\phi}_1)(\hat{\phi}_1\cdot\hat{\sigma}_1)}{2\pi a} \cdot \left(\frac{k\rho_\sigma}{2}\right)^{2/3} \cdot e^{-jk\sigma} \cdot f_0(\xi_{1s}) \cdot \frac{e^{-jkR}}{R} \qquad (3.9)$$

where

P_1: is the stationary point of Ω which turns out to be the same as the point of diffraction predicted by GTD.

$$\xi_{1s} = \left(\frac{ka}{2}\right)^{1/3} (\phi-\pi/2) \cdot \sin^{1/3}\theta$$

ρ_σ = radius of curvature of geodesic QP_1

σ = arc length QP_1

R = the distance between the point of diffraction P_1 and the observation point

$n_2 = \hat{\sigma}_2 \times \hat{\beta}_2$; normal to the surface at P_1

The details of the derivations of (3.8) and (3.9) are given in Appendix B.

Fig. 12 illustrates the geometric meaning of some of the parameters appearing in (3.8) and (3.9), for the observation point is located in the shadow region. In this case, ξ_{1s}, which is identical to ξ given in (2.16), is the reduced distance traveled by the surface ray before leaving the surface tangentially.

In the lit region, the geometric interpretations of σ and ξ are shown in Fig. 13. The rays, like QP_1P, that do not obey the generalized Fermat's principle are called "pseudo-rays" [25]. The ray QP_1P appears to travel along the surface up to the point P_1 and then leaves the surface at P_1 tangentially in the opposite direction, to reach the observation point P. It should be noted that formulas (3.8) and (3.9) give us the contribution of the ray which

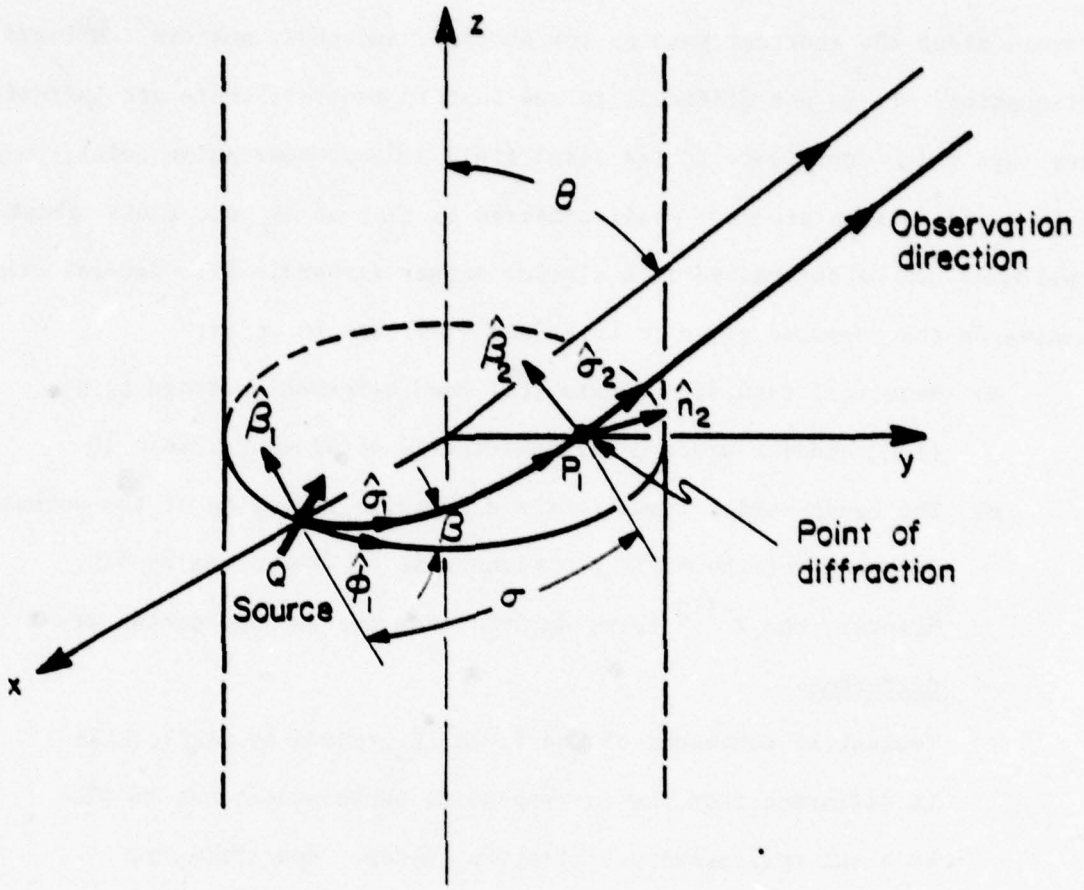

Figure 12: Diffraction of rays by a cylindrical body.

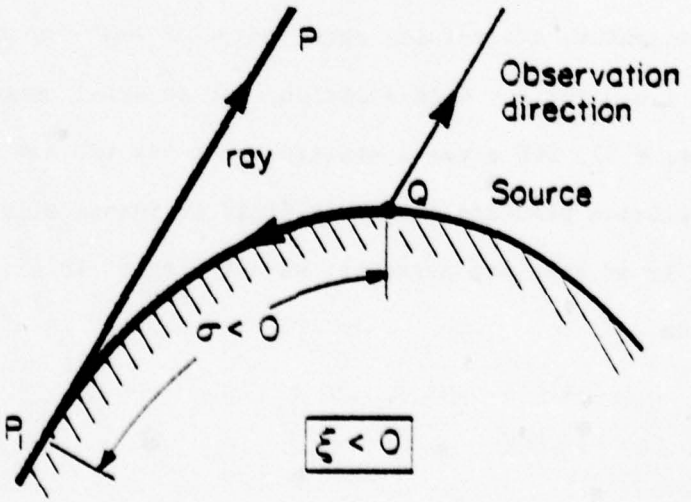

Figure 13: Diffraction of "psuedo-rays."

travels along the shortest path on the surface, and thus, suffers the least attenuation. It is not difficult to see that, in general, there are infinitely many rays which contribute to the total field at any observation point. However, their contributions are very small compared to that of QP_1 and their phases and amplitudes can be determined in a similar manner (Appendix B). Several other remarks on the formulas given in (3.8) and (3.9) are in order:

a) Numerical results indicate that good agreement between (3.8), (3.9), and the exact modal solution is obtained for ka > 10.

b) The zeroth-order terms in the asymptotic expansion of the normal component of the field E are identical to those given by GTD; however, the $k^{-1/3}$ terms derived from the two approaches are <u>different</u>.

c) Tangential component of the field, E_β, given by (3.9), also is different from the corresponding expression based on GTD by a multiplicative polarization factor. Specifically,

$$E_\beta \text{ in (45)} = \left[\frac{(\vec{M}\cdot\hat{\phi}_1)}{(\cos\beta)\cdot(\vec{M}\cdot\hat{\sigma}_1)}\right] \text{ (GTD)} \qquad (3.10)$$

Consequently, our results agree with GTD only for the circumferential ray, i.e., for $\beta = 0$. In addition, for an axial magnetic dipole ($\vec{M}\cdot\hat{\phi}_1 = 0$), GTD gives a nonzero value for the field in the $\hat{s}_2$ direction; our solution predicts that this field is identically zero, a result which is in complete agreement with the exact solution for the problem.

Yet another important distinguishing feature of the spectral domain formulas from the corresponding ones based on GTD is worth noting. As mentioned earlier, GTD neglects the effect of torsion on the diffraction of surface rays propagating along smooth objects. In contrast, the spectral domain formulas (3.8) and (3.9) indeed contain the torsion effect of the surface rays as may be seen from the discussion below.

To rearrange the formulas (3.8) and (3.9) in a manner such that the effect of the torsion on the surface rays is explicitly illustrated, it is necessary to examine the polarization factors in the above-mentioned formulas. Referring to Fig. 12, the helical path of a surface ray with initial angle β can be parametrized as:

$$\vec{x}(\sigma) = [a \cos(\frac{\sigma\cos\beta}{a}), a \sin(\frac{\sigma\cos\beta}{a}), \sigma \sin\beta] \tag{3.11}$$

The torsion of the ray, τ, is found from the relation,

$$\frac{d\hat{\beta}}{d\sigma} = -\tau \hat{n} \tag{3.12}$$

where $\hat{\beta}$ is the binormal vector given by

$$\hat{\beta} = \hat{n} \times \hat{\sigma} = \hat{n} \times \frac{\hat{dx}}{d\sigma} \tag{3.13}$$

and $\hat{n}$ is the outward unit normal to the surface of cylinder. For a helix on a circular cylinder, the torsion is constant along the path and depends solely on the initial angle of the curve. The torsion τ is given by the following simple formula:

$$\tau = \frac{\sin\beta \cdot \cos\beta}{a} \tag{3.14}$$

Combining the above relation with the expression for

$$\rho_\sigma = \frac{a}{\cos^2\beta} \tag{3.15}$$

one obtains,

$$\tan\beta = \tau\rho_\sigma \ . \tag{3.16}$$

The above relationship between β, τ and ρ_σ will be found useful in what follows.

Equation (3.16) enables one to rewrite the source polarization factors in (3.8) and (3.9) in the following form:

$$-\frac{(\vec{M}\cdot\hat{\phi}_1)\cdot(\hat{\phi}_1\cdot\hat{\beta}_1)}{2\cos^2\beta} = (\vec{M}\cdot\hat{\sigma}_1)\frac{\tan\beta_1}{2} - (\vec{M}\cdot\hat{\beta}_1)\frac{\tan^2\beta_1}{2}$$

$$= (\vec{M}\cdot\hat{\sigma}_1)\cdot\frac{(\tau\rho_\sigma)}{2} - (\vec{M}\cdot\hat{\beta}_1)\frac{(\tau\rho_\sigma)2}{2} \tag{3.17}$$

$$\frac{(\vec{M}\cdot\hat{\phi}_1)}{\cos\beta} = (\vec{M}\cdot\hat{\sigma}_1) - (\tau\rho_\sigma)\cdot(\vec{M}\cdot\hat{\beta}_1) \tag{3.18}$$

The explicit manifestation of the torsion effect can be seen very clearly if we use (3.17) and (3.18) in (3.8) and (3.9). The final result can be written as

$$E_{n_2} = E_{n2}^{GTD} + [(\vec{M}\cdot\hat{\sigma}_1)\cdot(\frac{\tau\rho_\sigma}{2}) - (\vec{M}\cdot\hat{\beta}_1)\cdot\frac{(\tau\rho_\sigma)^2}{2}]$$

$$\cdot\frac{ke^{-jk\sigma}}{4\pi}\left(\frac{k\rho_\sigma}{2}\right)^{-2/3} g_1(\xi_{1s})\cdot\frac{e^{-jkR}}{R} \qquad (3.19)$$

$$E_{\beta 2} = E_{\beta 2}^{GTD} - (\tau\rho_\sigma)(\vec{M}\cdot\hat{\beta}_1)\cdot\frac{ke^{-jk\sigma}}{4\pi}\cdot\left(\frac{k\rho_\sigma}{2}\right)^{-1/3}$$

$$\cdot f_0(\xi_{1s})\cdot\frac{e^{-jkR}}{R} \qquad (3.20)$$

where τ is the torsion of the surface ray. Note that the effect of the torsion on the surface rays has been isolated and explicitly expressed in the above expression. These appear as correction terms to GTD and are proportional to $\tau\rho_\sigma$ and $(\tau\rho_\sigma)$. As expected, the formulas given above reduce to the conventional GTD results for the limiting case of no torsion, i.e., $\tau = 0$.

In contrast to GTD, formulas (3.8) and (3.9) are valid irrespective of the location of the observation point, be it in the lit, shadow or transition regions. Although not valid in the paraxial region ($\beta\approx 90°$), they can be generalized to work along this direction also.

The solution to the problem of radiation of a normal electric dipole can be found from the expressions (3.8) and (3.9) for the radiated far field due to a magnetic dipole through an application of the reciprocity theorem. To show this, we apply this theorem to the following two reciprocal situations.

For the first case. let $\{\vec{E}, \vec{H}\}$ from an infinitesimal electric dipole source of moment $\vec{p}$, located far from the cylinder at a point P. In the second situation, let $\{\vec{E}^m, \vec{H}^m\}$ be the fields radiated by an infinitesimal dipole of moment $\vec{M}$, located at a point Q on the surface of the cylinder. As the outer boundary surface of the volume, where the theorem is applied, goes to infinity, the "cross flux" through it vanishes. Also there is no "cross flux" through the inner surface (cylinder). Therefore, invoking the reciprocity relation, one can derive

$$-\vec{M} \cdot \vec{H}(Q) = \vec{p} \cdot \vec{E}^m(P) \tag{3.21}$$

Now if we apply reciprocity to another pair of cases, in which the first one is the same as the first situation in the previous example and the second one consists of the radiation $\{\vec{E}^e, \vec{H}^e\}$ of a normal electric dipole of moment $\vec{J}$, we will have

$$\vec{J} \cdot \vec{E}(Q) = \vec{p} \cdot \vec{E}^e(P) \tag{3.22}$$

Suppose the magnitudes of $\vec{J}$ and $\vec{M}$ are unity, then it follows from (3.21) and (3.22)

$$H_\phi(Q) = -\vec{p} \cdot \vec{E}^{mc}(P) \tag{3.23a}$$

$$H_z(Q) = -\vec{p} \cdot \vec{E}^{ma}(P) \tag{3.23b}$$

$$E_\rho(Q) = \vec{p} \cdot \vec{E}^{en}(P) \tag{3.23c}$$

where $H_\phi(Q)$, $H_z(Q)$ and $E_\rho(Q)$ are the local field components in the cylindrical coordinate system coaxial with the conducting cylindrical surface. This field

is generated by $\vec{p}$ (Fig. 14). The following set of relations can be derived from (3.23) by replacing $\vec{p}$ by $\hat{\theta}_0$ and $\hat{\phi}_0$, respectively,

$$E_\rho^{\theta\theta_0}(Q) = E_{\theta_0}^{en}(P) \tag{3.24a}$$

$$E_\rho^{\phi 0}(Q) = E_{\phi_0}^{en}(P) \tag{3.24b}$$

$$H_\phi^{\theta_0}(Q) = -E_{\theta_0}^{mc}(P) \tag{3.25a}$$

$$H_z^{\theta_0}(Q) = -E_{\theta_0}^{ma}(P) \tag{3.25b}$$

$$H_\phi^{\phi_0}(Q) = -E_{\phi_0}^{mc}(P) \tag{3.25c}$$

$$H_z^{\phi_0}(Q) = -E_{\phi_0}^{ma}(P) \tag{3.25d}$$

where $E_\rho^\alpha(Q)$, $\alpha = \theta_0$ and ϕ_0 is the normal electric field at Q due to an electric dipole with moment $\vec{p} = \hat{\theta}_0, \hat{\phi}_0$ located at P. $H_\phi^\alpha(Q)$ and $H_z^\alpha(Q)$, $\alpha = \theta_0$, and ϕ_0 are the tangential components of the magnetic field generated by an electric dipole of moment $\vec{p} = \hat{\theta}_0, \hat{\phi}_0$ located at P. Invoking the Maxwell's equations, a relationship can be set up between the desired far field $E_{\theta_0,\phi_0}^{en}(P)$, due to a normal electric dipole of unit moment, and the known solutions $E_{\phi_0,\theta_0}^{mc,ma}(P)$ (Equations (3.8) and (3.9)) to the problem of the radiation of a circumferential (mc) and axial (ma) magnetic dipole on a cylinder. As a matter of fact, E_ρ^α and $\{H_\phi^\alpha, H_z^\alpha\}$ can be related by

$$E_\rho^\alpha(Q) = \frac{1}{j\omega\varepsilon}\left[\frac{1}{a}\cdot\frac{\partial H_z^\alpha}{\partial\phi} - \frac{\partial H_\phi^\alpha}{\partial z}\right], \quad \alpha = \theta_0, \phi_0 \tag{3.26}$$

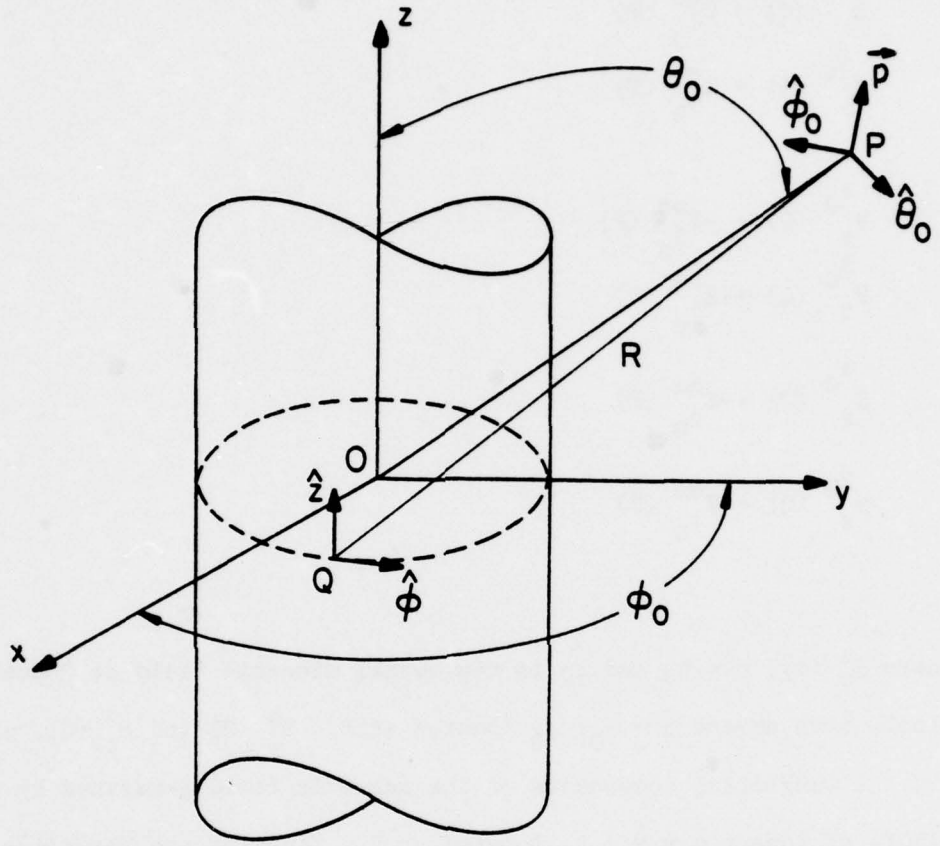

Figure 14. The source $\vec{M}$ or $\vec{J}$ (Equations 3.21 and 3.22) are located at Q and the elemental electrical dipole of moment $\vec{p}$ is located at P (the observation point).

where ϕ and z are cylindrical coordinates of a point on the surface of the cylinder. Using Equations (3.25), we have

$$E^{en}_{\theta_0}(P) = \frac{-1}{j\omega\varepsilon}\left[\frac{1}{a}\cdot\frac{\partial E^{ma}_{\theta_0}(P)}{\partial\phi} - \frac{\partial}{\partial z}E^{mc}_{\theta_0}(P)\right] \tag{3.27a}$$

$$E^{en}_{\phi_0}(P) = -\frac{1}{j\omega\varepsilon}\left[\frac{1}{a}\cdot\frac{\partial}{\partial\phi}\ E^{ma}_{\phi_0}(P) - \frac{\partial}{\partial z}E^{mc}_{\phi_0}(P)\right]. \tag{3.27b}$$

It is noted that the derivatives are taken with respect to the source coordinates, whereas Equations (3.8) and (3.9) give us the field components generated by a tangential mangetic dipole, as a function of the observation point P coordinates. However, the derivatives, with respect to the source coordinates, are related with those with respect to the observation point location through a sign reversal. Therefore,

$$E^{en}_{\theta_0}(P) = \frac{1}{j\omega\varepsilon}\left[\frac{1}{a}\cdot\frac{\partial}{\partial\phi_0}\ E^{ma}_{\theta_0}(P) - \frac{\partial}{\partial z_0}\ E^{mc}_{\theta_0}(P)\right] \tag{3.28a}$$

$$E^{en}_{\phi_0}(P) = \frac{1}{j\omega\varepsilon}\left[\frac{1}{a}\cdot\frac{\partial}{\partial\phi_0}\ E^{ma}_{\phi_0}(P) - \frac{\partial}{\partial z_0}\cdot E^{mc}_{\phi_0}(P)\right] \tag{3.28b}$$

where ϕ_0 and z_0 are the observation point coordinates. The far-zone radiated field due to a normal electric dipole of unit moment located on the surface of a cylinder can be found by evaluating relations (3.28) using (3.8) and (3.9)

$$E^{en}_{\theta_0} = \frac{-\sin\theta_0 \cos\theta_0}{2\pi Y_o a} \left(\frac{k\rho_\sigma}{2}\right)^{2/3} \cdot e^{-jk\sigma} \cdot f_0(\xi_{1s}) \cdot \frac{e^{-jkR}}{R} \qquad (3.29a)$$

$$E^{en}_{\phi_0} = \frac{jk(1+\cos^2\theta_0)}{Y_0} \frac{e^{-jk\sigma}}{4\pi} \cdot g_0(\xi_{1s}) \cdot \frac{e^{-jkR}}{R}$$

$$- \left(\frac{k\rho_\sigma}{2}\right)^{1/3} \cdot \frac{e^{-jk\sigma}}{4\pi a} \cdot g_1(\xi_{1s}) \frac{e^{-jkR}}{R} \quad . \qquad (3.29b)$$

Finally, let us consider the possibility of the generalization of (3.8) and (3.9) to other convex surfaces of more general nature. By "more general surfaces," we mean those surfaces which are not substantially different from cylinders, some examples being cylinders with noncircular (elliptical, hyperbolic, and parabolic) cross sections and conical surfaces with small apex angles. The key step in a systematic approach to generalizing (3.8) and (3.9) is to use the generalized definition of ξ given in (2.16).

Fig. 15 exhibits some initial results of the generalization of these formulas to the case of a cone. In these graphs, the Hughes results have been reproduced from [63]. It is evident that results obtained from the present approach agree quite well with the series solution which is rather tedious and time-consuming. We also observe from Fig. 16 that there is a noticeable discrepancy between the analytical solution and the experiment. Thus, within the range of experimental error, our results agree quite well with those published in the literature.

Before concluding this subsection, it is worth mentioning some basic points concerning the applicability of this formulation to the case of lossy surfaces which may be approximately described in terms of surface-impedances. For this case, the simplifying assumption of infinite conductivity for the

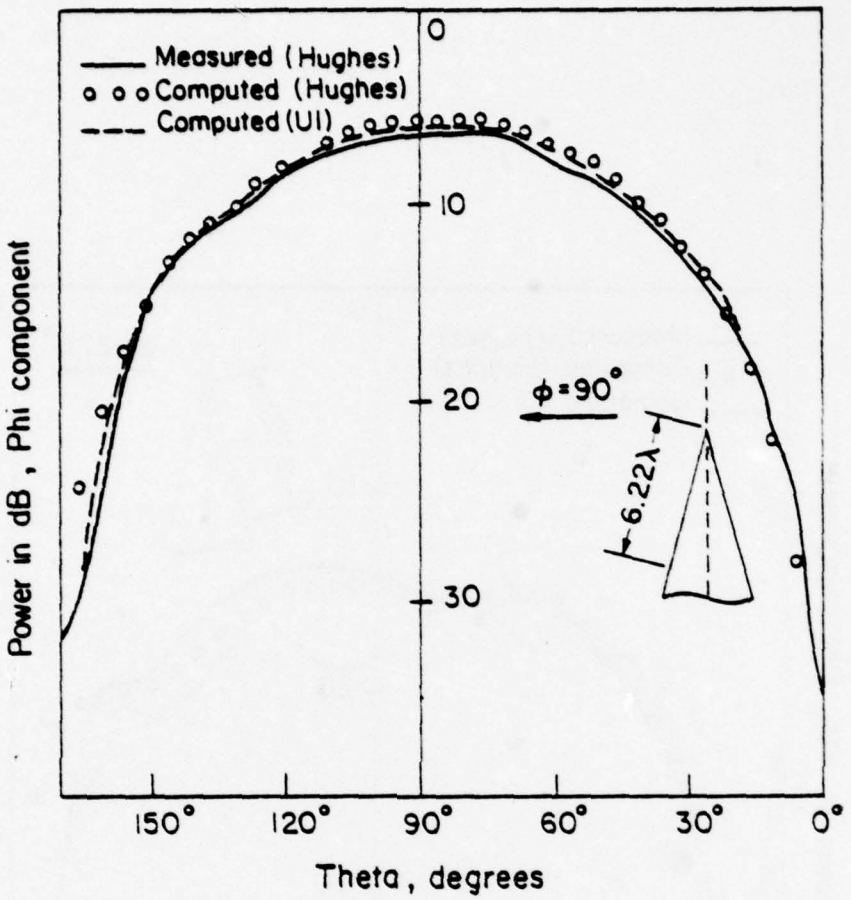

φ = 90° cut:

Figure 15 Comparison between spectral domain results (UI), modal approach (Hughes), and experimental measurements (Hughes). The UI results are derived from a generalized version of (3.8) and (3.9) for a cone. The Hughes results have been reproduced from [63] and are based on a modal series of 13 terms. All results are for λ/2 radial slot on a cone of half-angle 10°. (φ=90° cut)

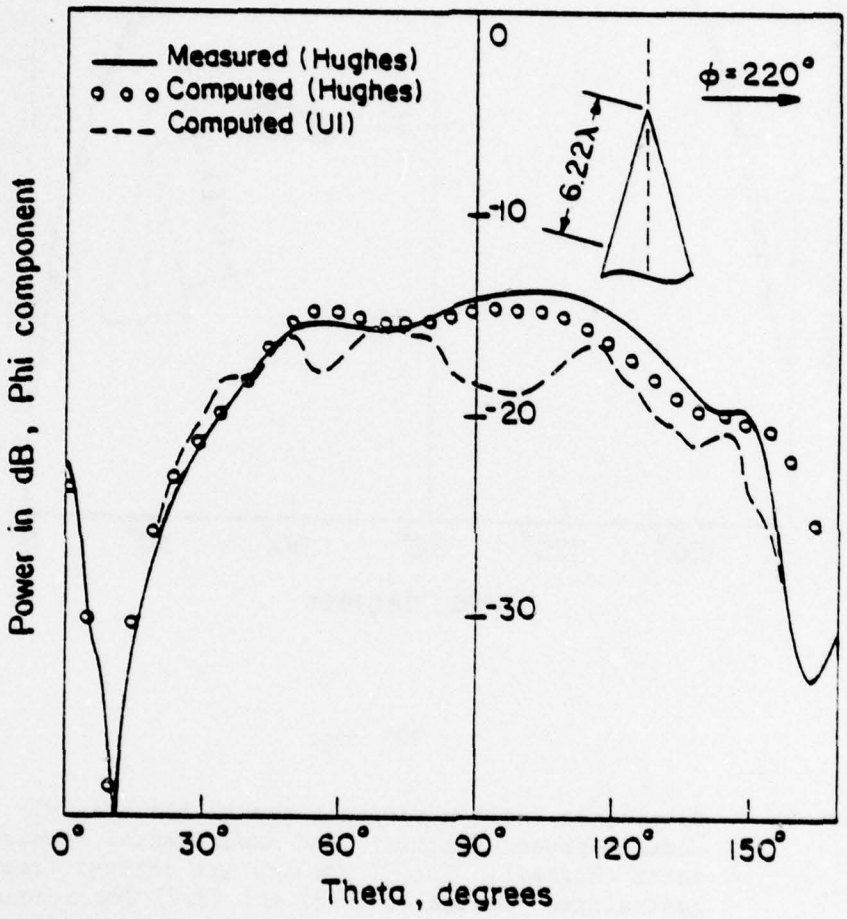

Figure 15b. ϕ = 220° cut.

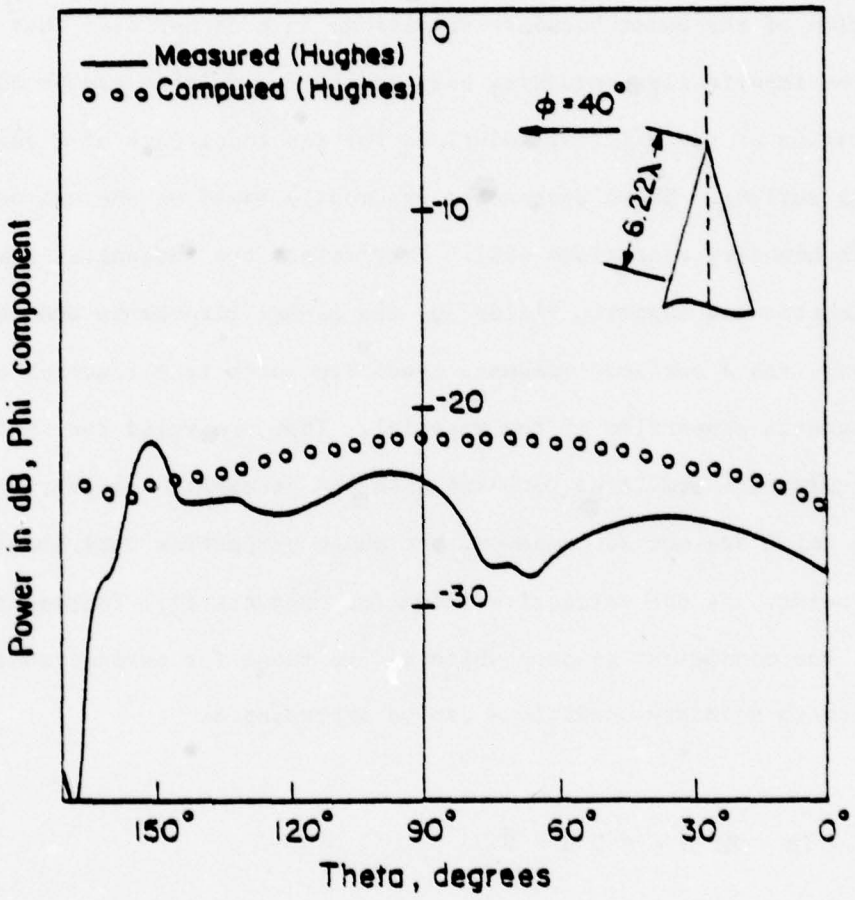

Figure 16. $\phi = 40°$ cut illustrating the discrepancy of thecretical (Hughes) and experimental (Hughes) presumably attributable to experimental error.

scatterer no longer holds, the problems become tremendously complicated, especially when the surface of the scatterer is curved. However, for special cases where the frequency is high and the geometry of the body satisfies some specific conditions, certain approximate procedures are available for solving the problem [64], [65], [66]. Some of these approaches are based on the modification of the exact boundary conditions in a manner such that the solution to the imperfectly conducting body scattering problem can be obtained as a perturbation of the existing solutions for the ideal case of a perfectly conducting surface. These approaches are mostly based on the use of the Leontovich boundary conditions [64]. They relate the tangential components of the electric and magnetic fields (or the normal components and their normal derivatives) via a surface impedance condition which is a function only of the electromagnetic properties of the material. They are valid for surfaces whose radii of curvature are large compared with the penetration depth, and also for materials which are not homogeneous, but whose properties vary slowly from point to point. As the refractive index (or conductivity) increases to infinity, the conditions go over uniformly to those for perfect conductivity. The Leontovich boundary conditions can be expressed as

$$\vec{E} - (\hat{n} \cdot E)\,\hat{n} = \eta Z\, \hat{n} \times \vec{H} \tag{3.30}$$

where $\hat{n}$ is the unit normal to the surface, Z is the impedance of free space and

$$\eta = \frac{1}{\sqrt{\frac{\mu_0}{\mu}\left(\frac{\varepsilon}{\varepsilon_0} + j\,\frac{\sigma}{\omega\varepsilon_0}\right)}} = \frac{\mu}{\mu_0 N}$$

σ, μ, ε = electromagnetic characteristic of the body

$Z = \sqrt{\mu/\varepsilon}$ = free space impedance

N = complex refractive index of the body.

The conditions for applicability of (3.30) to the curved surfaced can be formulated as

$$|N| >> 1 \tag{3.31a}$$

$$|\mathrm{Im}\, N|\ k\rho >> 1 \tag{3.31b}$$

where ρ is the smallest radius of curvature or dimension of the body [64].

When η is very small, we can expand the fields $\{\vec{E}, \vec{H}\}$ around their values $\{\vec{E}_0, \vec{H}_0\}$ for the case of perfectly conducting surfaces ($\eta=0$), in the ascending powers of η as

$$\vec{E} = \vec{E}_0 + \eta\vec{E}_1 + \eta^2 \vec{E}_2 + \ldots \tag{3.32a}$$

$$\vec{H} = \vec{H}_0 + \eta\vec{H}_1 + \eta^2\vec{H}_2 + \ldots \tag{3.32b}$$

Inserting (3.32) in (3.30) one finds

$$\vec{E}_0 - (\hat{n} \cdot \vec{E}_0)\, \hat{n} = 0 \tag{3.33a}$$

$$\vec{E}_1 - (\hat{n} \cdot \vec{E}_1)\, \hat{n} = \eta Z\, \hat{n} \times \vec{H}_0 \tag{3.33b}$$

$$\vec{E}_2 - (\hat{n} \cdot \vec{E}_2)\, \hat{n} = \eta Z\, \hat{n} \times \vec{H}_1,\ \vec{H}_1 = \frac{\nabla \times \vec{E}_1}{-j\omega\mu} \tag{3.33c}$$

Equation 3.33b is a first-order approximation for the boundary condition for the tangential electric field on the surface of the body. The function $\vec{H}_0$ is the known solution for a purely conducting surface. Using boundary condition (3.33b), one is able to find the first-order solution for the electric field in the presence of imperfectly conducting homogeneous or inhomogeneous objects. The higher-order solutions can be found in a similar manner.

3.3 Approach Based on an Asymptotic Evaluation of the Radiation Integral of the Surface Current

As a final topic in this chapter, we consider an approach based on the asymptotic evaluation of the radiation integral expressed in terms of the induced surface current which is itself derived in an asymptotic manner for surfaces with large radius of curvature.

It was shown in Chapter 2 that Fock's theory can provide us with an expression for the scattered field in the neighborhood of a smooth convex body illuminated by a plane wave. Using this solution in conjunction with the reciprocity principle, we can find the far field radiated by a point source located on the surface of the body. By generalizing the definition of ξ in Fock's theory, we can also write the final result in a GTD format and represent it as a surface ray. The total field at a point on the surface is obtained by adding all the possible rays which reach the observation point P. Various techniques can be used to determine the field propagation along these rays. For instance, when the source is located on the surface, and the surface is a conical one, the field at each point can be decomposed into two parts

$$F = F_1 + F_2 \tag{3.34}$$

where F_1 is the geometrical optics field when the observation point is directly illuminated by the source, and is the creeping-wave contribution derivable via an extension of Fock's theory when the point is in the shadow region. The other term, F_2, is the so-called tip contribution, and can be obtained by physical optics or GTD. Goodrich et al. [42] have applied this procedure to find the radiation pattern of slot arrays on cones.

The approximate induced surface current distribution can be obtained by Fock's theory, GTD [13], [14], [16], and [25] or some other appropriate high frequency technique. The induced surface current due to a magnetic dipole on a perfectly conducting circular cylinder and cone has been calculated by Chang, et al. [44], and Chan, et al. [45], whose procedure is based upon an asymptotic expansion of the exact modal solution to the above-mentioned problems. Lee, et al. [46] and [22] have treated the same problem by a method based on Fock's asymptotic solution of the problem of a sphere [47]. These expressions for the current distribution can be used in the radiation integral representation of the far field.

The numerical evaluation of this integral is a formidable task, especially when the frequency is very high. Thus, it is highly desirable to have an analytical and explicit formula for the far field expressed in terms of the surface current. We now discuss an approach for accomplishing this task and examine the problem of deriving an asymptotic expansion of the far field radiated due to a point source located on the surface of a smooth, conducting, and convex body of an arbitrary shape.

Consider an arbitrary smooth convex surface S shown in Fig. 17. Let a magnetic dipole source be located at a point Q on S. We parametrize the surface S introducing a "geodetical polar coordinate" system with the pole located at Q such that an arbitrary point P_1 on the surface is defined by a pair of numbers (σ,β), where σ is the arc length of the geodesic QP_1 and β is the angle between QP_1 and some reference direction at Q. Unit vectors along the constant parameter curves $\hat{\sigma}$ and $\hat{\beta}$ are locally orthogonal. The unit normal to the surface, $\hat{n}$, is given by $\hat{n} = \hat{\sigma} \times \hat{\beta}$. An element of length in this coordinate system may be written as

$$ds^2 = d\sigma^2 + G\, d\beta^2 \tag{3.35}$$

The radiation integral for the scattered far field can be written as

$$\vec{E} = \frac{-j\omega\mu}{4\pi} \int\int_S \vec{J}(1-\hat{R}\hat{R}) \cdot \frac{\exp(-jkR)}{R}\, dS \tag{3.36}$$

where R is the distance between any point on the surface and the observation point. In the geodetical polar coordinate system, we can rewrite a scalar component of (3.36), say M, in terms of a double integral of the following general form

$$M = \int\int_D F(\sigma,\beta;P)\, \frac{\exp[-jk(R+\sigma)]}{R}\, \sqrt{G}\, d\sigma\, d\beta \tag{3.37}$$

where we have assumed the following form for the surface current:

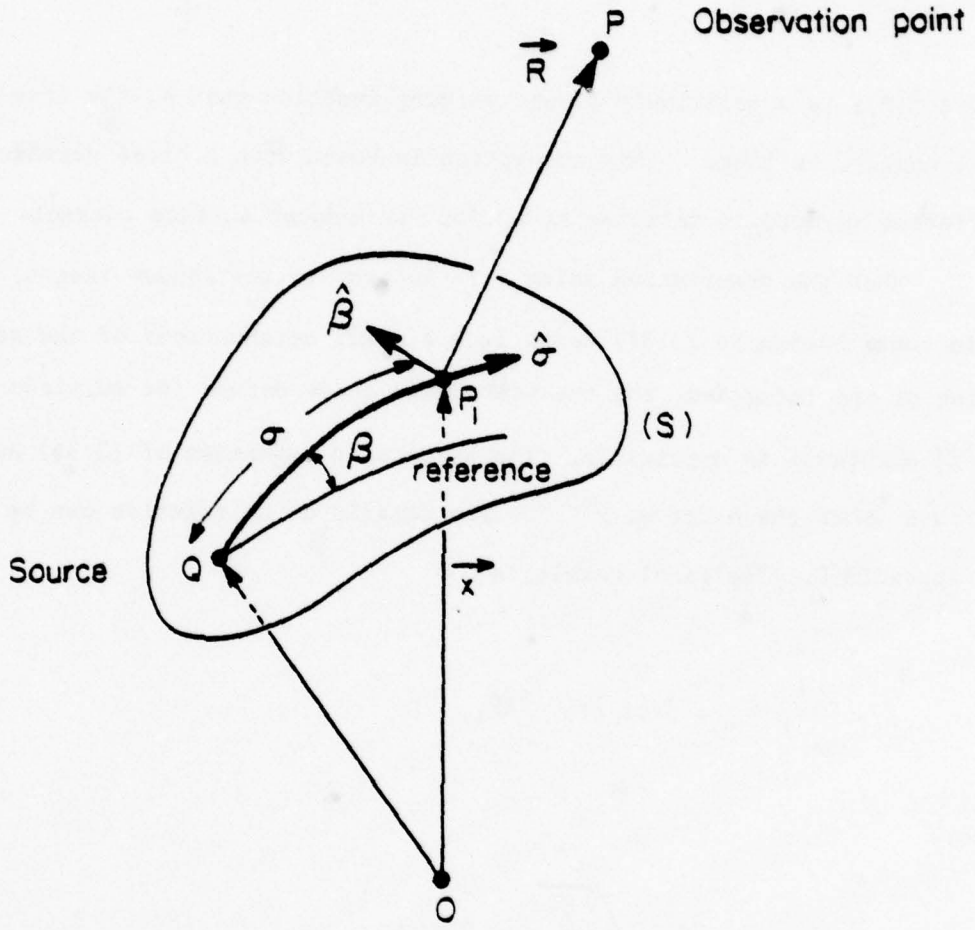

Figure 17: Source radiation in the presence of a smooth convex surface, parametrized by geodetical polar coordinate system.

$$\vec{J}(P_1) = \vec{f}(P_1)\exp(-jk_1\sigma) = J_\sigma\hat{\sigma} + J_\beta\hat{\beta}$$

$$k_1 = k - jk_2;\quad k = 2\pi/\lambda,\quad k_2 > 0,\quad k_2 << k \tag{3.38}$$

where $\vec{f}(P_1)$ is a relatively slowly varying function when k, the free-space wave number, is large. This assumption is based upon a close scrutiny of different asymptotic formulas given for the induced surface current.

When the observation point P is located in the shadow region, the main contribution to (3.37) comes from a small neighborhood of the stationary point of the integrand, and the stationary phase method for multiple integrals ([48] and [49]) is applicable. The asymptotic expansion of (3.36) has been derived up to the order of $k^{-5/3}$. The details of calculation can be found in Appendix C. The final result is

$$\vec{E} = \frac{-k^2}{8\pi^2}\,(\vec{U}_0 + \vec{U}_1 + 0(k^{-11/6})) \tag{3.39}$$

where

$$U_0 = \hat{\beta}\,J_\beta \cdot \frac{D_0}{k^{5/6}}\sqrt{\frac{\rho_g}{R(R+\rho_g)}} \cdot e^{-jkR} \tag{3.40}$$

$$U_1 = [(AJ_\beta + \frac{\partial}{\partial\sigma}(J_\beta e^{jk\sigma})e^{-jk\sigma})\hat{\beta} + (BJ_\beta + CJ_\sigma)\hat{n}]$$

$$\cdot \frac{D_1}{k^{7/6}}\sqrt{\frac{\rho_g}{(R+\rho_g)R}} \cdot e^{-jkR} \tag{3.41}$$

$$D_0 = e^{-j\pi/4} \cdot 6^{5/6} \cdot \Gamma(1/2) \cdot \Gamma(1/3) \cdot \rho_\sigma^{2/3} \tag{3.42}$$

$$D_1 = \frac{-je^{-j\pi/4}}{3} \cdot 6^{7/6} \cdot \Gamma(2/3) \cdot \Gamma(1/2) \cdot \rho_\sigma^{4/3} \tag{3.43}$$

A, B, and C are dependent upon geometric properties of the surface at the stationary point which turns out to be exactly the same as the "point of diffraction" of surface rays. The quantities A, B, and C are given by

$$A = \frac{1}{2G} \frac{\partial}{\partial\sigma} G - \frac{\rho_\sigma}{2} \cdot \frac{\partial}{\partial\sigma}\left(\frac{1}{\rho_\sigma}\right) + \frac{\rho_g}{2G}\left[\frac{L^{\beta\beta}}{\rho_\sigma} + (L^{\beta\sigma})^2 - (1/2)\frac{\partial^2 G}{\partial\sigma^2}\right] + 0\left(\frac{1}{R}\right) \tag{3.44}$$

$$B = L^{\beta\sigma}/G^{1/2}, \quad C = -1/\rho_\sigma \tag{3.45}$$

where

ρ_σ = radius of curvature of the geodesic

ρ_g = geodetic radius of curvature

$L^{\beta\beta}$, $L^{\beta\sigma}$ = coefficients of the second fundamental form of the surface (S).

A geometric interpretation of these parameters has been illustrated in Fig. 18. It is evident from this figure that $\left[\frac{\rho_g}{R(R+\rho_g)}\right]^{1/2}$ is simply the divergence factor of the rays leaving the surface tangentially at the point of diffraction. In using formula (3.43), we should bear in mind that the various terms in U_0 and U_1 are not of the same order. For example, in the deep shadow, J_σ is exponentially larger than J_β.

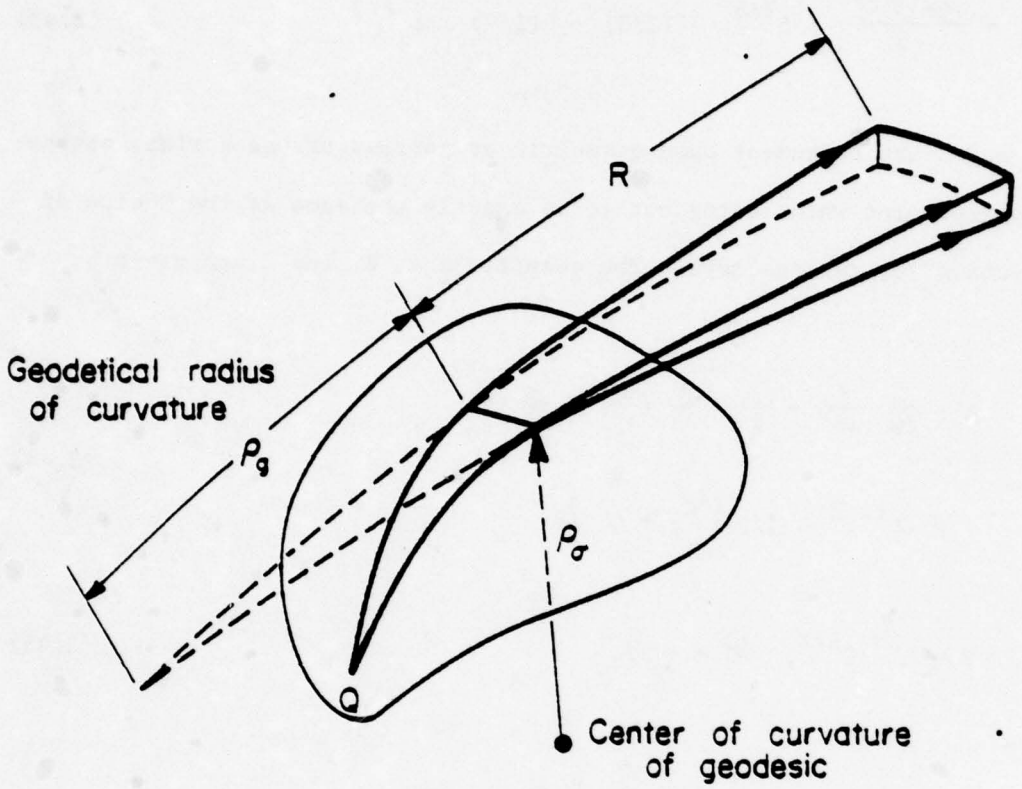

Figure 18: Diffraction of rays by a smooth convex body and geometric meaning of quantities ρ_g, ρ_σ and R.

The formulas given in (3.43) have been tested and compared with other available solutions. An important conclusion derived from this comparison is that although the method of radiation integral is based on less restrictive assumptions, it is perhaps not as useful as the spectral domain approach because the stationary point of the phase of the integrand in (3.37) is of the second order, and hence, the asymptotic expansion of this integral converges rather slowly except when $k\rho_\sigma$ is very large ($\simeq$40 or more).

4. SOURCE RADIATION IN THE PRESENCE OF AN INFINITELY CONDUCTING CIRCULAR CYLINDER OF FINITE LENGTH (GENERAL FORMULATION OF THE PROBLEM)

An asymptotic analysis of the problem of radiation of an electromagnetic point source located on a solid metallic cylinder of finite length is the topic which is studied in detail in the remaining chapters. Because of its theoretical and practical importance (small antennas mounted on the body of the satellites, conformal arrays, electromagnetic coupling through the slots on the surface of a cylinder, and etc.), the problem of radiation in the presence of or the diffraction by the finite cylinder has been treated by many investigators. Various numerical and asymptotic techniques have limited application since they are usually valid only for a special range of parameters, e.g., the length or radius of the cylinder, the location of the source, or a special type of incident field. When the length and the radius of the cylinder are small, compared to the wavelength (fraction of a wavelength), the 2-D integral equation for the surface magnetic field or the two one-dimensional (generally coupled) integral equations for the transverse and axial components of the induced surface current are solved by the moment method or point-matching techniques [67], [68], [69], [70], and [71]. Other approaches have been presented for the cases where the length of the cylinder is very large and its radius is relatively small or the incident field has some special characteristics [72], [73], [74], [75] and [76].

When the frequency is high or the length and the radius of the cylinder are large compared to the wavelength, several asymptotic procedures, mostly based on GTD and its modification, have been designed and applied to this problem [77], [78], [79], [80], and [81] with various degrees of success.

The asymptotic method described in this work is essentially a spectral domain approach and is very closely related to the Spectral Theory of Diffraction (STD) developed by R. Mittra et al. [82], [88], and [89].

The present approach is presumably more accurate than the other available methods because it avoids most of the restrictive assumptions underlying the conventional high frequency techniques. In this chapter, we merely outline the basic steps to this approach. The details are presented in the later chapters.

In the high frequency range where the ray formalism is the most convenient representation for the Maxwell's equations, the field at each point of the space can be expressed as the sum of the contributions of different rays passing through that point. Various diffraction or reflection mechanisms give rise to different types of reflected or diffracted rays which together with the direct ray constitute the total field. In the present problem, illustrated in Fig. 19, the effect of the finite solid cylinder on the radiated field at P due to the source Q (located on the surface) has been represented by three types of rays. F^s is the surface diffracted ray (or psuedoray, if the P is in the lit region of Q) corresponding to the radiated field due to current induced on the surface of the cylinder. F^{w1} and F^{w2} are wedge diffracted rays generated by the curved wedges at both ends of the cylinder. To calculate F^s, if the source is far from both ends, the infinite cylinder formula derived in Chapter 3 or in [85] can be used. These formulas are discussed in Chapter 5. Wedge diffracted fields F^{w1} and F^{w2} can be analyzed only when the surface field or current are available. Chapters 6 and 7 are devoted to computation of F^{w1} and F^{w2}. In Chapter 8, by calculating the effect of truncation, we remove the assumption made in Chapter 5 concerning the length of the cylinder and extend the range of applicability of the procedure to the cases where the source is not too far from the upper or lower wedge of the cylinder. Chapter 9 is devoted to the calculation of the field in the paraxial region. A summary of numerical results and conclusions are given in Chapters 10 and 11.

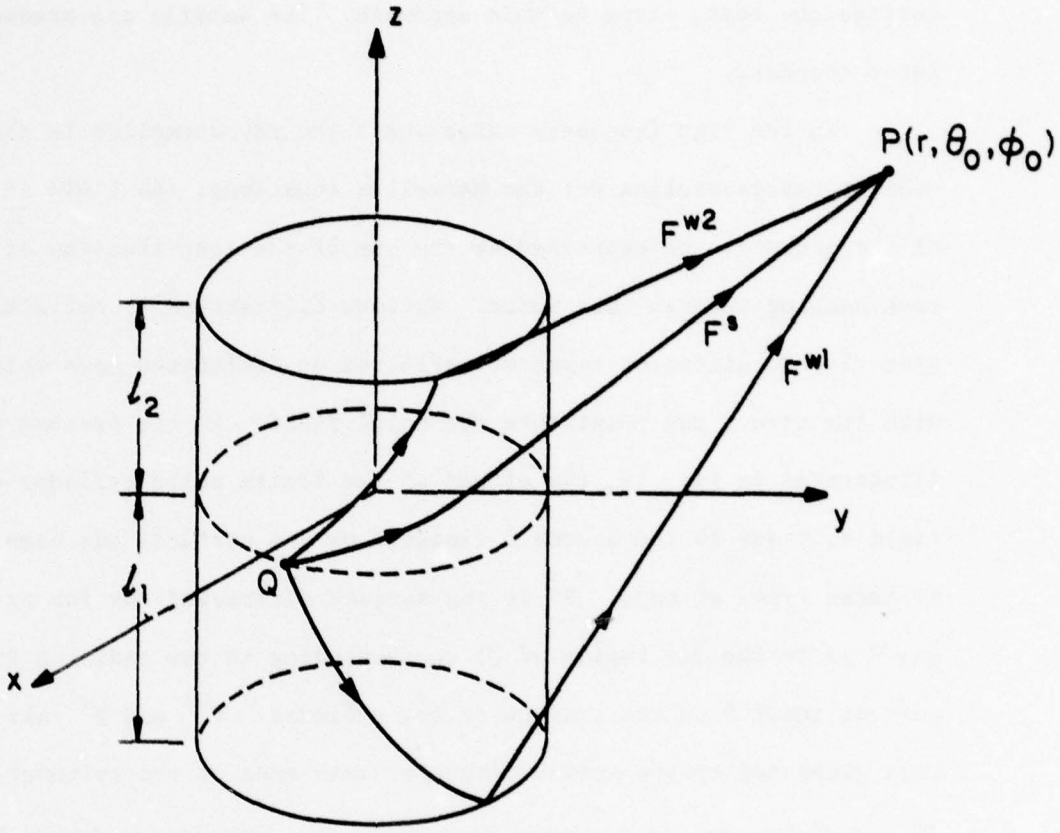

Figure 19. Different rays contributing to the field at the observation point P.

5. SURFACE DIFFRACTED RAYS

Let us consider the case where an infinitesimal magnetic dipole with the moment $\vec{M}$ placed on the surface at a location described by ($\rho = a$, $\phi = 0$, $z = 0$). The orientation of the dipole is tangent to the surface and the direction of observation is given by (θ_0, ϕ_0). If the observation point is not placed in the lit region, no direct ray can reach it. In this case only the surface diffracted rays that travel along the curved surface can pass through the observation point after leaving the surface tangentially. In general, there are an infinite number of rays which contribute to the field at P. In most of the cases, however, only two of these rays traveling in opposite directions around the cylinder are taken into consideration. If the radius of the cylinder is large, the others suffer strong attenuation and thus have negligible effect on the total field at P.

Propagation of the field along these rays is governed by formulas (3.8) and (3.9):

$$E_{n_2} = (\vec{M} \cdot \hat{\beta}_1) \cdot \left(\frac{jke^{-jk\sigma}}{4\pi}\right) \cdot g_0(\xi_{1S}) \cdot \frac{e^{-jkR}}{R} - \frac{(\vec{M} \cdot \hat{\phi}_1)(\hat{\phi}_1 \cdot \hat{\beta}_1)}{4\pi a} \cdot e^{-jk\sigma} \cdot \left(\frac{k\rho_\sigma}{2}\right)^{1/3} \cdot g_1(\xi_{1S}) \frac{e^{-jkR}}{R} \tag{5.1}$$

$$E_{\beta_2} = \frac{(\vec{M} \cdot \hat{\phi}_1)(\hat{\phi}_1 \cdot \hat{\sigma}_1)}{2\pi a} \cdot \left(\frac{k\rho_\sigma}{2}\right)^{2/3} \cdot e^{-jk\sigma} \cdot f_0(\xi_{1S}) \cdot \frac{e^{-jkR}}{R} \tag{5.2}$$

The far-zone fields along rays no. 1 and no. 2 should be calculated separately. The contribution of surface diffracted rays is the sum of these two fields. For circular cylinder geometry, simple relationships exist between (σ, β) and (θ_o, ϕ_o); (Figs. 20 and 21).

Ray no. 1:

$$\beta = \pi/2 - \theta_o \tag{5.3a}$$

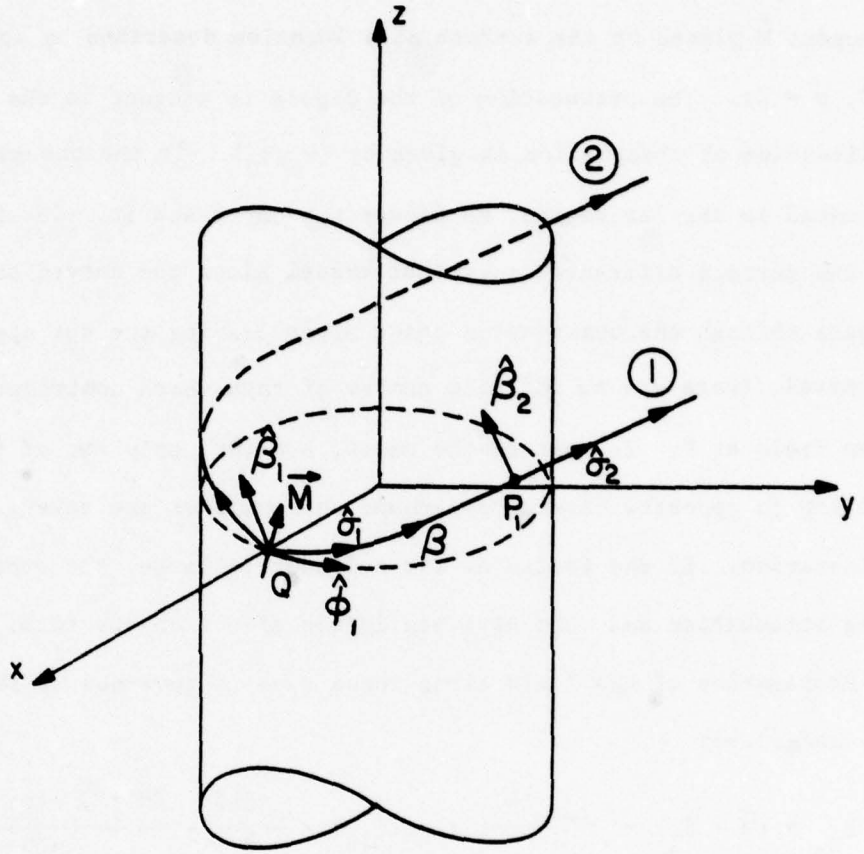

Figure 20. Surface rays launched by source $\vec{M}$ at point Q. These rays travel in opposite directions around the cylinder.

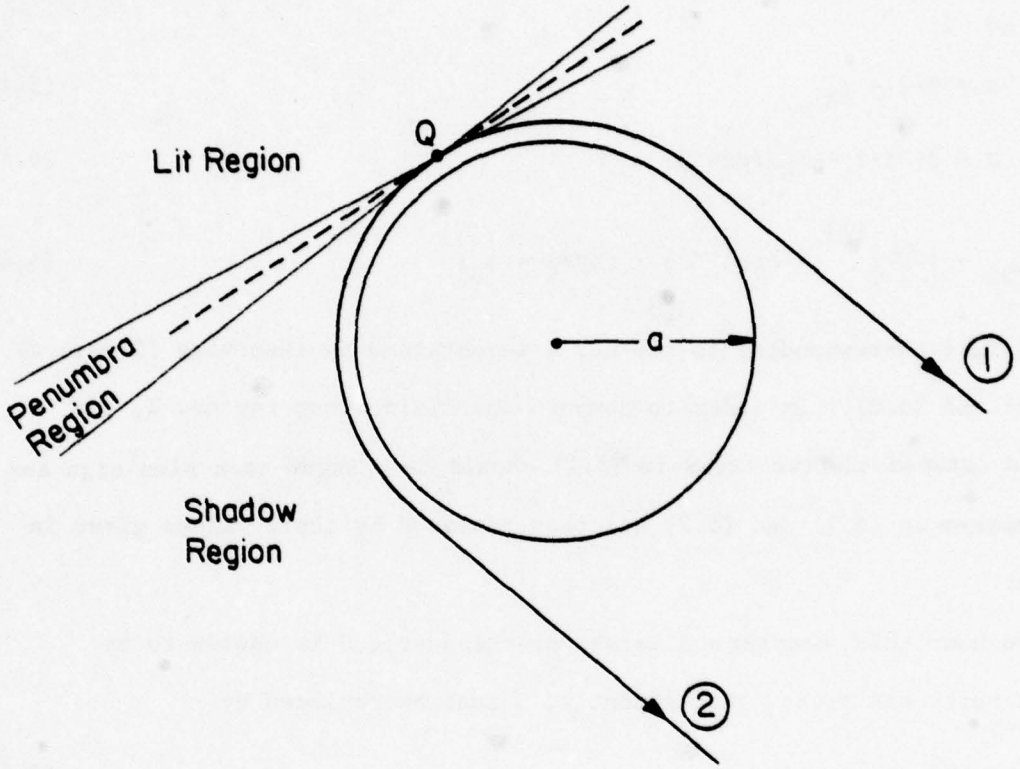

Figure 21. Cross section of the geometry shown in Fig. 20.

$$\sigma = a(\phi_o - \pi/2)/\cos\beta \tag{5.3b}$$

$$\xi_{1S} = \left(\frac{ka}{2}\right)^{1/3} \cdot \cos^{1/3}\beta \cdot (\phi_o - \pi/2) \tag{5.3c}$$

Ray no. 2:

$$\beta = \pi/2 - \theta_o \tag{5.4a}$$

$$\sigma = a(3\pi/2 - \phi_o)/\cos\beta \tag{5.4b}$$

$$\xi_{2S} = \left(\frac{ka}{2}\right)^{1/3} \cdot \cos^{1/3}\beta \cdot (3\pi/2 - \phi_o) \tag{5.4c}$$

The field corresponding to ray no. 1 is obtained by inserting (5.3a,b,c) into (5.1) and (5.2). In order to compute the field along ray no. 2, the minus sign between the two terms in (5.1) should be changed to a plus sign and the parameters in (5.1) and (5.2) are then replaced by their values given in (5.4a,b,c).

Throughout this chapter and later on, the source Q is chosen to be the phase reference point. Consequently, R must be replaced by

$$R = r - \vec{QP}_1 \cdot \hat{r} \tag{5.5}$$

or

$$R = r - (\sigma \cos^2\theta_0 - a \sin\theta_0 \cos\phi_0) \tag{5.6}$$

where r is the distance between the source and the observation point.

The components of the far-zone field along $\hat{\theta}_o$ and $\hat{\phi}_o$ can be found in terms of its components along $\hat{\beta}_2$ and $\hat{n}_2$ very easily:

$$E_{\theta_o} = -E_{\beta_2} \text{ (Ray no. 1 + Ray no. 2)} \tag{5.7}$$

$$E_{\phi_o} = -E_{n_2} \text{ (Ray no. 1 + Ray no. 2)} \tag{5.8}$$

The case in which the point source is a normal electric dipole is treated in a similar manner. In this case, the expressions (3.29a) and (3.29b) of Chapter 3 should be used instead of (3.8) and (3.9). The remaining steps remain exactly the same.

6. SURFACE FIELD DUE TO A POINT SOURCE ON A CIRCULAR CYLINDER

The cylinder problem has an exact modal solution, which is in the form of an infinite series with each term containing an infinite integral [86], [87]. For a large ka, this solution is very slowly convergent and becomes less useful. Among several asymptotic solutions, those given by Hwang, Kouyoumjian, Wang, and Pathak [88], [89], [90] and by Chang, Felsen, Hessel and Shmoys [91], [44] are approximately deduced from the exact modal solution under the condition $ka \to \infty$. In this work we use the asymptotic solution obtained by Lee and Safavi-Naini [21], [22] which gives the surface magnetic field everywhere from the source point to the deep shadow more accurately and is based on a classical work by Fock in 1949 on spheres [65]. A nondeductive part of this solution was later justified theoretically by Boersma and Lee [92].

Let us first consider the case of a tangential magnetic source. The normal electric source is discussed later. At a point Q on the surface of the cylinder (Fig. 22), there is a tangential magnetic dipole source described by a magnetic dipole moment $\vec{M}$. The problem is to determine $\vec{H}$ at another point $P(a,\phi,z)$ on the surface under the assumption that ka is large.

At this point we introduce several paramters. According to GTD [23], [24], [25], the dominant contribution of H at P is the field on the surface ray which is a geodesic on the conducting surface, and in the present case is a helical path (Fig. 22). The arclength of the surface ray is

$$\sigma = \sqrt{(a\phi)^2 + z^2} \tag{6.1}$$

The surface of the cylinder is parameterized by geodetical polar coordinates (σ,β) discussed in the previous chapter. The tangent, normal and binormal

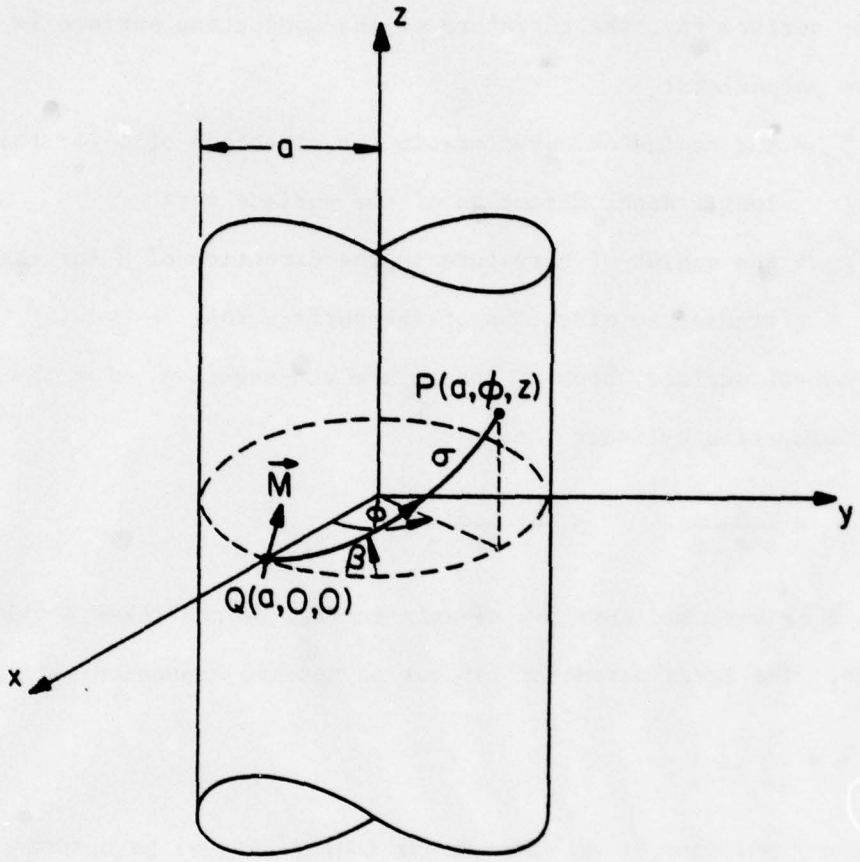

Figure 22. Geodetical polar coordinate system (σ,β) on the surface of a circular cylinder.

of the surface ray are $(\hat{\sigma}_Q, -n_Q, \hat{\beta}_Q)$ at Q and $(\hat{\sigma}_P, -n_P, \hat{\beta}_P)$ at P. At any point on the surface ray, the curvature of the conducting surface is described by two parameters:

ρ_σ = the radius of curvature in the direction of $\hat{\sigma}$ (or that in the longitudinal direction of the surface ray)

ρ_β = the radius of curvature in the direction of $\hat{\beta}$ (or that in the transverse direction of the surface ray)

On a convex surface, both ρ_σ and ρ_β are non-negative. For the present case of a conducting cylinder, one has

$$\rho_\sigma = \frac{a}{\cos^2 \beta} \qquad \rho_\beta = \frac{a}{\sin^2 \beta} \tag{6.2}$$

where β is measured from the $a\phi$-axis in Fig. 22 and takes a value between 0 and 2π. The large parameter for our asymptotic expansion is

$$m = \left(\frac{1}{2} k\rho_\sigma\right)^{1/3} . \tag{6.3}$$

Thus, our solution is an approximate (not rigorous) asymptotic solution valid for $m \to \infty$, up to and including terms of $O(m^{-3})$. Furthermore, let us introduce a distance parameter

$$\xi = \frac{m\sigma}{\rho_\sigma} = \left(\frac{k}{2\rho_\sigma}\right)^{1/3} \sigma = \frac{k\sigma}{2m^2} \tag{6.4}$$

which is the same as that defined in the previous chapter. Note that $\xi = 0$ defines the lit region ($\beta = \pi/2$), $\xi < 1$ defines the penumbra region, and $\xi >> 1$ defines the deep shadow. Our solution is uniformly valid for all $\xi \geq 0$.

Due to the point source M at Q, our final asymptotic solution for the magnetic field on the surface is given by

$$\vec{H}(P) = \vec{M} \cdot (\hat{\beta}_Q \hat{\beta}_P H_\beta + \hat{\sigma}_Q \hat{\sigma}_P H_\sigma) \tag{6.5a}$$

where the transverse component is

$$H_\beta(P) \sim \left[\left(1 - \frac{j}{k\sigma}\right) v(\xi) - \left(\frac{1}{k\sigma}\right)^2 u(\xi) + j(\sqrt{2}\, k\rho_\sigma)^{-2/3} \cdot v'(\xi) + j(\sqrt{2}\, k\rho_\sigma)^{-2/3} \cdot (\rho_\sigma/\rho_\beta) \cdot u'(\xi)\right] G(\sigma), \tag{6.5b}$$

the longitudinal component is

$$H_\sigma(P) \sim \left(\frac{j}{k\sigma}\right)\left[v(\xi) + \left(1 - \frac{2j}{k\sigma}\right)u(\xi) + j(\sqrt{2}\, k\rho_\sigma)^{-2/3} u'(\xi)\right] G(\sigma) \tag{6.5c}$$

and the function $G(\sigma)$ is

$$G(\sigma) = \frac{k^2 Y_o}{2\pi j} \frac{e^{-jk\sigma}}{k\sigma} \tag{6.5d}$$

Here $Y_o = (\varepsilon_o/\mu_o)^{1/2} = (120\pi)^{-1}$, v and u are defined in Appendix A, and v' is the derivative of v. It can be shown that if ka tends to infinity the exact solution for the ground flat plane will be recovered. When $\beta \to \pi/2$ (paraxial region) but the radius of the cylinder remains finite, we have

$$H_\beta(P) \sim [H_\beta(P)]_{\text{planar}} + B \cdot \frac{1}{ka} \cdot \frac{e^{-jk\sigma}}{\sqrt{k\sigma}} \tag{6.6}$$

as $k\sigma$ approaches infinity. Another limiting case of special importance to us is the case where

$$\xi \to \infty \quad , \tag{6.7}$$

which occurs when observation point P is in the deep shadow. Making use of (A-20) through (A-23), we have from (6.5) that

$$H_\beta(P) \sim \frac{k^2 \cos^{2/3}\beta}{1528\,(ka)^{1/3}(k\sigma)^{1/2}} \cdot \exp\left[-0.88\xi - j\left(\frac{5\pi}{12} + 0.51\xi + k\sigma\right)\right] \tag{6.8a}$$

$$H_\sigma(P) \sim \frac{j}{k\sigma} H_\beta(P) \quad . \tag{6.8b}$$

Therefore, in the deep shadow, the field is a slow wave and decays exponentially along the surface ray. In later applications, explicit field expressions are needed for axial and circumferential dipoles. They are listed below.

Axial dipole: $\vec{M} = \hat{z}$

$$H_z(P) = H_\beta(P) \cos^2 \beta + H_\sigma \sin^2 \beta \tag{6.9}$$

Circumferential dipole: $\vec{M} = \hat{\phi}$

$$H_\phi(P) = H_\beta(P) \sin^2 \beta + H_\sigma \cos^2 \beta \quad . \tag{6.10}$$

One can now derive similar expressions for the electromagnetic surface fields of a radial electric current J on a perfectly conducting circular cylinder. Let us define $\vec{J}$ as

$$\vec{J} = \frac{\vec{p}}{a} \delta(\rho - a)\delta(z)\delta(\phi) \quad . \tag{6.11}$$

This derivation has not been given in [21]. Here, the main steps are discussed briefly. It is noted that $\vec{p}$ is the dipole moment which is oriented normal to the surface at (a, 0, 0). The tangential magnetic field $\vec{H}_t^e(P)$ due to $\vec{J}$ can be obtained by applying the reciprocity theorem to the fields of $\vec{M}$ and $\vec{p}$ as follows:

$$\vec{H}_t^{e(Q)} \cdot \vec{M}\Big|_{\text{at } P} = -\vec{E}_\rho^{m(P)} \cdot \vec{p}\Big|_{\text{at } Q} \tag{6.12}$$

where $\vec{E}_\rho^{m(P)}$ is the radial component of the surface electric field at Q due to the tangential magnetic dipole $\vec{M}$ located at P, and $\vec{H}_t^{e(Q)}$ is the surface magnetic field at P due to the radial electric dipole of moment $\vec{p}$ located at Q. Employing Maxwell's equations, $E_\rho^{m(P)}\Big|_Q$ can be related to $\vec{H}_t^{m(P)}\Big|_Q$ by

$$E_\rho^{m(P)}\Big|_Q = \frac{1}{jkY_o}\left[\frac{1}{a}\frac{\partial H_z^{m(P)}}{\partial \phi'}\Big|_Q - \frac{\partial H^{m(P)}}{\partial z'}\Big|_Q\right] \tag{6.13}$$

where $H_z^{m(P)}\Big|_Q$ and $H_\phi^{m(P)}\Big|_Q$ are given by (6.9) and (6.10) when the source is located at P and the field is calculated at Q (Fig. 23). The axial and circumferential components of the surface magnetic field $\vec{H}_z^{e(Q)}$, $\vec{H}_\phi^{e(Q)}$ due to a radial electric point source now can be computed by (6.12) and (6.13) as follows:

Axial component $\vec{H}_z^{e(Q)}$ due to $\vec{p}$ at Q:

$$\vec{H}_z^{e(Q)}\Big|_P = -\vec{p} \cdot \vec{E}_\rho^{m(P)}\Big|_{Q,\vec{M}=\hat{z}} = \frac{(-\vec{p}\cdot\hat{\rho})}{j\omega\varepsilon a} \cdot \frac{\partial H_z^{m(P)}}{\partial \phi'}\Big|_{Q,\vec{M}=\hat{z}} \tag{6.14}$$

Circumferential component $\vec{H}_\phi^{e(Q)}$ due to p at Q:

$$\vec{H}_\phi^{e(Q)}\Big|_P = -\vec{p} \cdot \vec{E}^{m(P)}\Big|_{Q,\vec{M}=\hat{\phi}} = \frac{(\vec{p}\cdot\hat{\rho})}{j\omega\varepsilon} \cdot \frac{\partial H_\phi^{m(P)}}{\partial z'} \cdot \tag{6.15}$$

It is noted that the right-hand sides of the above equations are derivatives of the surface field due to a magnetic dipole $\vec{M}$ located at P, whereas the left-hand sides are the field quantities at P due to the source $\vec{p}$ at Q. Surface derivatives of $\vec{H}_t^{m(P)}$ can be written in terms of the derivatives of tangential and binormal components of $\vec{H}_t^{m(P)}$ with respect to β and σ:

$$\frac{\partial H_z^{m(P)}}{\partial \phi'} = \left(\frac{\partial H_{\beta'}}{\partial \beta'} \cdot \frac{\partial \beta'}{\partial \phi'} + \frac{\partial H_{\beta'}}{\partial \sigma'} \cdot \frac{\partial \sigma'}{\partial \phi'}\right) \cos^2 \beta' + \left(\frac{\partial H_{\sigma'}}{\partial \beta'} \cdot \frac{\partial \beta'}{\partial \phi'} + \frac{\partial H_{\sigma'}}{\partial \sigma'} \cdot \frac{\partial \sigma'}{\partial \phi'}\right) \cdot \sin^2 \beta' + (H_{\sigma'} - H_{\beta'}) \sin 2\beta' \cdot \frac{\partial \beta'}{\partial \phi'} \tag{6.16}$$

$$\frac{\partial H_\phi^{m(P)}}{\partial z'} = \left(\frac{\partial H_{\beta'}}{\partial \beta'} \cdot \frac{\partial \beta'}{\partial z'} + \frac{\partial H_{\beta'}}{\partial \sigma'} \cdot \frac{\partial \sigma'}{\partial z'}\right) \sin^2 \beta' + \left(\frac{\partial H_{\sigma'}}{\partial \beta'} \cdot \frac{\partial \beta'}{\partial z'} + \frac{\partial H_{\sigma'}}{\partial \beta'} \cdot \frac{\partial \sigma'}{\partial z'}\right) \cdot \cos^2 \beta' + (H_{\beta'} - H_{\sigma'}) \sin 2\beta' \cdot \frac{\partial \beta'}{\partial z'} \cdot \tag{6.17}$$

In deriving the relations (6.16) and (6.17), the Jacobian of transformation

between the two coordinate systems (σ',β') and (ϕ',z') is needed. Below, we list its elements:

$$\frac{\partial\sigma'}{\partial\phi'} = a\cos\beta' \quad ; \quad \frac{\partial\sigma'}{\partial z'} = \sin\beta' \quad ; \quad \frac{\partial\beta'}{\partial\phi'} = -\frac{a\sin\beta'}{\sigma'} \quad ; \quad \frac{\partial\beta'}{\partial z'} = \frac{\cos\beta'}{\sigma'} \tag{6.18}$$

The desired components of the surface field excited by a radial electric diple $\vec{p}$ are obtained by substituting (6.16) and (6.17) back into (6.14) and (6.15). The relationship between the (σ',β') coordinate system with the pole at P and the (σ,β) coordinate system with pole Q is illustrated in Fig. 23:

$$\sigma = \sigma' \quad , \quad \beta' = \beta - \pi \quad . \tag{6.19}$$

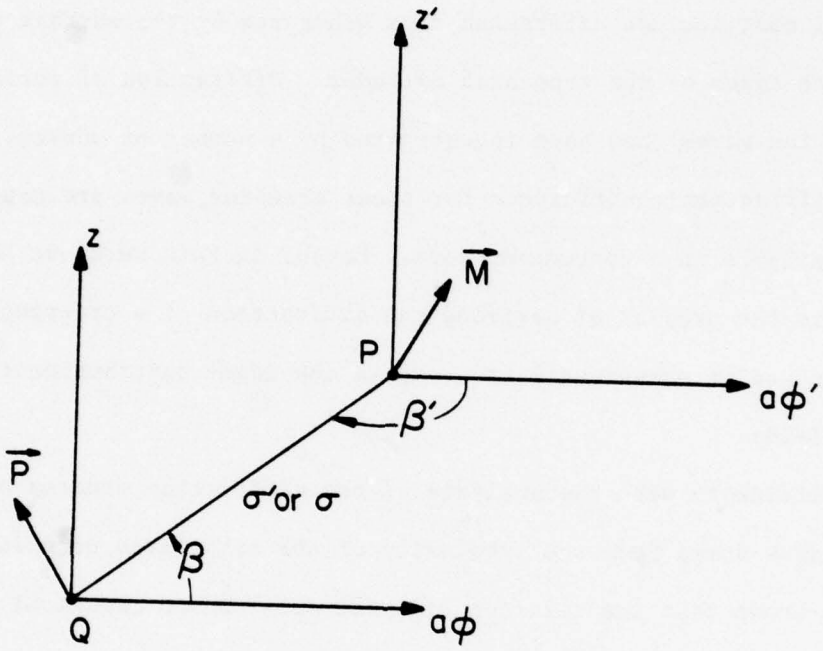

Figure 23. Relative locations of the $(z,a\phi)$ and $(z',a\phi')$ coordinate systems in reciprocity relation 6.12.

7. DIFFRACTION OF SURFACE RAYS BY CURVED WEDGE

As discussed previously, the computation of the radiated field for high-frequency electromagnetic point sources located on a finite solid cylinder it must include diffracted rays generated by the surface rays reaching the edges of the truncated cylinder. Diffraction of surface rays (creeping waves) has been investigated by a number of workers; however, diffraction coefficients for these creeping waves are not readily available in a convenient form. Hence, in this work, we address ourselves to the problem of deriving the diffraction of a creeping wave by a wedge and use it subsequently to compute the edge-contribution to the radiated fields.

The difficulty with the analysis of the diffraction process of surface rays at wedges stems from the complexity of the associated canonical problem. It is well-known that the solution of a suitably chosen canonical problem is a first step toward deriving the diffraction coefficient for a given problem with a complex geometry. The choice of the canonical problem is based on two principal considerations:

1) The geometry of the canonical problem should contain all the important features of the local geometry of the original problem.

2) The solution of the canonical problem must be expressible in a convenient, usable form.

As one example of such a geometry, Kouyoumjian and Burnside [93] considered the case of a cylinder-tipped half-plane. The case of ogive was treated by Peters and Ryan [94] in an empirical manner. Ryan [95] and Knott et al. [96] studied the finite cylinder. They assumed a wedge diffracted ray excited by creeping waves hitting the wedges of the cylinder could be

constructed by using equivalent currents, determined from the surface field of the waves and the wedge diffraction coefficients for a straight wedge. This approach was consistent with the results found by Albertsen and Christiansen [97], [41]. A somewhat similar procedure is applied to find the wedge diffracted fields.

7.1 Diffraction Points

For the case of the finite cylinder studied in this work, the surface rays emanate from the source Q (Fig. 19) and propagate along all directions on the surface of the cylinder along a helical path (geodesics). Surface rays creep over the surface until the curved wedges are reached. One of these rays has been shown in Fig. 24. After diffraction on the upper wedge (wedge no. 2) at diffraction point P_{w2}, a cone of diffracted rays with the axis $\hat{t}$ (unit tangent to the wedge at P_{w2}) and the half-angle β_{w2} is formed. β_{w2} is also the angle between the surface ray and circumferential direction at Q. $\hat{\sigma}^i$ indicates the direction of incidence of the surface ray on the wedge and is tangent to the ray at P_{w2}. The angle ϕ_{w2} counted from the x-axis determines the location of the diffraction point on the wedge. $\hat{n}_{w2}$ is the radial unit vector normal to the wedge lying in the plane of the upper end cap. $\hat{\sigma}^d$ is the unit vector along a diffracted ray. $\hat{\sigma}^i$ and $\hat{\sigma}^d$ both lie on the diffraction cone. β_{w2} and ϕ_{w2} are dependent upon the location of diffraction point P_{w2}. Therefore, each point of the wedge is assigned a cone of diffracted rays with a specified semiangle. The ensemble of directions defined by these cones covers the whole space. Conversely, associated with each direction (observation direction) in the space, there is a finite number of rays originating from specific points on the wedge, which contribute to the far-zone field in that direction. Hence, the first step in computing the contribution of wedge-diffracted rays to the total radiated field in a

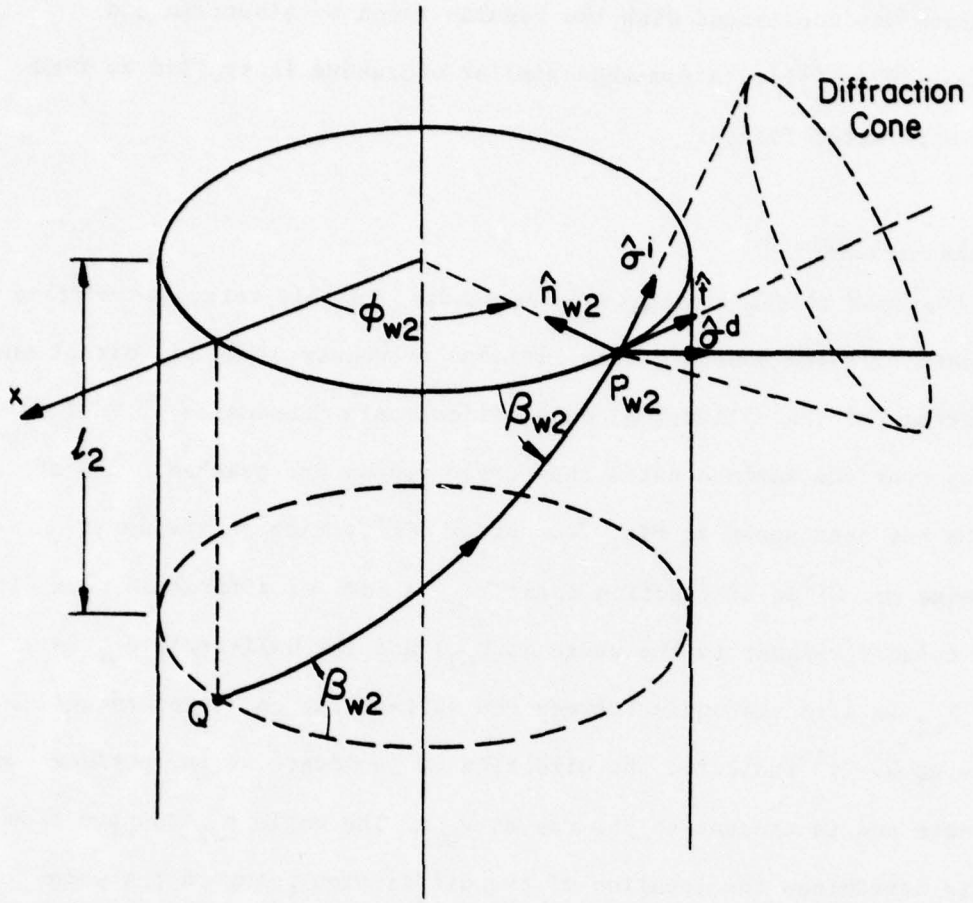

Figure 24. A surface ray reaching the wedge at Point P_{w2}.

given direction is to determine the location of the diffraction points on the wedge corresponding to that special direction. It is obvious that this location is solely determined by the value of ϕ_{w2}. Now let us derive the relationship between ϕ_{w2} and the observation direction defined by the observation angles (θ_o, ϕ_o).

To derive the above-mentioned relationship, it is noted that the direction of incidence $\hat{\sigma}^i$ and the observation direction $\hat{\sigma}^d$ must lie on the same cone. In other words,

$$\hat{\sigma}^i \cdot \hat{t} = \hat{\sigma}^d \cdot \hat{t} \tag{7.1}$$

All the quantities on both sides of (7.1) can be written in terms of ϕ_{w2} and (θ_o, ϕ_o) as follows (Fig. 24):

$$\hat{\sigma}^i = \cos \beta_{w2} \hat{t} + \sin \beta_{w2} \hat{z} \tag{7.2a}$$

$$\hat{\sigma}^d = \sin \theta_o \cos \phi_o \hat{x} + \sin \theta_o \sin \phi_o \hat{y} + \cos \theta_o \hat{z} \tag{7.2b}$$

$$\hat{t} = - \sin \phi_{w2} \hat{x} + \cos \phi_{w2} \cdot \hat{y} \tag{7.2c}$$

$$\cos \beta_{w2} = a\phi_{w2} / [(a\phi_{w2})^2 + \ell_2^2]^{1/2} \quad ; \tag{7.2d}$$

$$- \pi \leq \phi_{w2} \leq \pi$$

Substituting (7.2a,b,c,d) back into (7.1), the following transcendental Equation for ϕ_{w2} is obtained:

$$\frac{\phi_{w2}}{\sqrt{(\ell_2/a)^2 + \phi_{w2}^2}} = \sin \theta_o \cdot \sin (\phi_o - \phi_{w2}) \tag{7.3}$$

Equation (7.3) is solved for ϕ_{w2} when θ_o and ϕ_o (observation angles) are given. For each fixed value of parameters θ_o and ϕ_o, Equation (7.3) has several simple or multiple roots. Now let us study some interesting limiting cases.

When θ_o is equal to 0 or π (axial direction), the right-hand side of (7.3) vanishes. The single root of (7.3) in this case is

$$\phi_{w2} = 0 \tag{7.4}$$

which indicates that only the ray which travels along the generatrix of the cylinder passing through the source point contributes to the field in this direction. In the case where $\theta_o = \pi/2$ and $\phi_o = 0$ (direction normal to the surface of the cylinder at the source point), again we have the single root given in (7.4).

It should be noted that the range of variation of ϕ_{w2} has been chosen to be $[-\pi,\pi]$. This special choice excludes the rays which travel around the cylinder more than π. These rays, as mentioned previously, have negligible contribution.

Equation (7.3) locates the diffraction points on the upper wedge. A similar equation can be written for the diffraction points on the lower wedge (Fig. 25):

$$\frac{\phi_{w1}}{\sqrt{(\ell_1/a)^2 + \phi_{w1}^2}} = \sin\theta_o \sin(\phi_o - \phi_{w1}) \quad . \tag{7.5}$$

Once Equations (7.4) and (7.5) are solved, a set of values for ϕ_{w2} and ϕ_{w1} is obtained, with each of them a specific diffracted ray is associated. Construction of these diffracted rays is the subject matter of the next subsection.

7.2 Diffracted Rays

Surface rays reaching P_{w1} or P_{w2}, are diffracted at these points and generate cones of diffracted rays with their apex placed at these points. To

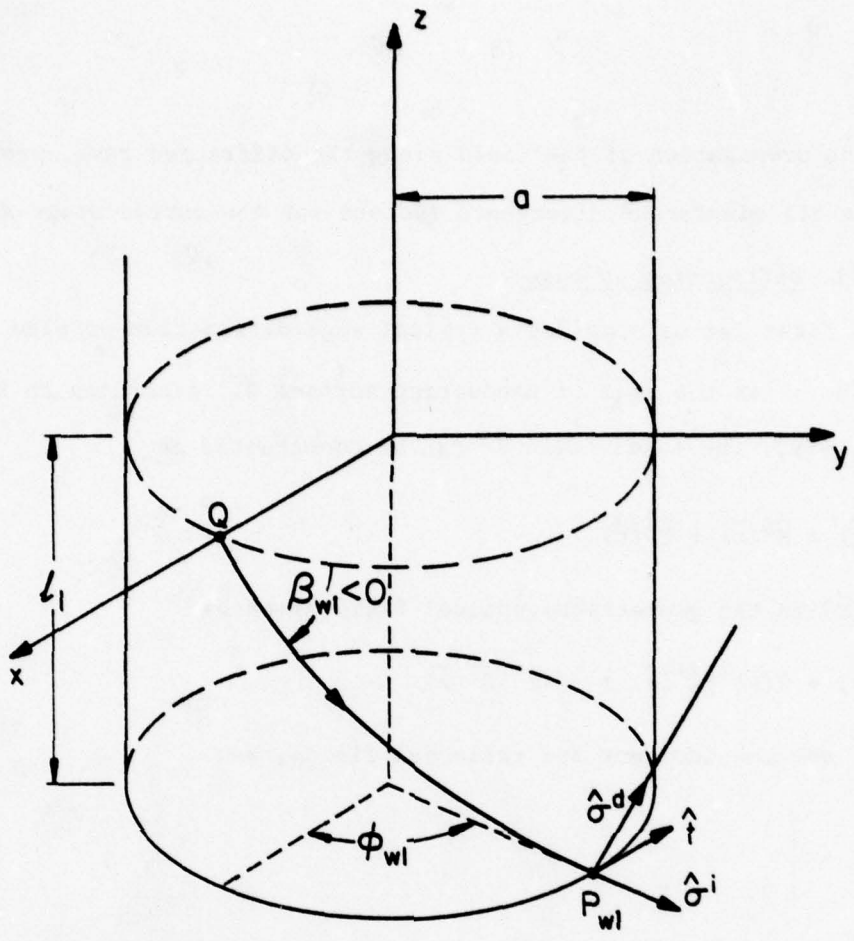

Figure 25. A typical surface ray reaching the lower wedge (wedge #1) at point P_{w1} (Diffraction point).

analyze the propagation of the field along the diffracted rays, proper diffraction coefficients and divergence factors for the curved wedge are needed.

7.2.1 Diffraction by edge

First let us consider a typical edge diffraction problem sketched in Fig. 26. Γ is the edge of conducting surface Σ. According to Keller's GTD [98], [99], the total field $\vec{E}^t$ can be constructed as

$$\vec{E}^t(\vec{r}) = \vec{E}^g(\vec{r}) + \vec{E}^d(\vec{r}) \tag{7.6}$$

where $\vec{E}^g(\vec{r})$ is the geometrical-optical field given by

$$\vec{E}^g(\vec{r}) = \theta(-\varepsilon^i)\vec{E}^i(\vec{r}) + \theta(-\varepsilon^r)\vec{E}^r(\vec{r}) \quad . \tag{7.7a}$$

$\vec{E}^i$ and $\vec{E}^r$ are the incident and reflected fields, and

$$\theta(x) = \begin{cases} 1 & x > 0 \\ 0 & x < 0 \end{cases} \quad . \tag{7.7b}$$

ε^i and ε^r are the shadow indicators for the incident and reflected fields defined as

$$\varepsilon^i(\vec{r}) = \begin{cases} +1 \ , & \vec{r} \text{ is in the shadow region of incident field} \\ -1 \ , & \vec{r} \text{ is in the lit region of incident field} \end{cases} \tag{7.7c}$$

$$\varepsilon^r(\vec{r}) = \begin{cases} +1 \ , & \vec{r} \text{ is in the shadow region of reflected field} \\ -1 \ , & \vec{r} \text{ is in the lit region of reflected field} \end{cases} \tag{7.7d}$$

$\vec{E}^d(\vec{r})$ is the diffracted field which is of order $k^{1/2}$ and is asymptotically smaller than E^g, which is of order k^o. As $\vec{E}^g$, $\vec{E}^d$ consists of two symmetrical parts: E^{di} associated with the incident field and E^{dr} with the reflected field,

$$\vec{E}^d(\vec{r}) = \vec{E}^{di}(\vec{r}) + \vec{E}^{dr}(\vec{r})$$

$$\sim k^{-1/2} e^{-jks^d(\vec{r})} \sum_{m=0}^{\infty} (-jk)^{-m} \left[\vec{e}_m^{di}(\vec{r}) + \vec{e}_m^{dr}(\vec{r}) \right] \tag{7.8}$$

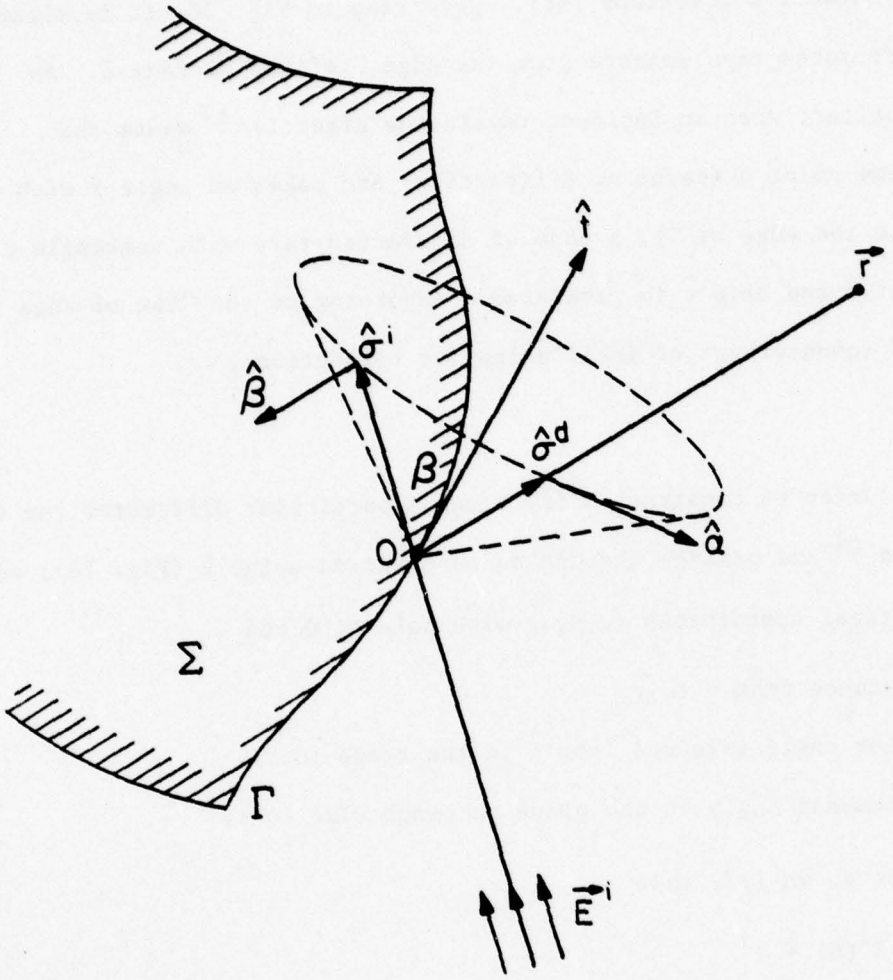

Figure 26. Diffraction of the rays by the edge of a conducting screen.

where $S^d(r)$ (phase function) and $\{e_m^{di}, e_m^{dr}\}$ are obtained by asymptotic solution of Maxwell's equations [98]. Referring to Fig. 26, it is clear that all diffracted rays emanate from the edge Γ of the surface Σ. As discussed earlier, when an incident ray in the direction $\hat{\sigma}^i$ meets the edge Γ at some point 0 (point of diffraction) and makes an angle β with $\hat{t}$ (tangent to the edge at 0), a cone of diffracted rays with semiangle β and vertex at 0 and axis $\hat{t}$ is generated. According to the "law of edge diffraction" (counterpart of Snell's law for reflection),

$$\beta = \beta^i \tag{7.9}$$

Now, in order to construct $S^d(\vec{r})$ along a particular diffracted ray in the direction $\hat{\sigma}^d$ and passing through an observation point $\vec{r}$ (Fig. 26), we use the spherical coordinates (σ,β,α) with pole at 0 and

σ^d = distance from 0 to $\vec{r}$,

β = polar angle measured from $\hat{t}$ in the range $(0,\pi)$,

α = azimuthal angle in the plane perpendicular to $\hat{t}$.

Then it can be shown [98] that

$$S^d(\vec{r}) = S^i(0) + \sigma^d \tag{7.10}$$

where $S^i(0)$ is the value of $S^i(\vec{r})$ at 0.

The variation of amplitude functions $\vec{e}_m^d(\vec{r})$ along a given ray, in general, depends upon the principal radii of curvature R_1 and R_2. But in this case, because of the fact that the edge Γ itself is a caustic line of the diffracted field, one of the principal radii of curvature is zero,

$$R_2 = 0 \tag{7.11}$$

and the final solution for $\vec{e}_m^d(\vec{r})$ can be written as

$$\vec{e}_m^{d}(\vec{r}) = \vec{e}_m^{di}(\vec{r}) + \vec{e}_m^{dr}(\vec{r})$$

$$= \left[(\sigma^d)^{1/2}\left(1 + \frac{\sigma^d}{R_1}\right)^{1/2}\right]^{-1} \vec{\delta}_m^{i} - \frac{1}{2}\int_0^{\sigma} \frac{\sigma'^{1/2}(\sigma' + R_1)^{1/2}}{(\sigma^d)^{1/2}(\sigma^d + R_1)^{1/2}}$$

$$\cdot \nabla^2 \vec{e}_{m-1}^{di}(\vec{r}') \cdot d\sigma' + \{i \to r\} \tag{7.12}$$

where $\vec{r}$ and $\vec{r}'$ have coordinates (σ,β,α) and (σ',β,α), respectively, and $\{i \to r\}$ means that the whole expression in the right-hand side of the equation is repeated for the reflected field. The determination of the initial values $\vec{\delta}_m^{i,r}$, in general, is very involved. In GTD only $\vec{\delta}_o^{i,r}$ are determined by comparison of (7.12) with the asymptotic expansion of the known solution to the Sommerfeld's half-plane problem. The zero-th order term (dominant term) in the asymptotic expansion of diffracted field $\vec{E}^d$ can be written as

$$\vec{E}^d(\vec{r}) = g(k\sigma^d) \frac{1}{\sqrt{1 + \sigma^d/R_1}} \cdot \frac{\chi^i}{\sin\beta}\left[e^{-jks^i(0)}\, \text{rot}\, \vec{e}_o^{i}(0)\right]$$

$$+ \{i \to r\} + O(k^{-3/2}) \tag{7.13}$$

where $g(k\sigma^d)$ is the cylindrical wave factor,

$$g(k\sigma^d) = \frac{1}{2\sqrt{2\pi k\sigma^d}} \cdot \exp[-j(k\sigma^d + \pi/4)] \tag{7.14}$$

$$\frac{1}{\sqrt{1 + \sigma^d/R_1}} = \text{divergence factor} = \text{DF} \tag{7.15}$$

$$\chi^i = \text{diffraction coefficient} \tag{7.16}$$

$$\text{rot} = \text{rotation operator} \tag{7.17}$$

DF (Divergence Factor) indicates the spreading of the tube of rays emanating from O as it travels into space. In general, the divergence factor DF depends upon the principal radii of curvature of the wavefront R_1 and R_2, but in our case, as discussed earlier, one of these radii is zero. The other radii of curvature R_1 can be computed in several ways [24], [100], [101] and [102]. R_1 is the radius of curvature of the diffracted wavefront in the direction $\hat{\sigma}_1$ defined by

$$\hat{\sigma}_1 = \hat{\sigma}_2 \times \hat{\sigma}^d \tag{7.18a}$$

$$\hat{\sigma}_2 = \frac{1}{\sin \beta} \hat{\sigma}^d \times \hat{t} \quad . \tag{7.18b}$$

In other words, R_1 is the radius of curvature of a curve formed by the diffracted wavefront intersected by a plane defined by $\hat{t}$ and $\hat{\sigma}^d$ at the point O. The method described by Lewis and Boersma [100] to calculate R_1 involves the computation of the Jacobian of the transformation from (η,α,σ), where η is the arclength along the edge measured positively in the direction $\hat{t}$ (Fig. 26) to the rectangular coordinate system. The resulting expression for R_1 is

$$R_1 = - \frac{\sin^2 \beta}{\kappa_\Gamma \hat{\sigma}^d \cdot \hat{n}_\Gamma + (d\beta/d\eta) \sin \beta} \tag{7.19}$$

where κ_Γ and $\hat{n}_\Gamma$ are the curvature and the unit normal of Γ at O ($\kappa_\Gamma \geq 0$ and $\hat{n}_\Gamma$ points toward the center of curvature).

Another procedure to determine R_1 has been given by Deschamps [102]. This procedure is based upon matching the phase of the incident and the diffracted rays on Γ. The resulting formula for R_1 is

$$R_1 = \left[\frac{1}{R_o^i} + \frac{\kappa_\Gamma}{\sin^2 \beta} (\hat{\sigma}^{i*} - \hat{\sigma}^d) \cdot \hat{n}_\Gamma \right]^{-1} \tag{7.20}$$

---

* Wave number k^i of the incident surface ray has been assumed to be the same as that of a plane wave in free space.

where R_o^i is the radius of curvature of the incident wavefront at O in the plane through $\hat{t}$ and $\hat{\sigma}^i$; in terms of the principal radii of curvature of the incident wavefronts (R_1^i, R_2^i) and their corresponding principal directions $(\hat{x}_1^i, \hat{x}_2^i)$ at O, R_o^i is given by

$$\frac{1}{R_o^i} = \frac{\cos^2 \Omega^i}{R_1^i} + \frac{\sin^2 \Omega^i}{R_2^i} \tag{7.21}$$

where Ω^i is the angle between $\hat{x}_1^i$ and the projection of $\hat{t}$ on the plane through $\hat{x}_1^i$ and $\hat{x}_2^i$. It can be shown that (7.19) and (7.20) are equivalent.

χ^i (Diffraction Coefficient): For a conducting surface, the diffraction coefficients $\chi^{i,r}$ are given by

$$\chi^{i,r} = \operatorname{cosec} \frac{\psi^{i,r}}{2} \tag{7.22}$$

To define $\psi^{i,r}$ we refer to Fig. 27, which is actually the projection of Fig. 26 on the plane through O perpendicular to $\hat{t}$. T is the tangent plane to Σ at O. As illustrated in Fig. 27, the magnitude of $\psi^{i,r}$, namely, $|\psi^{i,r}|$, is defined as the angle of rotation around t which brings $\hat{\sigma}^{i,r}$ to $\hat{\sigma}^d$ without crossing Σ, and the sign of $\psi^{i,r}$ is

$$\operatorname{sgn} \psi^{i,r} = \varepsilon^{i,r}(\vec{r}) \tag{7.23}$$

where $\varepsilon^{i,r}$ (shadow indicators) are defined (7.7).

Rotation Operator (rot): The operator rot in (7.13) denotes the rotation about $\hat{t}$ that brings $\hat{\sigma}^i$ onto $\hat{\sigma}^d$,

$$\text{rot } \hat{\sigma}^i = \hat{\sigma}^d \tag{7.24}$$

If we decompose the amplitude $\vec{e}_o^{\,i}$ into two transverse components:

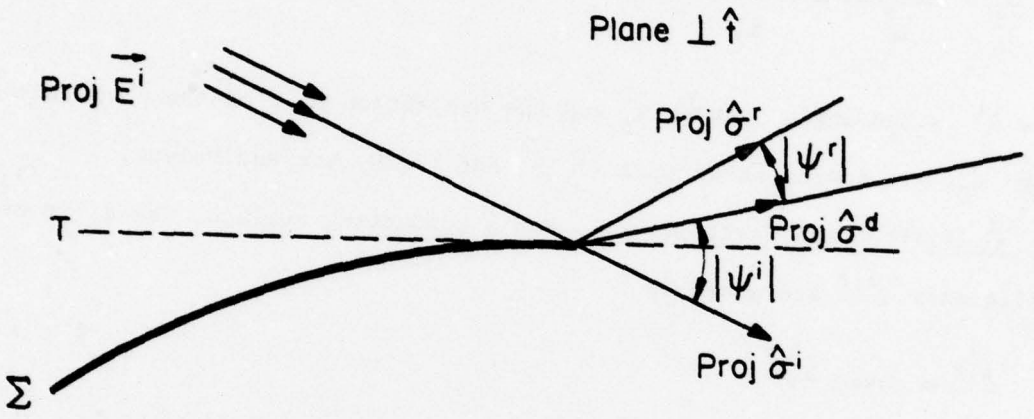

Figure 27. Projection of the geometry shown in Fig. 26 on a plane perpendicular to $\hat{t}$.

$$\vec{e}_o^{\,i}(\vec{r}) = \hat{\beta}^i e_{o\beta}^i(\vec{r}) + \hat{\alpha}^i e_{o\alpha}^i(\vec{r}) \tag{7.25}$$

then one would have

$$\text{rot } \vec{e}_o^{\,i}(\vec{r}) = \hat{\beta}^d e_{o\beta}^i(\vec{r}) + \hat{\alpha}^d e_{o\alpha}^i(\vec{r}) \tag{7.26}$$

where $(\hat{\beta}^i,\hat{\alpha}^i)$ and $(\hat{\beta}^d,\hat{\alpha}^d)$ are $(\hat{\beta},\hat{\alpha})$ unit vectors corresponding to incident and diffracted directions, respectively (Fig. 26).

7.2.2 Diffraction by wedge

The previous results for the edge diffraction problem can be applied to the analysis of diffraction by the wedge after a simple modification of diffraction coefficient $\chi^{i,r}$. Before explaining this modification, let us examine the geometry of the problem shown in Fig. 28. The wedge is composed of two conducting surfaces, Σ_1 and Σ_2, intersecting along the curved edge Γ. The half-planes T_1 and T_2, tangent at 0 to Σ_1 and Σ_2, respectively, form a planar wedge which approximates the curved wedge in the vicinity of 0 and has an exterior angle $m\pi$ with $1 < m < 2$. When the wedge is illuminated by the incident field $\vec{E}^i$ (Fig. 26), the total field solution is again composed of the geometrical-optical field $\vec{E}^g$ and diffracted field $\vec{E}^d$. For the case of a wedge, in general, we have two reflected fields: $\vec{E}_1^r$ from Σ_1 and $\vec{E}_2^r$ from Σ_2 (Fig. 29). Associated with each of these reflected fields exists a proper shadow indicator (ε_1^r and ε_2^r), illustrated in Fig. 29. Therefore, in the case of a wedge, the geometrical-optical field is given by

$$\vec{E}^g(\vec{r}) = \theta(-\varepsilon^i)\vec{E}^i(\vec{r}) + \theta(-\varepsilon_1^r)\vec{E}_1^r(\vec{r}) + \theta(-\varepsilon_2^r)\vec{E}_2^r(\vec{r}) \quad . \tag{7.27}$$

The diffracted field in this case is calculated as before, and the only modification necessary is the replacement of $\chi^{i,r}$ defined in (7.22) by the

AD-A070 827 ILLINOIS UNIV AT URBANA-CHAMPAIGN ELECTROMAGNETICS LAB F/G 20/3
SOURCE RADIATION IN THE PRESENCE OF CONVEX BODIES.(U)
JUN 79 S SAFAVI-NAINI, R MITTRA N00014-75-C-0293
UNCLASSIFIED UIEM-79-9 NL

2 OF 3
AD A070827

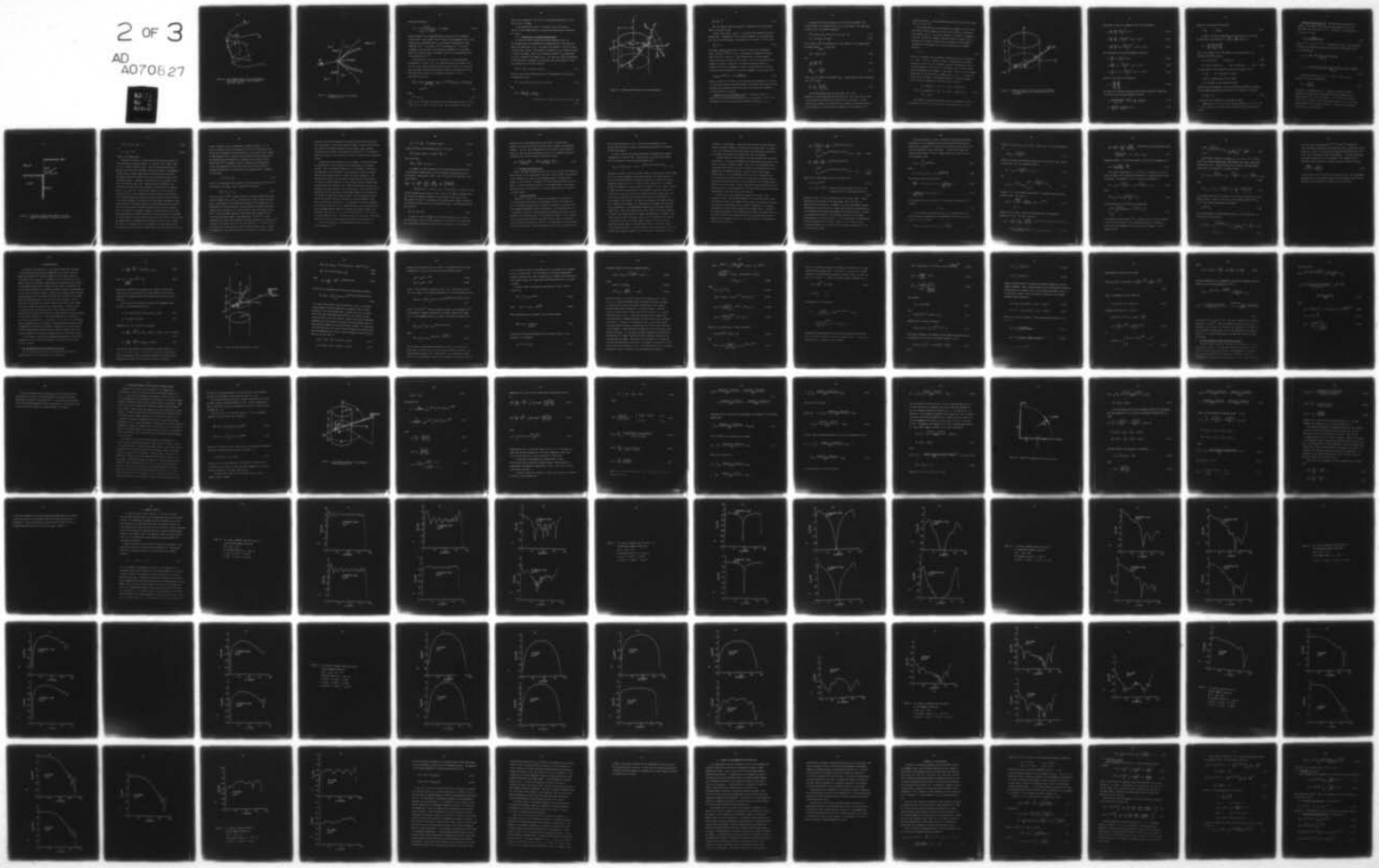

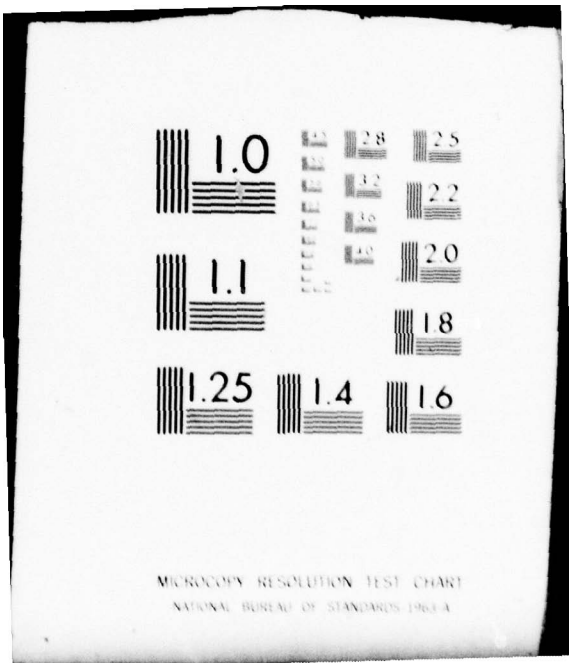
1.0
1.1
1.25
1.4
1.6
2.8
3.2
3.6
4.0
2.5
2.2
2.0
1.8
MICROCOPY RESOLUTION TEST CHART
NATIONAL BUREAU OF STANDARDS 1963-A

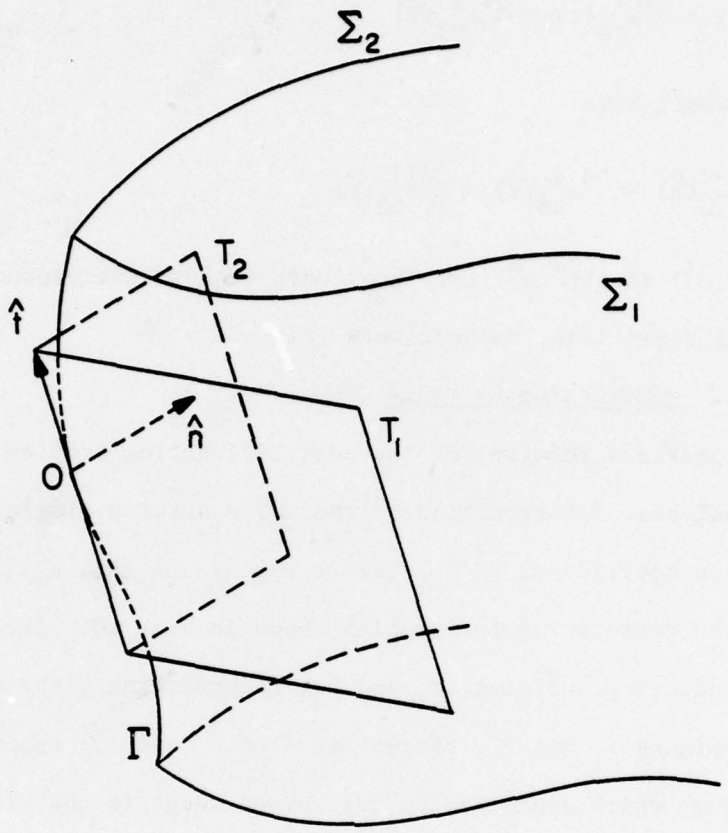

Figure 28. Curved wedge formed by the curved surfaces Σ_1 and Σ_2 and the planes T_1 and T_2 tangent to the faces Σ_1 and Σ_2.

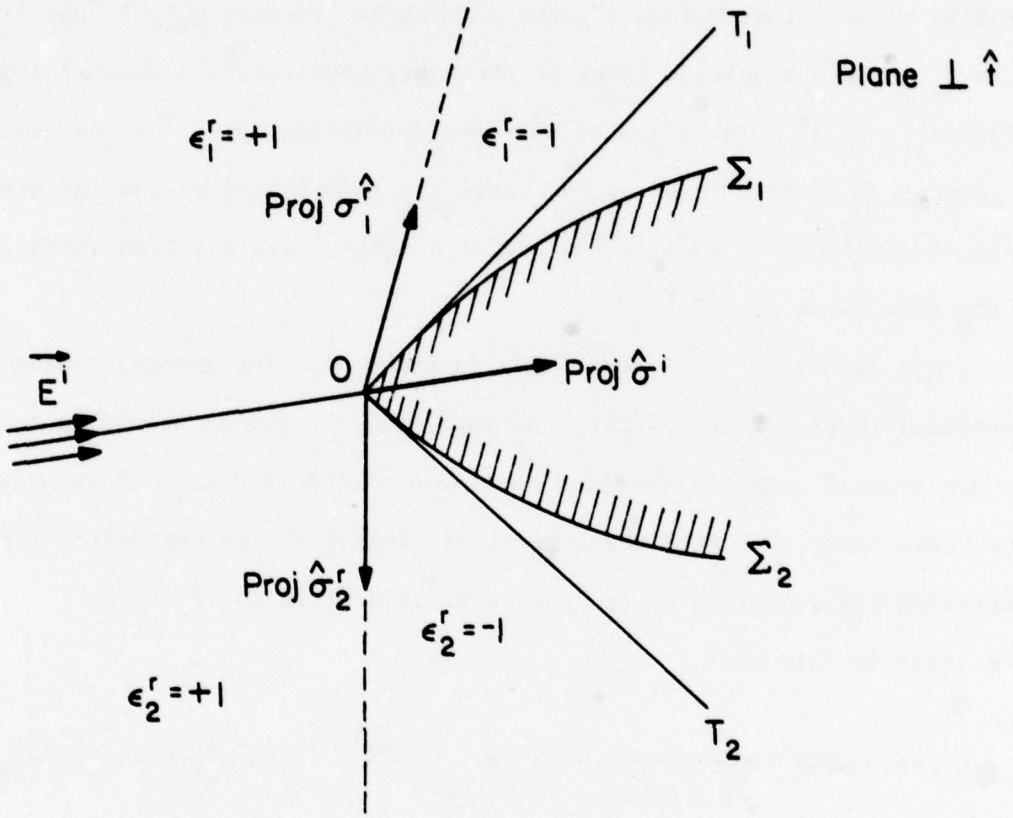

Figure 29. Projection of Fig. 28 on the plane perpendicular to t.

generalized definition

$$\chi^{i,r} = \frac{\frac{2}{m}\sin\frac{\pi}{m}}{\cos\frac{\pi}{m} - \cos\frac{\pi + \psi^{i,r}}{m}} \quad \text{(for wedge)} \tag{7.28}$$

where the angle ψ^i has a magnitude equal to the angle of the continuous rotation about $\hat{t}$ that brings $\hat{\sigma}^d$ onto $\hat{\sigma}^i$ without crossing <u>both</u> T_1 and T_2. The angle $\psi^r_{1,2}$ has a magnitude equal to the continuous rotation about $\hat{t}$ that brings $\hat{\sigma}^r_{1,2}$ on $\hat{\sigma}^d$. The signs of $\psi^{i,r}$ are determined by $\varepsilon^{i,r}$ as before. In general, when both faces of the wedge are illuminated by the incident field, two values for each of the angles ψ^i and ψ^r are obtained which lead to the same value for $\chi^{i,r}$.

Using Equations (7.6) and (7.13) together with the generalization introduced in (7.27) and (7.28), the total field solution according to GTD for the typical wedge diffraction problem sketched in Figure 28 is obtained. Here, once again, we write down the final version of the expression for the diffracted field excited by the incident field given in (7.25) as used later in this work,

$$\vec{E}^d(\vec{r}) = g(k\sigma^d)\frac{1}{\sqrt{1 + \sigma^d/R_1}} \cdot \frac{1}{\sin\beta} \cdot e^{-jks^i(0)}\left[\hat{\beta}^d D^s e^i_{o\beta}(0) + \hat{\alpha}^d D^h e^i_{o\beta}(0)\right]$$

$$+ O(k^{-3/2}) \tag{7.29}$$

where

$$D^{s,h} = \chi^i \mp \chi^r \tag{7.30}$$

$g(k\sigma^d)$, R_1, $\hat{\beta}^d$, $\hat{\alpha}^d$, $e^i_{o\beta}(0)$, and $e^i_{o\alpha}(0)$ have the same definition as in (7.14), (7.15), (7.19), (7.20), (7.25) and (7.26). The coefficients χ^i and χ^r are

given by the expression (7.28), which is the generalized version of (7.22) for the case of a wedge.

In the present work, we apply the formula (7.29) to the special case of a curved wedge formed by a circular cylindrical surface intersected by a plane.

7.2.3 Diffraction by a cylindrical-planar wedge

The structure under consideration has been sketched in Fig. 30. The incident field is the creeping wave originating from Q, which meets the wedge at an angle equal to β_{w2}. The curve of the wedge is a circle of radius a lying in the xy plane. The direction of incidence at P_{w2} (diffraction point) $\hat{\sigma}^i$ lies in the tangent plane to the cylindrical surface at P_{w2} making angle β_{w2} with $\hat{t}$ (tangent to the wedge at P_{w2}). The polar unit vector corresponding to the direction of incidence, $\hat{\beta}_p^i$, also lies in the plane formed by $\hat{\sigma}^i$ and $\hat{t}$. The azimuthal unit vector $\hat{\alpha}_p^i$ is given by

$$\hat{\alpha}_p^i = \hat{\sigma}^i \times \hat{\beta}_p^i = \cos \phi_{w2}\hat{x} + \sin \phi_{w2}\hat{y} \quad . \tag{7.31}$$

The unit vector along the diffracted ray $\hat{\sigma}^d$ is determined by the direction of observation (θ_o, ϕ_o)

$$\hat{\sigma}^d = (\sin \theta_o \cos \phi_o, \sin \theta_o \sin \phi_o, \cos \theta_o) \tag{7.32}$$

and

$$\hat{\alpha}_p^d = - \frac{\hat{\sigma}^d \times \hat{t}}{|\sin \beta_{w2}|} = \frac{1}{|\sin \beta_{w2}|} \cdot (\cos \phi_{w2} \cos \theta_o, \sin \phi_{w2} \cos \theta_o, -\sin \theta_o \cos (\phi_o - \phi_{w2})) \tag{7.33}$$

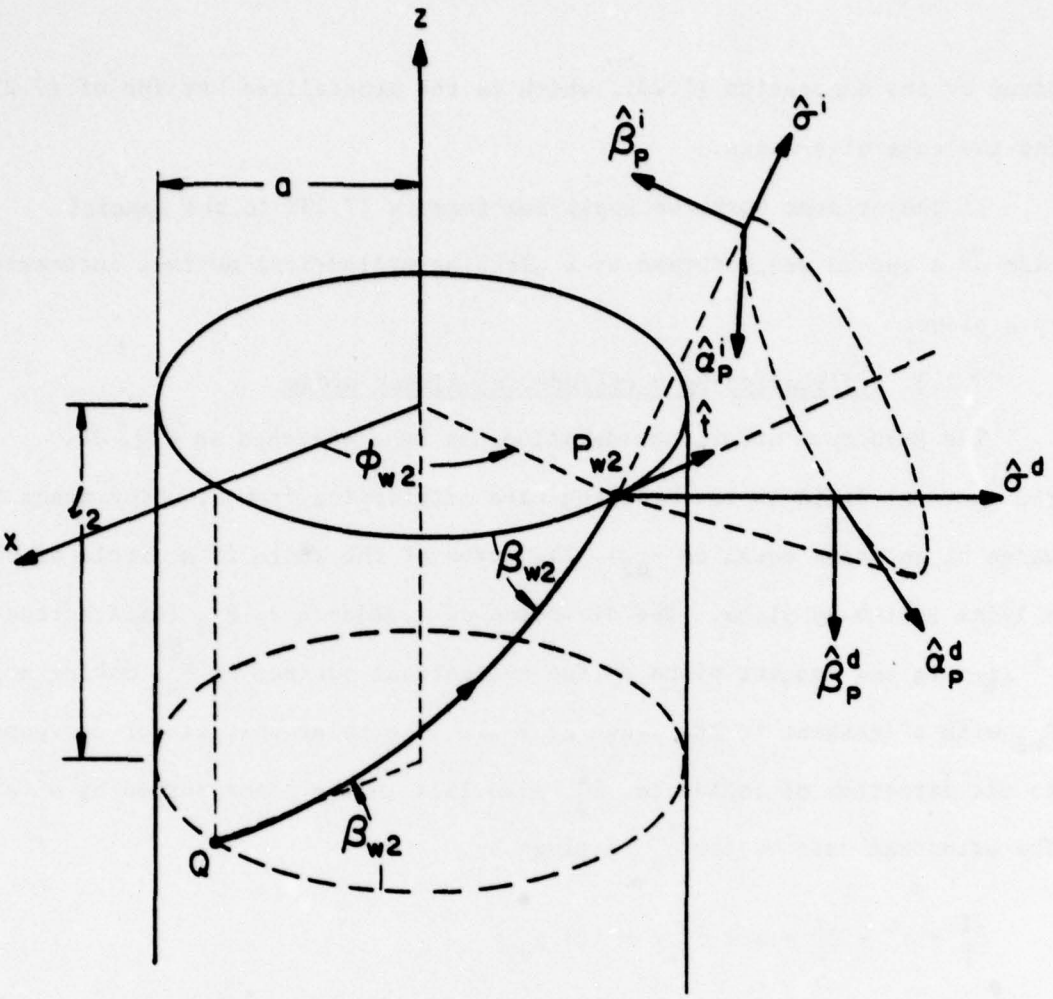

Figure 30. Incident and diffracted "ray fixed coordinates".

$$\hat{\beta}_p^d = \hat{\alpha}_p^d \times \hat{\sigma}^d \tag{7.34}$$

Now, we consider different quantities in expression (7.29) and evaluate them for this special case.

Incident field ($e^i_{o\beta}(0)$, $e^i_{o\alpha}(0)$): The incident field reaches the wedge at grazing angle. Consequently, the only nonzero component of the incident electric field is oriented normal to the surface of the cylinder. In other words,

$$\hat{e}^i_{P\beta}(P) = 0 \tag{7.35}$$

The normal component of the electric field (the phase factor eliminated), namely, $\hat{e}^i_{P\alpha}(P_{w2})e^{-jks^i(P_{w2})}$ at P_{w2}, is determined by evaluating the expressions (6.5a,b,c) at point P_{w2}. These formulas give the surface magnetic field at any point on the body of the cylinder. Now, if the surface field is assumed to be locally a plane wave, the simple relationship between the components of electric and magnetic vectors of a plane wave can be utilized to find the desired expression for the normal component of the electric field

$$\hat{e}^i_{P\alpha}(P_{w2})e^{-jks^i(P_{w2})} = -\frac{Z_o \quad H_\beta(P_{w2})}{2}\,\hat{\alpha}^i_P \tag{7.36}$$

where H_β is given by (6.5) and Z_o is the characteristic impedance of free space. It is noted that because of grazing incidence, the incident and reflected fields coincide so that one half of the total surface field should be considered as the incident field at the wedge.

Computation of R_1 and Divergence Factor: The principal radius of curvature R_1 of the diffracted wavefront at P_{w2} in the plane ($\hat{\sigma}^i$ and $\hat{t}$) can be determined by either of the procedures explained in subsection (7.1.1).

According to the first procedure, R_1 can be found by formula (7.19). In this formula, β is replaced by β_{w2}, κ_Γ is the curvature of the wedge which is equal to $\frac{1}{a}$ in the present problem and

$$\hat{\sigma}^d = (\sin\theta_o \cos\phi_o, \sin\theta_o \sin\phi_o, \cos\theta_o) = \hat{k}_o \tag{7.37}$$

$$\hat{n}_\Gamma = -\cos\phi_{w2}\hat{x} - \sin\phi_{w2}\hat{y} \quad . \tag{7.38}$$

Now in order to find the derivative of β with respect to the arclength along the wedge, $d\beta/d\eta\Big|_{\beta=\beta_{w2}}$, we note that

$$\tan\beta = \ell_2/a\phi = \ell_2/\eta \tag{7.39}$$

and

$$\frac{1}{\cos^2\beta}\frac{d\beta}{d\eta} = \frac{-\ell_2}{\eta^2} \tag{7.40}$$

$$\left.\frac{d\beta}{d\eta}\right|_{\beta_{w2}} = -\frac{\sin\beta_{w2}}{\sigma_{w2}} \tag{7.41}$$

where σ_{w2} is the length of the geodesic QP_{w2}. Substituting the above expressions into (7.19) leads to

$$\frac{1}{R_1} = \frac{1}{\sigma_{w2}} - \frac{\hat{k}_o \cdot \hat{n}_\Gamma}{a\sin^2\beta_{w2}} \quad . \tag{7.42}$$

The second procedure gives the same result as in (7.42); however, it is more complicated than the first one. Here, only the main steps of this method are explained and the details are not discussed. In order to apply this procedure, the first step is to construct the incident wavefront and to determine its local geometrical properties in the proximity of the

diffraction point P_{w2}. Having determined R_1^i and R_2^i, R_o^i and R_1 can be found from (7.21) and (7.20).

The incident wavefront can be defined as the geometrical locus of the end points of the rays emanating from the source located at Q and having equal lengths, say, S_o. The ray with length S_o, in general, is composed of two parts. One part is a geodesic along the surface of length σ and the other part is a straight line which can be considered as the tangential continuation of the geodesic part in the free space with the length d. Therefore,

$$\sigma + d = S_o \quad . \tag{7.43}$$

When S_o is a constant, each ray defines a specific point S on the wavefront S_o = const. (Fig. 31). Therefore, one way to parameterize the incident wavefront is to use the (σ,β) coordinate system of the cylindrical surface in the following way: Each value of (σ,β) defines a point on the cylinder and also determines a ray joining Q to this point. This ray can be continued tangentially in the free space at a length equal to $d = S_o - \sigma$ to reach the point S which is, indeed, on the desired wavefront. With this parameterization system, the equation of the surface can be written as

$$\vec{X}(\sigma,\beta) = \begin{Bmatrix} a\cos(\frac{\sigma}{a}\cos\beta) - (S_o - \sigma)\cdot\cos\beta\cdot\sin(\frac{\sigma}{a}\cos\beta) \\ a\sin(\frac{\sigma}{a}\cos\beta) + (S_o - \sigma)\cdot\cos\beta\cdot\cos(\frac{\sigma}{a}\cos\beta) \\ S_o\cdot\sin\beta \end{Bmatrix} \quad . \tag{7.44}$$

The principal curvatures and directions are now determined by means of expressions (9.6) and (9.7) in [43] or the formulas given in [44]. The

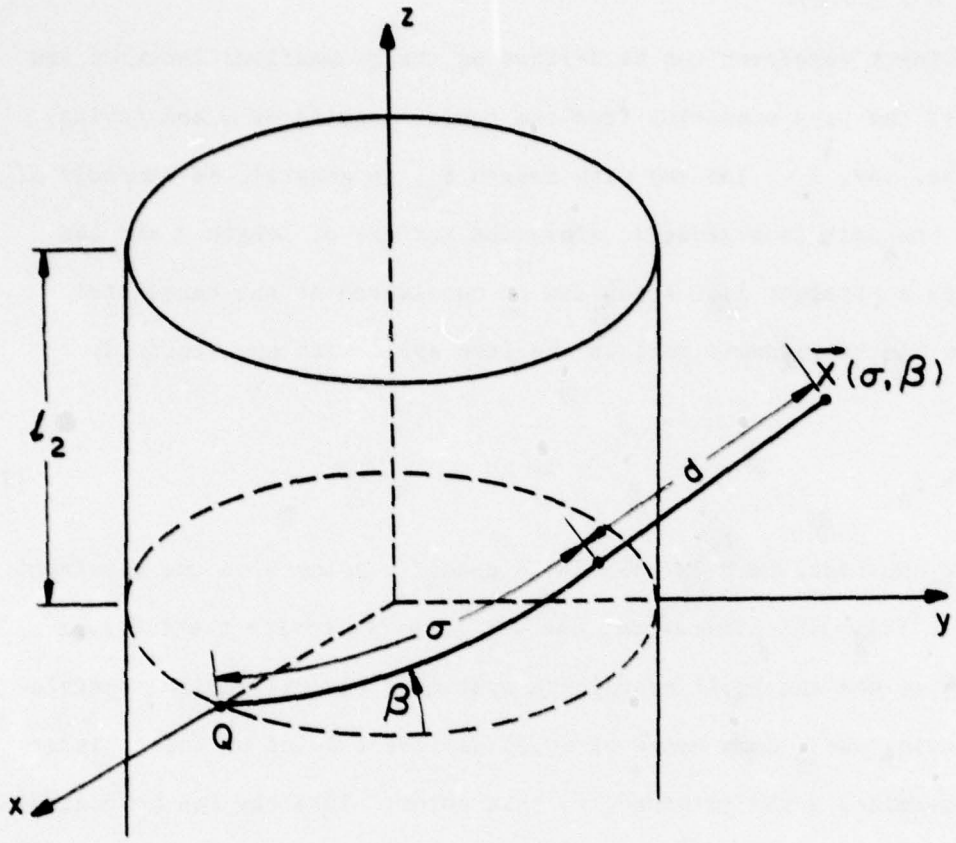

Figure 31. Defining a typical point $\vec{x}$ (σ,β) on the wavefront of the field along a ray originating from the point Q at angle β.

coefficients of the first fundamental form I are listed below:

$$E = \frac{\partial \vec{X}}{\partial \sigma} \cdot \frac{\partial \vec{X}}{\partial \sigma} = \frac{(S_o - \sigma)^2}{a^2} \cos^4 \beta \tag{7.45a}$$

$$F = \frac{\partial \vec{X}}{\partial \sigma} \cdot \frac{\partial \vec{X}}{\partial \beta} = - \frac{\sigma(S_o - \sigma)^2}{a^2} \cdot \sin \beta \cdot \cos^3 \beta \tag{7.45b}$$

$$G = \frac{\partial \vec{X}}{\partial \beta} \cdot \frac{\partial \vec{X}}{\partial \beta} = S_o^2 + \frac{\sigma^2 (S_o - \sigma)^2}{a^2} \cdot \sin^2 \beta \cdot \cos^2 \beta \quad . \tag{7.45c}$$

The coefficients of the second fundamental form II are

$$e = \frac{\partial^2 \vec{X}}{\partial \sigma^2} \cdot \hat{N} = \frac{S_o - \sigma}{a^2} \cos^4 \beta \tag{7.46a}$$

$$f = \frac{\partial^2 \vec{X}}{\partial \sigma \partial \beta} \cdot \hat{N} = - \frac{\sigma(S_o - \sigma)}{a^2} \cdot \sin \beta \cdot \cos^3 \beta \tag{7.46b}$$

$$g = \frac{\partial \vec{X}}{\partial \beta^2} \cdot \hat{N} = S_o + \frac{\sigma^2 (S_o - \sigma)}{a^2} \cdot \sin^2 \beta \cdot \cos^2 \beta \tag{7.46c}$$

where N is the normal to the wavefront,

$$\hat{N} = - \frac{\frac{\partial \vec{X}}{\partial \sigma} \times \frac{\partial \vec{X}}{\partial \beta}}{\left| \frac{\partial \vec{X}}{\partial \sigma} \times \frac{\partial \vec{X}}{\partial \beta} \right|} \quad . \tag{7.46d}$$

The "mean" and "Gaussian" curvatures can be derived through the coefficients of the first and the second fundamental forms via

$$\kappa_M = \frac{Eg - 2fF + eG}{2(EG - F^2)} = \frac{\kappa_1 + \kappa_2}{2} = \frac{1}{2S_o} + \frac{1}{2(S_o - \sigma)} \tag{7.47a}$$

$$\kappa_G = \frac{eg - f^2}{EG - F^2} = \frac{1}{S_o(S_o - \sigma)} = \kappa_1 \kappa_2 \quad . \tag{7.47b}$$

Therefore, the principal curvatures are

$$\kappa_1 = \frac{1}{S_o} \quad , \quad \kappa_2 = \frac{1}{S_o - \sigma} \quad . \tag{7.48}$$

In order to find the corresponding principal direction, we note that the curvature in the direction $\hat{u} = u_1 \frac{\partial \vec{X}}{\partial \sigma} + u_2 \frac{\partial \vec{X}}{\partial \beta}$ is given by

$$\kappa(\hat{t}) = \frac{eu_1^2 + 2fu_1u_2 + gu_2^2}{Eu_1^2 + 2Fu_1u_2 + Gu_2^2} \quad . \tag{7.49}$$

Using (7.49) together with (7.48) leads to the following results for principal directions $\hat{u}_1$ and $\hat{u}_2$:

$$\hat{u}_1 = (\cos(\tfrac{\sigma}{a}\cos\beta) \quad , \quad \sin(\tfrac{\sigma}{a}\cos\beta) \quad , \quad 0) \tag{7.50a}$$

$$\hat{u}_2 = (\sin\beta \sin(\tfrac{\sigma}{a}\cos\beta) \quad , \quad -\sin\beta\cos(\tfrac{\sigma}{a}\cos\beta) \quad , \quad \cos\beta) \tag{7.50b}$$

For those points of the wavefront that are on the surface, we have

$\kappa_1 = \frac{1}{S_o}$, $\kappa_2 = \infty$ (surface is a caustic)

$(\hat{u}_1, \hat{N})$ is a tangent plane to the cylinder

$\hat{u}_2$ is orthogonal to the cylindrical surface.

Based on these relationships, one can conclude that the radius of curvature of the incident wavefront in the direction of the tangent to the edge is

$$R_o^i = \frac{1}{\kappa_1} = S_o = \sigma \quad . \tag{7.51}$$

In deriving (7.51), Equation (7.21) has been utilized.

Substitution of (7.51) into (7.20) and the exploitation of the fact that $\hat{\sigma}^i \cdot \hat{n}_\Gamma = 0$ lead us to a result exactly the same as what has been given in (7.42).

Diffraction Coefficients $\chi^{i,r}$: The planar wedge whose faces are tangent to the original curved wedge and approximates it locally is a right angel wedge, sketched in Fig. 32. Referring to (7.28) and Fig. 32, m is equal to 3/2 and

$$\chi = \frac{-2\sqrt{3}\ /3}{1/2 + \cos\ (2\pi/3 + 2\psi/3)} \tag{7.52}$$

where $\chi = \chi^i = \chi^r$ and $\psi = \psi^i = \psi^r$. The magnitude of angle ψ can be expressed in terms of the observation angles and the location of diffraction points in the following way:

$$\cos\ |\psi| = \frac{[\hat{\sigma}^d - (\hat{\sigma}^d \cdot \hat{t})\hat{t}] \cdot [\hat{\sigma}^i - (\hat{\sigma}^i \cdot \hat{t})\hat{t}]}{\sin^2 \beta_{w2}} \tag{7.53}$$

or

$$\cos\ |\psi| = \frac{\sin \theta_o \cos \beta_{w2} \sin (\phi_o - \phi_{w2}) + \sin \beta_{w2} \cdot \cos \theta_o - \cos^2 \beta_{w2}}{\sin^2 \beta_{w2}} \ . \tag{7.54}$$

Using the relation $\cos \beta_{w2} = \hat{\sigma}^d \cdot \hat{t} = \sin \theta_o \cdot \sin (\phi_o - \phi_{w2})$, Equation (7.54) may be simplified as

$$\cos |\psi| = \frac{\cos \theta_o}{\sin \beta_{w2}} \ . \tag{7.55}$$

The sign of ψ is determined by $\varepsilon^{i,r}$. Therefore, in order to define ψ completely, the position of the observation point with respect to the shadow boundary (S.B.) should be examined. Fig. 30 shows that the plane $(\hat{t},\hat{\sigma}^i)$, which is tangent to the surface of the cylinder at P_{w2}, is the local shadow boundary for the incident surface ray. Therefore, the observation directions (θ_o,ϕ_o) which satisfy

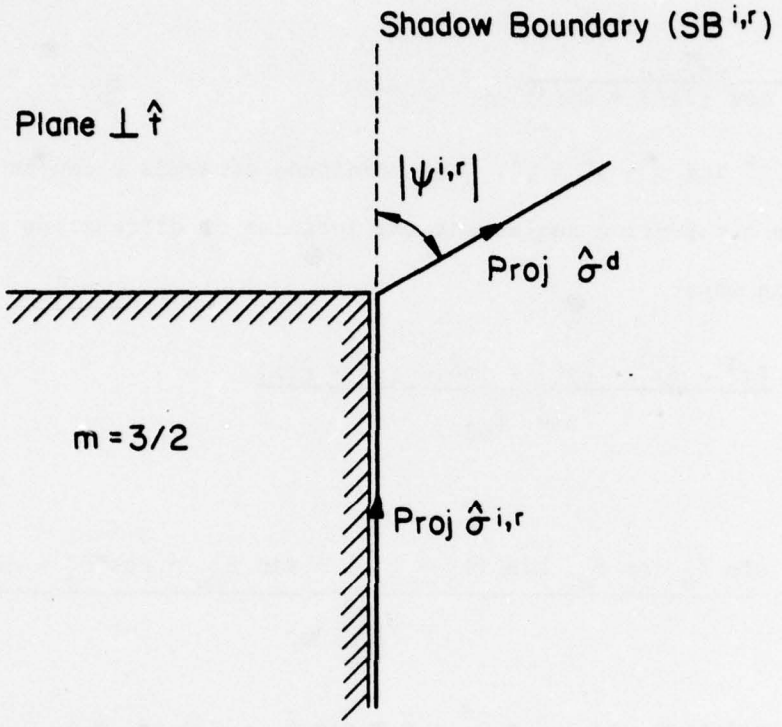

Figure 32. Right-angle straight wedge tangent to the upper wedge of the cylinder, projected on the plane ⊥ t.

$$\sin \theta_o \cos (\phi_o - \phi_{w2}) < 0 \tag{7.56a}$$

or

$$|\phi_o - \phi_{w2}| > \pi/2 \tag{7.56b}$$

belong to the shadow region.

The singular nature of χ causes some difficulty when the observation point approaches the shadow boundary. As a matter of fact, when ψ tends to zero, χ becomes infinitely large. This very well-known deficiency of Keller's GTD diffraction coefficient has been the subject of investigation by many authors. Several generalizations and modifications have been introduced to make GTD uniformly valid over the transition region (around the shadow boundary). Among the "Uniform" theories, we can refer to UTD [101], [25] and UAT [100], [98]. Another approach to circumvent this difficulty is to employ STD (Spectral Theory of Diffraction), developed by Mittra et al. [82], [83]. This approach attempts to correct the root of this difficulty by closely examining the earlier stages of the derivation of GTD formulas rather than attempting to modify the final results post-fact. In the familiar example of diffraction by the half-plane considered by them, it was shown that the singular nature of the diffracted field comes from the fact that the spectrum of the induced current on the half-plane contains a pole in the direction of incidence. When the observation point is far from the shadow boundary, the simple saddle-point technique applied to the integral of the spectrum of the induced current leads one to Keller's GTD. However, when the shadow boundary is approached in the observation space, the pole becomes very close to the saddle point of the integrand, the simple method used in the previous case fails, and more refined methods are required to carry out the

current integration (e.g., introduction of Fresnel integrals, ...). It was also pointed out that the existence of the pole in the spectrum of the current can be considered as the contribution of the physical optics currents of semi-infinite extent. Therefore, the scattered field was interpreted as the superposition of the spectrum of a physical optics current J^0 and a higher-order ($k^{-1/2}$) component, called J^1, without the pole singularity. In the later application of STD to the strip, the diffracted field was considered proportional to the spectrum of the induced current J, composed of three terms,

$$J = J^b + J_1^{tr} + J_2^{tr} \tag{7.57}$$

where J^b is the physical optics current on the strip and $J_{1,2}^{tr}$ are the $O(k^{-1/2})$ contribution of the edges 1 and 2 truncated over the strip,

$$J_{1,2}^{tr} = J_{1,2}^{l} - J_{1,2} \tag{7.58}$$

where $J_{1,2}^{l}$ are the $O(k^{-1/2})$ currents induced on the semi-infinite half-planes erected at edges 1 and 2, and $J_{1,2}$ are portions of these currents outside the strip. Final results for the field were the same as those predicted by UAT. Generalization of this procedure to the curved surfaces required some special remarks on the definition of J^b. When the case of the curved wedge is dealt with, J^b cannot be simply replaced by the physical optics current on the fictitious half-planes tangent to the wedge faces. The $O(k^{-1/2})$ current components $J_{1,2}^{tr}$, more or less represent localized distribution of current in the proximity of the wedge, therefore, the local properties of the surface should be sufficient to provide us with a fairly accurate estimate of that. Whereas J^b corresponds to the global distribution of the induced current on the whole

body which can deviate substantially from what one would obtain based upon the local geometry of the surface around the wedge. Initial results indicate that using the approximate expression for the surface current (instead of physical optics current on the tangent half-plane) for J^b will hopefully improve the accuracy of the existing solution for a curved-surface diffraction problem.

In applying the above principles to our problem, J^b has been obtained by truncating the current distribution that would exist on an infinite cylinder. Thus, the radiated field due to J^b is derivable by subtracting the contribution of the currents of the extension of the finite cylinder from the field radiated when the cylinder is infinite (Chapter 8). The contributions of $J^{tr}_{1,2}$ to the far zone scattered field are proportional to the spectrum (Fourier Transform) of these currents which are computed under the same assumptions employed in GTD. These contributions do not have any singularity and behave smoothly over the whole space. The fields F^{w1} and F^{w2} (diffracted from the lower and the upper wedge, Figure 19) are generated by J^{tr}_1 and J^{tr}_2 and, based upon these principles, can be approximately deduced from the GTD solution upon the subtraction of the pole singularity from Keller's diffraction coefficients χ. In conclusion, the point is emphasized once more that using GTD's χ as it stands provides us with a scattered field due to the <u>total</u> induced current on an infinite half-plane, whereas in our formulation (see Fig. 19), F^w is just the localized effect of the wedges on the total diffracted field. As a matter of fact, the field due to the current induced on the body has been calculated separately and represented by F^s.

In view of the above, the following definition has been used for χ for the computation of F^w

$$\chi_F^{i,r} = \chi^{i,r}(\text{GTD}) - \chi^{PO} \text{ (physical optics)} \tag{7.59}$$

where $\chi^{i,r}(\text{GTD})$ has the expression given in (7.52) and

$$\chi^{PO} \text{ (physical optics)} = \text{cotan } \frac{\psi}{2} = \frac{A_{-1}}{\psi} + \cdots \tag{7.60}$$

and we also have

$$\chi(\text{GTD}) = \frac{A_{-1}}{\psi} + A_o + A_1\psi + \cdots . \tag{7.61}$$

In summary, the final expression for the far-zone diffracted field due to diffraction at wedge point P_{w2} in the observation direction (θ_o,ϕ_o) can be obtained by substituting (7.59), (7.42), (7.36) and (7.35) back into (7.19) which leads to

$$\vec{E}^d_{w2}(\vec{r}) \sim \hat{\alpha}^d_P \cdot \frac{e^{-jkr}}{kr} \cdot \frac{e^{-j\pi/4}}{2\sqrt{2\pi}} \cdot \frac{\sqrt{kR_1}}{\sin \beta_{w2}} \cdot D^h_F \cdot \left[\frac{-Z_o H_\beta(P_{w2})}{2}\right]$$

$$\cdot \exp\{jk[a \sin\theta_o \cdot \cos(\phi_o - \phi_{w2}) - a \sin\theta_o \cos\phi_o + \ell_2 \cos\theta_o]\} \tag{7.62}$$

Several remarks should be made on (7.62). First of all, $\vec{E}^d_{w2}$ is polarized along $\hat{\alpha}^d_P$, because the tangential component of the incident field at P_{w2} is zero. The observation vector $\vec{r}$ is connecting Q (the source point), which is chosen to be the phase reference center, to the observation point. The diffraction factor D^h_F is given by

$$D^h_F = \chi^i_F + \chi^r_F = 2\chi^i_F \quad . \tag{7.63}$$

It should be noted that $\vec{E}^d_{w2}(\vec{r})$ is the diffracted field due to a point on the upper wedge. Diffracted fields generated by the points on the lower wedge are constructed in the same way only when ℓ_2 is replaced by $-\ell_1$ and geometric

quantities of the lower wedge points replace those of the upper ones. Formula (7.62) gives the far-zone scattered field in terms of its single $\hat{\alpha}_p^d$ component. The unit vector $\hat{\alpha}_p^d$ depends upon the location of the diffraction point P_{w2}, which can also be expressed in terms of its components along the transversal unit vectors along the observation direction;

$$\hat{\alpha}_p^d = \frac{\cos(\phi_o - \phi_{w2})}{\sin|\beta_{w2}|}\hat{\theta}_o - \frac{\cos\theta_o \sin(\phi_o - \phi_{w2})}{\sin|\beta_{w2}|}\hat{\phi}_o \quad . \tag{7.64}$$

7.2.4 Blockage of diffracted rays

Some of the wedge diffracted rays may not be able to reach the observation point because of their interception by the body of the cylinder. The condition of the blockage by the object can be determined easily by looking at the geometry of the structure. Blockage of the upper wedge diffracted rays occurs when $\theta_o > \frac{\pi}{2}$ and the observation point is in the shadow region. Lower wedge diffracted rays are blocked when $\theta_o < \frac{\pi}{2}$ and the observation point is again in the shadow region.

7.2.5 Caustic directions

Equations (7.19) and (7.62) express the dependence of the amplitude of the diffracted field upon R_1 as it propagates along the diffracted ray. R_1 is the distance between one of the caustic lines and the diffraction point. This parameter determines the rate of divergence of the diffracted rays. As it increases, the pencil of the diffracted rays diverges more slowly, and consequently, the diffracted field in that direction increases. In the limiting case, in those directions where R_1 becomes infinitely large, the diffracted field according to GTD blows up. However, it is known that real fields remain finite in these regions. These directions are called "caustic directions" and

are determined by Equation (7.42). From the above explanation, it is obvious that GTD cannot be applied in these directions unless it is modified in some proper manner.

In order to derive the desired modification, we reexamine the integral representation of the far field. The expression for the far-zone radiated field can be shown to have the following general form

$$F(\theta_o,\phi_o) = \int\int_S \psi(\theta_o,\phi_o) \cdot f(\phi,z) \cdot e^{jk[a\sin\theta_o\cos(\phi-\phi_o)+z\cos\theta_o]} ds \quad (7.65)$$

(derivation is given in the next section), where S is the surface of the cylinder and f is a typical component of the surface current. For large values of k, the stationary phase method for multiple integrals can be applied to derive an asymptotic expansion for (7.65). Because of the finiteness of S, in general, we have two classes of critical points for the phase of (7.65). Class 1 consists of those stationary points which are in the interior region of S, and their contribution to the total field can be identified with the surface rays. The other class contains the critical points which locate on the boundary of S or the wedge of the cylinder. The latter class generates the wedge diffracted rays. Based on this argument, it is expected that the wedge diffracted field can be represented by a one-dimensional integral around the wedge stationary phase points. Some of the authors ([95], [105], [106], [107]) have attempted to identify this integral with the integral representation of a fringe current flowing along the rim of the wedge. Ryan et al. [105] applied this technique to evaluate the field at the axial caustic formed by an axially incident plane wave upon the edge of planar apertures, disks, or the wedge formed by a ring slope discontinuity. In this procedure, the GTD diffraction coefficients for the planar wedges and edges are used to determine an equivalent current at

the edge of a discontinuity. These equivalent currents are then integrated using the radiation integral to determine the scattered field. As a matter of fact, the diffraction coefficients specify the diffraction at each point on the wedge and the radiation integral sums these contributions.

The major drawback of this method is the way one defines the "equivalent edge current". The function determined by the diffraction coefficients is not really a current in a physical sense. First of all, the expression used as "equivalent edge current" is not only a function of the wedge point but also depends upon the observation angles. Second, at points on the wedge, removed from $\phi_w = 0$, the diffracted rays lie on a cone and therefore do not contribute to the radiated field in all directions in the entire space. Consequently, we should not expect accurate results by this technique in the regions far from the caustic, and the "equivalent current" representation may be valid only in a close neighborhood of the stationary point which contributes significantly to the field in the caustic region.

In this report we have applied a procedure very similar to that discussed in [105]. The type and expression of the equivalent edge current, which should be placed on the wedge of the cylinder, are determined by comparison between the GTD formulas and the asymptotic expansion of the integral representation of the far field radiated by the fringe current. Because of the normal polarization of the incident electric field at the wedge (Fig. 30) and $\hat{\imath}^d$-polarization of the diffracted field, the equivalent edge current is assumed to be of magnetic type $K(\phi)$. The radiated field can be expressed in terms of this function as

$$E_{\phi}^{w2} = \frac{jk^2 a \cos\theta_o}{4\pi} \cdot \frac{e^{-jkr}}{kr} \cdot e^{-jk(a\sin\theta_o\cos\phi_o - \ell_2\cos\theta_o)}$$

$$\cdot \int_{\phi_{w2}-\Delta\phi}^{\phi_{w2}+\Delta\phi} K_o(\phi) e^{-jk\sigma(\phi)+jka\sin\theta_o\cos(\phi-\phi_o)} \sin(\phi_o - \phi)d\phi \qquad (7.66a)$$

$$E_{\theta}^{w2} = \frac{-jk^2 a}{4\pi} \cdot \frac{e^{-jkr}}{kr} \cdot e^{-jk(a\sin\theta_o\cos\phi_o - \ell_2\cos\theta_o)}$$

$$\cdot \int_{\phi_{w2}-\Delta\phi}^{\phi_{w2}+\Delta\phi} K_o(\phi) e^{-jk\sigma(\phi)+jka\sin\theta_o\cos(\phi-\phi_o)} \cos(\phi_o - \phi)d\phi \qquad (7.66b)$$

(7.66b)

where $K(\phi)$ has been assumed to have the following form:

$$K(\phi) = K_o(\phi)e^{-jk\sigma(\phi)} \qquad (7.66c)$$

$\sigma(\phi) = [(a\phi)^2 + \ell_2^2]^{1/2}$ = geodetical distance between the source Q and an arbitrary point on the wedge defined by ϕ.

(7.66d)

Equations (7.66a) - (7.66d) have been written for the upper wedge. Similar expressions can be derived for the lower wedge. Here, once more, we emphasize that we would prefer to consider (7.66) as an approximate integral representation of the field in the caustic region rather than interpreting $K(\phi)$ as an equivalent edge current which generates the diffracted field. The angle ϕ_{w2} determines the location of the stationary phase point on the wedge corresponding to the caustic direction. It is believed that a one-dimensional integral representation for the field similar to (7.66) can be derived by treating asymptotically the exact surface integral representation of the far field near the wedge.

As discussed earlier, our basic criterion for determining the unknown function $K_o(\phi)$ is the assumption that one must recover the GTD results by asymptotically expanding (7.66) around the stationary phase points far from those corresponding to caustic directions. To this end, we apply the stationary phase method to (7.66). Integrals given in (7.66) are of the following general form:

$$I(\phi_o,\theta_o) = \int_{\phi_1}^{\phi_2} h(\phi)e^{jk\Omega(\phi)}d\phi \tag{7.67}$$

where

$$\Omega(\phi) = a \sin\theta_o \cos(\phi - \phi_o) - \sqrt{(a\phi)^2 + \ell_2^2} \quad . \tag{7.68}$$

The stationary phase point is given by

$$\frac{d\Omega(\phi)}{d\phi} = - a \sin\theta_o \sin(\phi - \phi_o) - \frac{a^2\phi}{\sqrt{\ell_2^2 + (a\phi)^2}} = 0 \tag{7.69}$$

$$\text{or} \quad \frac{a\phi}{\sqrt{\ell_2^2 + (a\phi)^2}} = \sin\theta_o \sin(\phi_o - \phi) \quad . \tag{7.70}$$

The stationary point ϕ_s is the root of (7.70), which is the same as (7.3). Therefore,

$$\phi_s = \phi_{w2} \tag{7.71}$$

In other words, the stationary point ϕ_s of $\Omega(\phi)$ coincides with the diffraction point corresponding to the observation direction (θ_o,ϕ_o) given by ϕ_{w2}. At $\phi = \phi_s$, we have

$$\Omega^{(2)}(\phi_s) = -a \sin\theta_o \cos(\phi_s - \phi_o) - \frac{a^2 \sin^2\beta_s}{\sigma_s} \tag{7.72}$$

where $\sigma_s = \sigma(\phi_s)$ and $\beta_s = \sin^{-1}(\ell/\sigma_s)$. Using (7.42), (7.72) can be rewritten as

$$\Omega^{(2)}(\phi_s) = \frac{-a^2 \sin^2 \beta_s}{R_1} \tag{7.73}$$

when R_1 is finite or the observation point does not lie in the caustic region. In this case, $\Omega(\phi)$ can be expanded around ϕ_s:

$$\Omega(\phi) \approx \Omega(\phi_s) - \frac{a^2 \sin^2 \beta_s}{R_1} (\phi - \phi_s)^2 + \cdots \tag{7.74}$$

and

$$I(\phi_o,\theta_o) \approx e^{jk\Omega(\phi_s)} h(\phi_s) \int_{\phi_s-\Delta\phi}^{\phi_s+\Delta\phi} e^{-\frac{jka^2\sin^2\beta_s}{2R_1}(\phi-\phi_s)^2} d\phi \tag{7.75}$$

Integral (7.75) can be computed approximately by changing variables and using Euler's formula. The result is

$$I(\phi_o,\theta_o) \approx \sqrt{\frac{2\pi|R_1|}{k}} \cdot \frac{e^{\pm j\pi/4}}{a|\sin\beta_s|} \cdot h(\phi_s) \cdot e^{jk\Omega(\phi_o)} \tag{7.76}$$

$$R_1 \gtrless 0 \ .$$

Formula (7.76) is used to derive the first-order term in the asymptotic expansion of (7.66). The final results are

$$E_\phi^{w2} = -\frac{e^{-jkr}}{kr} \cdot \frac{e^{\pm j\pi/4}}{2\sqrt{2\pi}} \cdot \frac{\sqrt{k|R_1|}}{\sin|\beta_s|} \cdot e^{jk[a\sin\theta_o\cos(\phi_s-\phi_o)-a\sin\theta_o\cos\phi_o+\ell_2\cos\theta_o]}$$

$$\cdot \frac{\cos\theta_o \cdot \sin(\phi_o-\phi_s)}{\sin|\beta_s|} \cdot [-jk \cdot \sin\beta_s \cdot K(\phi_s)] \tag{7.77a}$$

$$E_\theta^{w2} = \frac{e^{-jkr}}{kr} \cdot \frac{e^{\mp j\pi/4}}{2\sqrt{2\pi}} \cdot \frac{\sqrt{k|R_1|}}{\sin|\beta_s|} \cdot e^{jk[a\sin\theta_o\cos(\phi_s-\phi_o)-a\sin\theta_o\cos\phi_o+\ell_2\cos\theta_o]}$$

$$\cdot \frac{\cos(\phi_o - \phi_s)}{\sin|\beta_s|} \cdot [-jk \cdot \sin\beta_s \cdot K(\phi_s)] \quad . \tag{7.77b}$$

Comparison between (7.77) and GTD formulas (7.62) and (7.64) determines $K(\phi)$:

$$K(\phi) = \frac{Z_o \cdot D_F^h(\phi)}{jk \sin\beta(\phi)} \cdot \frac{H_\beta(\phi)}{2} \quad . \tag{7.78}$$

In a caustic region where $R_1 \to \infty$ or $\Omega^{(2)}(\phi_s) \to 0$, formula (7.76) is not valid any longer, and the third-order derivative of the phase should be taken into account. The expansion (7.74), in this case, is replaced by

$$\Omega(\phi) \approx \Omega(\phi_s) + \frac{\Omega^{(2)}(\phi_s)}{2}(\phi - \phi_s)^2 + \frac{\Omega^{(3)}(\phi_s)}{6}(\phi - \phi_s)^3 \tag{7.79a}$$

where

$$\Omega^{(3)}(\phi_s) = a\cos\beta_s\left(\frac{3a^2\sin^2\beta_s}{\sigma_s^2} - 1\right) \tag{7.79b}$$

and the integral in (7.75) takes the following form,

$$\int_{\phi_s-\Delta\phi}^{\phi_s+\Delta\phi} e^{jk\left[\frac{\Omega^{(2)}(\phi_s)}{2}(\phi-\phi_s)^2 + \frac{\Omega^{(3)}(\phi_s)}{6}(\phi-\phi_s)^3\right]} \quad . \tag{7.80}$$

At the caustic direction where $\Omega^{(2)}(\phi_s)$ vanishes, a fairly accurate estimate of (7.80) can be obtained by first extending the domain of integration to infinity and then expressing the resulting infinite integral in terms of Gamma functions.

$$\int_{\phi_s-\Delta\phi}^{\phi_s+\Delta\phi} e^{jk\left[\frac{\Omega^{(3)}(\phi_s)}{6}\right](\phi-\phi_s)^3} d\phi \simeq \left[\frac{6}{|k\Omega^{(3)}(\phi_s)|}\right]^{1/3} \cdot \frac{\Gamma(1/3)}{\sqrt{3}} \quad . \tag{7.81}$$

In very special regions (for example at $\theta_o = \pi/2$ and $\phi_o \simeq \pi$), $\Omega^{(2)}(\phi_s)$ and $\Omega^{(3)}(\phi_s)$ become extremely small simultaneously and, hence, higher-order caustics will occur. These situations can be treated by including higher-order terms in the expansion of the phase function

$$\Omega(\phi) \simeq \Omega(\phi_s) + \frac{\Omega^{(2)}(\phi_s)}{2}(\phi - \phi_s)^2 + \frac{\Omega^{(3)}(\phi_s)}{6}(\phi - \phi_s)^3 + \frac{\Omega^{(4)}(\phi_s)}{24}(\phi - \phi_s)^4 \tag{7.82a}$$

where

$$\Omega^{(4)}(\phi_s) = -\Omega^{(2)}(\phi_s) - \frac{a^2 \sin^2 \beta_s}{\sigma_s} \cdot \left[1 + \frac{3a^2}{\sigma_s^2} + \frac{15a^2 \cos^2 \beta_s}{\sigma_s^2}\right] \tag{7.82b}$$

and the phase function in the integral (7.75) should be replaced by its value given in (7.82b). Again, in this case, in those directions where $\Omega^{(2)}(\phi_s)$ and $\Omega^{(3)}(\phi_s)$ vanish simultaneously, the integral

$$\int e^{jk\Omega(\phi)} d\phi \tag{7.83}$$

can be approximated in the same manner discussed in the previous case. In this case, the final result is

$$\int e^{jk\Omega(\phi)} d\phi \simeq \int e^{j\frac{k\Omega^{(4)}(\phi_s)}{24}(\phi-\phi_s)^4} d\phi \simeq \left[\frac{24}{|k\Omega^{(4)}(\phi_s)|}\right]^{1/4} \cdot \frac{e^{\pm j\pi/8}}{2} \cdot \Gamma\left(\tfrac{1}{4}\right) \quad ,$$

$$\Omega^{(4)}(\phi_s) \gtrless 0 \quad . \tag{7.84}$$

A careful study of the expressions $\Omega^{(2)}$, $\Omega^{(3)}$, and $\Omega^{(4)}$ reveals that their simultaneous vanishing is not possible and, hence, higher-order caustics cannot occur. Also, it is obvious that closed-form expressions like (7.76), (7.81), and (7.84) cannot be used in the proximity of the caustic directions. One possible approach is to use the integral (7.83) together with the expression (7.82a) and derive a transition function to replace the factor

$$\sqrt{\frac{2\pi|R_1|}{k}} \cdot \frac{e^{\mp j\pi/4}}{a \sin|\beta_s|} \tag{7.85}$$

in the formula (7.62) for the field in the caustic region. This replacement provides us with a fairly smooth transition into the caustic region from the observation directions where the formula (7.62) is applicable.

8. TRUNCATION EFFECT

According to our formulation of the present problem given in Chapter 4, the far-zone radiated field was decomposed into the upper- and lower-wedge contributions $F^{w1,w2}$ and that generated by the current induced on the surface of the cylinder F^{s}. In Chapter 5 the far field due to a point source located on an infinitely long cylinder was calculated and the surface ray representation was used to express the final results. Frequently, the far-zone field formulas for the infinite cylinder are used as an approximation for the case of the finite cylinder. However, this technique yields inaccurate results, especially for the observation points near the axis of the cylinder where the expressions given in (5.1) and (5.2) are not valid, or in the cases where the distance of the source from one of the ends of the cylinder or the total length of the object is not large enough. In order to carry out a more accurate approximate solution to this problem, the current distribution on the finite cylinder will be taken identical to the distribution on the infinite cylinder [73]. Then the contributions of the portions of the infinite cylinder above $z = \ell_2$ and below $z = -\ell_1$ (Fig. 19) are determined with the assumption that the current on these semi-infinite cylinders remains unchanged when the cylinder is truncated. Subtraction of the contributions of the two semi-infinite cylinders from the infinite cylinder field yields a better estimate for the far-zone radiated field due to the finite cylinder.

In this chapter, we derive the approximate expressions for the far-zone radiated field due to current distributions of the upper and lower semi-infinite cylinders.

8.1 Far Field Radiated by Upper Semi-Infinite Cylinder

The far radiated field due to a current distribution confined to a region of space with a finite extent can be expressed as

$$E_\alpha = \frac{-jk}{4\pi Y_0} \cdot \frac{e^{-jkr}}{r} \quad [\tilde{J}_\alpha - (\hat{k}\cdot\tilde{\vec{J}})k_\alpha] \quad \alpha = x,y,z \tag{8.1a}$$

$$\text{where} \quad \tilde{J}_\alpha = \int_{\substack{\text{Source} \\ \text{Region}}} J_\alpha(\vec{r}') \, e^{j\vec{k}\cdot\vec{r}'} \, d_3\vec{r}' \tag{8.1b}$$

Obviously the semi-infinite cylinder is not "finite." But the fact that the decay of the current due to a point source is very fast and strong at far distances from the source allows us to use (8.1) in this case, too.

The far field (8.1) can be put in terms of its components along $\hat{\theta}_0$ and $\hat{\phi}_0$ in the observation direction:

$$E_\theta = E_x \cos\theta_0 \cos\phi_0 + E_y \cos\theta_0 \sin\phi_0 - E_z \sin\theta_0 \tag{8.2}$$

$$E_\phi = -E_x \sin\phi_0 + E_y \cos\phi_0 \tag{8.3}$$

Combining (8.1), (8.2), and (8.3), one obtains

$$E_\theta = \frac{-jk}{4\pi Y_0} \cdot \frac{e^{-jkr}}{r} \quad [\tilde{J}_x \cos\theta_0 \cdot \cos\phi_0 + \tilde{J}_y \cos\theta_0 \cdot \sin\phi_0 - \tilde{J}_z \sin\theta_0] \tag{8.4}$$

$$E_\phi = \frac{-jk}{4\pi Y_0} \cdot \frac{e^{-jkr}}{r} \quad [-\tilde{J}_x \sin\phi_0 + \tilde{J}_y \cos\phi_0] \tag{8.5}$$

Applying the above formulas to a semi-infinite cylinder erected at $z = \ell_2$, ($\ell_2 < z < +\infty$) (see Fig. 33), we note that in this case two-dimensional Fourier transforms of axial and azimtuhal components of surface current distribution are dealt with, so that the field may be written as

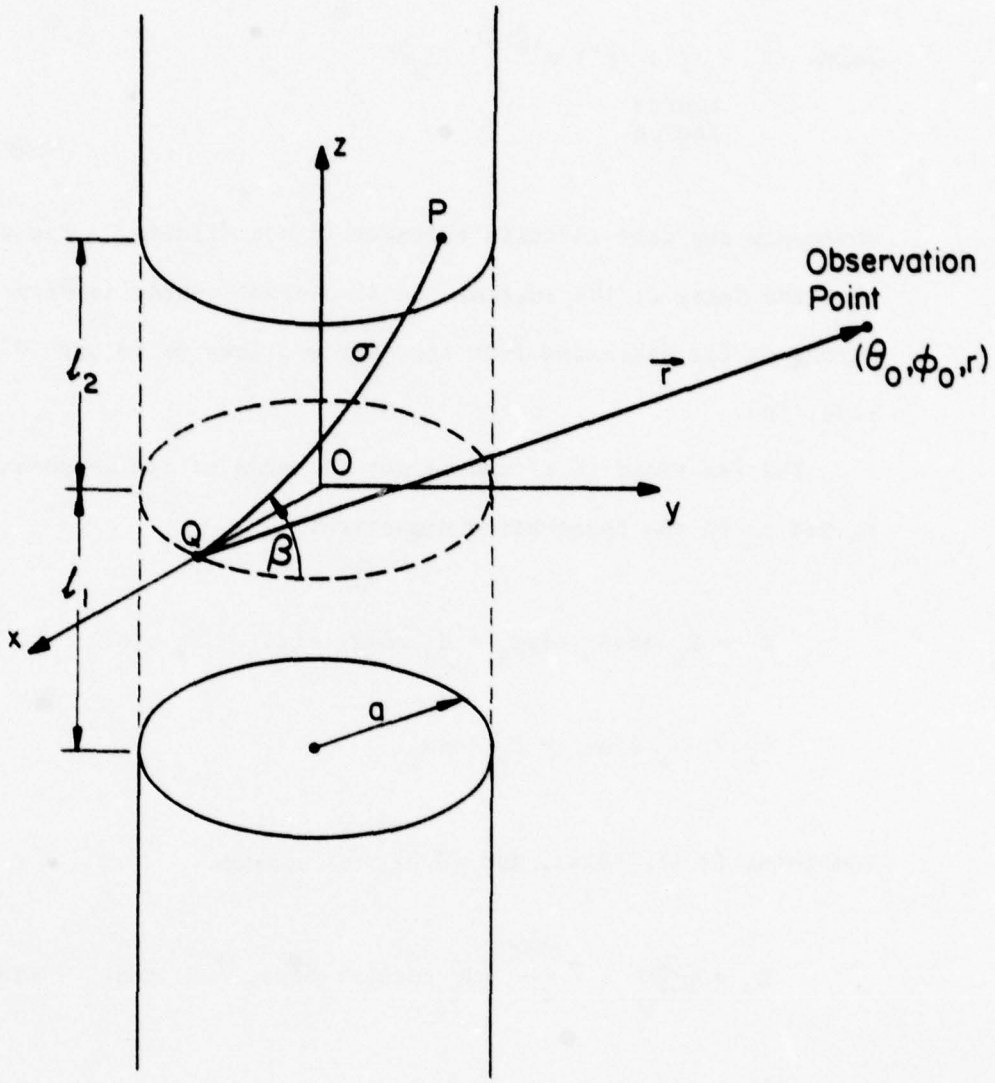

Figure 33. Upper and lower semi-infinite cylinders.

$$E_{\theta}^{Up} = A(\vec{r}) \left\{ a\cos\theta_0 \cdot T^{Up} [\sin(\phi_0-\phi)J_{\phi}] - a\sin\theta_0 \, T^{Up} [J_z] \right\} \tag{8.6a}$$

$$E_{\phi}^{Up} = A(\vec{r}) \left\{ a \cdot T^{Up} [\cos(\phi_0-\phi)J_{\phi}] \right\} \tag{8.6b}$$

where

$$A(\vec{r}) = \frac{-jk}{4\pi Y_0} \cdot \frac{e^{-jkr}}{r} \cdot e^{-jka\sin\theta_0 \cdot \cos\phi_0} \tag{8.6c}$$

and T^{Up} is the two-dimensional Fourier-type transformation defined as

$$T^{Up} [h(\phi,z)] = \int_0^{2\pi} d\phi \int_{\ell_2}^{\infty} dz \; h(\phi,z) \; e^{j[ka \sin\theta_0 \cos(\phi-\phi_0)+kz \cos\theta_0]} \tag{8.6d}$$

It is obvious that using the exact solutions for J and J_z in the above equations makes the double integrations a formidable task to perform, especially in the high-frequency range. Besides this point, we should bear in mind that expressions being derived in this chapter are only corrective terms to our final solution. Based on these facts, approximate expressions (6.8) were chosen to represent the surface magnetic field or surface current components on the semi-infinite cylinder. The expressions (6.8) have been shown to be fairly accurate estimates of the surface field when the observation point is two or more wavelengths far from the source. Therefore, we have (Fig. 33)

$$J_z(P) = H_{\phi}(P) = (\vec{M} \cdot \hat{\phi}) \; [H_{\beta} \sin^2\beta + H_{\sigma}\cos^2\beta] \tag{8.7a}$$

$$J_{\phi}(P) = -H_z(P) = (\vec{M} \cdot \hat{z}) \; [-H_{\beta}\cos^2\beta - H_{\sigma}\sin^2\beta] \tag{8.7b}$$

where $H_\sigma(P)$ and $H_\beta(P)$ are given by (6.8a,b). The special form of the final expressions for J_z and J_ϕ are such that we can represent them as

$$J_z(P) = J_{z0}(P) \cdot e^{-jk\sigma} \tag{8.8a}$$

$$J_\phi(P) = J_{\phi 0}(P) \cdot e^{-jk\sigma} \tag{8.8b}$$

where σ is the arclength of geodesic QP (Fig. 33). Substitution of (8.8) into (8.6) leads us to the double integrations of the following general form:

$$F^U(\theta_0,\phi_0) = \int_0^{2\pi} a\,d\phi \int_{\ell_2}^{\infty} dz\; f(\phi,z)\; e^{-jk\sigma} e^{jk[a\sin\theta_0 \cos(\phi-\phi_0)+z\cos\theta_0]} \tag{8.9}$$

where $\sigma = [z^2+(a\phi)^2]^{1/2}$. Here, we attempt to simplify the computation of F^U by deriving an asymptotic expansion for the inner integral (with respect to z) on the assumption that $k\ell_2$ is large. To this end, we rewrite (8.9) as

$$F^U(\theta_0,\phi_0) = \int_0^{2\pi} a\,d\phi\;\; \bar{f}(\phi)\; e^{jka\,\sin\theta_0 \cos(\phi_0-\phi)} \tag{8.10}$$

where

$$\bar{f}^U(\phi) = \int_{\ell_2}^{\infty} dz\; f(\phi,z)\; e^{jk[z\cos\theta_0 - \sqrt{(a\phi)^2+z^2}\,]} \tag{8.11}$$

and then apply the stationary phase method to (8.11). At this point one might raise the question why it is not possible to apply this method to the original double integral (8.9). Theoretically, it is possible to evaluate (8.9) by the two-dimensional version of the stationary phase method, however,

it can be shown [85] that the stationary point of the phase of the integrand (8.9) is of second order. This fact makes the resulting two-dimensional asymptotic expansion very slowly convergent and, in addition, the coefficients of the double infinite sum become highly complicated when order of the terms increases.

In order to apply the stationary phase method to (8.11), first we rewrite it as

$$\tilde{f}^U(\phi) = \int_{\ell_2}^{\infty} f(\phi,z)\, e^{jkq(z,\phi)} \tag{8.12a}$$

where $$q(z,\phi) = z\cos\theta_0 - \sqrt{(a\phi)^2+z^2} \tag{8.12b}$$

The stationary point of q is given by the following equation

$$\frac{\partial q}{\partial z} = \cos\theta_0 - \frac{z}{\sqrt{(a\phi)^2+z^2}} = 0 \tag{8.13}$$

from which the following expression for the stationary value of z as a function of ϕ is obtained:

$$z_s(\phi) = a|\phi|\ \mathrm{cotg}\theta_0 \tag{8.14}$$

The phase function $q(z,\phi)$ can be expanded around z_s

$$q(z,\phi) \simeq q(z_s,\phi) + \frac{q^{(2)}(z_s,\phi)}{2} (z-z_s)^2 + \ldots \tag{8.15a}$$

where

$$q(z_s,\phi) = -a|\phi|\sin\theta_0 \tag{8.15b}$$

$$q^{(2)}(z_s,\phi) = \frac{-\sin^3\theta_0}{a|\phi|} < 0 \quad (\phi \neq 0) \tag{8.15c}$$

The case in which $\phi = 0$ is of no interest to us because $z_s(\phi) \to 0$, and if $k\ell_2 >> 1$, then the stationary point is located far outside the domain of integration and thus has negligible contributions to the integral. The most significant contributions to a typical integral of the form given in (8.12a), when k is large, come from the end point $z = \ell_2$ and the stationary point $z = z_s(\phi)$. When these two points are far apart, these contributions can be computed separately and then added to give an estimate for (8.12a). Of course, if the stationary point z_s is far from the end point and outside the domain of integration, only the end point contributes to the integral. A more complicated situation can occur when the two points approach each other. In this case, the simple formulas for calculating the contributions of a single isolated end point or stationary phase point are not applicable any longer. The details of the procedure for treating this case have been explained by many authors (for example, see page 421 of [108]). We apply the final formulas to (8.12a). The first-order term in the asymptotic expansion of (8.12a), according to the above-mentioned procedure, is

$$\bar{f}^{U}(\phi) \sim e^{jkq(z_s,\phi)} \left\{ \frac{f(z_s,\phi)\, h_s(\phi)}{\sqrt{k}}\, Q\left[s_2(\phi) \cdot \sqrt{k} \cdot e^{\mp j\pi/4}\right] + \frac{e^{\pm j(ks_2^2+\pi/4)}}{2k\, s_2(\phi)} \left[f(\ell_2,\phi) \cdot h_2(\phi) - f(z_s,\phi) \cdot h_s(\phi)\right] \right\}$$

$$, \; q^{(2)}(z_s,\phi) \gtrless 0 \tag{8.16a}$$

where

$$Q(y) = \int_y^{\infty} e^{-x^2}\, dx \tag{8.16b}$$

$$s_2(\phi) = \left|q(z_s,\phi) - q(\ell_2,\phi)\right|^{1/2} \cdot \operatorname{sgn}\left(\ell_2 - z_s(\phi)\right) \tag{8.16c}$$

$$h_s(\phi) = \sqrt{\frac{2}{\left|q^{(2)}(z_s,\phi)\right|}} \cdot e^{\pm j\pi/4}, \quad q^{(2)}(z_s,\phi) \gtrless 0 \tag{8.16d}$$

$$h_2(\phi) = \frac{2\left|s_2(\phi)\right| e^{\pm j\pi/4}}{\left|q'(\ell_2,\phi)\right|}, \quad q^{(2)}(z_s,\phi) \gtrless 0 \tag{8.16e}$$

When, $z_s = \ell_2$, one has $s_2(\phi) = 0$ and, consequently,

$$Q\left(s_2 \sqrt{k}\, e^{\mp j\pi/4}\right) = Q(0) = \sqrt{\pi}/2 \tag{8.17a}$$

and

$$\bar{f}^{U}(\phi) \sim (1/2) \cdot \sqrt{\frac{2\pi}{k\left|q^{(2)}(z_s,\phi)\right|}}\, f(z_s,\phi)\, e^{jkq(z_s,\phi) \pm j\pi/4} \tag{8.17b}$$

which is the well-known formula for computing the contribution of a single isolated stationary phase point. The factor 1/2 in front of this formula accounts for the semi-infinite integration interval. When z_s is quite far from ℓ_2 or $\sqrt{k}\, s_2(\phi) \gg 1$, using the following asymptotic expansion for Q,

$$Q(z) \sim \frac{e^{-z^2}}{2z} + \sqrt{\pi}\theta\,(-\mathrm{Re}z) \tag{8.18a}$$

$$\theta(x) = \begin{cases} 1 & x > 0 \\ 0 & x < 0 \end{cases}$$

the expression (8.12a) reduces to

$$\bar{f}^U(\phi) \sim \frac{\sqrt{2\pi}}{\sqrt{k\,|q^{(2)}(z_s,\phi)|}}\, f(z_s,\phi)\, e^{jkq(z_s,\phi)\pm j\pi/4} \cdot \theta(z_s-\ell_2)$$

$$- \frac{f(\ell_2,\phi)\cdot e^{jkq(z_s,\phi)}}{jkq'(\ell_2,\phi)}\,,\quad q^{(2)}(z_s,\phi) \gtrless 0$$

The important limiting cases (8.17) and (8.18) indicate that the formula (8.16a), indeed, satisfies the criteria discussed earlier. In the special case where $q(z,\phi)$ is given by (8.12b), one has

$$s_2(\phi) = \mathrm{sgn}(\ell_2 - z_s(\phi)) \left| -a|\phi| \sin\theta_0 - \ell_2 \cos\theta_0 + \sqrt{(a\phi)^2 + \ell_2^2} \right|^{1/2} \tag{8.19a}$$

$$h_s(\phi) = \sqrt{\frac{2a|\phi|}{\sin^3\theta_0}} \cdot e^{-j\pi/4} \tag{8.19b}$$

$$h_2(\phi) = \frac{2\,|s_2(\phi)| \cdot e^{-j\pi/4}}{\left|\cos\theta_0 - \dfrac{\ell_2}{\sqrt{(a\phi)^2 + \ell_2^2}}\right|} \tag{8.19c}$$

Let us denote

$$\zeta_2(\phi) = s_2(\phi)\sqrt{k/2} \tag{8.20}$$

then

$$Q(s_2(\phi)\sqrt{k}\, e^{j\pi/4}) = Q[(1+j)\,\zeta_2(\phi)] \tag{8.21}$$

Equation (8.21) can also be written as

$$Q[(1+j)\,\zeta_2(\phi)] = \sqrt{\frac{\pi}{2}} - \int_0^{(1+j)\zeta_2} e^{-x^2}\, dx \tag{8.22}$$

After proper changing of the variable and some algebraic manipulations, one can express (8.22) in terms of the Fresnel integrals C and S,

$$Q[(1+j)\zeta_2] = \sqrt{\frac{\pi}{2}} \left\{ 1 - (1+j)\left[C\left(\frac{2\zeta_2}{\sqrt{\pi}}\right) - jS\left(\frac{2\zeta_2}{\sqrt{\pi}}\right)\right] \right\} \tag{8.23}$$

where

$$C(z) = \int_0^z \cos(\tfrac{\pi}{2} t^2)\, dt \tag{8.24a}$$

$$S(z) = \int_0^z \mathrm{Sin}(\tfrac{\pi}{2} t^2)\, dt \tag{8.24b}$$

Several procedures exist for evaluating the Fresnel integrals for various ranges of argument. Some of these procedures involve some auxiliary functions. One efficient way to compute C and S, which has been discussed in [62], is to write them in terms of some new auxiliary functions f_0 and g_0 having reasonably simple expressions:

$$C(z) = \tfrac{1}{2} + f_0(z)\cdot\sin(\tfrac{\pi}{2} z^2) - g_0(z) \cdot \cos(\tfrac{\pi}{2} z^2) \tag{8.25a}$$

$$S(z) = 1/2 - f_0(z)\cdot\cos(\tfrac{\pi}{2} z^2) - g_0(z) \cdot \sin(\tfrac{\pi}{2} z^2) \tag{8.25b}$$

where $f_0(z)$ and $g_0(z)$ are given by following approximate expressions [62]: $(0 \le x < \infty)$

$$f_0(x) = \frac{1 + 0.926x}{2 + 1.792x + 3.104x^2} + \varepsilon \tag{8.25c}$$

$$g_0(x) = \frac{1}{2 + 4.142x + 3.492x^2 + 6.670x^3} + \varepsilon \tag{8.25d}$$

$$|\varepsilon| \le 2 \times 10^{-3}$$

Substitution of (8.25) in (8.23) yields

$$Q[(1+j)\zeta_2] = \sqrt{\frac{\pi}{2}} \{1-(1+j)\ [\frac{1-j}{2} + jf_0\ (\frac{2\zeta_2}{\sqrt{\pi}})\ e^{-j2\zeta_2^2} - g_0(\frac{2\zeta_2}{\sqrt{\pi}}) \cdot e^{-j2\zeta_2^2}]\}$$

$$\zeta_2 > 0 \qquad (8.26)$$

When ζ_2 is negative, it can be shown that

$$Q[-(1+j)|\zeta_2|] = \sqrt{\pi} - Q[(1+j)|\zeta_2|] \qquad (8.27)$$

Combining (8.26) and (8.27) results in

$$Q[(1+j)\zeta_2] = \sqrt{\pi}\ \{\theta(-\zeta_2) - \mathrm{sgn}(\zeta_2) \cdot \frac{e^{j\pi/4}}{\sqrt{2}} \cdot$$

$$[j\ f_0\ (\frac{2|\zeta_2|}{\sqrt{\pi}})\ e^{-j2\zeta_2^2} - g_0(\frac{2|\zeta_2|}{\sqrt{\pi}}\ e^{-j2\zeta_2^2}]\ \} \qquad (8.28)$$

or

$$Q[(1+j)\zeta_2] = \begin{cases} \sqrt{\pi}\ \theta(-\zeta_2) - W(\zeta_2)e^{-j2\zeta_2^2}, & \zeta_2 \neq 0 \\ \sqrt{\frac{\pi}{2}}\ , & \zeta_2 = 0 \end{cases} \qquad (8.29a)$$

where

$$W(x) = \sqrt{\pi}\ \mathrm{sgn}\ (x) \cdot \frac{e^{j\pi/4}}{\sqrt{2}} \cdot \left[j f_0\left(\frac{2|x|}{\sqrt{\pi}}\right) - g_0\left(\frac{2|x|}{\sqrt{\pi}}\right)\right] \qquad (8.29b)$$

The above expression for Q is employed in (8.16a) which together with (8.19) leads us to the following expression for $\bar{f}^U(\phi)$,

$$f^{-U}(\phi) \sim e^{jk[\ell_2 \cos\theta_0 - \sqrt{(a\phi)^2+\ell_2^2}]} \left\{ \frac{-h_s(\phi) f(z_s,\phi)}{\sqrt{k}}\ W(\zeta_2) \right.$$

$$\left. + e^{-j\pi/4}\ \frac{f(\ell_2,\phi)h_2(\phi) - f(z_s,\phi)h_s(\phi)}{2\sqrt{2}\cdot\sqrt{k}\cdot\zeta_2} \right\} + \frac{e^{-jka|\phi|\sin\theta_0}\ h_s(\phi)\cdot f(z_s,\phi)\cdot\theta(-\zeta_2)}{\sqrt{k/\pi}}$$

(8.30)

The function $\bar{f}^U(\phi)$ is used in (8.10). Then the ϕ-integration is carried out numerically to obtain F^U. When the arbitrary function $f(\phi,z)$ in (8.9) is replaced by $J_{\phi 0} \sin(\phi_0-\phi)$, $J_{\phi 0}\cos(\phi_0-\phi)$, and J_{z0} (given in (8.8) and (8.7)), various terms of the expressions (8.6) for the components of the radiated field due to the current distribution on the upper semi-infinite cylinder are obtained.

8.2 Far Field Radiated by Lower Semi-Infinite Cylinder

The same procedure is applied to evaluate the contribution of the lower semi-infinite cylinder. The final result is exactly the same as for the previous case except for minor changes in some parameters. As a matter of fact, in this case, $T^{Up}, F^U, \bar{f}^U$ are replaced by $T^{LO}, F^L, \bar{f}^L$ in which the z-integration is carried out over the interval $(-\infty, -\ell_1)$. Here we list only

the final results,

$$\bar{f}^{L}(\phi) \sim e^{jk[-\ell_1\cos\theta_0-\sqrt{(a\phi)^2+\ell_1^2}]} \left\{ \frac{-h_s(\phi)\cdot f(z_s,\phi)}{\sqrt{k}} \; W(\zeta_1) \right.$$

$$\left. + e^{-j\pi/4} \; \frac{f(-\ell_1,\phi)\cdot h_1(\phi)-f(z_s,\phi)\cdot h_s(\phi)}{2\sqrt{2}\cdot\sqrt{k}\cdot\zeta_1} \right\} \; + e^{-jka|\phi|\sin\theta_0}$$

$$\cdot \frac{h_s(\phi)\cdot f(z_s,\phi)\cdot\vartheta(-\zeta_1)}{\sqrt{k/\pi}} \tag{8.31a}$$

where

$$s_1(\phi) = \mathrm{sgn}(\ell_1+z_s(\phi)) \; \left| -a|\phi|\sin\theta_0+\ell_1\cos\theta_0 + \sqrt{(a\phi)^2+\ell_1^2} \right|^{1/2} \tag{8.31b}$$

$$\zeta_1(\phi) = s_1(\phi)\cdot\sqrt{\frac{k}{2}} \tag{8.31c}$$

$$h_1(\phi) = \frac{2|s_1(\phi)|e^{-j\pi/4}}{\left|\cos\theta_0+\dfrac{\ell_1}{\sqrt{(a\phi)^2+\ell_1^2}}\right|} \; . \tag{8.31d}$$

The total contribution due to those parts of the cylinder that have been removed is the sum of the fields generated by the upper- and lower-semi-infinite cylinders as discussed above. It is expected that subtraction of the radiated field generated by the truncated parts of the structure from the total field will improve the overall accuracy of the results.

9. APPROXIMATE EXPRESSION FOR THE FIELD IN PARAXIAL REGION

Equations (5.1) and (5.2) used in Chapter 2 for computing the contribution of surface rays are not valid in the paraxial region $\theta_0 \simeq 0$, or $\theta_0 \simeq \pi$ (this point is discussed in more detail in [85] or in Sec. 3.2). It is well-known that field components in this region do not have any strange behaviour and their variation in polar region is more or less smooth. Based on this fact, which is supported by theoretical analysis and experimental data, several techniques have been suggested for field evaluation in paraxial regions. In some cases where simple field expressions are available outside the paraxial region, Huygen's principle can be invoked to find the field in paraxial directions by integrating the field over an arbitrary surface enclosing the object. When the asymptotic formulas based on certain canonical problems are involved (for example, in GTD or our case), it may be possible to modify the existing formulas by studying the exact solution to corresponding canonical problems for the special directions in which the existing formulas are not valid [24].

Our problem is to find the far-zone radiated field generated by a surface current distribution excited by a point source on a finite cylinder in the paraxial region. Using the same argument given in the previous section, we assume that the current distribution on the finite cylinder is the same as that of an infinite one truncated to a finite length. The effects of the wedges are accounted for when the wedge diffracted fields are added to the total field. In the present case, as shown later, it turns out that one can compute the field along the axis ($\theta_0 = 0, \pi$) by a very efficient numerical procedure. Based on the fact that the field behaves smoothly in the polar region, one can utilize the field value along the axis given by the method discussed later and the field quantities at the points not very close to the axial region obtained by our asymptotic formulas in some interpolation scheme

the field in the paraxial region. We will now outline a very efficient approach for calculating the field along the axis ($\theta_0 = 0,\pi$).

The far-zone radiated field due to a current distribution on a finite cylinder is given by equations similar to (8.6). The only difference is that, in the present case, the z-integration in (8.6d) is carried out over the range $[-\ell_1, \ell_2]$.

Referring to Fig. 34 in the axial region $\theta_0 = \begin{matrix}0\\ \pi\end{matrix}$, the rectangular components of the far field can be written as

$$E_x^{ax} = A(r) \cdot \int_{-\pi}^{\pi} ad\phi \int_{-\ell_1}^{\ell_2} dz\, J_x(\phi,z)e^{\pm jkz} \tag{9.1a}$$

$$E_y^{ax} = A(r) \cdot \int_{-\pi}^{\pi} ad\phi \int_{-\ell_1}^{\ell_2} dz\, J_y(\phi,z)e^{\pm jkz} \tag{9.1b}$$

where A(r) is defined in (8.6c), and J_x and J_y are rectangular components of the surface current which can be given in the term of J_ϕ,

$$J_x = -J_\phi \sin\phi\ , \quad J_y = J_\phi \cos\phi \tag{9.2}$$

Equations (9.1) have been obtained by evaluating (8.1) along the axis. It follows from (9.1) and (9.2) that only the ϕ-component of the surface current contributes to the field along the axis.

The exact modal solution for the surface current J_ϕ due to a magnetic dipole of moment

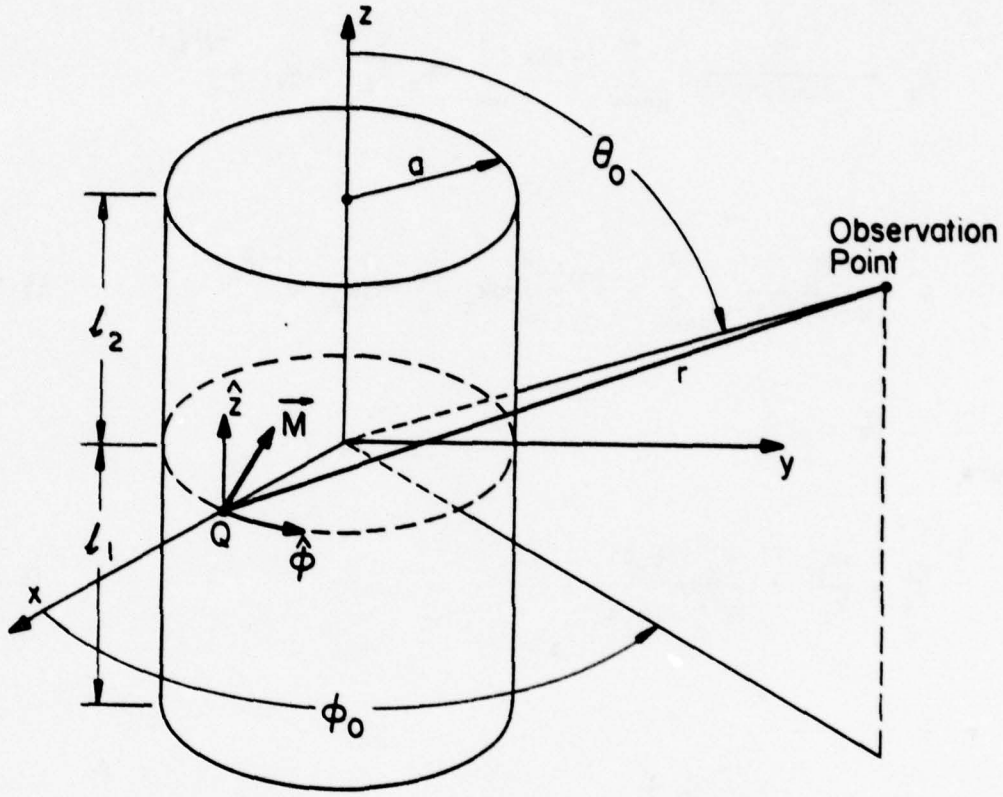

Figure 34. The geometrical meaning of the parameters used in Equations (9.1).

$$\vec{M} = M_\phi \hat{\phi} + M_z \hat{z} \tag{9.3}$$

can be written as

$$J_\phi = \frac{-M_\phi}{j\omega\mu(2\pi a)^2} \sum_{n=-\infty}^{\infty} e^{-jn\phi} \int_{-\infty}^{\infty} dk_z \tilde{J}_\phi^c(n,k_z)\, e^{-jk_z z}$$

$$+ \frac{M_z}{j\omega\mu(2\pi)^2 a} \cdot \sum_{n=-\infty}^{\infty} e^{-jn\phi} \int_{-\infty}^{\infty} dk_z \tilde{J}_\phi^a(n,k_z)\, e^{-jk_z z} \tag{9.4a}$$

where

$$\tilde{J}_\phi^c = \frac{nk_z}{k_t} \cdot \frac{H_n^{(2)}(k_t a)}{H_n^{(2)'}(k_t a)} \tag{9.4b}$$

$$\tilde{J}_\phi^a = k_t \cdot \frac{H_n^{(2)}(k_t a)}{H_n^{(2)'}(k_t a)} \tag{9.4c}$$

$$k_t = \sqrt{k^2 - k_z^2} = \begin{cases} \sqrt{k^2 - k_z^2}, & k_z < k \\ -j\sqrt{k_z^2 - k^2}, & k < k_z \end{cases} \tag{9.4d}$$

Insertion of (9.4) into (9.1) and some algebraic manipulation leads us to

$$E_x^{ax} = \frac{jM_\phi}{8\pi^2 a} \cdot \frac{e^{-jkr}}{r} \cdot \int_{-\infty}^{\infty} dk_z \, V(k_z \mp k) \cdot \frac{k_z H_1^{(2)}(k_t a)}{k_t H_1^{(2)'}(k_t a)} \tag{9.5a}$$

$$E_y^{ax} = \frac{-M_z}{8\pi^2} \cdot \frac{e^{-jkr}}{r} \cdot \int_{-\infty}^{\infty} dk_z \, V(k_z \mp k) \cdot \frac{k_t H_1^{(2)}(k_t a)}{H_1^{(2)'}(k_t a)} \tag{9.5b}$$

where

$$V(t) = \int_{-\ell_1}^{\ell_2} e^{-jtz} \, dz = \frac{e^{-jt\ell_2} - e^{+jt\ell_1}}{-jt} \tag{9.5c}$$

(minus sign is for $\theta_0 = 0$ and plus sign is for $\theta_0 = \pi$). It can easily be shown that the above integrals are very slowly convergent in many cases, the fact which makes their accurate evaluation a tedious task.

In this work we have employed a technique used by Duncan [109] in the study of cylindrical antenna problems. Here the method is illustrated by discussing its application to (9.5a). For (9.5b), only the final results are given.

In order to apply this technique to (9.5a), let us rewrite the integral in (9.5a) in the following form:

$$I_x = \int_0^\infty dk_z \cdot U_x(k_z) \cdot F(k_z) \tag{9.6a}$$

where

$$F(k_z) = \frac{k_z H_1^{(2)}(k_t a)}{k_t H_1^{(2)'}(k_t a)} = \begin{cases} F_1(k_z) + j\, F_2(k_z) & , \quad k \geq k_z \\ F_3(k_z) & , \quad k \leq k_z \end{cases} \tag{9.6b}$$

$$F_1(k_z) = \frac{k_z}{k_t} \left[\frac{J_1(k_t a) J_1'(k_t a) + Y_1(k_t a) Y_1'(k_t a)}{J_1'^2(k_t a) + Y_1'^2(k_t a)} \right] \tag{9.6c}$$

$$F_2(k_z) = \frac{2k_z}{\pi k_t^2 a} \cdot \frac{1}{J_1'^2(k_t a) + Y_1'^2(k_t a)} \tag{9.6d}$$

$$F_3(k_z) = \frac{k_z}{|k_t|} \cdot \frac{K_1(|k_t|a)}{K_1'(|k_t|a)} \tag{9.6e}$$

When $k_z \to k$, it can be shown that $F \to -ka$. The function U_x can also be written as follows:

$$U_x(k_z) = \frac{\sin(k_z-k)\ell_2 + \sin(k_z-k)\ell_1}{k_z-k} - \frac{\sin(k_z+k)\ell_2 + \sin(k_z+k)\ell_1}{k_z+k}$$

$$+ j \left\{ \frac{\cos(k_z-k)\ell_2 - \cos(k_z-k)\ell_1}{k_z-k} + \frac{\cos(k_z+k)\ell_2 - \cos(k_z+k)\ell_1}{k_z+k} \right\} \tag{9.7}$$

Inserting (150) in (149a), one will be dealing with integrals of the following general form:

$$\int_0^\infty dk_z \; \frac{\binom{\sin}{\cos}(k_z \mp k)\ell_2 \pm \binom{\sin}{\cos}(k_z \mp k)\ell_1}{k_z \mp k} \cdot F(k_z)\, dk_z \tag{9.8}$$

Let us consider the following typical integral

$$C_1^x = \int_0^\infty dk_z \; \frac{\cos(k_z-k)\ell_2 - \cos(k_z-k)\ell_1}{k_z-k} \cdot F(k_z) \tag{9.9}$$

which can be rewritten as

$$C_1^x = \int_0^k dk_z \; \frac{\cos(k_z-k)\ell_2 - \cos(k_z-k)\ell_1}{k_z-k} \; F_1(k_z)$$

$$+ \int_k^\infty dk_z \cdot \frac{\cos(k_z-k)\ell_2 - \cos(k_z-k)\ell_1}{k_z-k} \; F_3(k_z)$$

$$+j \left\{ \int_0^k dk_z \frac{\cos(k_z-k)\ell_2 - \cos(k_z-k)\ell_1}{k_z-k} \right\} F_2(k_z) \tag{9.10}$$

From (9.9), one can derive

$$\text{Re } C_1^x = \text{Re } \{ -j \int_0^\infty dk_z \left[\frac{\sin(k_z-k)\ell_2 - \sin(k_z-k)\ell_1}{k_z-k}\right] F(k_z)$$

$$+ \int_0^\infty dk_z \frac{e^{j(k_z-k)\ell_2} - e^{j(k_z-k)\ell_1}}{k_z-k} \cdot F(k_z) \} \tag{9.11}$$

The first term on the right-hand side of (9.11) can be computed by (9.6b),

$$\text{Re } \{ -j \int_0^\infty dk_z \left[\frac{\sin(k_z-k)\ell_2 - \sin(k_z-k)\ell_1}{k_z-k}\right] F(k_z) \} =$$

$$\int_0^k dk_z \frac{\sin(k_z-k)\ell_2 - \sin(k_z-k)\ell_1}{k_z-k} F_2(k_z) \tag{9.12}$$

In the second term of (9.11) given below

$$\text{Re} \left\{ \int_0^\infty dk_z \, \frac{e^{j(k_z-k)\ell_2} - e^{j(k_z-k)\ell_1}}{k_z-k} \cdot F(k_z) \right\} \tag{9.13}$$

the k_z-integration is along the path C_1 in the complex k_z-plane (Fig. 35). It can be shown that the integrand has no pole in the first quadrant and also the integrand exponentially decays as $|k_z| \to \infty$, as long as Im $k_z > 0$. Therefore, if the integration inside the curly brackets of (9.13) is carried out along a closed contour composed of C_1, a quarter circle at infinity in the first quadrant going from Re k_z to Im k_z, and C_2 (Fig. 35), the result is zero. Consequently, the integral (9.13) can be evaluated along the path C_2. After proper change of variable, (9.13) can be rewritten as

$$\text{Re} \int_0^\infty d\zeta \cdot \frac{e^{-jk\ell_2-\zeta\ell_2} - e^{-jk\ell_1-\zeta\ell_1}}{-k+j\zeta} \cdot [jF(j\zeta)] =$$

$$\text{Re} \left[I_F^-(\ell_2) - I_F^-(\ell_1) \right] \tag{9.14}$$

where

$$I_F^-(\ell) = \int_0^\infty d\zeta \cdot \frac{[k\cos k\ell + \zeta \sin k\ell + j(\zeta \cos k\ell - k\sin k\ell)]e^{-\zeta\ell}}{\zeta^2+k^2} \cdot [-jF(j\zeta)] \tag{9.15a}$$

$$I_F^+(\ell) = I_F^-(\ell) \{k \to -k\} \tag{9.15b}$$

Combining (9.15), (9.13) and (9.12), we have

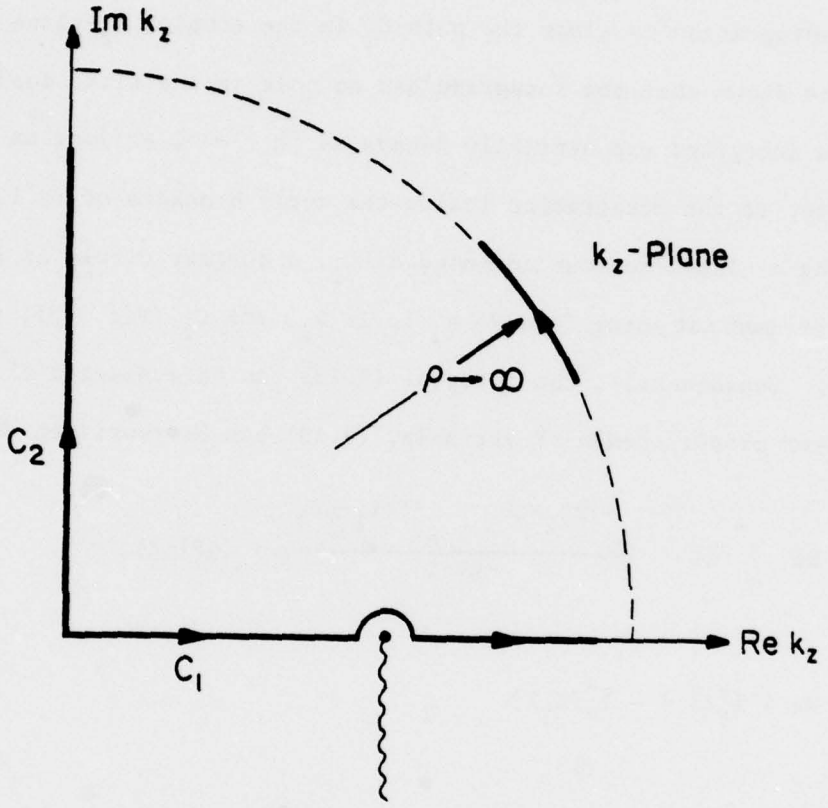

Figure 35. Contours of integration in (9.13) and (9.14).

$$C_1^x = j \int_0^k dk_z \left[\frac{e^{-j(k_z-k)\ell_2} - e^{-j(k_z-k)\ell_1}}{k_z-k}\right] F_2(k_z)$$

$$+ \text{Re} \left[I_F^-(\ell_2) - I_F^-(\ell_1)\right] \tag{9.16}$$

The other terms in (9.6a) can be computed in exactly the same manner. The final expression for I_x in terms of the auxiliary integrals $I_F^{\pm}(\ell_{1,2})$ reads

$$I_x = 2 \int_0^{|k|} \left[\frac{e^{-j(k_z-k)\ell_2}}{k_z-k} - \frac{e^{-j(k_z+k)\ell_1}}{k_z+k}\right] F_2(k_z)\, dk_z$$

$$+ \text{Im} \left[I_F^-(\ell_2) + I_F^-(\ell_1) - I_F^+(\ell_2) - I_F^+(\ell_1)\right]$$

$$+ j\text{Re} \left[I_F^-(\ell_2) - I_F^-(\ell_1) + I_F^+(\ell_2) - I_F^+(\ell_1)\right] \tag{9.17}$$

The same technique can be applied to the integral

$$I_y = \int_0^{\infty} dk_z\, U_y(k_z) \cdot G(k_z) \tag{9.18a}$$

where

$$G(k_z) = \frac{k_t H_1^{(2)}(k_t a)}{H_1^{(2)'}(k_t a)} \tag{9.18b}$$

$$U_y(k_z) = \frac{\sin(k_z-k)\ell_2 + \sin(k_z-k)\ell_1}{k_z-k} + \frac{\sin(k_z+k)\ell_2 + \sin(k_z+k)\ell_1}{k_z+k}$$

$$+ j \left\{ \frac{\cos(k_z-k)\ell_2 - \cos(k_z-k)\ell_1}{k_z-k} - \frac{\cos(k_z+k)\ell_2 - \cos(k_z+k)\ell_1}{k_z+k} \right\} \qquad (9.18c)$$

almost in the same manner as discussed earlier. We have

$$I_y = -2 \int_0^{|k|} dk_z \left[\frac{e^{-j(k_z-k)\ell_2}}{k_z-k} + \frac{e^{-j(k_z+k)\ell_1}}{k_z+k} \right] G_2(k_z)\, dk_z$$

$$+ \text{Im} \left[I_G^-(\ell_2) + I_G^-(\ell_1) + I_G^+(\ell_2) + I_G^+(\ell_1) \right]$$

$$+ j\text{Re} \left[I_G^-(\ell_2) - I_G^-(\ell_1) - I_G^+(\ell_2) + I_G^+(\ell_1) \right] \qquad (9.19a)$$

where

$$I_G^+(\ell) = \int_0^\infty d\zeta \, \frac{(\zeta\cos k\ell - k\sin k\ell) + j(k\cos k\ell + \zeta\sin k\ell)}{k^2+\zeta^2} \, G(j\zeta) e^{-\zeta\ell} \qquad (9.19b)$$

$$I_G^-(\ell) = I_G^+(\ell) \quad \{k \to -k\} \qquad (9.19c)$$

$$G(k_z) = \begin{cases} G_1(k_z) + j\, G_2(k_z) & , \quad k \geq k_z \\ G_3(k_z) & , \quad k \leq k_z \end{cases} \qquad (9.19d)$$

$$G_1(k_z) = k_t \cdot \frac{J_1(k_t a)J_1'(k_t a) + Y_1(k_t a)Y_1'(k_t a)}{J_1'^2(k_t a) + Y_1'^2(k_t a)} \tag{9.19e}$$

$$G_2(k_z) = \frac{2}{\pi a} \cdot \frac{1}{J_1'^2(k_t a) + Y_1'^2(k_t a)} \tag{9.19f}$$

$$G_3(k_z) = -|k_t| \frac{K_1(|k_t|a)}{K_1'(|k_t|a)} \tag{9.19g}$$

Formulas (9.17) and (9.19) have been derived from $\theta_0 = 0$. The same formulas can be applied to $\theta_0 = \pi$, after replacing k by -k.

For numerical computation the expressions derived for the integrals I_x and I_y are much more convenient than the original ones. The new expressions (9.18) and (9.19) consist of two parts. The first part is a finite integral with an oscillatory integrand. Because of finiteness of the integration domain, many efficient algorithms exist to perform the task. The second part is a linear combination of infinite integrals whose integrands are fastly decaying because of the presence of the factor $e^{-\zeta\ell}$, therefore, their numerical evaluation can be easily accomplished. It is observed that from computational points of view, (9.18) and (9.19) are much more suitable than (9.6a) and (9.18a).

Once I_x and I_y are determined, the field components can be obtained from:

$$E_x^{ax} = \frac{jM_b}{8\pi^2 a} \cdot \frac{e^{-jkr}}{r} \cdot I_x \tag{9.20a}$$

$$E_y^{ax} = \frac{-M_z}{8\pi^2} \cdot \frac{e^{-jkr}}{r} \cdot I_y \tag{9.20b}$$

It should be mentioned that the above formulas have been derived for a finite cylinder and therefore the truncation effect has already been taken into consideration. The only corrective term which should be added to (9.20) is the wedge diffracted field which has been discussed in Chapter 7.

10. NUMERICAL RESULTS

A computer program for the calculation of the far-zone radiated field has been developed based upon the expressions derived in the previous sections. The program first computes the main constituents of the total field (surface rays, wedge diffracted field, and truncation effect) and then sums them up to obtain the final value for the field. Special situations such as field evaluation in paraxial and caustic regions are being handled properly by the program itself. The complete listing of the main program with all of its subroutines and some additional clarifying remarks has been given in Appendix D.

Extensive numerical results have been obtained by this program. Only some typical results for various cases are presented here. The geometry chosen for the numerical analysis is characterized by the following parameters:

$$a = 2\lambda, \quad \ell_1 = 6\lambda, \quad \ell_2 = 2\lambda \tag{10.1}$$

All of the lengths are normalized with respect to the wavelength (λ). The numbers given in (10.1) indicate that the sample geometry is a circular cylinder of radius 2λ and length 8λ, on which a point source is placed 2λ below the upper wedge. The E-plane and H-plane far-radiated field patterns have been generated for different polarizations of an elemental dipole of unit moment, $|\vec{M}|=1$. As far as the polarization of the source is concerned, two cases, the circumferential magnetic dipole ($M_z=0$) and the axial one ($M_\phi=0$), have been studied. It is abvious that any other polarization of the source can be considered as a linear combination of the two previous cases. In each case, the graphs (Figs. 36 to 43) illustrate the variation of the amplitudes

Figure 36. $|E_\theta|$ versus θ_0(degrees) when the source is a circumferential magnetic dipole and $\ell_1=6\lambda$, $\ell_2=2\lambda$, $a=2\lambda$ for different values of ϕ_0. (Fig. 19)

a) $\phi_0=0°$, b) $\phi_0=30°$, c) $\phi_0=60°$,

d) $\phi_0=90°$ e) $\phi_0=120°$, f) $\phi_0=160°$.

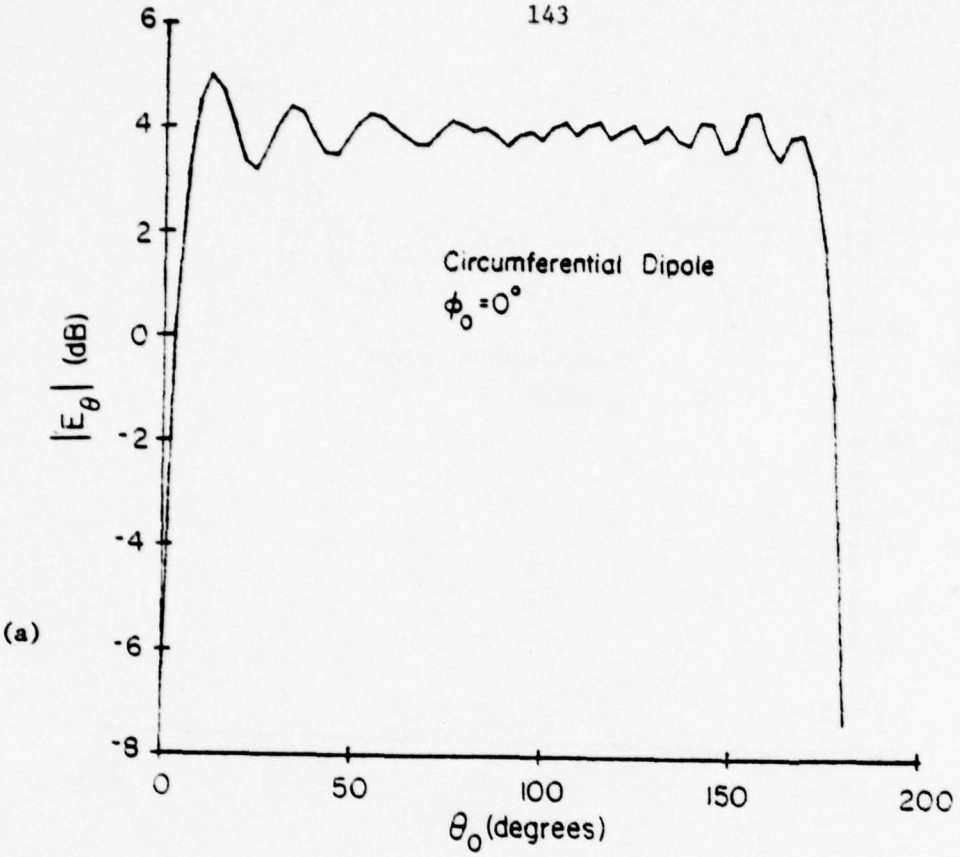
6
4
2
0
-2
-4
-6
-8
$|E_\theta|$ (dB)
Circumferential Dipole
$\phi_0 = 0°$
0
50
100
150
200
θ_0 (degrees)

(a)

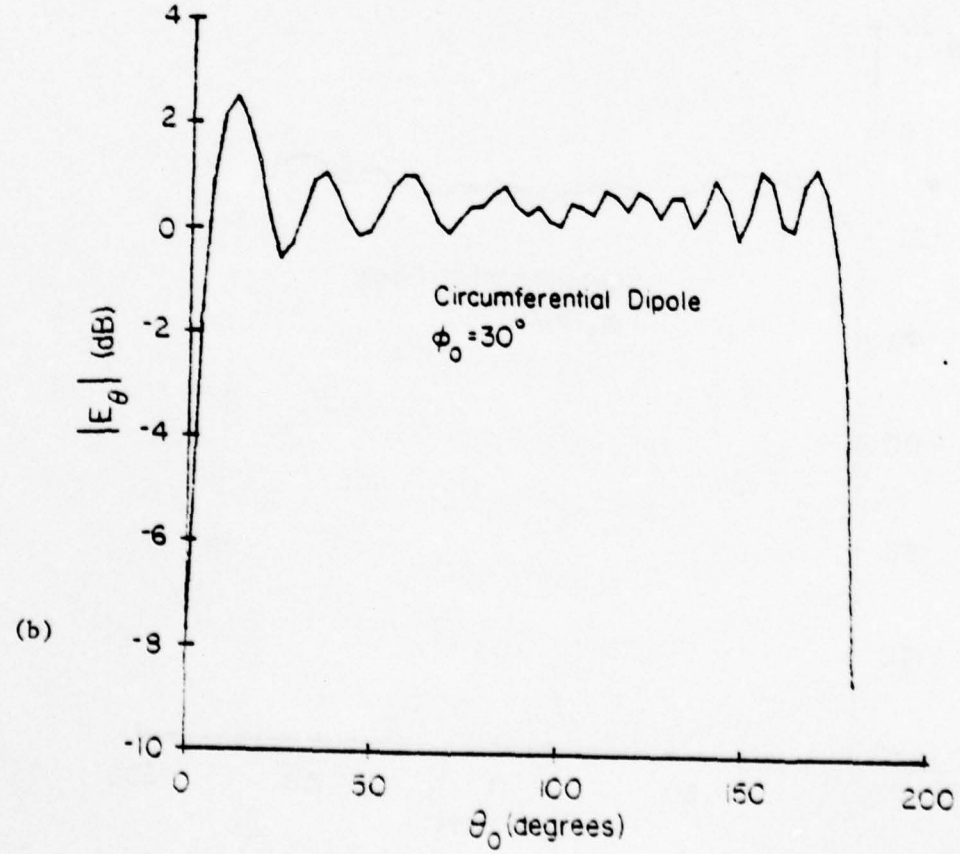
4
2
0
-2
-4
-6
-8
-10
$|E_\theta|$ (dB)
Circumferential Dipole
$\phi_0 = 30°$
0
50
100
150
200
θ_0 (degrees)

(b)

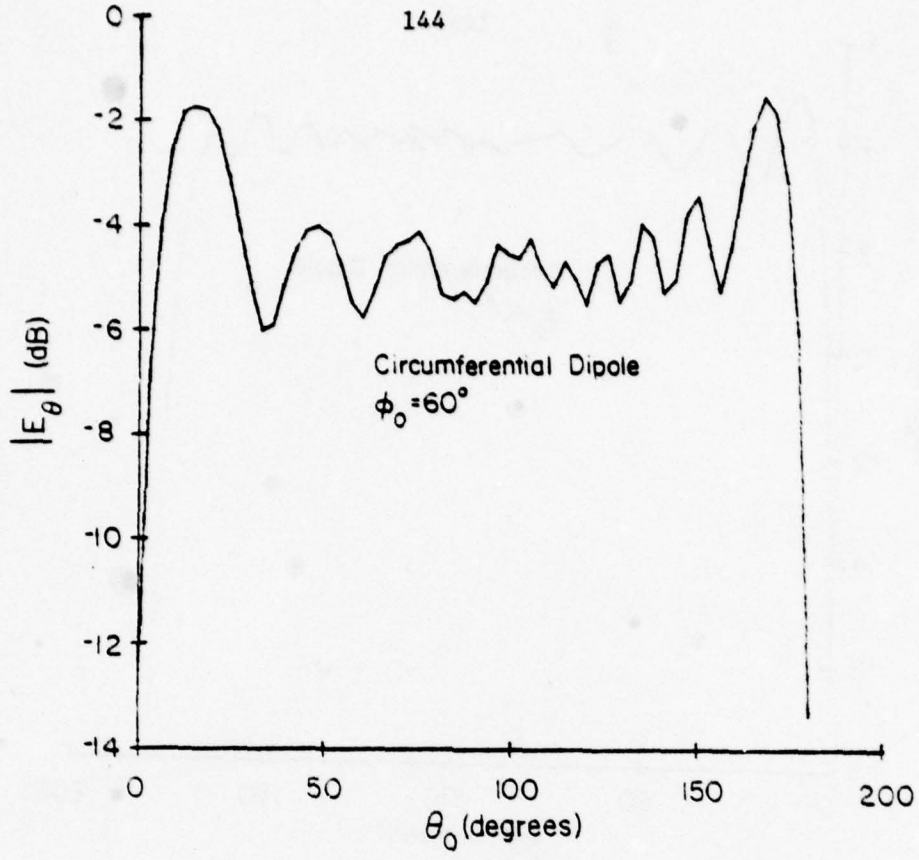
0
-2
-4
-6
-8
-10
-12
-14
$|E_\theta|$ (dB)
Circumferential Dipole
ϕ_0=60°
0
50
100
150
200
θ_0 (degrees)

(c)

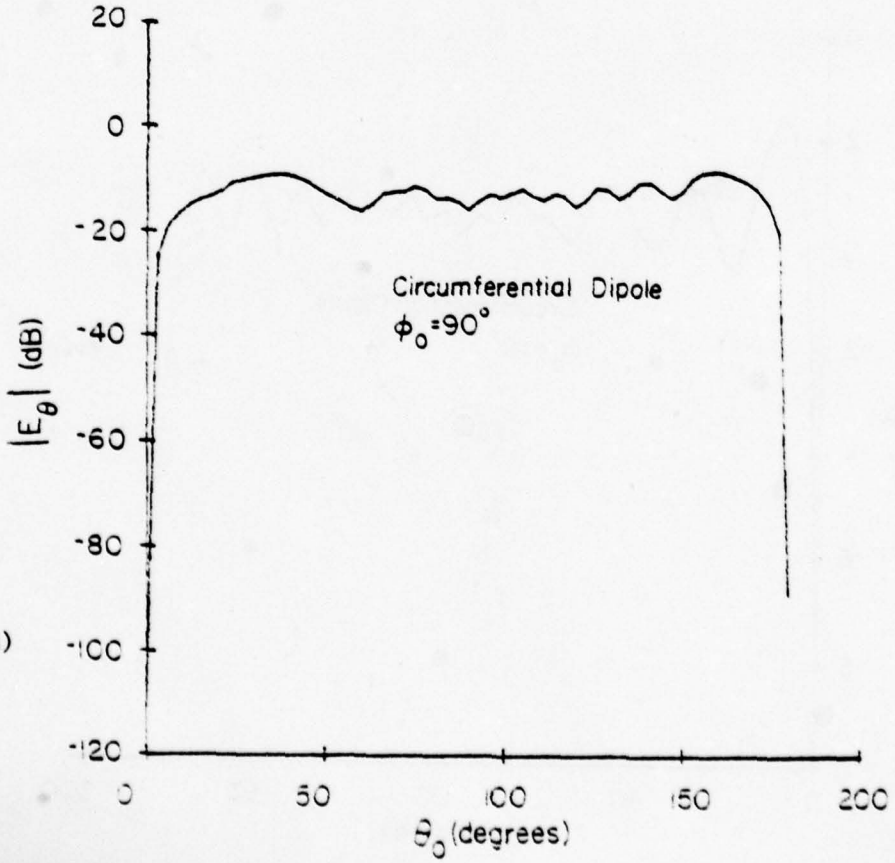
20
0
-20
-40
-60
-80
-100
-120
$|E_\theta|$ (dB)
Circumferential Dipole
ϕ_0=90°
0
50
100
150
200
θ_0 (degrees)

(d)

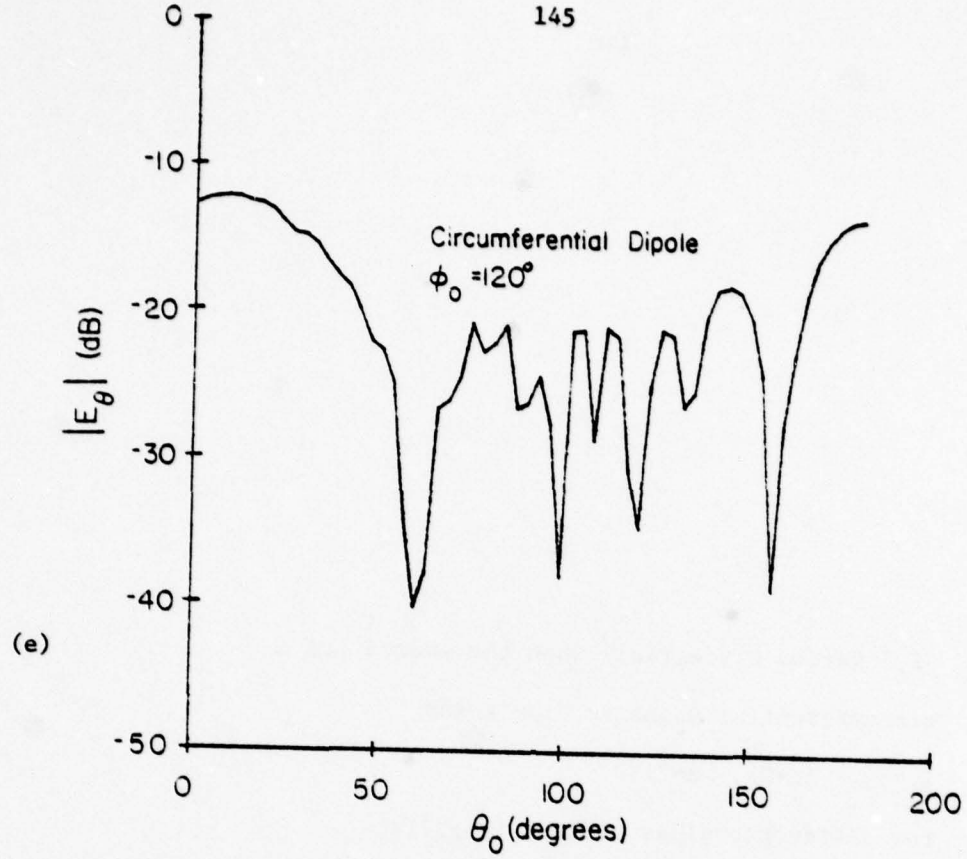
0
-10
-20
-30
-40
-50
$|E_\theta|$ (dB)
Circumferential Dipole
ϕ_0 =120°
0
50
100
150
200
θ_0 (degrees)

(e)

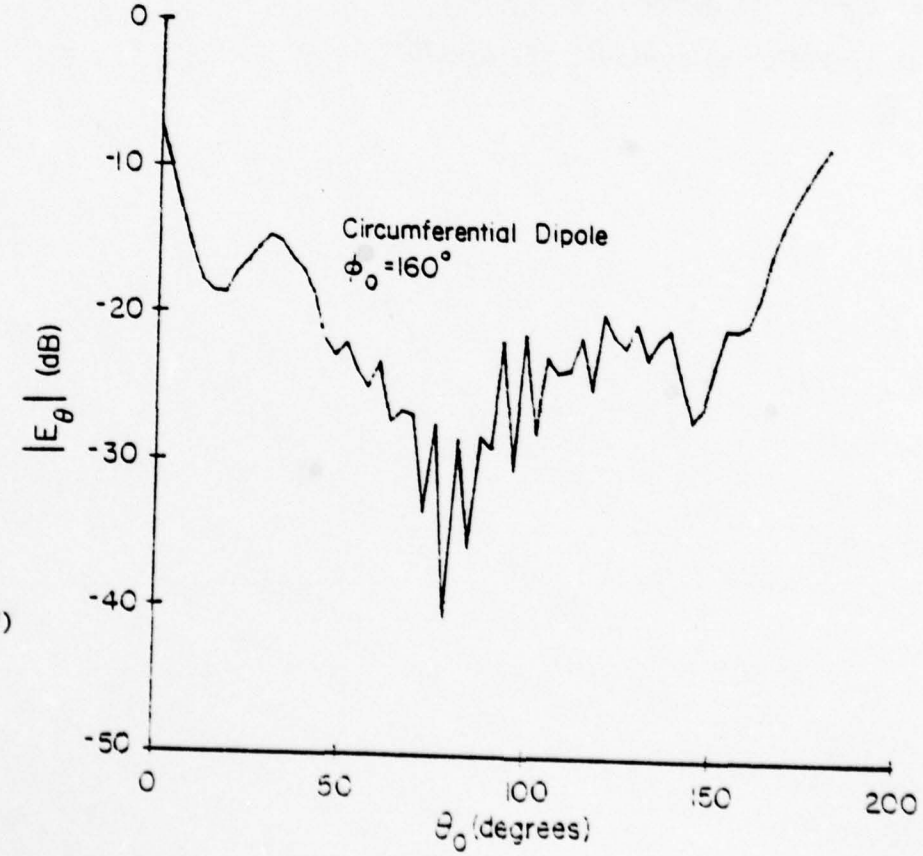
0
-10
-20
-30
-40
-50
$|E_\theta|$ (dB)
Circumferential Dipole
ϕ_0 =160°
0
50
100
150
200
θ_0 (degrees)

(f)

Figure 37. $|E_\phi|$ versus θ_0(degrees) when the source is a circumferential magnetic dipole and $\ell_1=6\lambda$, $\ell_2=2\lambda$, $a=2\lambda$ for different values of ϕ_0. (Fig. 19)
a) $\phi_0=0°$, b) $\phi_0=60°$, c) $\phi_0=90°$,
d) $\phi_0=120°$, e) $\phi_0=150°$, f) $\phi_0=170°$

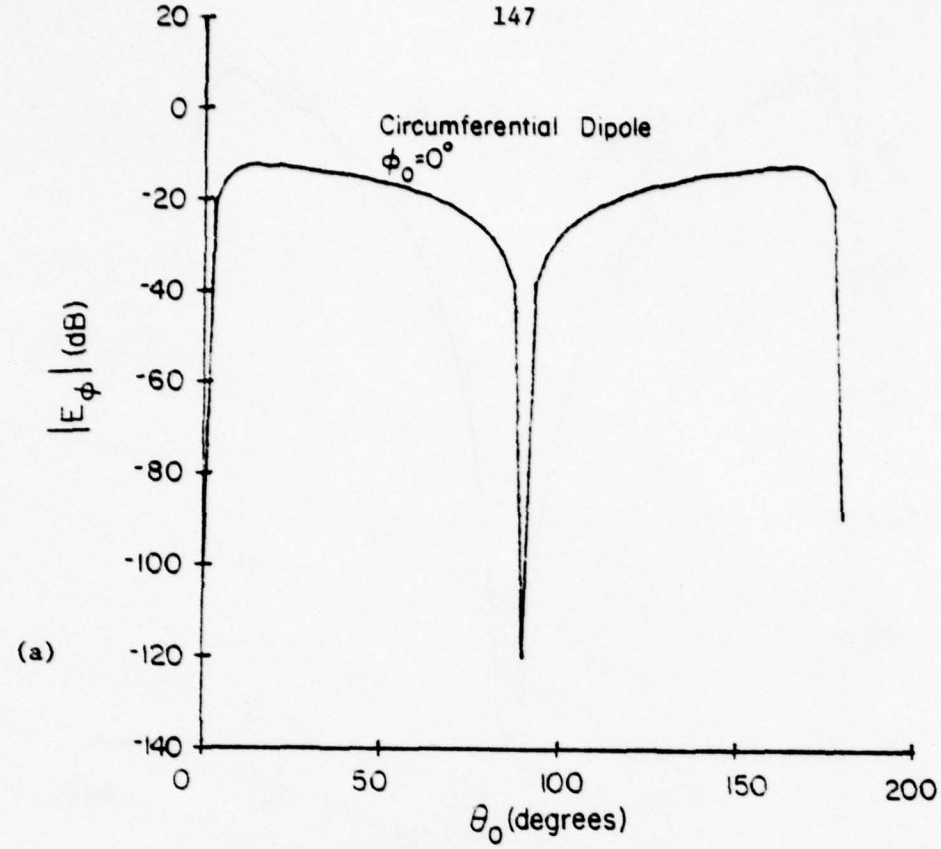
Circumferential Dipole
ϕ_0=0°
$|E_\phi|$ (dB)
20
0
-20
-40
-60
-80
-100
-120
-140
0
50
100
150
200
θ_0 (degrees)

(a)

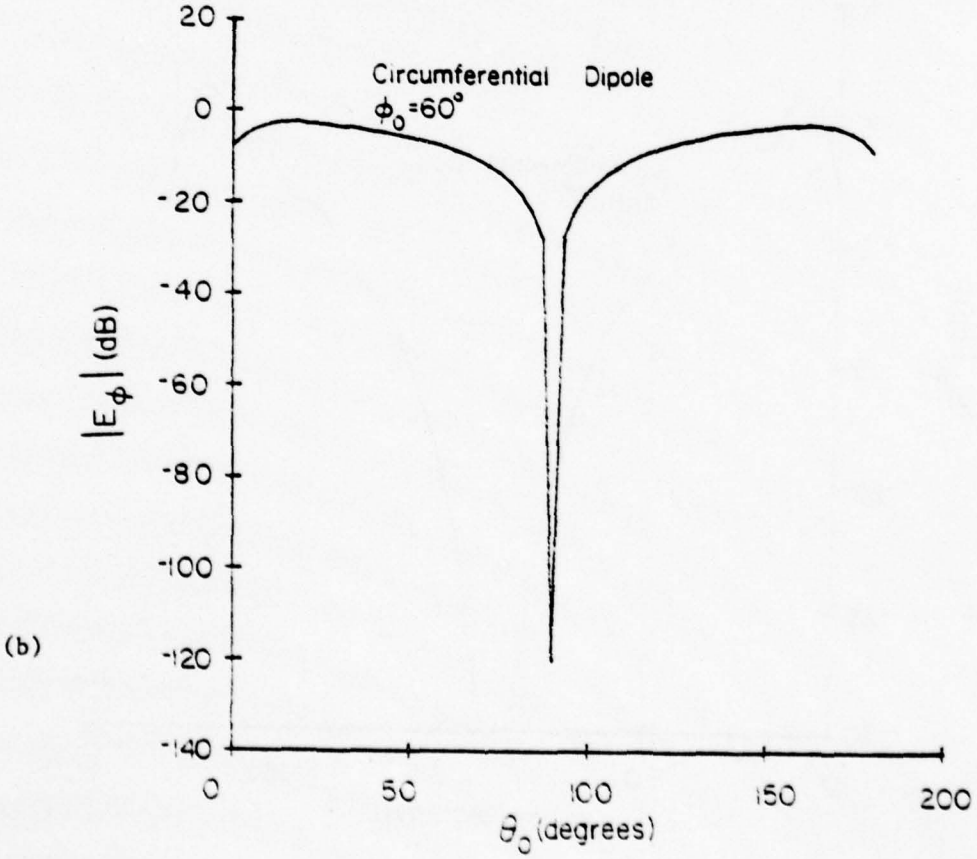
Circumferential Dipole
ϕ_0=60°
$|E_\phi|$ (dB)
20
0
-20
-40
-60
-80
-100
-120
-140
0
50
100
150
200
θ_0 (degrees)

(b)

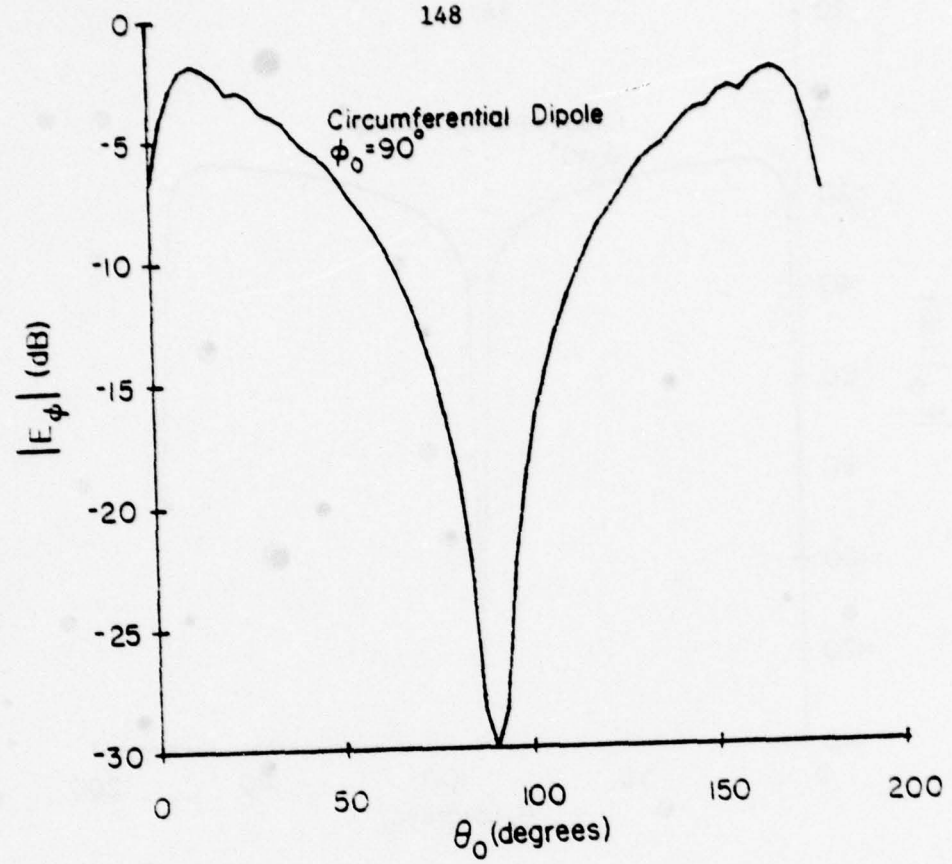
Circumferential Dipole
ϕ_0=90°
$|E_\phi|$ (dB)
0
-5
-10
-15
-20
-25
-30
0
50
100
150
200
θ_0(degrees)

(c)

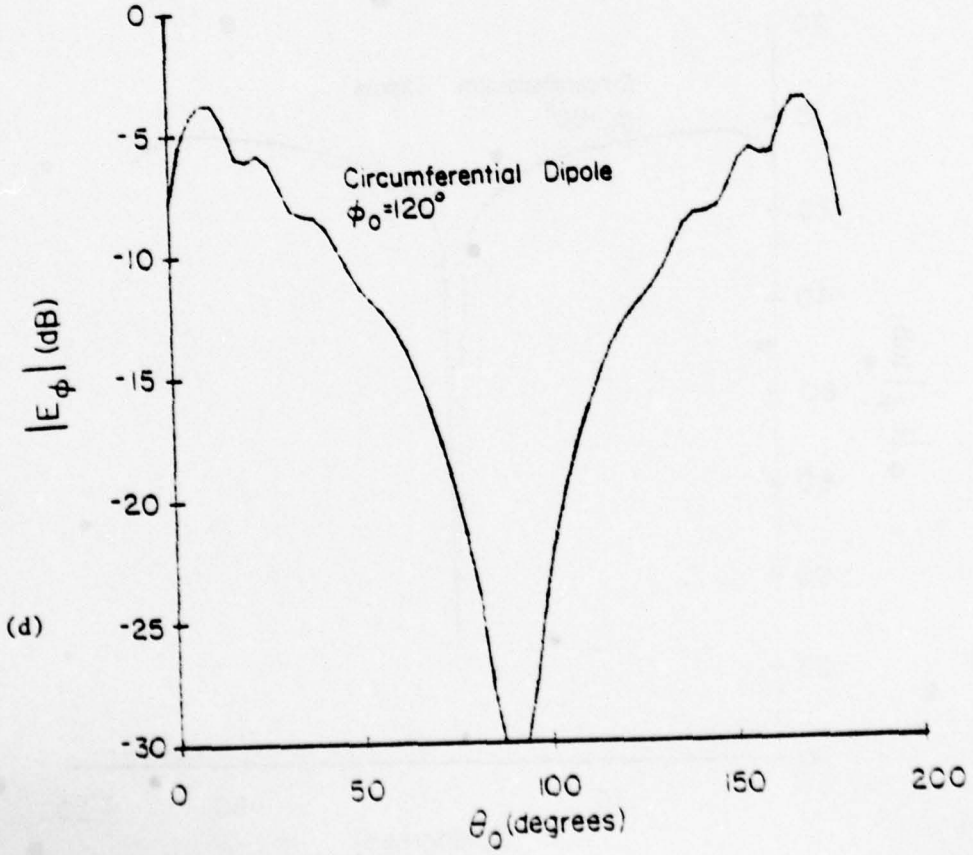
Circumferential Dipole
ϕ_0=120°
$|E_\phi|$ (dB)
0
-5
-10
-15
-20
-25
-30
0
50
100
150
200
θ_0(degrees)

(d)

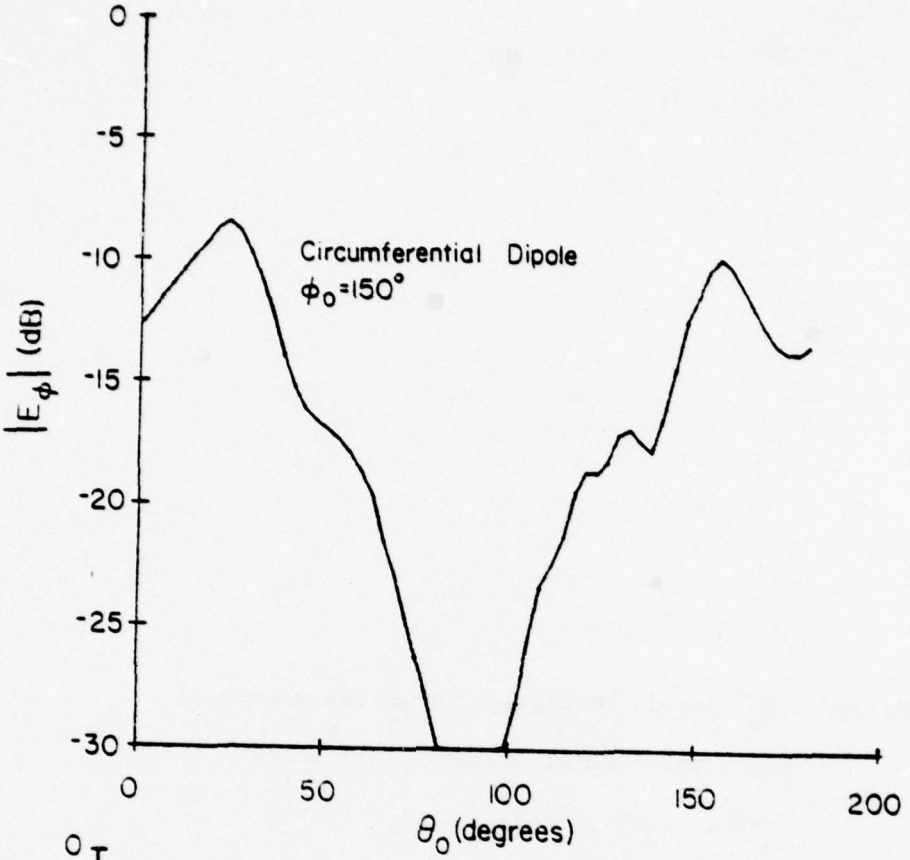
0
-5
-10
-15
-20
-25
-30
$|E_\phi|$ (dB)
Circumferential Dipole
ϕ_0=150°
0
50
100
150
200
θ_0 (degrees)

(e)

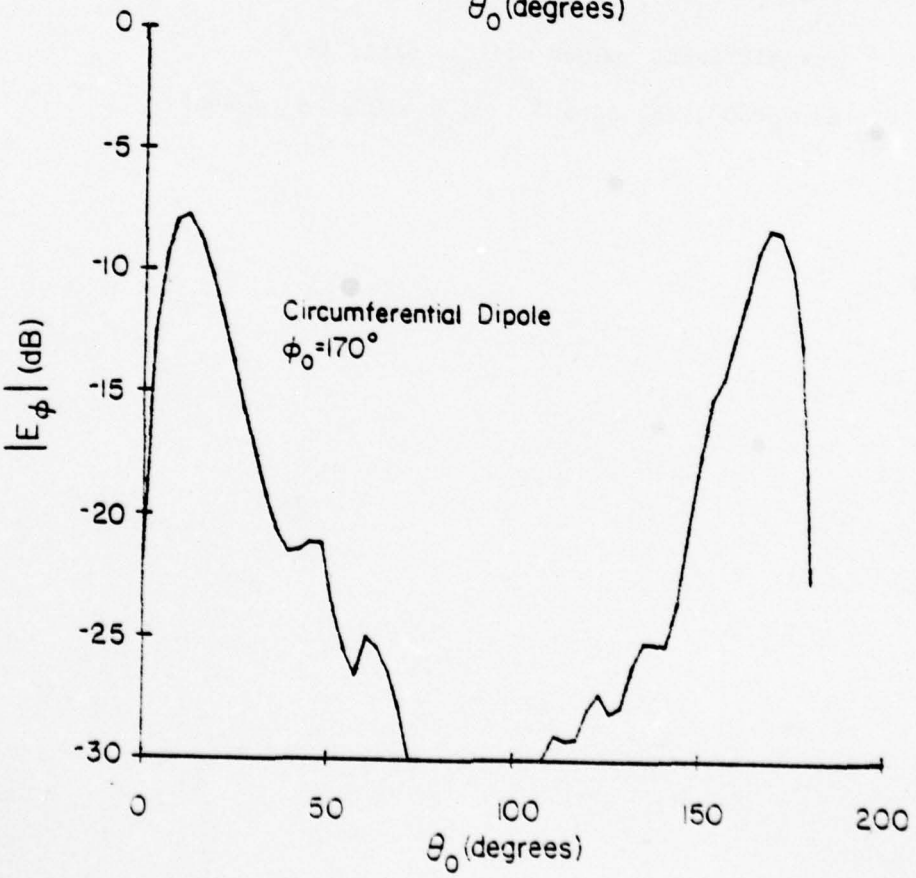
0
-5
-10
-15
-20
-25
-30
$|E_\phi|$ (dB)
Circumferential Dipole
ϕ_0=170°
0
50
100
150
200
θ_0 (degrees)

(f)

Figure 38. $|E_\theta|$ versus ϕ_0(degrees) when the source is a circumferential magnetic dipole and $\ell_1=6\lambda$, $\ell_2=2\lambda$, $a=2\lambda$ for different values of θ_0. (Fig. 19)
a) $\theta_0=30°$, b) $\theta_0=50°$, c) $\theta_0=70°$, d) $\theta_0=90°$

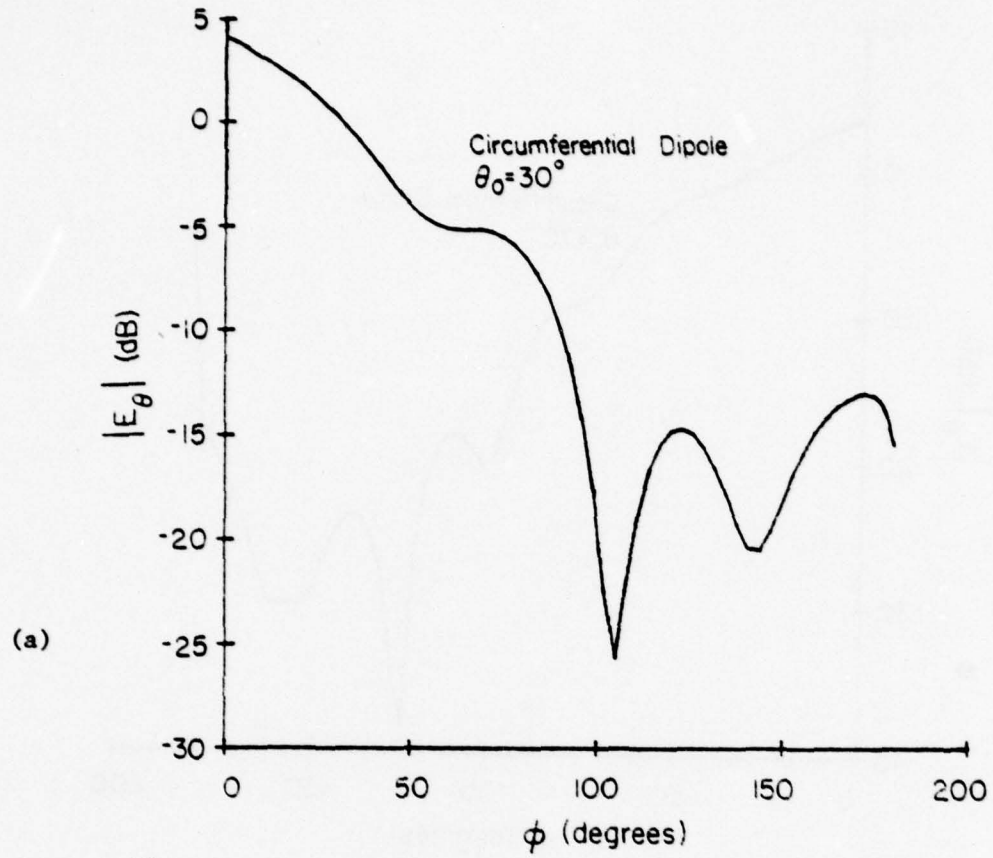
Circumferential Dipole
θ_0=30°
$|E_\theta|$ (dB)
5
0
-5
-10
-15
-20
-25
-30
0
50
100
150
200
ϕ (degrees)

(a)

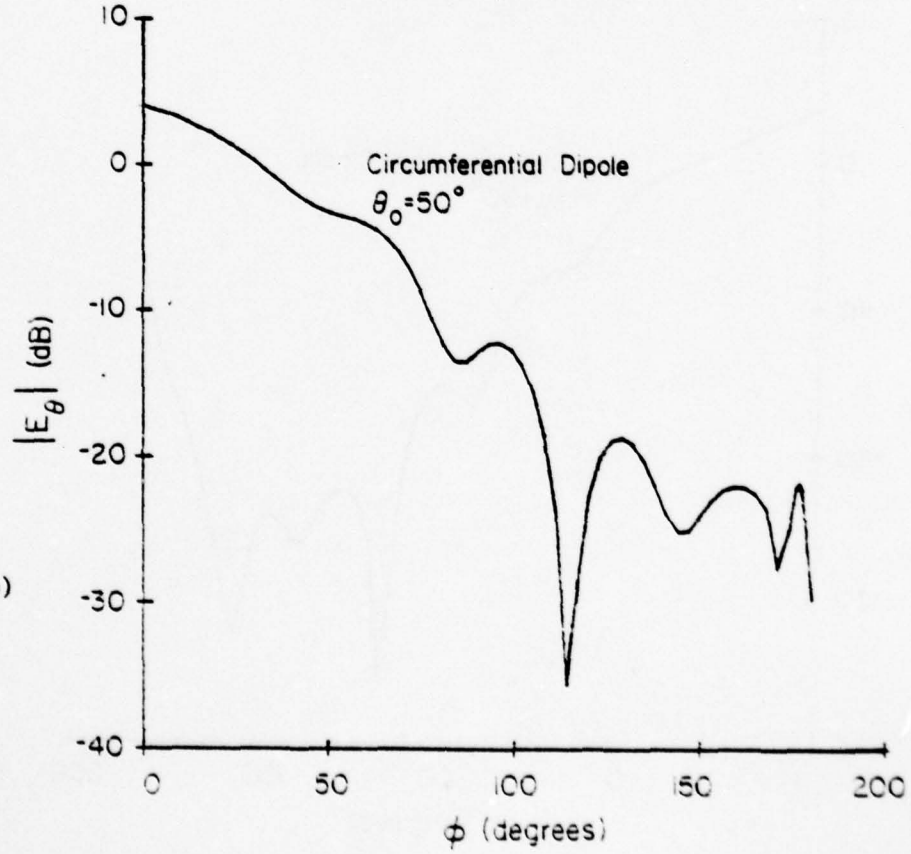
Circumferential Dipole
θ_0=50°
$|E_\theta|$ (dB)
10
0
-10
-20
-30
-40
0
50
100
150
200
ϕ (degrees)

(b)

(c)

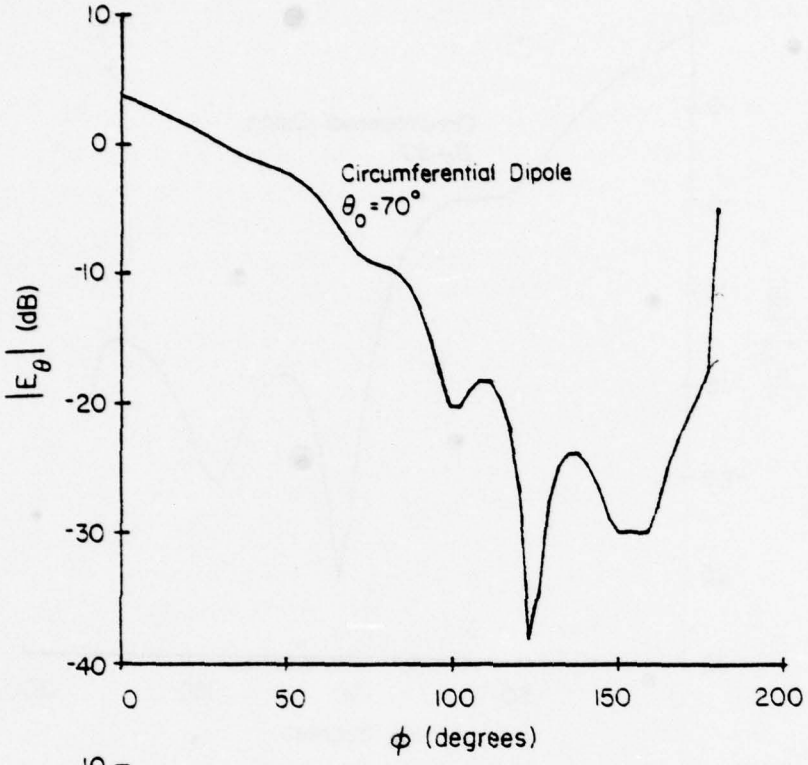
Circumferential Dipole
θ_0=70°
$|E_\theta|$ (dB)
10
0
-10
-20
-30
-40
0
50
100
150
200
ϕ (degrees)

(d)

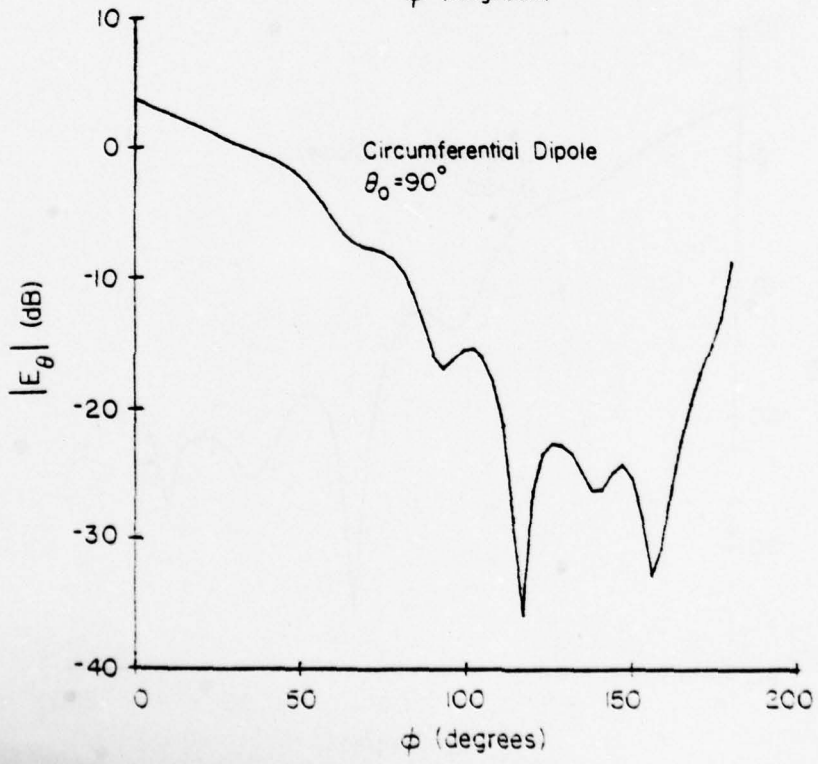
Circumferential Dipole
θ_0=90°
$|E_\theta|$ (dB)
10
0
-10
-20
-30
-40
0
50
100
150
200
ϕ (degrees)

Figure 39. $|E_\phi|$ versus ϕ_0 (degrees) when the source is a circumferential magnetic dipole and $\ell_1=6\lambda$, $\ell_2=2\lambda$, $a=2\lambda$ for different values of θ_0. (Fig. 19)

a) $\theta_0=30°$, b) $\theta_0=50°$, c) $\theta_0=70°$, d) $\theta_0=80°$.

(a)

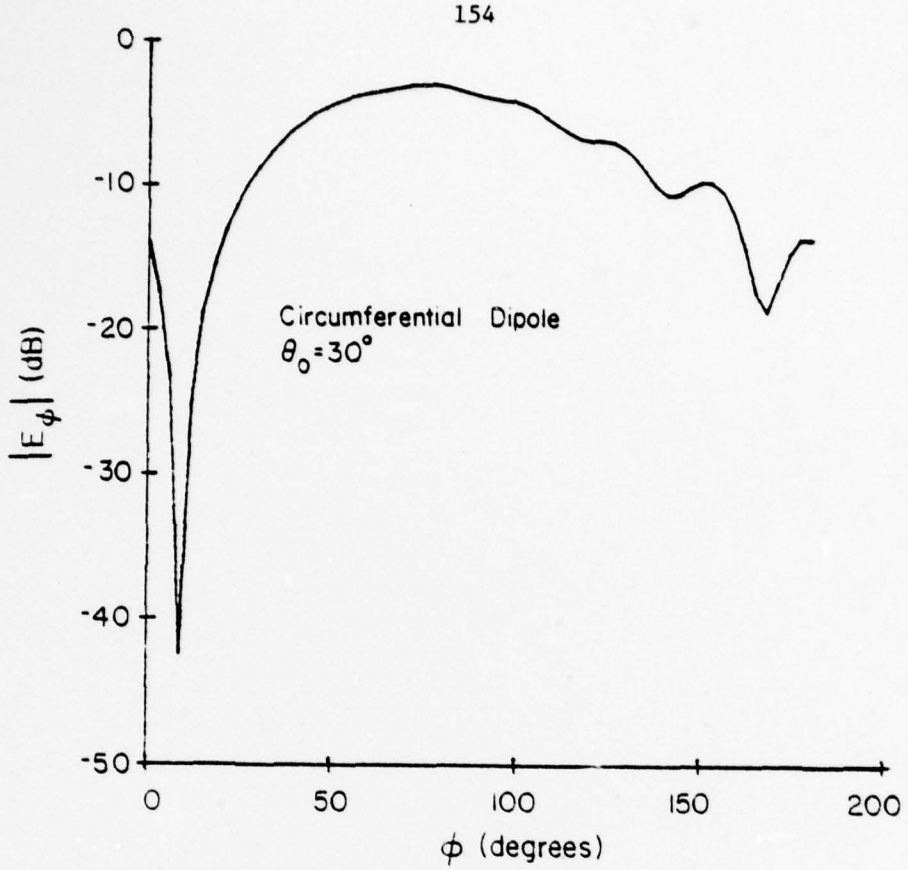
0
-10
-20
-30
-40
-50
$|E_\phi|$ (dB)
Circumferential Dipole
$\theta_0 = 30°$
0
50
100
150
200
ϕ (degrees)

(b)

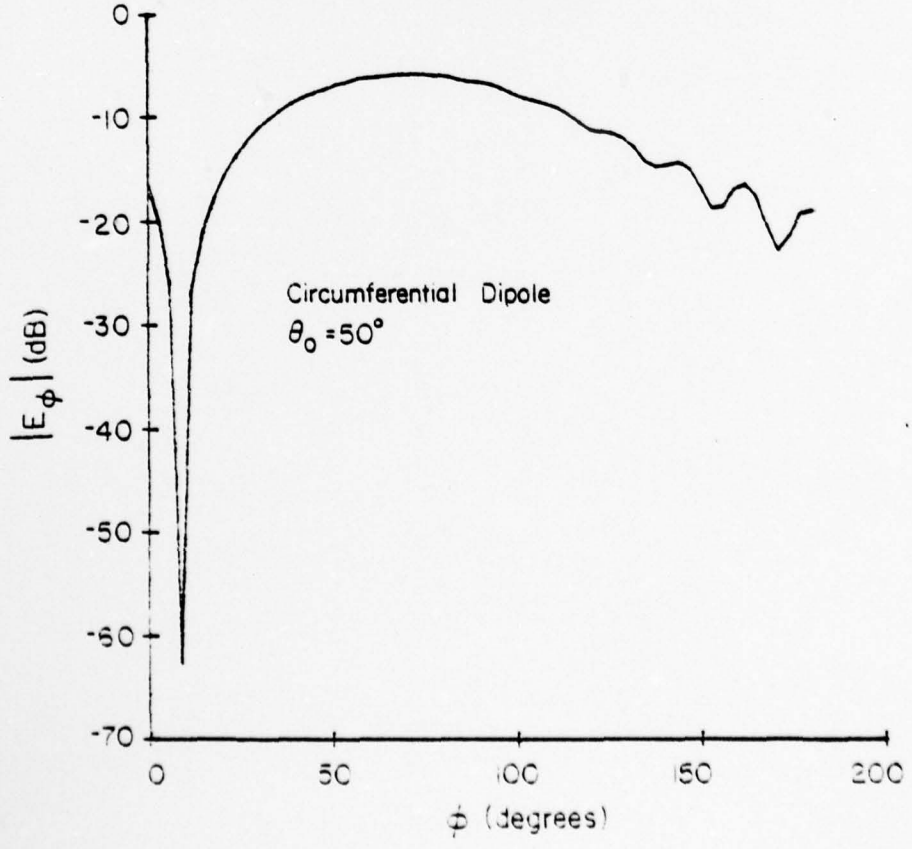
0
-10
-20
-30
-40
-50
-60
-70
$|E_\phi|$ (dB)
Circumferential Dipole
$\theta_0 = 50°$
0
50
100
150
200
ϕ (degrees)

(c)

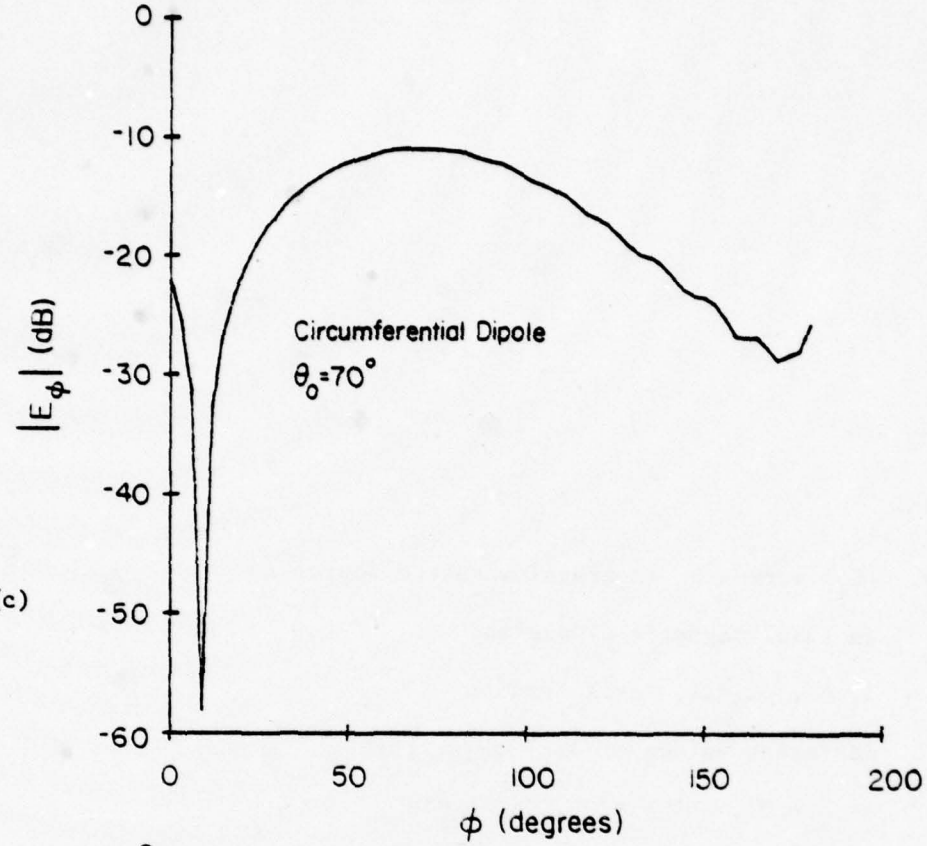
0
-10
-20
-30
-40
-50
-60
$|E_\phi|$ (dB)
Circumferential Dipole
θ_0=70°
0
50
100
150
200
ϕ (degrees)

(d)

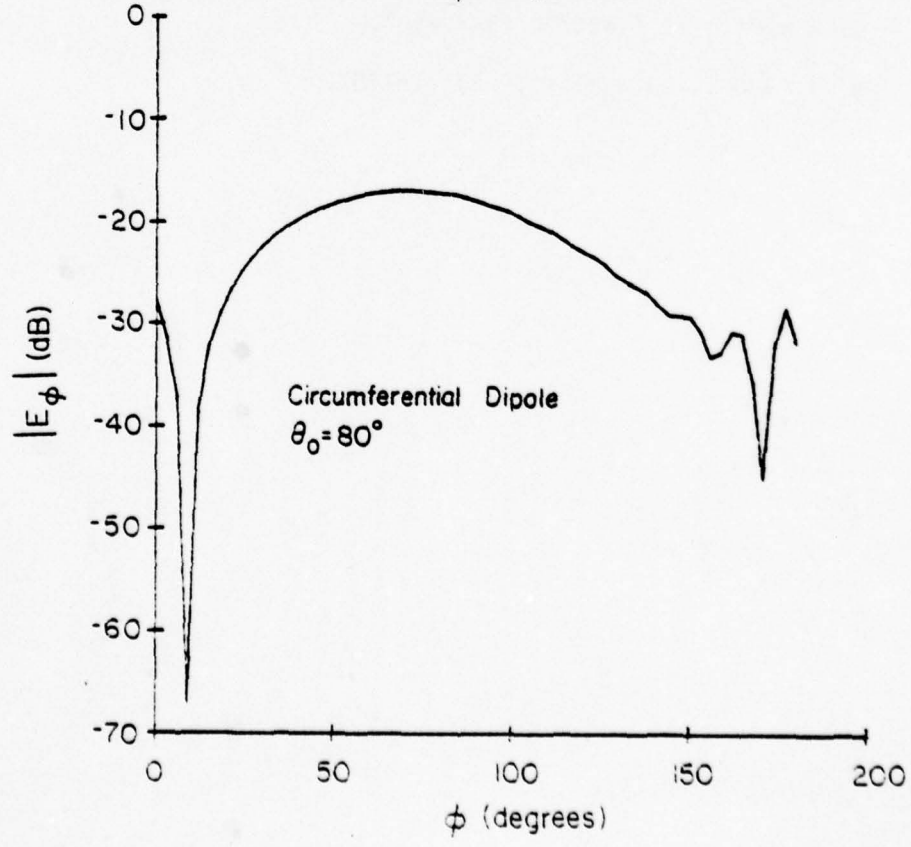
0
-10
-20
-30
-40
-50
-60
-70
$|E_\phi|$ (dB)
Circumferential Dipole
θ_0=80°
0
50
100
150
200
ϕ (degrees)

Figure 40. $|E_\phi|$ versus θ_0 (degrees) when the source is an axial magnetic dipole and $\ell_1=6\lambda$, $\ell_2=2\lambda$, $a=2\lambda$ for different values of ϕ_0. (Fig. 19)

a) $\phi_0=10°$, b) $\phi_0=20°$, c) $\phi_0=50°$

d) $\phi_0=70°$, e) $\phi_0=80°$, f) $\phi_0=90°$,

g) $\phi_0=120°$, h) $\phi_0=150°$, i) $\phi_0=170°$.

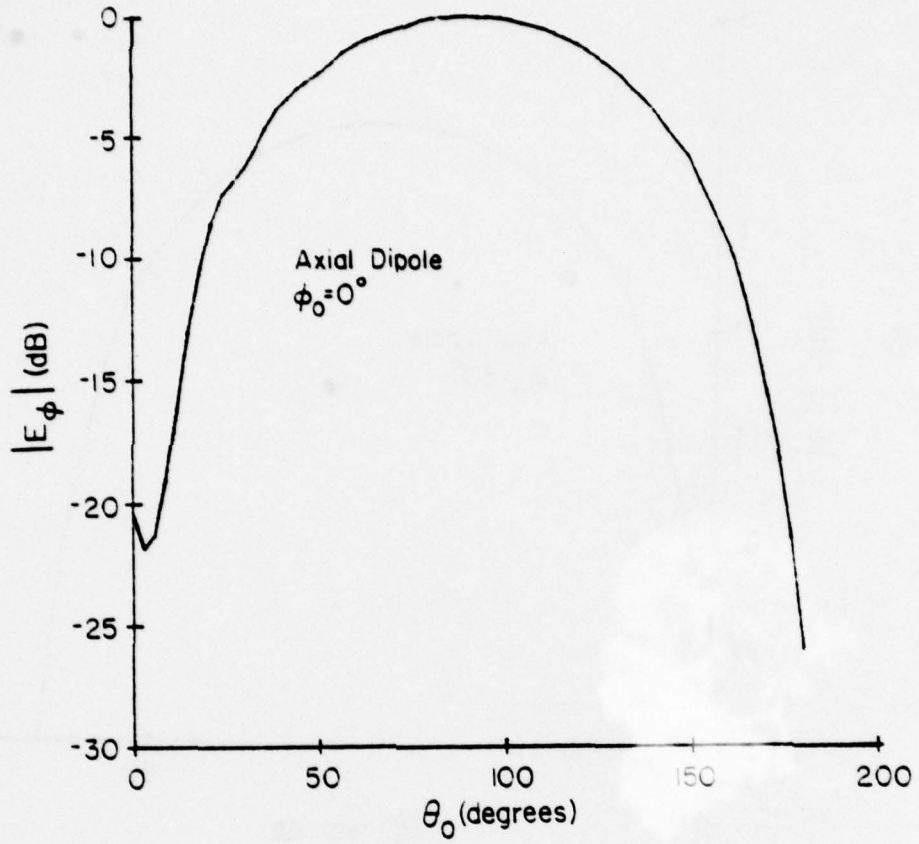
0
-5
-10
-15
-20
-25
-30
$|E_\phi|$ (dB)
Axial Dipole
$\phi_0=0°$
0
50
100
150
200
θ_0 (degrees)

(a)

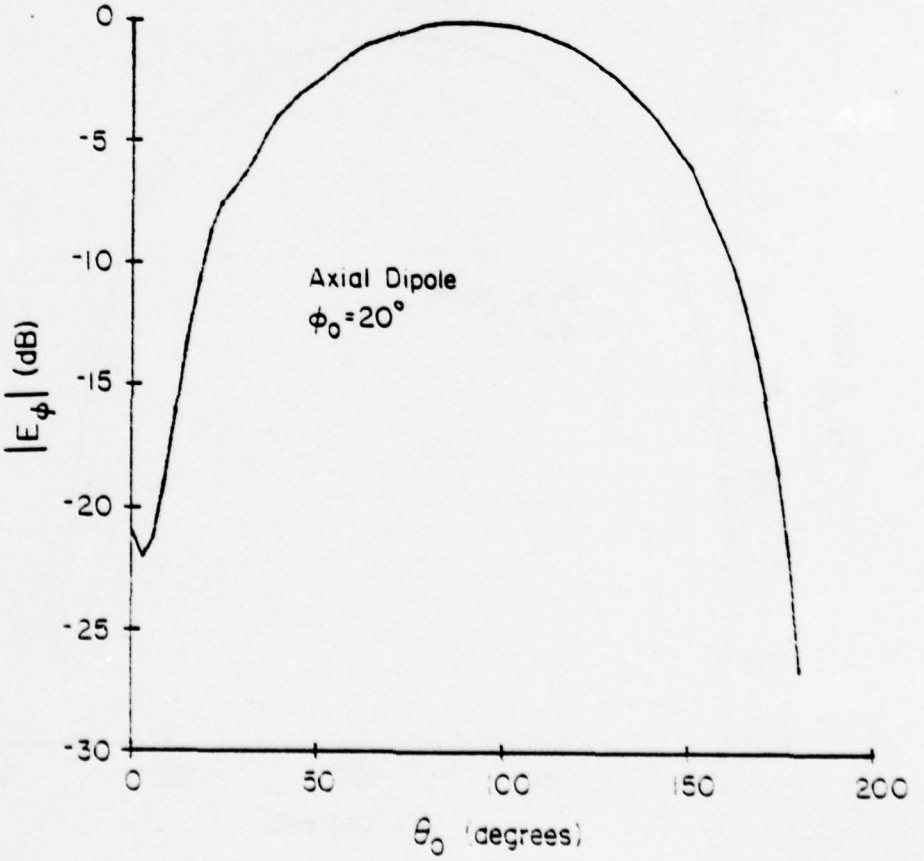
0
-5
-10
-15
-20
-25
-30
$|E_\phi|$ (dB)
Axial Dipole
$\phi_0=20°$
0
50
100
150
200
θ_0 (degrees)

(b)

(c)

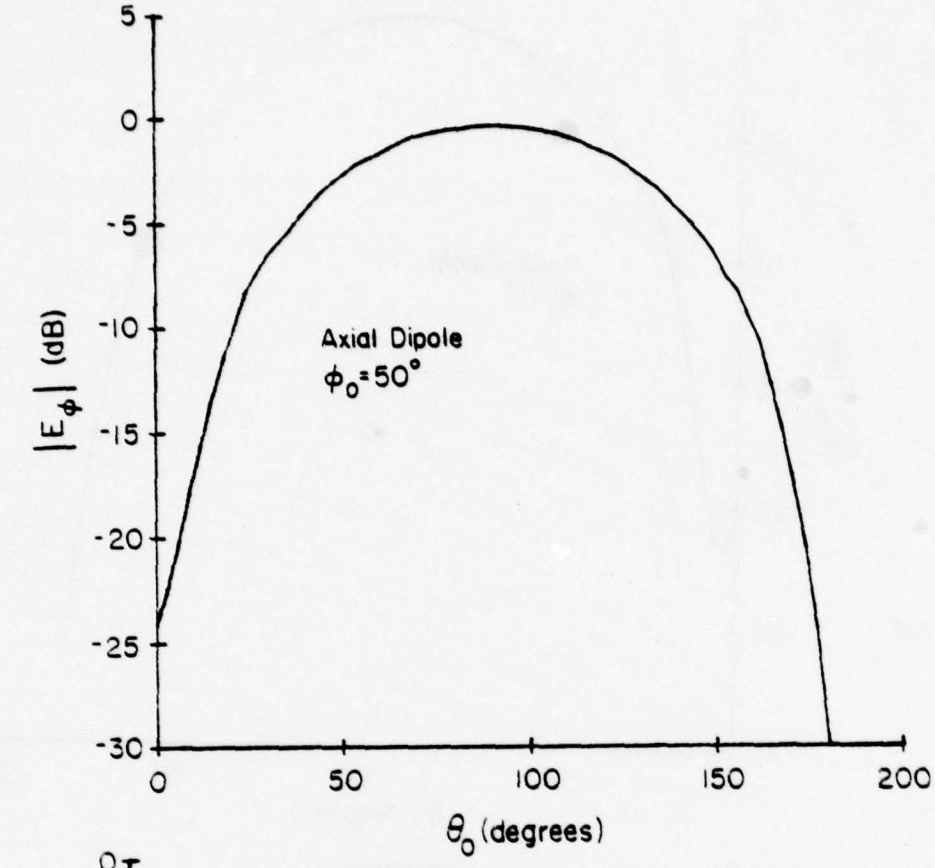
5
0
-5
-10
-15
-20
-25
-30
$|E_\phi|$ (dB)
Axial Dipole
$\phi_0 = 50°$
0
50
100
150
200
θ_0 (degrees)

(d)

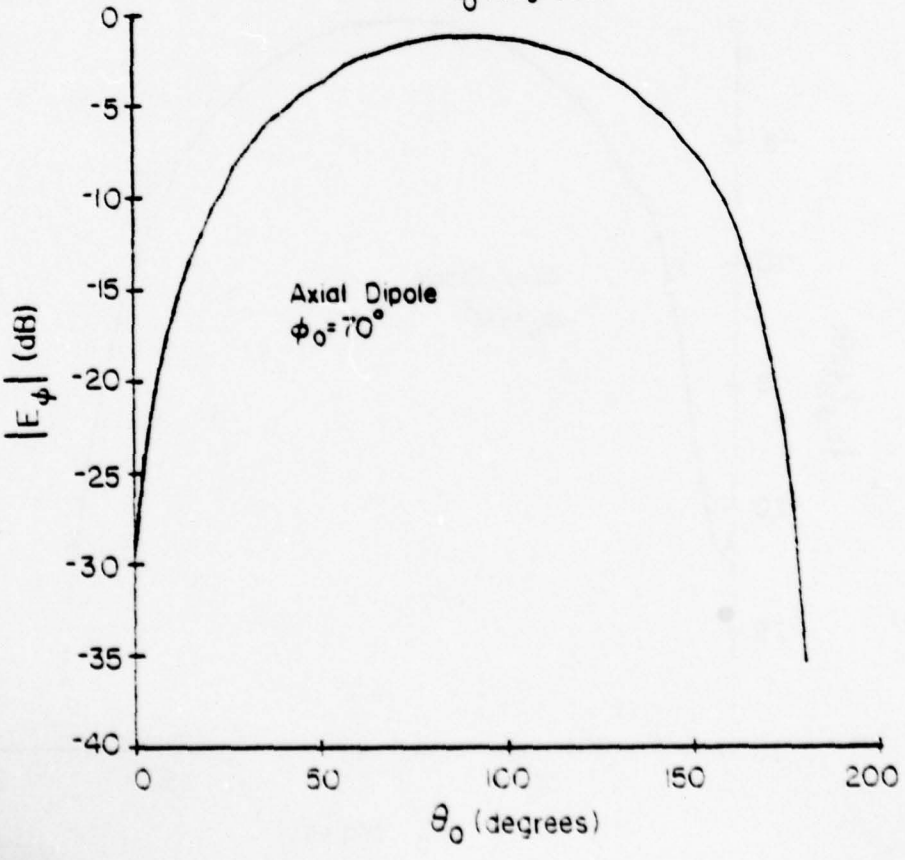
0
-5
-10
-15
-20
-25
-30
-35
-40
$|E_\phi|$ (dB)
Axial Dipole
$\phi_0 = 70°$
0
50
100
150
200
θ_0 (degrees)

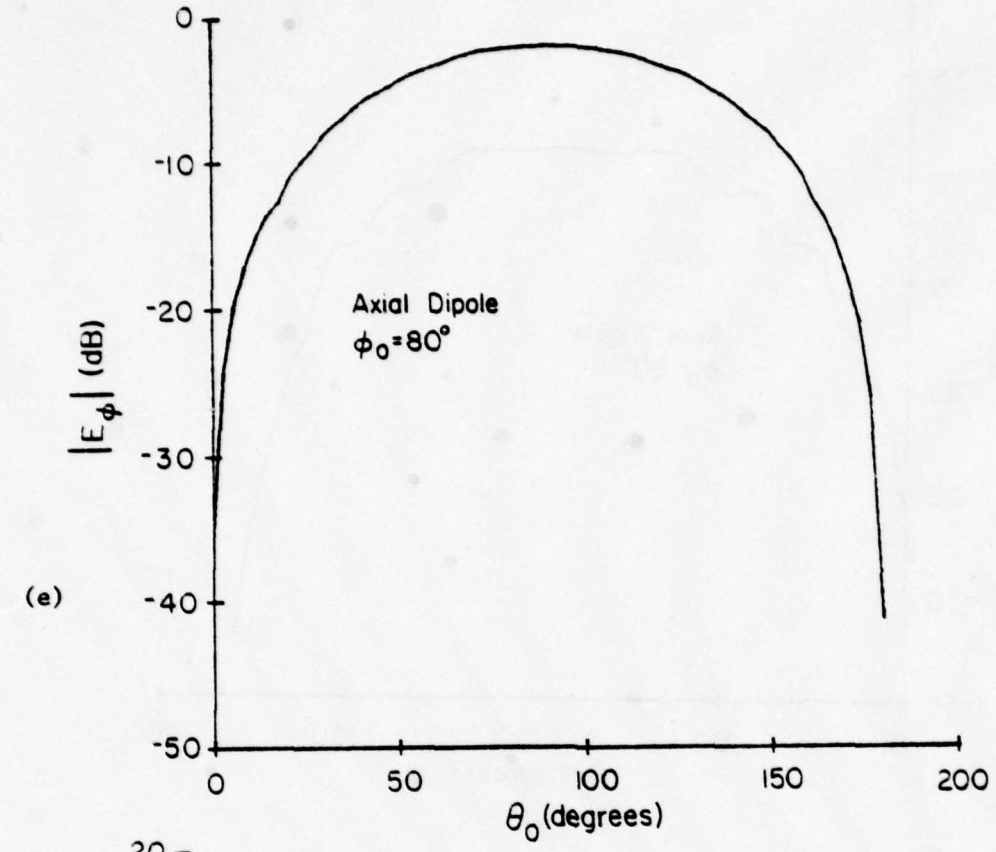
0
-10
-20
-30
-40
-50
$|E_\phi|$ (dB)
Axial Dipole
$\phi_0=80°$
0
50
100
150
200
θ_0 (degrees)

(e)

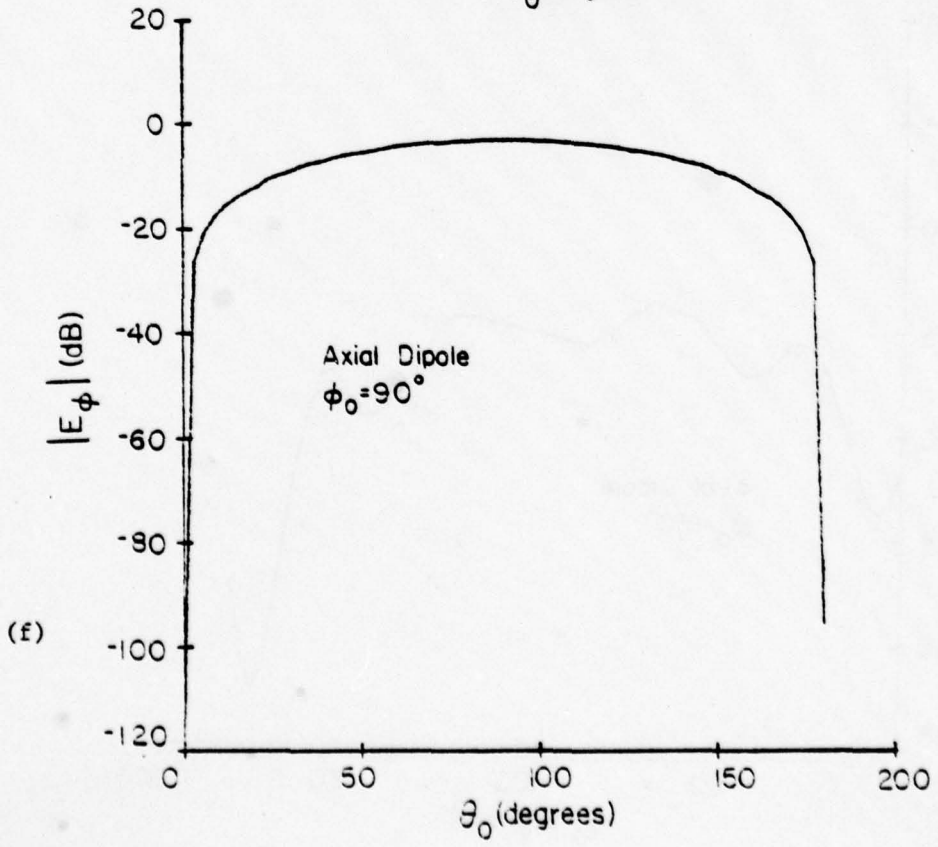
20
0
-20
-40
-60
-80
-100
-120
$|E_\phi|$ (dB)
Axial Dipole
$\phi_0=90°$
0
50
100
150
200
θ_0 (degrees)

(f)

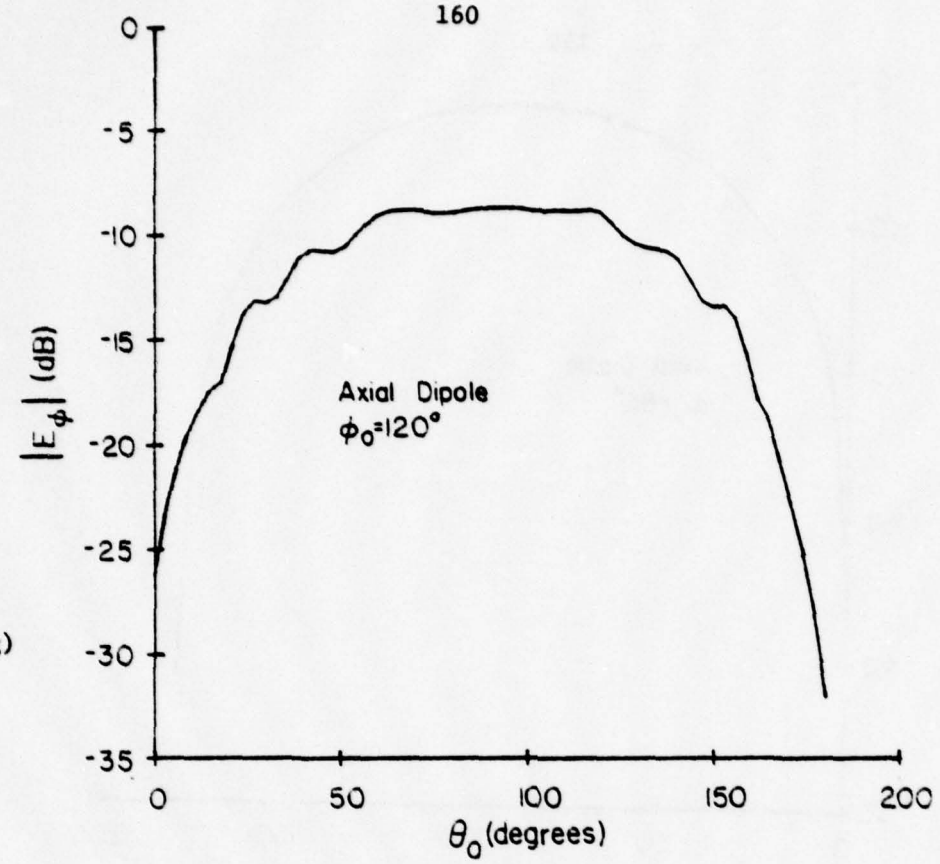
0
-5
-10
-15
-20
-25
-30
-35
$|E_\phi|$ (dB)
Axial Dipole
ϕ_0=120°
0
50
100
150
200
θ_0 (degrees)

(g)

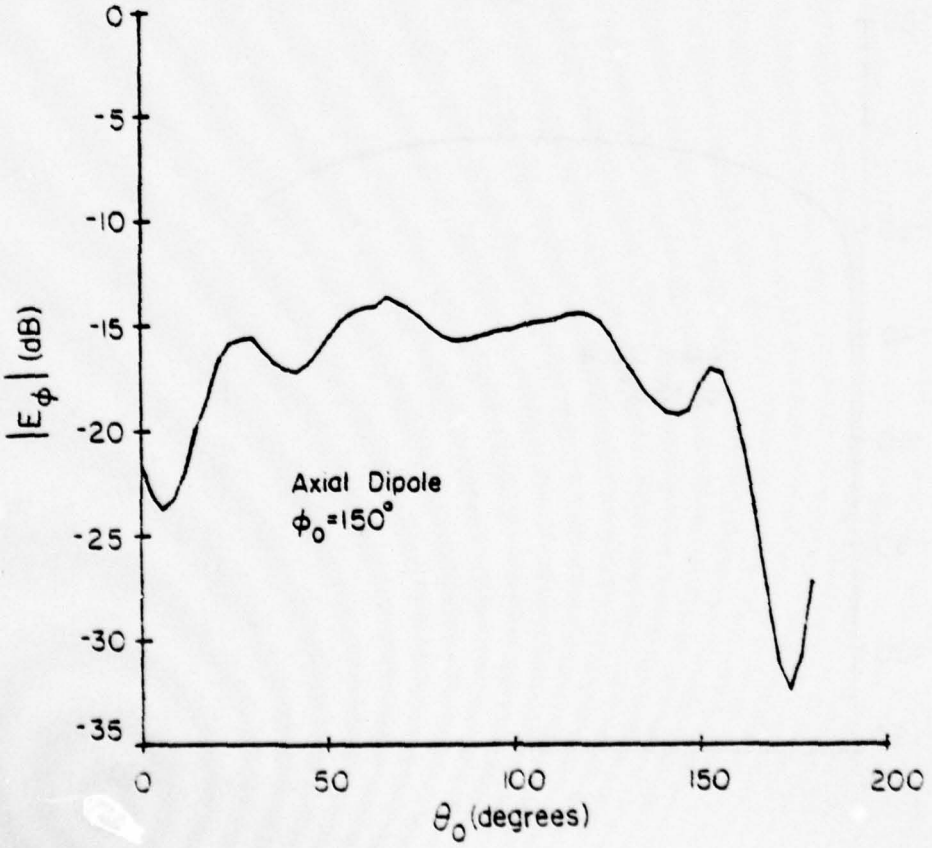
0
-5
-10
-15
-20
-25
-30
-35
$|E_\phi|$ (dB)
Axial Dipole
ϕ_0=150°
0
50
100
150
200
θ_0 (degrees)

(h)

(i)

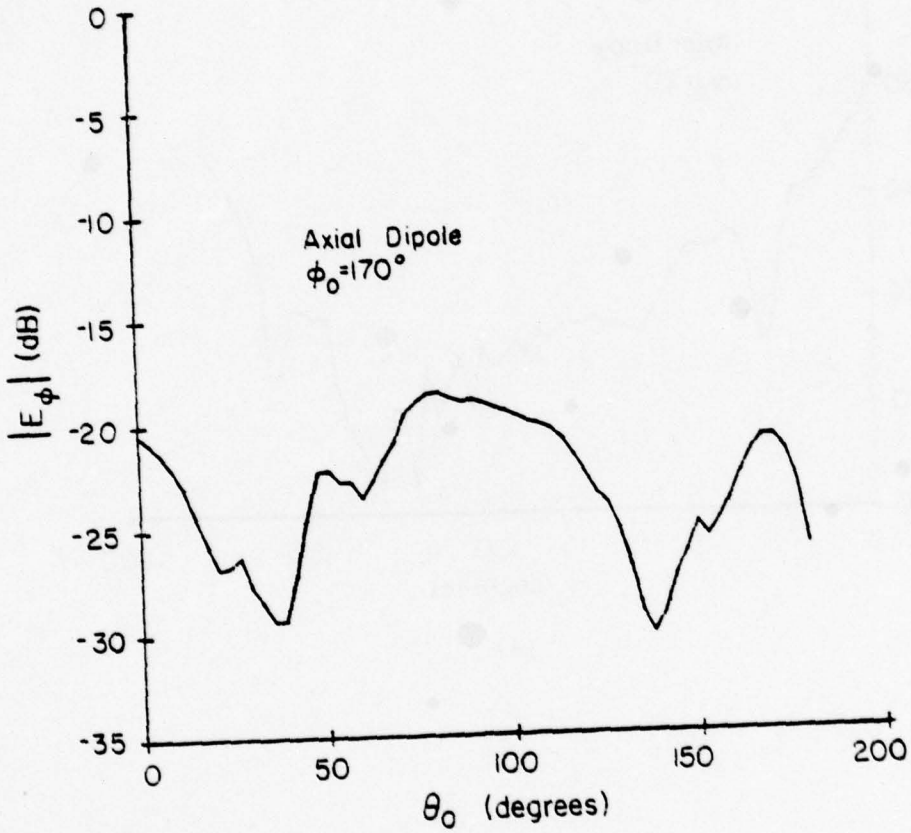
Axial Dipole
ϕ_0=170°
$|E_\phi|$ (dB)
0
-5
-10
-15
-20
-25
-30
-35
0
50
100
150
200
θ_0 (degrees)

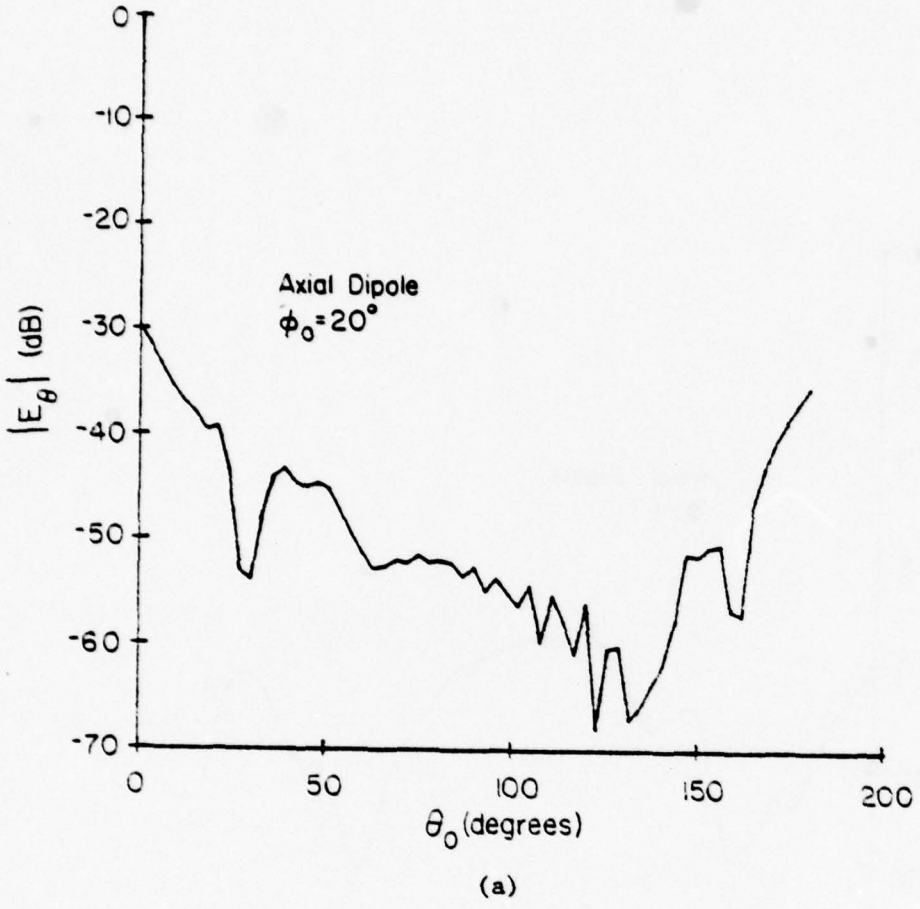

(a)

Figure 41. $|E_\theta|$ versus θ_0 (degrees) when the source is an axial magnetic dipole and $\ell_1=6\lambda$, $\ell_2=2\lambda$, $a=2\lambda$ for different values of ϕ_0. (Fig. 19)

a) $\phi_0=20°$, b) $\phi_0=40°$, c) $\phi_0=70°$, d) $\phi_0=120°$

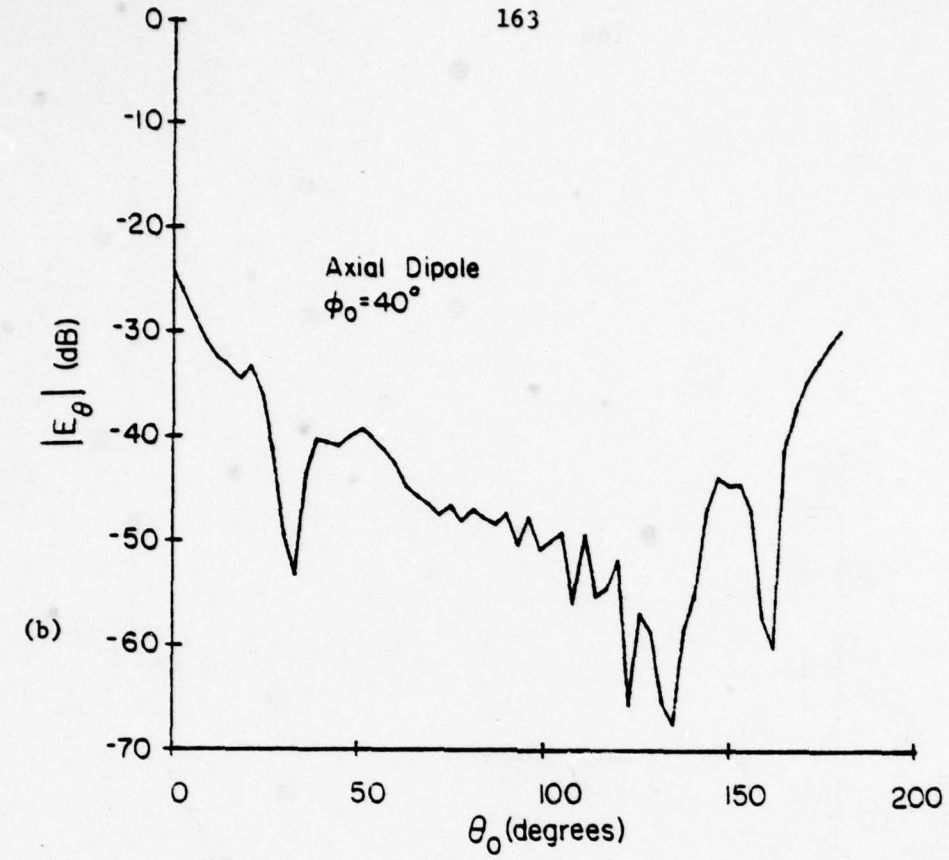
0
-10
-20
-30
-40
-50
-60
-70
Axial Dipole
$\phi_0 = 40°$
$|E_\theta|$ (dB)
0
50
100
150
200
θ_0 (degrees)

(b)

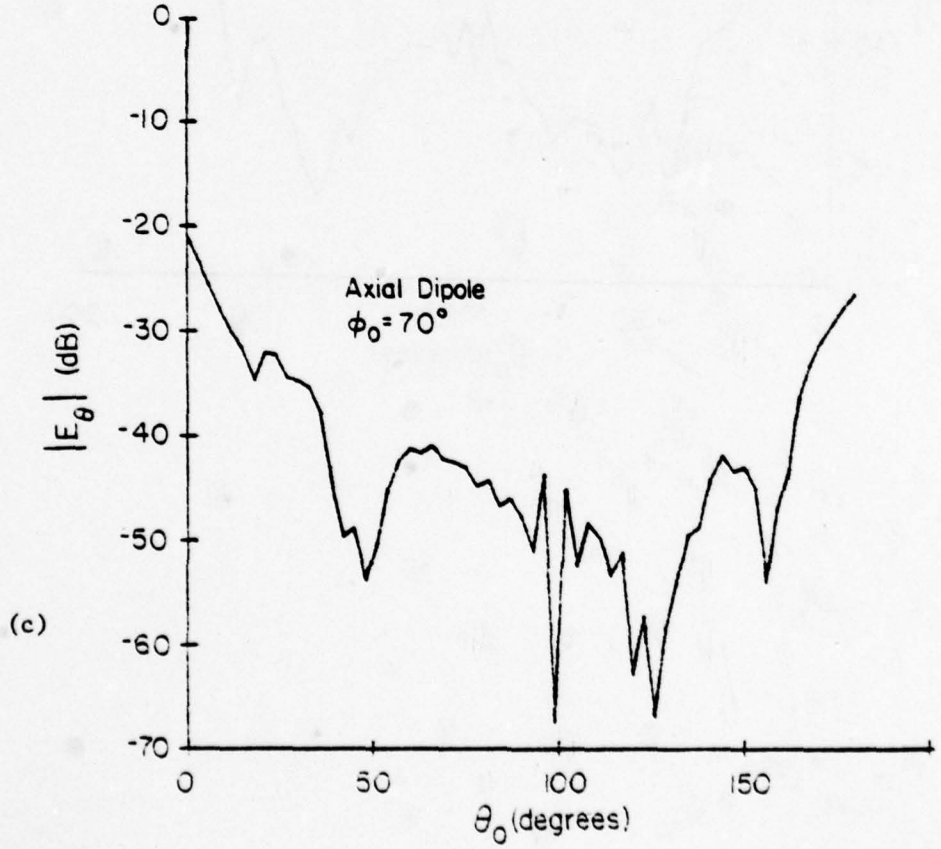
0
-10
-20
-30
-40
-50
-60
-70
Axial Dipole
$\phi_0 = 70°$
$|E_\theta|$ (dB)
0
50
100
150
θ_0 (degrees)

(c)

(d)

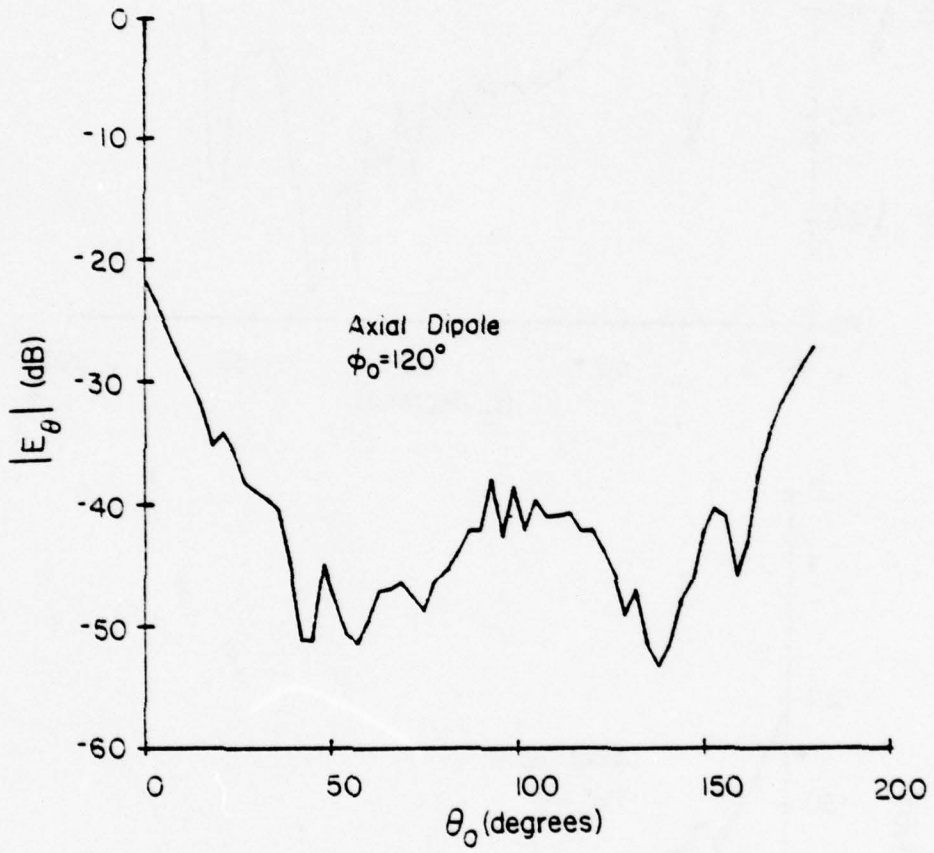
0
-10
-20
-30
-40
-50
-60
$|E_\theta|$ (dB)
Axial Dipole
ϕ_0=120°
0
50
100
150
200
θ_0 (degrees)

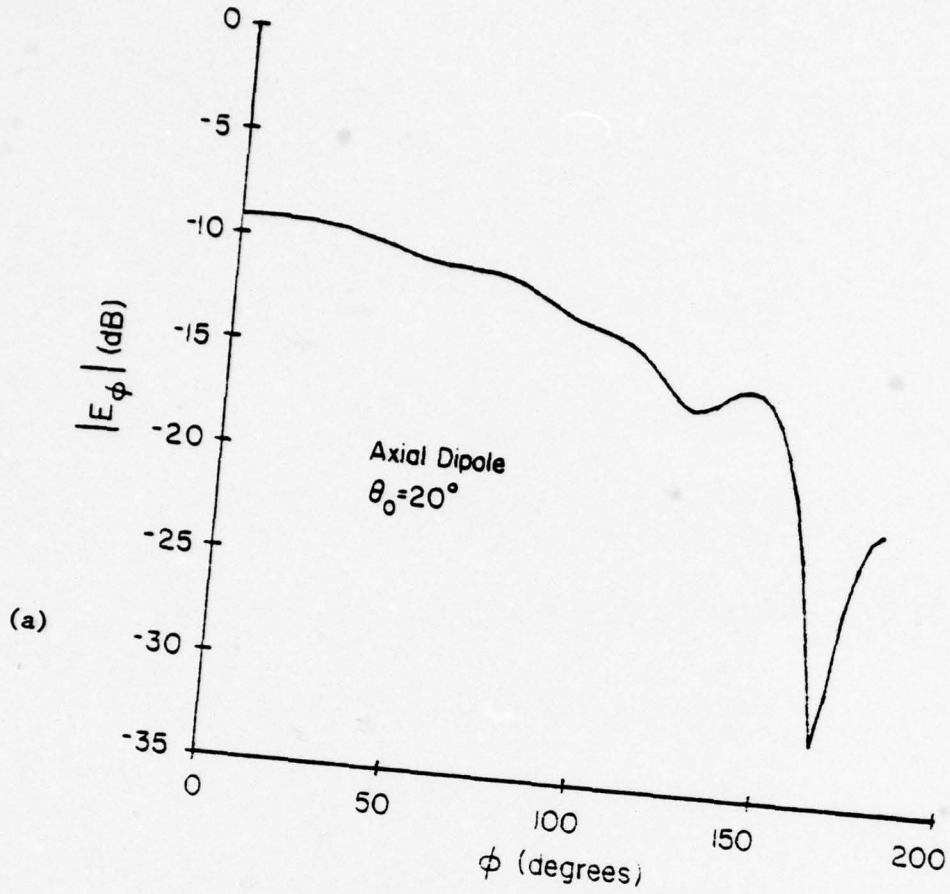

(a)

Figure 42. $|E_\phi|$ versus ϕ_0 when the source is an axial magnetic dipole and $\ell_1=6\lambda$, $\ell_2=2\lambda$, $a=2\lambda$ for different values of θ_0. (Fig. 19) a) $\theta_0=20°$, b) $\theta_0=30°$, c) $\theta_0=50°$, d) $\theta_0=70°$, e) $\theta_0=90°$, f) $\theta_0=120°$

(b)

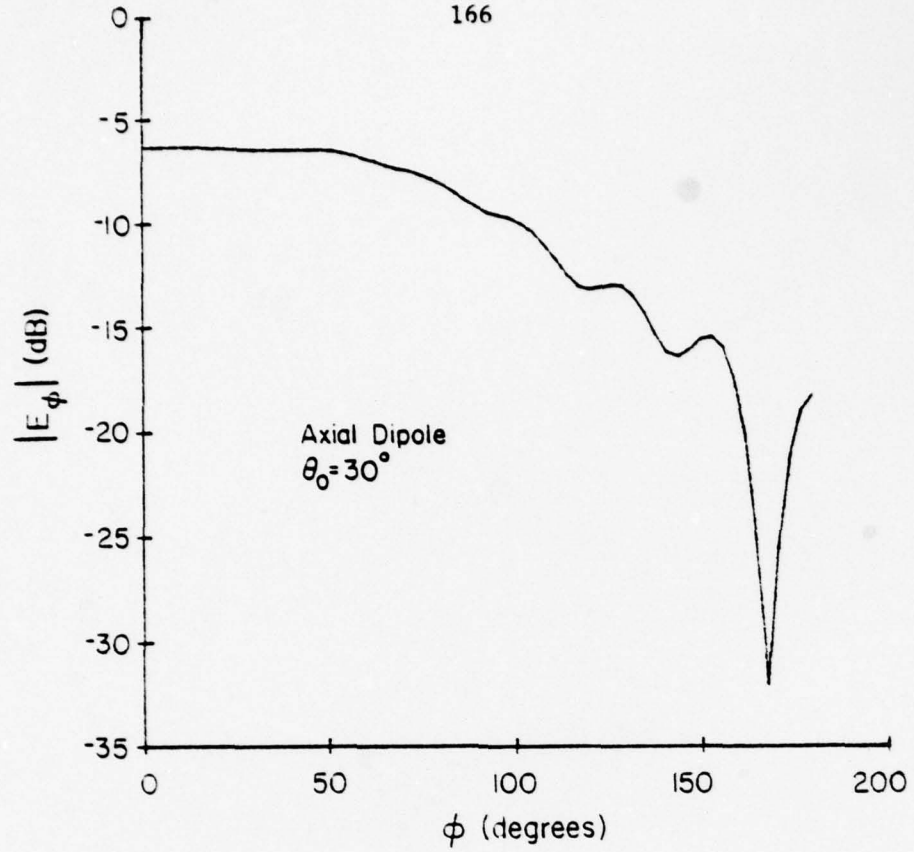
0
-5
-10
-15
-20
-25
-30
-35
$|E_\phi|$ (dB)
Axial Dipole
$\theta_0 = 30°$
0
50
100
150
200
ϕ (degrees)

(c)

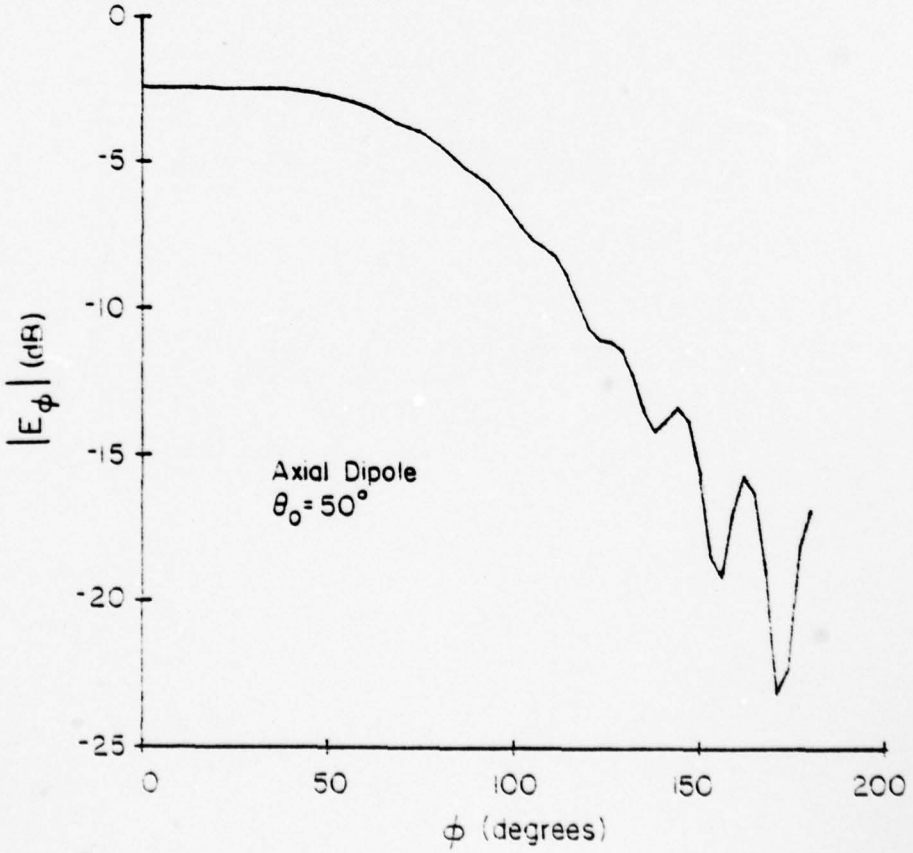
0
-5
-10
-15
-20
-25
$|E_\phi|$ (dB)
Axial Dipole
$\theta_0 = 50°$
0
50
100
150
200
ϕ (degrees)

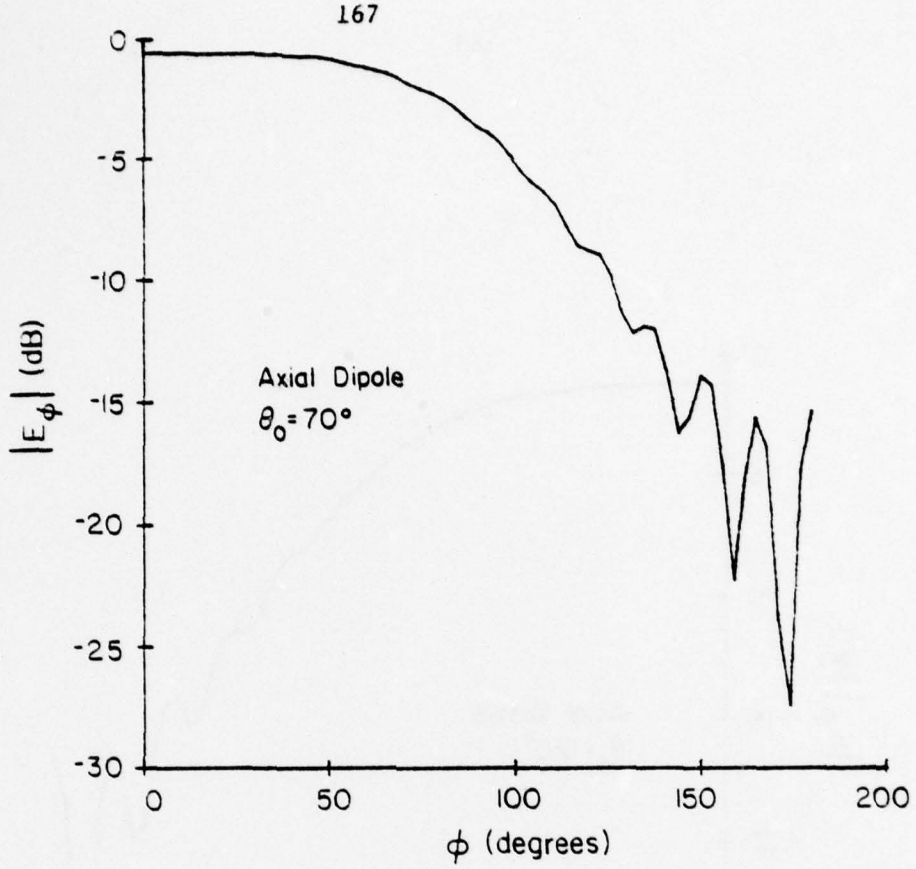
0
-5
-10
-15
-20
-25
-30
$|E_\phi|$ (dB)
Axial Dipole
$\theta_0 = 70°$
0
50
100
150
200
ϕ (degrees)

(d)

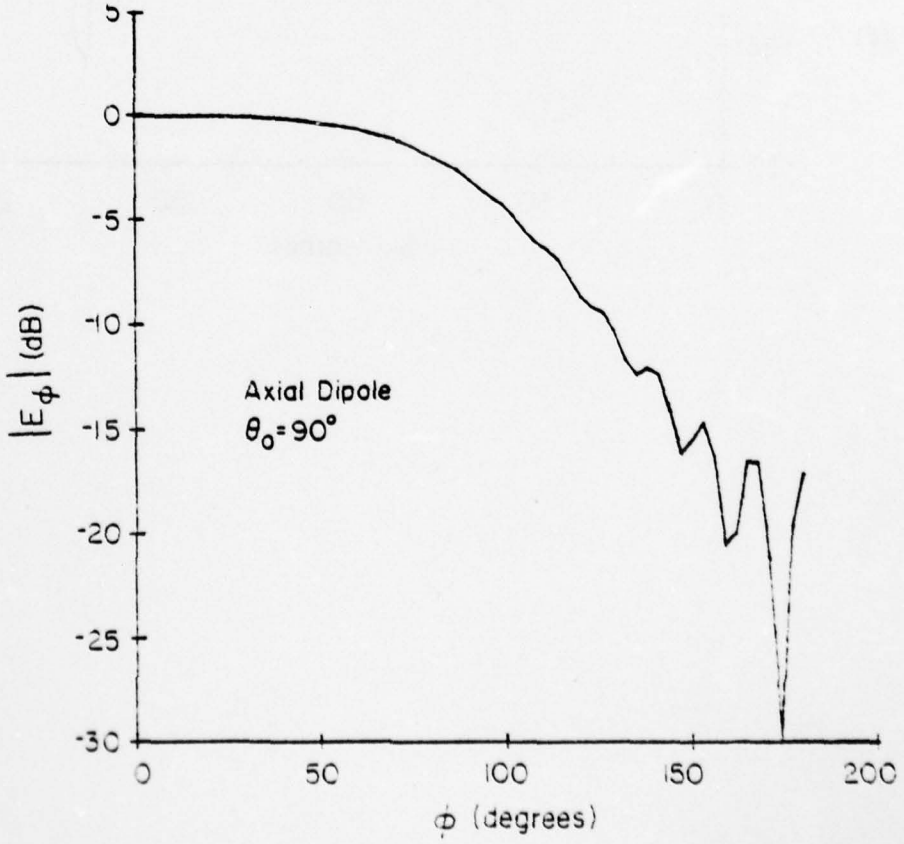
5
0
-5
-10
-15
-20
-25
-30
$|E_\phi|$ (dB)
Axial Dipole
$\theta_0 = 90°$
0
50
100
150
200
ϕ (degrees)

(e)

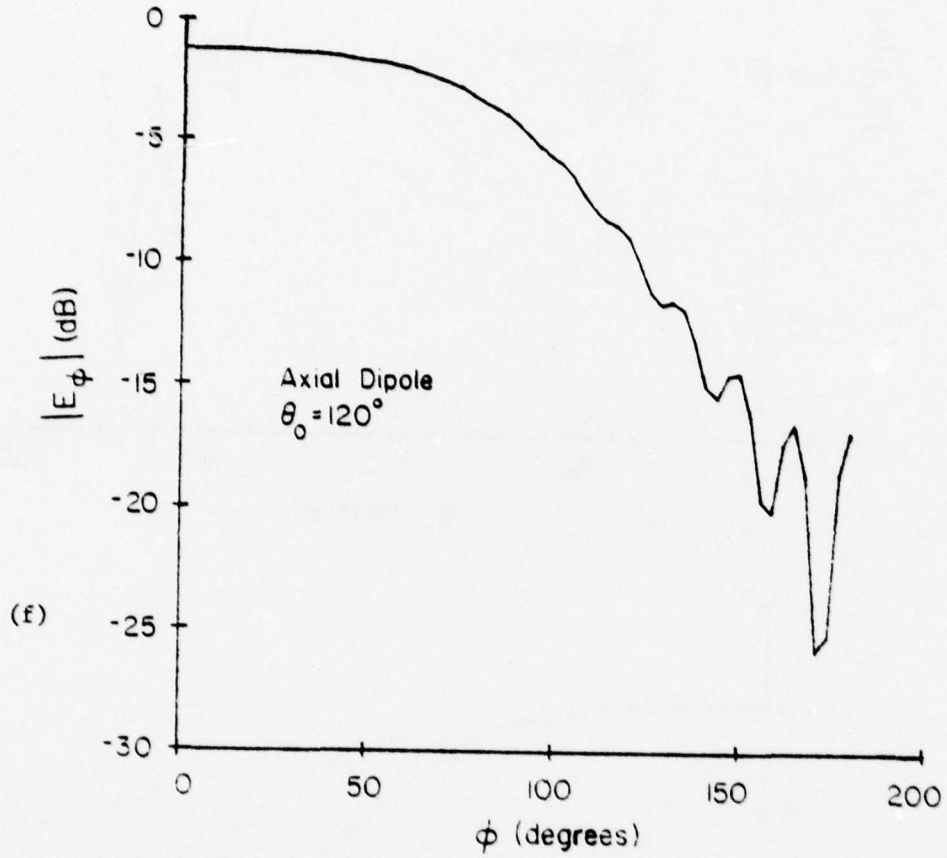
0
-5
-10
-15
-20
-25
-30
$|E_\phi|$ (dB)
Axial Dipole
$\theta_0 = 120°$
0
50
100
150
200
ϕ (degrees)

(f)

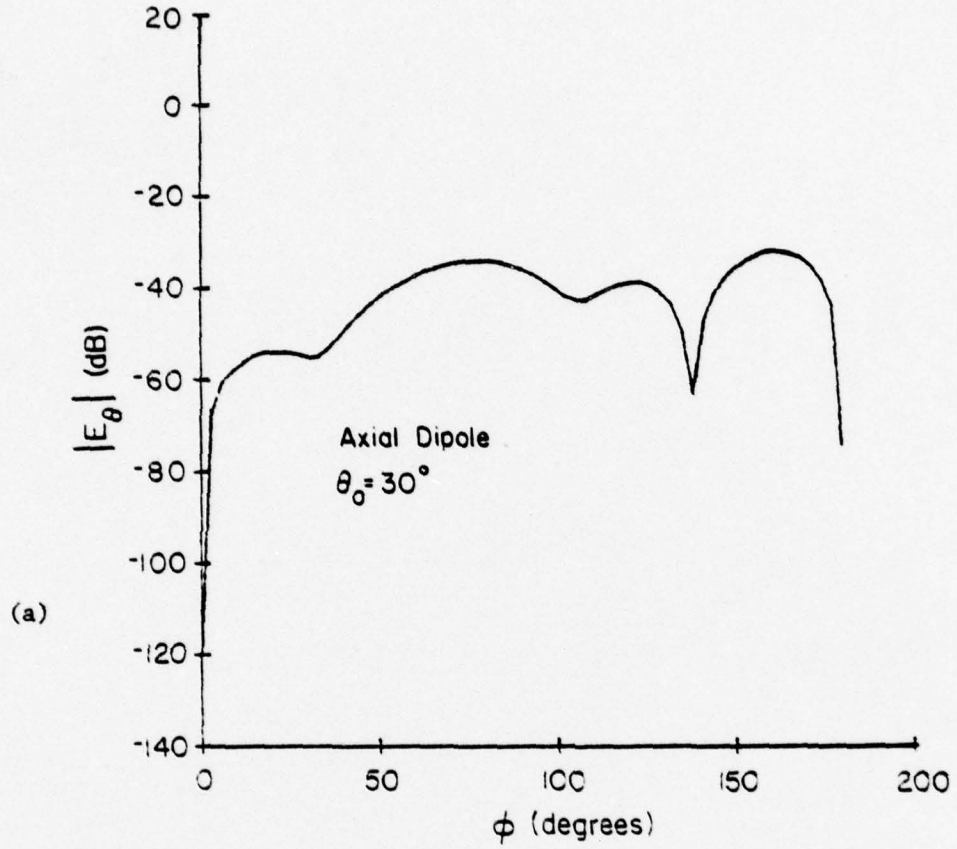

(a)

Figure 43. $|E_\theta|$ versus ϕ_0 when the source is an axial magnetic dipole and $\ell_1 = 6\lambda$, $\ell_2 = 2\lambda$, $a = 2\lambda$ for different values of θ_0. (Fig. 19) a) $\theta_0 = 30°$, b) $\theta_0 = 50°$, c) $\theta_0 = 120°$.

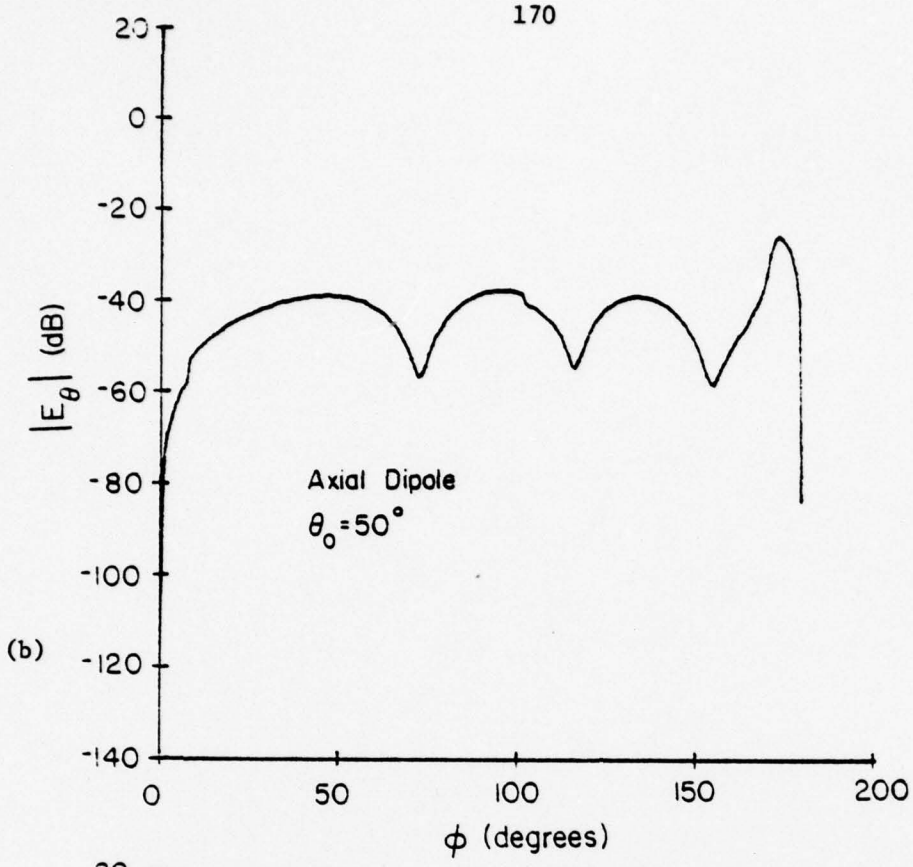
20
0
-20
-40
-60
-80
-100
-120
-140
$|E_\theta|$ (dB)
Axial Dipole
$\theta_0 = 50°$
0
50
100
150
200
ϕ (degrees)

(b)

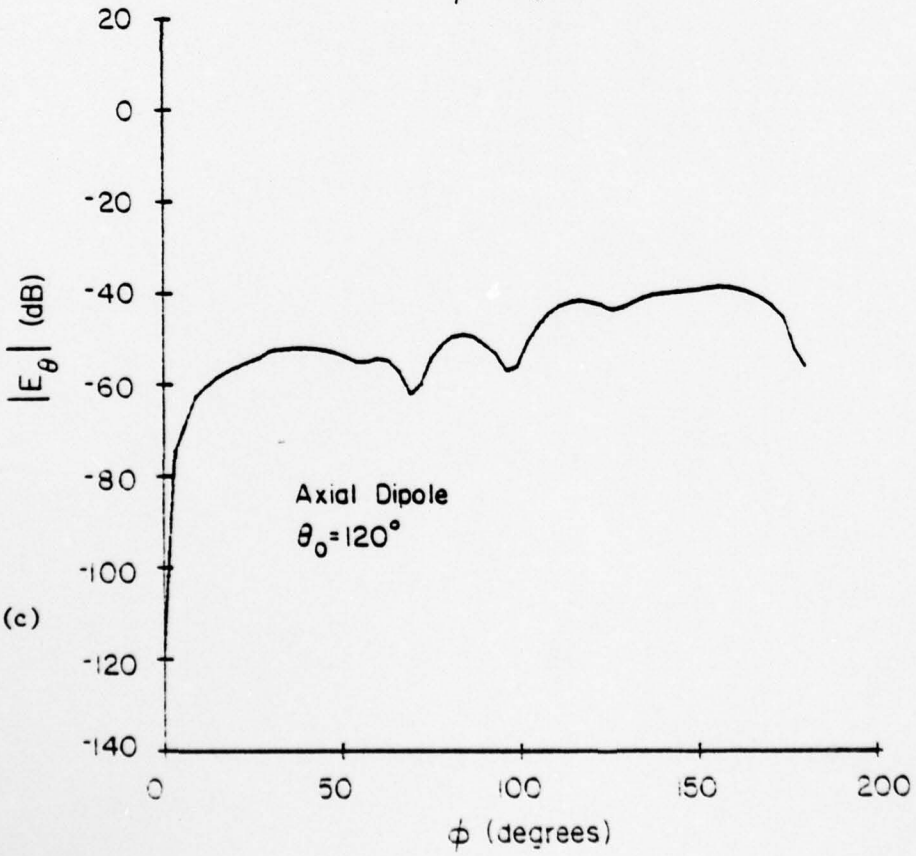
20
0
-20
-40
-60
-80
-100
-120
-140
$|E_\theta|$ (dB)
Axial Dipole
$\theta_0 = 120°$
0
50
100
150
200
ϕ (degrees)

(c)

of the two spherical components of the radiated electric field with respect to ϕ_0 (for different θ_0 cuts) and θ_0 (for different ϕ_0 cuts). The amplitude of the various components of the field have been given in dB:

$$|E_\theta| \text{ in dB} = 20 \log_{10}(|E_\theta|) \tag{10.2a}$$

$$|E_\phi| \text{ in dB} = 20 \log_{10}(|E_\phi|) \tag{10.2b}$$

Figs. 36 to 39 show the radiation patterns of the spherical components of the electric field on ϕ_0 = constant planes and θ_0 = constant cones, for the case where the elemental magnetic dipole has circumferential polarization ($M_z = 0$). The variations of the dominant component $|E_\theta|$ and nondominant component $|E_\phi|$ have been shown. It is observed in the lit region ($|\phi_0| < \frac{\pi}{2}$) that the amplitude of the nondominant component is about 10 or 20 dB below the dominant one. But as the shadow region is approached, the difference tends to decrease. Lack of smoothness of the plots is mainly due to the finiteness of the number of points in each curve. Of course, the fine structure of the curves can be studied by increasing the number of the points. In all the cases in the deep lit region ($|\phi_0| < 45°$ and $\theta_0 \simeq 90°$), the basic structure of the plots can be identified with those of the $\hat{y}$-directed magnetic dipole on a flat ground plane. In this region, the geometrical optical field is a reasonable approximation. In the paraxial and shadow region, the more accurate results deviate substantially from geometrical optical predictions. In these regions, wedge diffracted and surface diffracted rays contribute significantly. These latter contributions are also responsible for too many fluctuations observed in the field amplitude specially in the deep shadow.

Special narrow peaks near the $\phi_0 = 180°$-end of the graphs of the field components versus ϕ_0 (Figs. 38 and 39) are mostly due to the formation of a caustic region for the wedge diffracted fields along these directions (the detailed discussion of this case was given at the end of Chapter 7). The formation of the caustic generates a relatively strong field in the corresponding directions in the shadow region. The strong peaks at the polar regions in Fig. 37 indicate the significant deviation from the G.O. (Geometrical Optical) and even the exact solution for the infinite cylinder when paraxial regions are approached. Once more it should be emphasized that the curves show a rough estimate of the variations. The other point which should be mentioned is that for the field amplitude below some certain level the computational error can exceed the value of the results.

The precise study of our extensive numerical results indicates that for the specific geometry chosen for computations the truncation effect can amount to up to 20% of the final result in some cases. Of course, as ℓ_1 and ℓ_2 increase this effect decreases.

Figs. 40 and 43 illustrate the field variation with respect to θ_0 and ϕ_0 when the source has a $\hat{z}$-polarization (M_ϕ=0). The general properties described in the previous case can also be observed in these curves. The behavior of the dominant component of the field E_ϕ in the deep lit region is almost similar to what can be predicted by G.O. expressions. In this region, E_θ (Fig. 41) is much weaker than the dominant polarization. Again, when we approach the shadow region, the patterns deteriorate and significant deviation from G.O. is observed (Figs. 40f, g, h, i). The field variations versus ϕ_0 are depicted in Figs. 42 and 43. In the deep lit region, (Figs. 42c, d, e, f), E_ϕ patterns are quite analogous to those of a magnetic current

filament on an infinite cylinder, and the finiteness of the object affects only the shadow part of the plots. In this case too, like in previous ones, a high-order caustic formation is responsible for a fairly sharp peak towards the ϕ_0=180° end of the plots.

11. SUMMARY AND RECOMMENDATION FOR FUTURE WORK

In the beginning of this work (Chapters 2 and 3) we have examined the problem of radiation from sources in the presence of smooth, convex, impenetrable objects. First, a brief survey of various high frequency techniques was presented. A generalization of the geometrical theory of diffraction and two new techniques based on the spectral domain approach and an asymptotic evaluation of the radiation integral for the surface current, were discussed. It was shown that is is possible to extend the range of applicability and to improve upon the accuracy of the existing asymptotic theories by solving new canonical problems in which some of the earlier restricting assumptions underlying GTD and other high frequency techniques have been removed. The accuracy of the new approach was evaluated by comparing the numerical results derived from the new formulas with the available theoretical and experimental data.

In the second part of the present work (Chapters 5 through 10), the special case of source radiation in the presence of a finite solid cylinder was studied. For the problem of high frequency radiation of an electromagnetic point source on the surface of a conducting circular cylinder with finite length, a technique combining the main features of different asymptotic theories has been presented. The STD interpretation has been employed to derive the diffracted field and the total radiated field has been obtained by adding the contribution of the "body" currents and the field scattered by the wedges. A modified version of GTD has been applied to wedge diffraction. The modification consists of removing the singularity of Keller's diffraction coefficient which, according to STD, can be associated with the field radiated by a current distribution with a semi-infinite support on the faces of a straight wedge. The incident surface field at the wedge has

been obtained by asymptotic expressions derived by Lee and Safavi-Naini [28]. The contributions of "body" current have been determined by approximate asymptotic formulas developed by Safavi-Naini and Mittra [20]. The effect of finiteness of the cylinder has also been studied and accounted for in the final expressions for the total field. The special situations where the field evaluation in the first- or higher-order caustics are involved have been treated successfully by introducing the notion of "non-uniform equivalent edge current" [46] and modifying the GTD in a proper manner.

Based upon this new formulation of the problem, a computer program has been developed which can achieve field computation for all observation angles taking into account all various effects or specific situations whose handling requires special care.

The accuracy of the procedure has been partially justified by the demonstrated validity of the different theories used in the present method when applied to other similar problems. Finally, it is recommended that a thorough testing of the accuracy of the procedure outlined in this paper be carried out in order to fully evaluate its usefulness. This can be done by following a procedure suggested in [110].

APPENDIX A: FOCK FUNCTIONS

In studies of radio-wave propagation around the earth by Van der Pol, Bremmer, Pryce, Fock, and others, and also the later studies of diffraction of electromagnetic waves by certain bodies of revolutions ([51], [52], [53], [54], [55], [48], [56], [57], [58], [59], [60] and [50]), a class of universal functions was introduced which can be used to predict the amplitude and the phase of the reflected or diffracted field by smooth convex surfaces [17]. An exhaustive treatment of these functions which, in general, are defined as Fourier integrals having combinations of Airy integrals in their integrants, has been carried out by N. A. Logan [61]. (See also Bowman, et al. [1] and Logan and Yee [17].

Since the first extensive application of these functions to diffraction theory was done by Fock, many authors named them after him. Here we list only the most important formulas and expressions for these functions without going through the details of their derivations. We have followed Logan's set of notations for these functions [61]. However, since his time dependence factor, $\exp(-i\omega t)$, is different from one we have used throughout this paper, namely $\exp(+j\omega t)$, our expressions, listed below, are conjugates of what have been presented in [61].

First we start with general definitions. Fock's most general form of the "Van der Pol-Bremmer diffraction formula" is

$$V(x,y_1,y_2,q) = \exp(j\pi/4) \cdot \sqrt{\frac{x}{\pi}} \cdot \int_{-\infty}^{\infty} \cdot e^{-jxt} \cdot w_2(t - y_>) \cdot \left\{ v(t - y_<) - \frac{v'(t) - qv(t)}{w_2'(t) - qw_2(t)} \cdot w_2(t - y_>) \right\} dt \qquad (A.1)$$

where $w_1(t)$, $w_2(t)$, $u(t)$ and $v(t)$ are Fock-type Airy functions, defined as

$$u(t) = \sqrt{\pi}\ \mathrm{Bi}(t) \quad , \quad v(t) = \sqrt{\pi}\ \mathrm{Ai}(t)$$

$$w_1(t) = u(t) + jv(t) \quad , \quad w_2(t) = w_1(t)^*$$

We note that w_1 and w_2 can also be defined as in Sec. 2. $y_>$ and $y_<$ are the larger and smaller of the two numbers y_1 and y_2. $V(x,y_1,y_2,q)$ is proportional to the attenuation suffered by an electromagnetic wave generated by a source located at reduced height y_1 above the surface of a smooth convex body, when it reaches the observation point located at reduced height y_2 above the same surface. x is the reduced distance between the source and the observation point along the surface, and q is dependent upon the impedance of the surface. Let us consider some useful limiting cases.

When $y_1 = y_2 = 0$, then $V(x,0,0,q)$ is denoted by V_0, where

$$V_0(x,q) = \frac{e^{j\pi/4}}{2} \cdot \sqrt{\frac{x}{\pi}} \cdot \int_{-\infty}^{\infty} \frac{e^{-jxt}\ w_2(t)}{w_2'(t) - qw_2(t)} \cdot dt \tag{A.2}$$

We also have

$$v(x) = V_0(x,0) = \frac{e^{j\pi/4}}{2} \sqrt{\frac{x}{\pi}} \int_{-\infty}^{\infty} \frac{e^{-jxt}\ w_2(t)}{w_2'(t)}\, dt \tag{A.3}$$

$$u(x) = \lim_{q\to\infty} \left(-2jxq^2 V_0(x,q)\right) = \frac{e^{j3\pi/4}}{\sqrt{\pi}} \cdot x^{3/2} \int_{-\infty}^{\infty} \frac{e^{-jxt}\ w_2'(t)}{w_2(t)} \tag{A.4}$$

When $y_1 = 0$ and $y_2 \to \infty$, then $V \to V_1(x,q)$:

$$V_1(x,q) = \frac{1}{\sqrt{\pi}} \cdot \int_{-\infty}^{\infty} \frac{e^{-jxt}}{w_2'(t) - qw_2(t)} \cdot dt \tag{A.5}$$

and also

$$g(x) = V_1(x,0) = \frac{1}{\sqrt{\pi}} \cdot \int_{-\infty}^{\infty} \frac{e^{-jxt}}{w_2'(t)}\, dt \tag{A.6}$$

$$f(x) = \lim_{q\to\infty}\left[-qV_1(x,q)\right] = \frac{1}{\sqrt{\pi}}\cdot\int_{-\infty}^{\infty}\frac{e^{-jxt}}{w_2(t)}\,dt \qquad (A.7)$$

A.1. Functions f_n and g_n

Based on Equations (A.6) and (A.7), a class of functions can be defined:

$$f^{(n)}(x) = \frac{(-j)^n}{\sqrt{\pi}}\cdot\int_{\Gamma}\frac{t^n\cdot e^{-jxt}}{w_2(t)}\cdot dt = \frac{d^n f(x)}{dx^n} \qquad (A.8)$$

$$g^{(n)}(x) = \frac{(-j)^n}{\sqrt{\pi}}\cdot\int_{\Gamma}\frac{t^n\, e^{-jxt}}{w_2'(t)}\cdot dt = \frac{d^n g(x)}{dx^n} \qquad (A.9)$$

where Γ is any path in the complex t-plane which comes from $-\infty$ in a sector defined by $-\pi \le \arg(t) < -\frac{\pi}{3}$ and goes to $+\infty$ in the sector $-\frac{\pi}{3} < \arg(t) < \frac{\pi}{3}$. In what follows, we will give the suitable formulas for $f(x)$ and $g(x)$ in different ranges. Tabulated values and graphs of these functions can be found in [57], [54], and [61].

When x is very large and negative, the following asymptotic expansions for $f(x)$ and $g(x)$ can be used [61].

$$f(x) \sim -2jxe^{jx^3/3}\left\{1 + \frac{j}{4x^3} + \frac{1}{2x^6} - \frac{j175}{64x^9} - \frac{395}{16x^{12}} + \frac{j318175}{1024x^{15}} + \ldots\right\} \qquad (A.10)$$

$$g(x) \sim 2e^{jx^3/3}\left\{1 - \frac{j}{4x^3} - \frac{1}{x^6} + \frac{j469}{64x^9} + \frac{5005}{64x^{12}} - \frac{j1122121}{1024x^{15}} - \ldots\right\} \qquad (A.11)$$

The above formulas are valid and accurate for $x \ll -1$. For moderate values of x, namely, $-1 \le x \le 1$, it is difficult to find an appropriate expression. Although there are some analytical techniques like "stationary phase method" or "Poisson summation formula" which may be used to evaluate $f^{(n)}$ and $g^{(n)}$ for these values, another possible way which is probably easier and more efficient is to interpolate the tabulated values of these functions in this range.

In the vicinity of zero ($|x| \approx 0$), the Taylor expansion can be used to calculate f and g. The coefficients are given by

$$f^{(n)}(0) = e^{-j(5n\pi/6-\pi/3)} \cdot \sqrt{\pi} \cdot \left(\frac{3\pi}{2}\right)^{(2/3)(n-1/4)} \cdot \sum_{m=0}^{\infty} A_m(n) \cdot \left(\frac{2}{3\pi}\right)^{2m} \cdot \tau\left(2m - \frac{4n-1}{6}, \frac{3}{4}\right) \tag{A.12}$$

$$g^{(n)}(0) = e^{-j5n\pi/6} \cdot \sqrt{\pi} \cdot \left(\frac{3\pi}{2}\right)^{(2/3)(n-3/4)} \cdot \sum_{m=0}^{\infty} B_m(n) \cdot \left(\frac{2}{3\pi}\right)^{2m} \cdot \tau\left(2m - \frac{4n-3}{6}, \frac{1}{4}\right) \tag{A.13}$$

where $\tau(\lambda,\mu)$ is the generalized "tau" function:

$$\tau(\lambda,\mu) = \sum_{n=0}^{\infty} \frac{(-1)^n}{(n+\mu)^{\lambda}}, \quad \lambda > 1 \tag{A.14}$$

$$A_0(n) = 1, \quad A_1(n) = \frac{5}{48}(n-1)$$

$$A_2(n) = 5\left(5n^2 - 143n + \frac{26385}{16}\right)/(2^9 \cdot 3^2)$$

$$B_0(n) = 1, \quad B_1(n) = -7(n-3/2)/48$$

$$B_2(n) = (49n^2 + 364n + 39849/16)/(2^9 \cdot 3^2)$$

When x is large, and positive, residue series can be used to compute $f^{(n)}$ and $g^{(n)}$:

$$f^{(n)}(x) = e^{j(2+7n)\pi/6} \sum_{p=1}^{\infty} \frac{(r_p)^n \exp(r_p \cdot x \cdot e^{-j5\pi/6})}{Ai'(-r_p)} \tag{A.15}$$

$$g^{(n)}(x) = e^{j7\pi n/6} \sum_{p=1}^{\infty} \frac{(r'_p)^{n-1} \exp(r'_p \cdot x \cdot e^{-j5\pi/6})}{Ai(-r'_p)} \qquad (A.16)$$

where $Ai(-r_p) = 0$ and $Ai'(-r'_p) = 0$ for $p = 1,2,3,\ldots$.

A.2. Functions u, v, u', v':

Fock's functions u and v defined in (A.3) and (A.4) may be re-expressed as,

$$v(\xi) = \frac{1}{2} e^{j\pi/4} \xi^{1/2} \frac{1}{\sqrt{\pi}} \int_{\Gamma_1} \frac{w_2(t)}{w'_2(t)} e^{-j\xi t} dt \qquad (A.17)$$

$$u(\xi) = e^{j3\pi/4} \xi^{3/2} \frac{1}{\sqrt{\pi}} \int_{\Gamma_1} \frac{w'_2(t)}{w_2(t)} e^{-j\xi t} dt \qquad (A.18)$$

where integration contours Γ_1 and Γ_2 are sketched in Figure 44, and $w'_2(t)$ is the derivative of $w_2(t)$.

A.2.1 Zeroes of $w_2(t)$ and $w'_2(t)$: They are given by

$$t_n = |r_n| e^{-j\pi/3} \text{ , and } t'_n = |r'_n| e^{-j\pi/3} \text{ ,} \qquad (A.19)$$

respectively. The magnitudes of the first ten zeroes are listed in Table A.1.

A.2.2 Residue series representation. For real positive ξ,

$$v(\xi) = e^{-j\pi/4} \sqrt{\pi}\, \xi^{1/2} \sum_{n=1}^{\infty} (t'_n)^{-1} e^{-j\xi t'_n} \qquad (A.20)$$

$$u(\xi) = e^{j\pi/4} 2\sqrt{\pi}\, \xi^{3/2} \sum_{n=1}^{\infty} e^{-j\xi t_n} \qquad (A.21)$$

$$v'(\xi) = \frac{1}{2} e^{-j\pi/4} \sqrt{\pi}\, \xi^{-1/2} \sum_{n=1}^{\infty} (1 - j2\xi t'_n)(t'_n)^{-1} e^{-j\xi t'_n} \qquad (A.22)$$

$$u'(\xi) = e^{j\pi/4} 3\sqrt{\pi}\, \xi^{1/2} \sum_{n=1}^{\infty} \left(1 - j \frac{2}{3} \xi t_n\right) e^{-j\xi t_n} \text{ .} \qquad (A.23)$$

AD-A070 827 ILLINOIS UNIV AT URBANA-CHAMPAIGN ELECTROMAGNETICS LAB F/G 20/3
SOURCE RADIATION IN THE PRESENCE OF CONVEX BODIES.(U)
JUN 79 S SAFAVI-NAINI, R MITTRA N00014-75-C-0293
UNCLASSIFIED UIEM-79-9 NL

3 OF 3
AD A070827

END
DATE FILMED
8-79
DDC

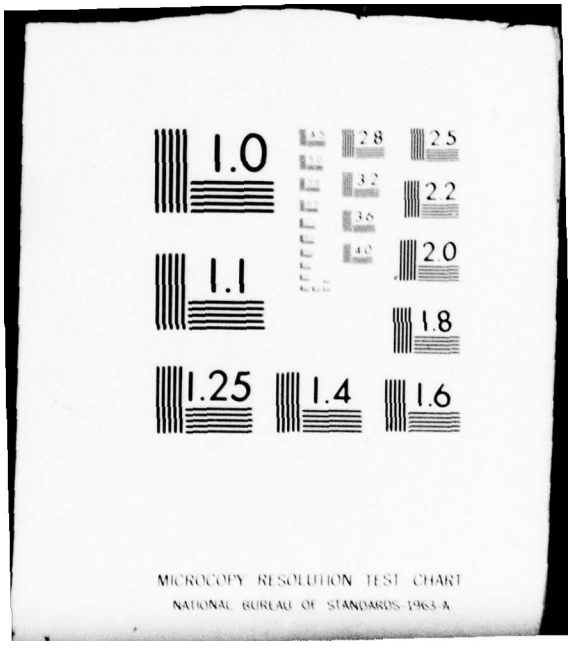
1.0
1.1
1.25
1.4
1.6
1.8
2.0
2.2
2.5
2.8
3.2
3.6
4.0
MICROCOPY RESOLUTION TEST CHART
NATIONAL BUREAU OF STANDARDS 1963 A

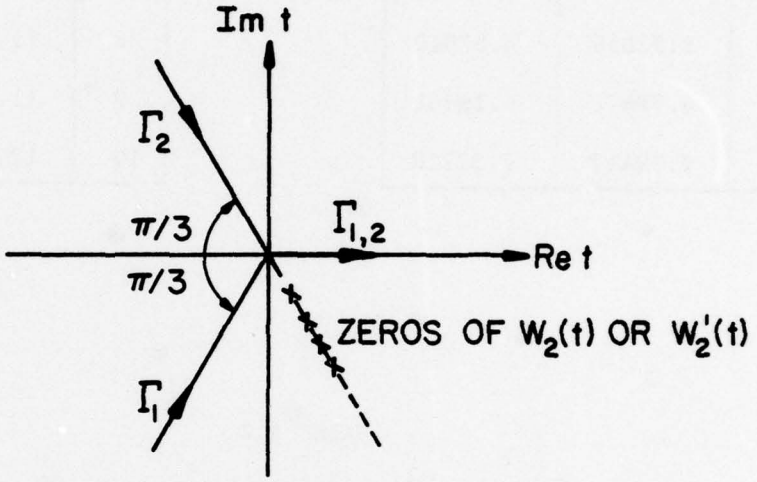

Figure 44. Contours Γ_1 and Γ_2 on the complex t (or z) plane. Γ_1, for example, goes from ∞ to 0 along the line Arg $t = -2\pi/3$ and from 0 to ∞ along the real axis.

TABLE A.1

The modulas of the zeroes of the functions $w_2(t)$ and $w_2'(t)$

n	$\lvert r_n \rvert$	$\lvert r_n' \rvert$
1	2.33811	1.01879
2	4.08795	3.24820
3	5.52056	4.82010
4	6.78671	6.16331
5	7.99417	7.37218

n	$\lvert r_n \rvert$	$\lvert r_n' \rvert$
6	9.02265	8.48849
7	10.04017	9.53545
8	11.00852	10.52766
9	11.93602	11.47506
10	12.82878	12.38479

TABLE A.2

*% = |1 - (Residue/small arg.)| x 100

Difference at ξ = 0.7		
	Mag. (%)*	Phase (deg.)
v	0.00	0.00
u	0.11	0.01
v_1	0.02	0.08
v'	0.09	0.15
u'	0.10	0.90

A.2.3. Small argument asymptotic expansion. For real positive ξ and $\xi \to 0$,

$$v(\xi) \sim 1 - \frac{\sqrt{\pi}}{4} e^{j\pi/4}\xi^{3/2} + \frac{7j}{60}\xi^3 + \frac{7\sqrt{\pi}}{512} e^{-j\pi/4}\xi^{9/2} - 4.141 \times 10^{-3}\xi^6 + \ldots \quad \text{(A.24)}$$

$$u(\xi) \sim 1 - \frac{\sqrt{\pi}}{2} e^{j\pi/4}\xi^{3/2} + \frac{5j}{12}\xi^3 + \frac{5\sqrt{\pi}}{64} e^{-j\pi/4}\xi^{9/2} - 3.701 \times 10^{-2}\xi^6 + \ldots \quad \text{(A.25)}$$

$$v'(\xi) \sim \frac{3\sqrt{\pi}}{8} e^{-j3\pi/4}\xi^{1/2} + \frac{7j}{20}\xi^2 + \frac{63\sqrt{\pi}}{1024} e^{-j\pi/4}\xi^{7/2} - 2.485 \times 10^{-2}\xi^5 + \ldots \quad \text{(A.26)}$$

$$u'(\xi) \sim \frac{3}{4}\sqrt{\pi}\, e^{-j3\pi/4}\xi^{1/2} + \frac{5j}{4}\xi^2 + \frac{45\sqrt{\pi}}{128} e^{-j\pi/4}\xi^{7/2} - 2.221 \times 10^{-1}\xi^5 + \ldots \quad \text{(A.27)}$$

A.2.4. Numerical evaluation. For $\xi \geq \xi_0$, the residue series representation with the first ten terms in the summation may be used. For $\xi \leq \xi_0$, the small argument asymptotic expansion with the first five terms may be used. It can be shown that the smoothest crossover is obtained if $\xi_0 = 0.6$. In the present study, we set $\xi_0 = 0.7$, where the difference in the two representations shown in Table A.2.

APPENDIX B: DERIVATION OF FORMULAS (3.8)and (3.9)

Here, we consider only the derivation of the asymptotic expansion of Φ for a circumferential magnetic dipole. In this case, Φ may be written as:

$$\Phi = \frac{j\omega\varepsilon M_\phi}{(2\pi)^2}\int_{-\infty}^{\infty} dk_z \cdot \frac{e^{-jk_z z}\cdot S(k_t)}{k_t^2} \tag{B.1}$$

where

$$S(k_t) = \sum_{n=-\infty}^{\infty} e^{-jn\phi}\cdot\frac{H_n^{(2)}(k_t\rho)}{H_n^{(2)}(k_t a)} \tag{B.2}$$

Applying the Watson transformation to (B.2),

$$S(k_t) = \frac{j}{2}\cdot\int_{C+D}\frac{H_\nu^{(2)}(k_t\rho)}{H_\nu^{(2)}(k_t a)}\cdot\frac{e^{-j\nu(\phi-\pi)}}{\sin\nu\pi}\cdot d\nu \tag{B.3}$$

where C and D are shown in Fig.45 . Or,

$$S(k_t) = j\cdot\int_{+\infty-j\delta}^{-\infty-j\delta}\frac{\cos\nu(\pi-\phi)\quad H_\nu^{(2)}(k_t\rho)}{\sin\nu\pi\cdot H_\nu^{(2)}(k_t a)}\cdot d\nu \tag{B.4}$$

Substituting the expansion

$$\frac{\cos\nu(\pi-\phi)}{\sin\nu\pi} = j\sum_{i=1}^{2}\sum_{l=0}^{\infty} e^{-j\nu(\phi_i+2\pi l)} \tag{B.5}$$

where $\phi_1 = \phi$ and $\phi_2 = 2\pi - \phi$, in (B.4), the result will be:

$$S(k_t) = \sum_{i=1}^{2}\sum_{l=0}^{\infty}\int_{-\infty-j\delta}^{\infty-j\delta}\frac{H_\nu^{(2)}(k_t\rho)}{H_\nu^{(2)}(k_t a)}\cdot e^{-j\nu(\phi_i+2\pi l)}\cdot d\nu \tag{B.6}$$

Each term of the above expansion is associated with a "creeping wave" travelling in a counterclockwise (i = 1) or clockwise (i = 2) direction around the cylinder. Following the ray concept, each creeping wave

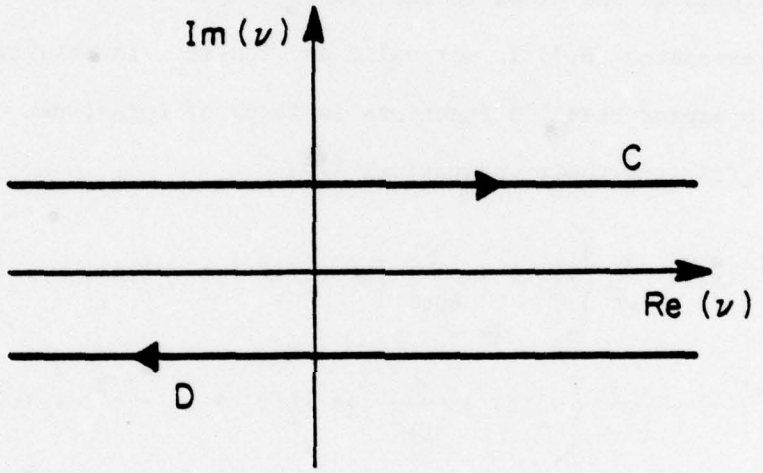

Figure 45 : Paths C and D in Watson transformation.

appears to be travelling along a specific surface ray. Now, as $\rho \to \infty$ (far zone) for each fixed ν, we have [62]

$$H_\nu^{(2)}(k_t\rho) \sim \sqrt{\frac{2}{\pi k_t \rho}} \cdot e^{-j(k_t\rho - \nu\pi/2 - \pi/4)} \tag{B.7}$$

On the other hand, it can be shown that the significant contribution to $S(k_t)$ comes from a small neighborhood of $k_t a$. In this neighborhood, where $k_t a$ and ν are large and close to each other ($|k_t a - \nu| \leq |\nu|^{1/3}$), the Hankel's asymptotic expansion (B.7) is not valid any longer. In this case, it is necessary to expand Bessel's functions in terms of Fock-type, Airy functions, $w_1(t)$ and $w_2(t)$, and their derivatives [16]

$$H_\nu^{(2)}(x) \sim \frac{1}{m\sqrt{\pi}} \left\{ w_2(t) - \frac{1}{60m^2} \left[4t\, w_2(t) + t^2 w_2'(t) \right] + \ldots \right\} \tag{B.8}$$

$$H^{(2)'}(x) \sim \frac{-j}{m^2\sqrt{\pi}} \left\{ w_2'(t) + \frac{1}{60m^2} \left[4t\, w_2'(t) + (6 - t^3)\, w_2(t) \right] + \ldots \right\} \tag{B.9}$$

where

$$m = \left(\frac{x}{2}\right)^{1/3} \quad , \quad t = \frac{\nu - x}{m} \quad \text{(m is very large)}$$

Inserting (B.7) and the first-order terms of (B.8) and (B.9) into (B.6) and (B.1), we obtain

$$\phi \sim \frac{\omega\varepsilon M_\phi}{(2\pi)^2} \cdot \sqrt{\frac{2\pi}{\rho}} \cdot e^{j\pi/4} \cdot \sum_{i=1}^{2} \sum_{l=0}^{\infty} \int_{-\infty}^{\infty} dk_z \cdot e^{-j\Omega_{il}} \cdot f_0(\xi_{il}) \cdot \frac{m^2}{k_t^{5/2}} \tag{B.10}$$

where

$$m = (k_t a/2)^{1/3}$$

$$\Omega_{il} = k_z z + k_t[\rho + a(\phi_i + 2\pi l - \pi/2)]$$

$$\xi_{il} = m(\phi_i + 2\pi l - \pi/2)$$

Introducing a new integration variable α:

$$k_z = k \sin \alpha \tag{B.11}$$

$$k_t = k \cos \alpha \tag{B.12}$$

and $$\beta_{il} = \tan^{-1}\{z/[\rho + a(\phi_i + 2\pi l - \pi/2)]\} \tag{B.13}$$

we have:

$$\Omega_{il} = kR_{il} \cos(\beta_{il} - \alpha) \tag{B.14}$$

where

$$R_{il} = \left\{z^2 + [\rho + a(\phi_i + 2\pi l - \pi/2)]\right\}^{1/2}$$

Now (B.10) takes the following form:

$$\phi \sim \frac{\omega\varepsilon M_\phi}{(2\pi)^2} \cdot \sqrt{\frac{2\pi}{\rho}} \cdot \frac{m_0^2}{k^{3/2}} \cdot e^{j\pi/4} \cdot \sum_{i=1}^{2} \sum_{l=0}^{\infty} \int_\gamma d\alpha \cdot e^{-jkR_{il}\cos(\alpha-\beta_{il})}$$

$$\cdot \cos^{-5/6} \alpha \cdot f_0(\xi_{il}) \tag{B.15}$$

γ is the path of integration in the complex α-plane, which is shown in Fig.46.

Now we deform the path of integration into the "steepest descent path," SDP, passing through the saddle point of the phase of the integrand. Performing the "saddle-point integration," we can derive the asymptotic expansion of (B.15) for large kR_{il}. The first order term is:

$$\phi \sim \frac{\omega\varepsilon M_\phi}{2\pi k^2} \cdot e^{j\pi/2} \cdot \left(\frac{ka}{2}\right)^{1/3} \cdot \sum_{i=1}^{2} \sum_{l=0}^{\infty} (\cos \beta_{il})^{-4/3} \cdot \frac{e^{-jkR_{ils}}}{R_{ils}} \cdot f_0(\xi_{ils}) \tag{B.16}$$

where R_{ils} and ξ_{ils} are the values of these parameters at the stationary point specified by $\alpha = \beta_{il}$.

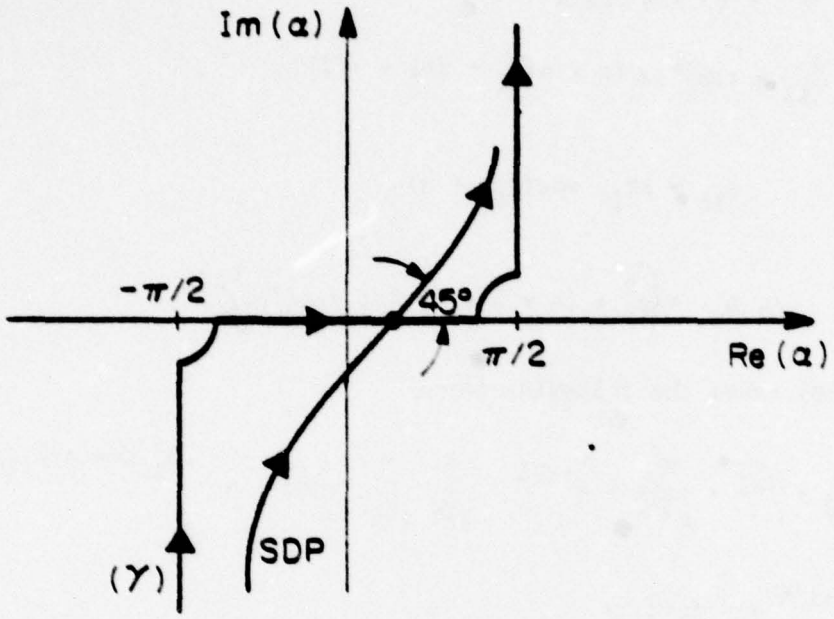

Figure 46: Steepest descent path (SDP) for integral (B.15).

Equation (B.16) is the creeping-wave representation of the far field. If the cylinder is large ($ka \gg 1$) and $|\phi|$ is not very close to π, then only the first term ($i = 0$, $l = 1$) has the most important contribution to the total infinite sum, and the other terms are not significant. Neglecting the other terms, we obtain the result given in (3.8) and (3.9). It should be emphasized that (3.8) and (3.9) are not valid when $|\beta|$ is close to $\pi/2$ (paraxial region), because in this case, $k_t a$ is very small, and (B.7), (B.8) and (B.9) no longer apply.

The other formulas can be derived in a similar manner.

APPENDIX C: ASYMPTOTIC EVALUATION OF THE RADIATION INTEGRAL

Consider the following double integral:

$$U(k) = \int_D\int g(x,y) \cdot e^{jk\phi(x,y)}\, dxdy \tag{C.1}$$

where $g(x,y)$ is rather slowly varying, and $\phi(x,y)$ has a stationary point (x_s,y_s) inside domain D. The objective is to derive an asymptotic expansion for (C.1) when k is large.

Suppose g and ϕ have the following forms around (x_s,y_s):

$$\begin{cases} g(x,y) = (x - x_s)^{\lambda_0 - 1} (y - y_s)^{\mu_0 - 1} g_1(x,y), \quad \lambda_0, \mu_0, > 1 \\ \phi(x,y) = \phi(x_s,y_s) + a_{\delta,0}(x - x_s)^{\delta}[1 + P(x,y)] + b_{0,\tau}(y - y_s)^{\tau}[1 + Q(x,y)] \end{cases} \tag{C.2}$$

N. Chako [48] has derived the following asymptotic series for U:

$$U(k) \sim B_0 \cdot \sum_{p,q=0}^{\infty} A_{pq}(\alpha_1 + \alpha_2)(\beta_1 + \beta_2) \cdot \Gamma\left(\frac{\lambda_0 + p}{\delta}\right) \cdot \Gamma\left(\frac{\mu_0 + q}{\tau}\right) \frac{1}{(ka_{\delta,0})^{p/\delta}} \cdot \frac{1}{(kb_{0,\tau})^{q/\tau}} \tag{C.3}$$

where

$$B_0 = \frac{1}{(ka_{\delta,0})^{\lambda_0/\delta}} \cdot \frac{1}{(kb_{0,\tau})^{\mu_0/\tau}} \cdot \frac{1}{(\delta\tau)} \cdot e^{jk\phi(x_s,y_s)}$$

$$\alpha_1 = \exp[j\pi(\lambda_0 + p)/(2\delta)], \quad \alpha_2 = \exp\left\{[j\pi/(2\delta)]\left[(\lambda_0 + p)(2\delta + e^{j\pi\delta}) - 2\delta\right]\right\}$$

$$\beta_1 = \exp[j\pi(\mu_0 + q)/(2\tau)], \quad \beta_2 = \exp\left\{[j\pi/(2\tau)]\left[(\mu_0 + q)(2\tau + e^{j\pi\tau}) - 2\tau\right]\right\}$$

$$g_1(x,y) = \sum_{k,l=0}^{\infty} g_{k\ l}(x - x_s)^k(y - y_s)^l$$

$$P(x,y) = \sum_{m+n\geq 1} a_{mn}(x - x_s)^m(y - y_s)^n$$

$$Q(x,y) = \sum_{m+n\geq 1} b_{mn}(x - x_s)^m(y - y_s)^n$$

$$A_{00} = g_{00} \quad , \quad A_{10} = g_{10} - g_{00}\left\{(\lambda_0 + 1)\frac{a_{10}}{\delta} + \frac{b_{10}}{\tau}\right\}$$

$$A_{01} = g_{01} - g_{00}\left\{\frac{a_{01}}{\delta} + (\mu_0 + 1)\cdot\frac{b_{01}}{\tau}\right\}$$

In order to apply this procedure to the integrals of the type (50) for which

$$\phi(x,y) = -\Omega(\sigma,\beta) = -(R + \sigma) \tag{C.4}$$

$$g(x,y) = F(\sigma,\beta,P)\frac{\sqrt{G}}{R} \tag{C.5}$$

When F is one of the components of $\vec{J}(1 - \hat{R}\hat{R})$, one should first determine the stationary point of Ω, wherein its first-order derivatives vanish. The second step is to compute the various order derivatives of Ω, J, $\hat{R}$, ...,at this point, and then insert them into (C.3). We just give the main formulas needed for these derivations.

Suppose the surface of the body, $\vec{x}(\sigma,\beta)$, is parametrized by a geodetical polar coordinate system. As discussed previously,in this system, σ is the arc length of the surface geodesic connecting the pole Q to $\vec{x}(\sigma,\beta)$, and β is the angle between the geodesic and some fixed reference geodesic at Q (Fig.17)

The element of length in this system is given by

$$ds^2 = d\sigma^2 + G(\sigma,\beta)\, d\beta^2 \tag{C.6}$$

Let us denote $d\vec{x}(u)/du$ by $\vec{x}_u$; then we have the following set of relations

$$\vec{x}_{\beta\beta} = \frac{-\partial G/\partial\sigma}{2} \cdot \vec{X}_\sigma + \frac{\partial G/\partial\rho}{2G} \vec{x}_\beta + L^{\beta\beta} \vec{x}_3 \tag{C.7}$$

$$\vec{x}_{\beta\sigma} = \vec{x}_{\sigma\beta} = \frac{\partial G/\partial\sigma}{2G} \vec{x}_\beta + L^{\beta\sigma} \vec{x}_3 \tag{C.8}$$

$$\vec{x}_\sigma = \frac{-\vec{x}_3}{\rho_\sigma} \tag{C.9}$$

where $\vec{x}_\sigma = \hat{\sigma}$, and $\vec{x}_\beta/\sqrt{G} = \hat{\beta}$ are unit vectors along β = const. and σ = const. curves, and

$$\vec{x}_3 = \hat{n} = \frac{\vec{x}_\sigma \times \vec{x}_\beta}{\sqrt{G}} \tag{C.10}$$

is the outward unit normal to the surface. Another quantity of interest is the "geodetical curvature" κ_g given by

$$\kappa_g = \frac{\partial G/\partial\sigma}{2G} \tag{C.11}$$

Using the above relations, we can derive the following expressions which hold true at the stationary point:

$$\frac{\partial\Omega}{\partial\sigma} = 1 - \hat{R} \cdot \vec{X}_\sigma = 0 \tag{C.12}$$

$$\frac{\partial\Omega}{\partial\beta} = -\hat{R} \cdot \vec{x}_\beta = 0 \tag{C.13}$$

$$\frac{\partial^2\Omega}{\partial\sigma^2} = 0 \quad , \quad \frac{\partial^2\Omega}{\partial\sigma\partial\beta} = 0 \quad , \quad \frac{\partial^2\Omega}{\partial\beta^2} = G\left(\frac{1}{R} + \frac{1}{\rho_g}\right) \tag{C.14}$$

where $\rho_g = 1/\kappa_g$, and

$$\frac{\partial^3\Omega}{\partial\sigma^3} = \frac{1}{\rho_\sigma^2} \quad , \quad \frac{\partial^3\Omega}{\partial\sigma^2\partial\beta} = -L^{\beta\sigma}/\rho_\sigma \tag{C.15}$$

$$\frac{\partial^3\Omega}{\partial\beta^2\partial\sigma} = \frac{G}{R^2} + \frac{\partial G/\partial\sigma}{R} + \frac{\partial^2 G/\partial\sigma^2}{2} - \frac{L^{\beta\beta}}{\rho_\sigma} \qquad (C.16)$$

$$\frac{\partial^3\Omega}{\partial\beta^3} = \frac{3\partial G/\partial\beta}{2R} + \frac{\partial G}{\partial\beta}\cdot\frac{\partial G}{\partial\sigma}\cdot\frac{1}{4G} + L^{\beta\sigma}\cdot L^{\beta\beta} + \frac{1}{2}\cdot\frac{\partial^2 G}{\partial\sigma\partial\beta} \qquad (C.17)$$

where ρ_σ is the radius of curvature of the geodesic.

Equations (C.12) and (C.13) determine the location of the stationary point. At this point $\hat{R} = \vec{x}_\sigma$, which, if we introduce the ray concept, tells us that the surface rays leave the surface at the "point of diffraction" tangentially. Equation (C.14) indicates that the stationary point is of second order, so that we need higher-order derivatives of the phase. $L^{\sigma\sigma}$, $L^{\beta\sigma}$ and $L^{\beta\beta}$ are coefficients of the second fundamental form of the surface evaluated at the stationary point. They are defined as

$$L^{\sigma\sigma} = \vec{x}_{\sigma\sigma}\cdot\vec{x}_3 \quad , \quad L^{\sigma\beta} = \vec{x}_{\sigma\beta}\cdot\vec{x}_3 \quad , \quad L^{\beta\beta} = \vec{x}_{\beta\beta}\cdot\vec{x}_3$$

Using the relationships given above, one can find the expansion coefficients g_{kl}, a_{mn}, b_{mn} and A_{pq} in (C.3). Zeroth and first-order terms in (C.3) give us formulas (3.39), (3.40), and (3.41).

A few remarks should be made concerning the expansion presented in (C.3). First of all, (C.3) is a doubly infinite series; therefore, for each fixed power of k^{-1} a finite number of terms should be summed up. The coefficients of various terms in these finite sums, namely A_{pq}'s, become very complicated when p and q are greater than 0 or 1. Another difficulty with this series is that when the stationary point of the phase is of an order higher than 1, the difference between the order of the successive terms (when they are ordered according to the descending power of k) becomes very

small, and consequently the infinite series converges very slowly. For instance, in our problem where $\delta = 3$ and $\tau = 2$ (stationary point is of second order), sometimes the difference between the orders of successive terms is $k^{-1/6}$, which indicates the weak convergence (in an asymptotic sense) of the expansion in the cases where the frequency is not very large.

APPENDIX D:
COMPUTER PROGRAM FOR COMPUTATION OF THE FAR ZONE FIELD RADIATED BY A TANGENTIAL MAGNETIC DIPOLE ON A FINITE CYLINDER

Based upon the formulas derived in this report, a computer program for calculating different constituents of the far field has been written. The organization of the program is shown below and its listing is given in the next pages.

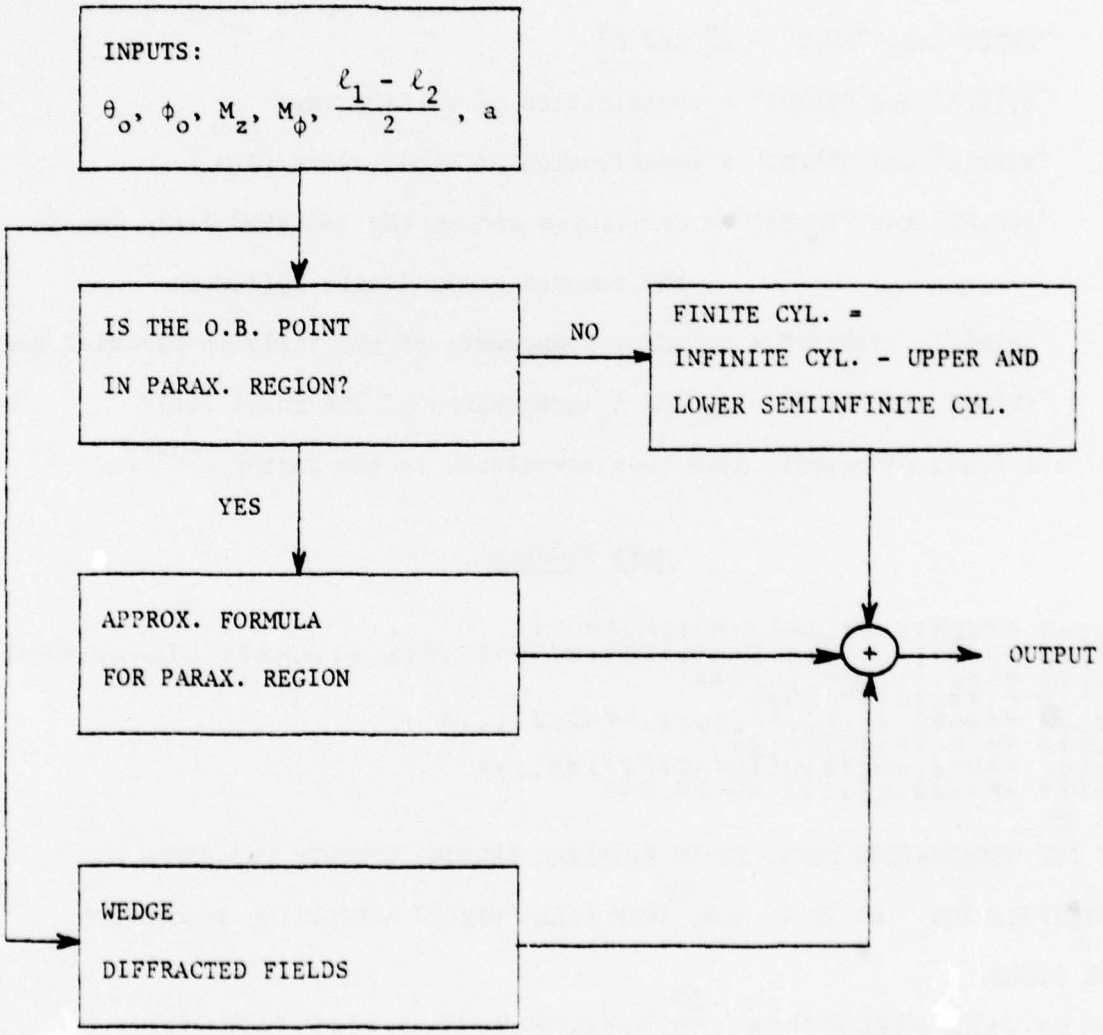

The symbols used in this program have been listed below.

Input parameters:

"PHID" = ϕ_o(in degrees)

"TETAD" = θ_o (in degrees)

"MZ" = M_z , "MPHI" = M_ϕ

"ZO" = $(\ell_1 - \ell_2)/2$ (in wavelength)

"A" = a , the radius of the cylinder (in wavelength)

"EWTET" and "EWFI" = E_θ^w and E_ϕ^w

"ESTETA" and "ESPHI" = contribution of surface rays

"EDTETA" and "EDPHI" = contribution of direct rays (G.O.)

"TRUNEF" and "TRUNET" = truncation effect; the radiated field due to the removed semiinfinite cylinders

"PARAXX", "PARAXY" = x- and y-components of the field in paraxial region

"ETETA" and "EPHI" = θ_o-and ϕ_o-components of the total field.

All the field components have been normalized to the factor e^{-jkr}/r.

MAIN PROGRAM

```
00100 PROGRAM CYLIN(INPUT,OUTPUT)
00110 COMPLEX ETETA,EPHI,ETETAD,EPHID,ETETA1,EPHI1,ETETA2,EPHI2
00120 REAL MZ,MPHI,L,KAS
00130 PI=3.141592653
00140 READ90,TETAD,PHID,MZ,MPHI,ZO,L,A
00150 90 FORMAT(7F7.2)
00160 KAS=2.*PI*SIN(TETAD*PI/180.)*A
00170 IF(KAS.LT.1.) GO TO 100
```

IF THE OBSERVATION POINT IS IN PARAXIAL REGION, COMPUTE THE FIELD BY INTERPOLATION. IF IT IS NOT, THEN CALL "FIELD" SUBROUTINE TO COMPUTE THE FIELD.

```
00180 CALL FIELD(TETAD,PHID,MZ,MPHI,ZO,L,A,ETETA,EPHI)
00190 ET=CABS(ETETA)*CEF=CABS(EPHI)
00200 PRINT 95,ET,EF
00210 95 FORMAT(5X,3H(ETETA)=,F9.4,5X,7H(EPHI)=,F9.4)
00220 GO TO 200
```

FIELD COMPUTATION IN PARAXIAL REGION BY PARABOLIC INTERPOLATION

```
00250 100 CONTINUE
00260 PRINT 110,TETAD,PHID,MZ,MPHI,ZO,L,A
00270 110 FORMAT(5X,5HTETA=,F7.2,5X,4HPHI=,F7.2,5X,3HMZ=,F5.2,5X
00280+,5HMPHI=,F5.2,5X,3HZO=,F6.2,5X,2HL=,F6.2,5X,2HA=,F6.2)
00290 TETAD0=0.$IF(TETAD.GT.90.) TETAD0=180.
00300 PRINT*,"                                *PARAXIAL REGION*    "
00310 PRINT*,"      FIELD COMPUTATION BY 3-POINT INTERPOLATION"
00320 TETAD1=ASIN(1./(2.*PI*A))*180./PI+1.
00330 IF(TETAD.GT.90.) TETAD1=180.-TETAD1
00340 TETAD2=TETAD1+5.$IF(TETAD.GT.90.) TETAD2=TETAD1-5.
00350 IF(TETAD.GT.90.) TETAD2=TETAD1-5.
00360 PRINT*,"  POINT NO. 1"
00370 CALL FIELD(TETAD1,PHID,MZ,MPHI,ZO,L,A,ETETA1,EPHI1)
00380 PRINT*,"  POINT NO. 2"
00390 CALL FIELD(TETAD2,PHID,MZ,MPHI,ZO,L,A,ETETA2,EPHI2)
00400 PRINT*,"  POINT NO. 0"
00410 CALL FIELD(TETAD0,PHID,MZ,MPHI,ZO,L,A,ETETA0,EPHI0)
00420 PRINT*,"                "
00430 PRINT*,"                                *INTERPOLATED FIELD*"
00440 ET1=CABS(ETETA1)$EF1=CABS(EPHI1)
00450 ET2=CABS(ETETA2)$EF2=CABS(EPHI2)
00460 ET0=CABS(ETETA0)$EF0=CABS(EPHI0)
00470 DERIVT=(ET2-ET1)/(TETAD2-TETAD1)
00480 DERIVF=(EF2-EF1)/(TETAD2-TETAD1)
00490 CT1=DERIVT/(TETAD1-TETAD0)-(ET1-ET0)/(TETAD1-TETAD0)**2
00500 CT2=DERIVT-2.*TETAD1*CT1
00510 CT3=ET0-CT1*TETAD0**2-CT2*TETAD0
00520 CF1=DERIVF/(TETAD1-TETAD0)-(EF1-EF0)/(TETAD1-TETAD0)**2
00530 CF2=DERIVF-2.*TETAD1*CF1
00540 CF3=EF0-CF1*TETAD0**2-CF2*TETAD0
00550 ET=CT1*TETAD**2+CT2*TETAD+CT3
00560 EF=CF1*TETAD**2+CF2*TETAD+CF3
00570 PRINT 150,ET,EF
00580 150 FORMAT(5X,8H(ETETA)=,F9.4,5X,7H(EPHI)=,F9.4)
00590 CONTINUE
00600 200 CONTINUE
00610 STOP
00620 END
```

SUBROUTINE "FIELD"

THIS SUBROUTINE COMPUTES DIFFERENT CONSTITUENTS OF THE RADIATED FIELDS AS A FUNCTION OF THE OBSERVATION POINT AND GEOMETRIC CHARACTERISTICS OF THE STRUCTURE AS DISCUSSED ABOVE. THE FINAL OUTPUT OF THIS SUBROUTINE ARE

"ETETA" = E_θ AND "EPHI" = E_ϕ

```
00630 SUBROUTINE FIELD(TETAD,PHID,MZ,MPHI,ZO,L,A,ETETA,EPHI)
00640 COMPLEX EIALFA,GSIGMA,FUCKU,FUCKV,DFUCKU,DFUCKV,GR
00650+,EWEDGE,ENTETA,ENPHI,EN1,EDETA1,EN2,EDETA2,CSTETA,ESPHI,FU
00660+,G0,G1,ETETA,EPHI,ENTET,ENFI,CSTETA,ECPHI,EY
00670+,FPHI1,FZ,FZ1,FPHI,FPHI2,CJPHI1,CJPHI2,CJPHIS,CJZ1,CJZ2,
00680+CJZ3,MF01,MF02,MF03,MFT1,MFT2,MFT3,EJAL1,EJAL2,CHSFI,
00690+CHAMFI,CHAMFI,MFUNC,CONST,NZETAP,NZETAM,TRUNET,TRUNEF,
00700+C2FML1,C2FML2,C2FPL1,C2FPL2,C2GML1,C2GML2,C2GPL1,C2GPL2,
00710+CJZETA,GJZETA,IIL1L2,I2L1L2,III,I21,EJL1,EJL2,EX,PARAXX,
00720+PARAXY,PARAXZ,PHIDEL
```

```
00710 REAL L,KSI,DIFPT1(10),DIFPT2(10),MBETA,MZ,MPHI,KSI1,KSI2
00720+,L1,L2,KL1S,KL2S,KAS,LI,LJ,KSIS,K,KZ
00730 PI=3.1415926536
00740 PRINT 100,TETAD,PHID,MZ,MPHI,ZO,L,A
00750 100 FORMAT(5X,5HTETA=,F7.2,5X,4HPHI=,F7.2,5X,3HMZ=,F5.2,5X
00760+,5HMPHI=,F5.2,5X,3HZO=,F6.2,5X,2HL=,F6.2,5X,2HA=,F6.2)
00770 TETA=TETAD*PI/180.$PHI=PHID*PI/180.
00780 UO=SIN(TETA)*COS(PHI)$VO=SIN(TETA)*SIN(PHI)
00790 WO=COS(TETA)$KAS=2.*PI*SIN(TETA)*A
00800 UOVO=UO*VO/(4.*PI)$UOWO=UO*WO/(4.*PI)$VOWO=VO*WO/(4.*PI)
00810 VO2I=-(1-VO*VO)/(4.*PI)$WO2I=-(1.-WO*WO)/(4.*PI)
00820 L1=L/2.+ZO$L2=L/2.-ZO$BETAI=ATAN(L2/(PI*A))
00830 BETA2=ATAN(L1/(PI*A))
00840 SINT=SIN(TETA)$COST=COS(TETA)
```

COMPUTATION OF WEDGE DIFFRACTED FIELDS:

FIRST STEP: FIND THE WEDGE DIFFRACTION POINTS BY SUBROUTINE "WDGPT"

SECOND STEP: COMPUTE THE DIFFRACTED FIELD CORRESPONDING TO EACH WEDGE DIFFRACTION POINT.

```
00850 PRINT 210
00860 PRINT*,"                    CONTRIBUTION OF WEDGE DIFFRACTED RAYS"
00870 NMAX=50
00880 CALL WDGPT((L/2.-ZO)/A,TETA,PHI,NMAX,DIFPT1,IROOT1)
00890 PRINT 110,(DIFPT1(J),J=1,IROOT1)
00900 110 FORMAT(5X,38HDIFFRACTION POINTS ON THE UPPER WEDGE:,2X
00910+,8F9.3)
00920 CALL WDGPT((-L/2.-ZO)/A,TETA,PHI,NMAX,DIFPT2,IROOT2)
00930 PRINT 120,(DIFPT2(J),J=1,IROOT2)
00940 120 FORMAT(5X,38HDIFFRACTION POINTS ON THE LOWER WEDGE:,2X
00950+,8F9.3)
00960 IROOT=IROOT1+IROOT2
00970 EWTET=EWPI=0.
00980 DO 200 I=1,IROOT
00990 IF(I.GT.IROOT1) GO TO 150
01000 PHIO=DIFPT1(I)*PI/180.$SM=L/2.-ZO
01010 IF((ABS(PHI-PHIO).GT.PI/2.).AND.(TETA.GT.PI/2.)) GO TO 175
01020 GO TO 160
01030 150 PHIO=DIFPT2(I-IROOT1)*PI/180.$SM=-L/2.-ZO
01040 IF((ABS(PHI-PHIO).GT.PI/2.).AND.(TETA.LT.PI/2.)) GO TO 175
01050 160 SIGMA=SQRT((A*PHIO)**2+M**2)
01060 BETA=ATAN2(M,A*PHIO)
01070 IF(SIN(TETA)*COS(PHI-PHIO).NE.0.) GO TO 170
01080 180 CONTINUE
01090 PRINT*,"   OBSERVATION POINT IS ON SHADOW BOUNDARY"
01100 170 CONTINUE
01110 MBETA=-MPHI*SIN(BETA)+MZ*COS(BETA)$BETA1=BETA
01120 IF((BETA.EQ.PI/2.).OR.(BETA.EQ.0.)) BETA1=BETA+0.000001
01130 RHOSIG=A/COS(BETA1)**2$RHOBET=A/SIN(BETA1)**2
01140 KSI=(PI/RHOSIG**2)**(1./3.)*SIGMA
01150 GSIGMA=(0.,-0.500)*CEXP((0.,-1.)*2.*PI*SIGMA)/SIGMA
01160 EIALFA=-MBETA*((1.-(0.,1.)/(2.*PI*SIGMA))*FOCKV(KSI)
01170+-FOCKU(KSI)/(2.*PI*SIGMA)**2+(0.,1.)*UFOCKV(KSI)/(1.01021*
01180+PI*2.*RHOSIG)**(2./3.)*(-(4.,1.)*UFOCKU(KSI)*(RHOSIG/RHOBET)
01190+/(SQRT(2.)*2.*PI*RHOSIG)**(2./3.))*GSIGMA
01200 RHO=1./((1./SIGMA+SIN(TETA)*COS(PHI-PHIO)/(A*SIN(BETA1)**2)
01210+)$RHP=ABS(RHO)
01220 EPSLN=1.$IF(ABS(PHI-PHIO).LT.PI/2.) EPSLN=-1.
01230 SBETA1=SIN(BETA1)
01240 IF(ABS(SIN(BETA1)).LE.ABS(COS(TETA))) SBETA1=ABS(COS(TETA)
01250+)*SIGN(1.0,SIN(BETA1))
```

```
01260 PSI=EPSLN*ABS(ACOS(COS((ETA)/SBETA1*1.0))*1.00
01270 IF(ABS(PSI).LE.0.0001) GO TO 169
01275 IF(ABS(COS(PSI/2.)).LE.0.000001) PSI=PSI+0.000001
01280 DM=6.9282032/(1.5+3.*COS(2.*PI/3.+2.*PSI/3.))*(-1.)-2./TAN
01285+(PSI/2.)
01290 GO TO 171
01300 169 DM=6.9282032/9.,SGN=1.
01310 171 CONTINUE
01320 OMEGA2=-A*A*SIN(BETA)**2/RHO
01330 OMEGA3=A*COS(BETA)*(3.*A*A*SIN(BETA)**2/SIGMA**2
01340+-1.)
01350 OMEGA4=-OMEGA2-A*A*SIN(BETA)**2*(1.+3.*A*A/SIGMA**2
01360+-15.*A*A*COS(BETA)**2/SIGMA**2)/SIGMA
01370 IF(ABS(OMEGA3).LT.0.0000001) OMEGA3=0.0000001
01380 IF(ABS(OMEGA4).LT.0.0000001) OMEGA4=0.0000001
01390 T23=ABS(OMEGA2/OMEGA3),T24=ABS(OMEGA2/OMEGA4)
```

IF THE POINT IS IN THE CAUSTIC REGION, USE EQUATION (7.83) BY CALLING FUNCTION "PHIDEL" OTHERWISE EMPLOY GTD FORMULA TO FIND THE DIFFRACTED FIELD.

```
01400 IF((T23.LE.15.).AND.(T24.LE.10.)) GO TO 1777
01410 ENEDGE=GM*(1.,-1.)*(SQRT(RMP/2.)/2.)*CEXP((0.,+1.)*2.*PI*(
01420+A*SIN(TETA)*(COS(PHI-PHI0)-COS(PHI))+M*COS(TETA))
01430+)*DM*EIALFA/(SIN(ABS(BETA1))*2.*PI)
01440 IF(RHO.LT.0.) ENEDGE=(0.,1.)*ENEDGE
01450 GO TO 1778
01460 1777 CONTINUE$PRINT*,"          CAUSTIC DIRECTION"
01470 ENEDGE=A*GM*CEXP((0.,1.)*2.*PI*(A*SIN(TETA)*(COS
01480+(PHI0-PHI)-COS(PHI))+M*COS(TETA)))*DM*EIALFA*PHI0
01490+CL(PI*OMEGA2,PI*OMEGA3/3.,PI*OMEGA4/12.)/(2.*PI)
01500 1778 CONTINUE
01510 ENTETA=ENEDGE*COS(PHI-PHI0)/SIN(ABS(BETA))
01520 ENPHI=ENEDGE*COS(TETA)*SIN(PHI-PHI0)*(-1.000000)/
01530+SIN(ABS(BETA))
01540 PRINT 130,I,ENTETA,ENPHI
01550 100 FORMAT(5X,7HRAY NO.,I2,5X,6HETETA=,F6.3,F9.3,5X,
01560+5HEPHI=F6.3,F9.3)
01570 GO TO 179
01580 175 ENTETA=ENPHI=0.,$PRINT 177,I
01590 177 FORMAT(5X,7HRAY NO.,I2,2X,24HIS BLOCKED BY THE OBJECT)
01600 179 CONTINUE
01610 ENTET=ENTET+ENTETA$ENPI=ENPI+ENPHI
01620 200 CONTINUE
01630 PRINT 105,ENTET,ENPI
01640 105 FORMAT(10X,7HENTETA=,F9.5,F10.5,5X,6HENPHI=,F9.5,F10.5)
01650 PRINT 210
01660 210 FORMAT(10X,/)
```

COMPUTATION OF THE FIELD GENERATED BY THE "BODY" CURRENT:

IF THE OBSERVATION POINT IS IN THE DEEP LIT REGION OR PARAXIAL REGION, USE SPECIAL EXPRESSIONS DERIVED FOR THESE CASES, OTHERWISE PROCEED TO COMPUTE SURFACE DIFFRACTED RAYS BY FORMULAS (5.1) AND (5.2).

```
01670      IF(RAS.LT.1.) GO TO 815
01680      IF((PHI.LE.PI/4.).OR.(PHI.GE.7.*PI/4.)) GO TO 450
01690      PRINT*,"                                CONTRIBUTION OF SURFACE RAYS "
01700      BETA=-MPHI*COS(TETA)+MZ*SIN(TETA)$BETA=PI/2.-TETA
01710      PRINT*,"          RAY NO.1"
01720      SIGMA1=A*(PHI-PI/2.)/COS(BETA)$RHOSIG=A/COS(BETA)**2
01730      XSI1=(PI*A*COS(BETA))**(1./3.)*(PHI-PI/2.)
01740      EN1=MBETA*(0.,1.)*0.5*CEXP((0.,1.)*2.*PI*(-SIGMA1*SIN(TETA
01750+)**2-A*SIN(TETA)*COS(PHI)))*G0(XSI1)+MPHI*SIN(BETA)*CEXP((
01760+0.,-1.)*2.*PI*(SIGMA1*SIN(TETA)**2+A*SIN(TETA)*COS(PHI)))*
01770+(PI*RHOSIG)**(1./3.)*G1(XSI1)/(4.*PI*A)
01780      EBETA1=MPHI*COS(BETA)*(PI*RHOSIG)**(2./3.)*CEXP((0.,-1.)*
01790+2.*PI*(SIGMA1*SIN(TETA)**2+A*SIN(TETA)*COS(PHI)))*F0(XSI1)
01800+/(2.*PI*A)
01810      PRINT 240 ,EN1,EBETA1
01820      240 FORMAT(10X,4HEN1=,F9.5,F10.5,5X,7HEBETA1=,F9.5,F10.5)
01830      250 PRINT*,"          RAY NO.2"
01840      SIGMA2=A*(3.*PI/2.-PHI)/COS(BETA)
01850      XSI2=(PI*A*COS(BETA))**(1./3.)*(3.*PI/2.-PHI)
01860      EN2=MBETA*(0.,1.)*0.5*CEXP((0.,-1.)*2.*PI*(SIGMA2*SIN(TETA
01870+)**2+A*SIN(TETA)*COS(PHI)))*G0(XSI2)-MPHI*SIN(BETA)*CEXP((
01880+0.,-1.)*2.*PI*(SIGMA2*SIN(TETA)**2+A*SIN(TETA)*COS(PHI)))*
01890+(PI*RHOSIG)**(1./3.)*G1(XSI2)/(4.*PI*A)
01900      EBETA2=MPHI*COS(BETA)*CEXP((0.,-1.)*2.*PI*(SIGMA2*SIN(TETA
01910+)**2+A*SIN(TETA)*COS(PHI)))*(PI*RHOSIG)**(2./3.)*F0(XSI2)
01920+/(2.*PI*A)
01930      PRINT 270,EN2,EBETA2
01940      270 FORMAT(10X,4HEN2=,F9.5,F10.5,5X,7HEBETA2=,F9.5,F10.5)
01950      PRINT 210
01960      350 CONTINUE
01970      ESTETA=-(EBETA1+EBETA2)$ESPHI=-(EN1+EN2)
01980      PRINT 360,ESTETA,ESPHI
01990      360FORMAT(10X,7HESTETA=,F9.5,F10.5,5X,6HESPHI=,F9.5,F10.5)
02000      PRINT 210
02010      PRINT*,"                                INFINITE CYLINDER "
02020      ETETA=ESTETA+CNTETSEPHI=ESPHI+CNPI+0.
02030      PRINT360,ETETA,EPHI
02040      360 FORMAT(10X,6HETETA=,F9.5,F10.5,5X,5HEPHI=,F9.5,F10.5)
02050      400 CONTINUE
02060      GO TO 510
```

THIS SECTION COMPUTES THE GEOMETRICAL OPTICAL FIELD

```
02070      450 CONTINUE
02080        EDTETA=(0.,-1.)*MPHI*COS(PHI)
02090      EDPHI=(0.,1.)*(MPHI*SIN(PHI)*COS(TETA)-MZ*SIN(TETA))
02100      ETETA=EDTETA+CNTETSEPHI=EDPHI+CNPI
02110      PRINT*,"                                DIRECT RAY CONTRIBUTION"
02120      PRINT 460,EDTETA,EDPHI
02130      460FORMAT(10X,7HEDTETA=,F9.5,F10.5,5X,6HEDPHI=,F9.5,F10.5)
02140      PRINT*,"                                INFINITE CYLINDER "
02150      PRINT 360,ETETA,EPHI
02160      510 CONTINUE
```

COMPUTATION OF TRUNCATION EFFECT USING FORMULAS (8.30) AND (8.31)

```
02170      PRINT*,"                    TRUNCATION EFFECT"
02180      NPTRUN=30.*SQRT((A*PI)**2+(AMAX1(L1,L2)**2))+1.
02190      DPHIP=2.*PI/(NPTRUN-1)
02200      EQUAL2=CEXP((0.,1.)*2.*PI*L2*COST)
02210      EQUAL1=CEXP((0.,-1.)*2.*PI*L1*COST)
02220      PHI1=PHI2=PI/2.-0.000000400
02230      CONST=4.*PI*PI*CEXP((0.,-5.)*PI/12.)/(1536.*(2.*PI*A)**
02240+(1./3.))
02250      DO 600 ITRNF=1,NPTRUN
```

```
      DIVID=1.
      IF((ITRNFI.EQ.1).OR.(ITRNFI.EQ.NPTRUN)) DIVID=2.
      PHIP=PI*(ITRNFI-1)*DPHIP
      IF(PHIP.EQ.0.0)PHIP=.000001
      ZSPHI=A*ABS(PHIP)*COST/SINT+1.0000
      IF(L2.EQ.ZSPHI) L2=L2+2.0000E
      ZETAP=SQRT(PI)*SQRT(ABS(-A*ABS(PHIP)*SINT-L2*COST+
     +SQRT((A*PHIP)**2+L2*L2)))*SIGN(1.,L2-ZSPHI)
      CMSFI=SQRT(2.*A*ABS(PHIP)/SINT**3)*CEXP((0.,-1.)*PI/4.)
      CMAPFI=2.*SQRT(1./PI)*ABS(ZETAP)*CEXP((0.,-1.)*PI/4.)/
     +ABS(COST-L2/SQRT((A*PHIP)**2+L2*L2))
      IF(ABS(L2-ZSPHI).LE..05) CMAPFI=CMSFI
      IF(-L1.EQ.ZSPHI) L1=L1+0.20000
      ZETAM=SQRT(PI)*SQRT(ABS(-A*ABS(PHIP)*SINT+L1*COST+
     +SQRT((A*PHIP)**2+L1*L1)))*SIGN(1.,L1+ZSPHI)
      CMAMFI=2.*SQRT(1./PI)*ABS(ZETAM)*CEXP((0.,-1.)*PI/4.)/
     +ABS(COST+L1/SQRT((A*PHIP)**2+L1**2))
      IF(ABS(L1+ZSPHI).LE.0.05) CMAMFI=CMSFI
      SIGMAS=SQRT((A*PHIP)**2+ZSPHI**2)
      SIGMA1=SQRT((A*PHIP)**2+L1*L1)
      SIGMA2=SQRT((A*PHIP)**2+L2*L2)
      COSBS=A*PHIP/SIGMAS
      COSB1=A*PHIP/SIGMA1
      COSB2=A*PHIP/SIGMA2
      RMUTS=A/COSBS**2
      RMUT1=A/COSB1**2
      RMUT2=A/COSB2**2
      KSIS=(PI/RMUTS**2)**(1./3.)*SIGMAS
      KSI1=(PI/RMUT1**2)**(1./3.)*SIGMA1
      KSI2=(PI/RMUT2**2)**(1./3.)*SIGMA2
      MFBS=CSHS2**(1./3.)*CEXP(-.88*KSIS-(0.,1.)*.5I*KSIS)*
     +CONST/SQRT(2.*PI*SIGMAS)IF(SIGMAS.LE.0.1)MFBS=0.00000000
      MFB1=CSH12**(1./3.)*CEXP(-.88*KSI1-(0.,1.)*.5I*KSI1)*
     +CONST/SQRT(2.*PI*SIGMA1)
      MFB2=CSH22**(1./3.)*CEXP(-.88*KSI2-(0.,1.)*.5I*KSI2)*
     +CONST/SQRT(2.*PI*SIGMA2)
      MFTS=(0.,1.)*MFBS/(2.*PI*SIGMAS)
      MFT1=(0.,1.)*MFB1/(2.*PI*SIGMA1)
      MFT2=(0.,1.)*MFB2/(2.*PI*SIGMA2)
      CJPHIS=-MZ*(MFBS*COSBS**2+MFTS*SINBS**2)
      CJZS=PHI*(MFBS*SINBS**2+MFTS*COSBS**2)
      CJPHI1=-MZ*(MFB1*COSB1**2+MFT1*SINB1**2)
      CJZ1=PHI*(MFB1*SINB1**2+MFT1*COSB1**2)
      CJPHI2=-MZ*(MFB2*COSB2**2+MFT2*SINB2**2)
      CJZ2=PHI*(MFB2*SINB2**2+MFT2*COSB2**2)
      ZETAP=FUNC(ZETAP)
      ZETAM=FUNC(ZETAM)
      SUZETAP=FUNC(-ZETAP)
      SUZETAM=FUNC(-ZETAM)
      IF(MZ.EQ.0.) GO TO 780
      PHIS=EJAL2*CEXP((0.,-1.)*2.*PI*SQRT((A*PHIP)**2+L2*L2))*
     +(-CMSFI*CJPHIS*ZETAP/SQRT(2.*PI)+CEXP((0.,-1.)*PI/4.)*
     +(CJPHI2*CMAPFI-CJPHIS*CMSFI)/(2.*SQRT(4.*PI)*ZETAM))+
     +CEXP((0.,-1.)*2.*PI*A*ABS(PHIP)*SINT)*CMSFI*CJPHIS*
     +UZETAP/SQRT(2.)
     +EJAL1*CEXP((0.,-1.)*2.*PI*SQRT((A*PHIP)**2+L1*L1))*(
     +-CMSFI*CJPHIS*ZETAM/SQRT(2.*PI)*CEXP((0.,-1.)*PI/4.)*(
     +CJPHI1*CMAMFI-CJPHIS*CMSFI)/(2.*SQRT(4.*PI)*ZETAM))+
     +CEXP((0.,-1.)*2.*PI*A*ABS(PHIP)*SINT)*CMSFI*CJPHIS*
     +UZETAM/SQRT(2.)
      GO TO 785
  780 IF(PHI.EQ.0.) GO TO 785
      PHIS=EJAL2*CEXP((0.,-1.)*2.*PI*SQRT((A*PHIP)**2+L2**2))*
     +(-CMSFI*CJZS*ZETAP/SQRT(2.*PI)*CEXP((0.,-1.)*PI/4.)*(
     +CJZ2*CMAPFI-CJZS*CMSFI)/(2.*SQRT(4.*PI)*ZETAP))*CEXP((0.,
     +-1.)*2.*PI*A*ABS(PHIP)*SINT)*CMSFI*CJZS*UZETAP/SQRT(2.)
     +EJAL1*CEXP((0.,-1.)*2.*PI*SQRT((A*PHIP)**2+L1*L1))*(-
     +CMSFI*CJZS*ZETAM/SQRT(2.*PI)*CEXP((0.,-1.)*PI/4.)*(CJZ1*
     +CMAMFI-CJZS*CMSFI)/(2.*SQRT(4.*PI)*ZETAM))*CEXP((0.,-1.)*
     +2.*PI*A*ABS(PHIP)*SINT)*CMSFI*CJZS*UZETAM/SQRT(2.)
  785 CONTINUE
```

```
      PPHI1=PPHI1+(DPHIP/DIVID)*A*PPHI*SIN(PHI-PHIP)
      PPHI2=PPHI2+(DPHIP/DIVID)*A*PPHI*COS(PHI-PHIP)
      PZ1=PZ1+(DPHIP/DIVID)*PZ*A
  800 CONTINUE
      TRUNET=CEXP((0.,-1.)*2.*PI*A*UO)*(0.,-1.)*(50.*PI)*(COST*
     1*PPHI1-SINT*PZ1)
      TRUNEF=CEXP((0.,-1.)*2.*PI*A*UO)*(0.,-1.)*(50.*PI)*PPHI2
      PRINT 799,TRUNET,TRUNEF
  799 FORMAT(5X,7HTRUNET=,F8.4,F9.4,5X,7HTRUNEF=,F8.4,F9.4)
```

SUBTRACT THE FIELDS DUE TO THE REMOVED PARTS OF THE CYLINDER FROM THE

INFINITE CYLINDER SOLUTION TO FIND THE FINITE CYLINDER SOLUTION:

```
      ETETA=ETETA-TRUNET
      EPHI=EPHI-TRUNEF
      PRINT*,"                                        TOTAL FIELD"
      PRINT 800,ETETA,EPHI
      GO TO 900
```

THIS SECTION COMPUTES THE FIELD IN PARAXIAL REGION BY USING EXPRESSIONS

(9.20a) AND (9.20b)

```
  810 PRINT*,"                                  PARAXIAL REGION"
      K= 2.*PI
      IF(ABS(TETA-PI).LT.TETA) K=-2.*PI
      SINAL1=SIN(K*L1)
      COSAL1=COS(K*L1)
      SINAL2=SIN(K*L2)
      COSAL2=COS(K*L2)
      I21=(1.,0.)
      NI=AMAX1(L1,L2,A)*40.+150*Z=ABS(K)/(NI-1)
      DO 111 IKZ=1,NI
      DIVIDK=1.
      IF((IKZ.EQ.1).OR.(IKZ.EQ.NI)) DIVIDK=2.
      KZ=(IKZ-1)*DKZ
      IF(KZ.EQ.ABS(K)) KZ=KZ-.0001
      ARG=SQRT(K*K-KZ*KZ)
      CALL BESSEL(X,FM,FN)
      F2KZ=2.*KZ/(PI*(K*K-KZ*KZ)*A*FM)
      G2KZ=2./(PI*A*FM)
      EJL2=CEXP((0.,-1.)*(KZ-K)*L2)/(KZ-K)
      EJL1=CEXP((0.,-1.)*(KZ+K)*L1)/(KZ+K)
      III=III+(DKZ/DIVIDK)*(EJL2-EJL1)*F2KZ
      I21=I21+(DKZ/DIVIDK)*(EJL2+EJL1)*G2KZ
  111 CONTINUE
      C2FML1=C2FML2=C2FPL1=C2FPL2=C2GML1=C2GML2=C2GPL1=C2GPL2=.0
      ZETAMX=-ALOG10.0001)/AMIN1(L1,L2)
      DZETA=PI/(10.*A)
      NZETA=ZETAMX/DZETA
      DO 222 IZ=1,NZETA
      DIVIDZ=1.
      IF(IZ.EQ.1) DIVIDZ=2.
      ZETA=(IZ-1)*DZETA
      IF(ZETA.GT.ZETAMX) GO TO 333
      EZL1=EXP(-ZETA*L1)
      EZL2=EXP(-ZETA*L2)
      IF(AMIN1(EZL1,EZL2).LE.0.001) DZETA=1.*DZETA
      A1=K*COSAL1+ZETA*SINAL1
      A2=K*COSAL2+ZETA*SINAL2
      A=K*K+ZETA*ZETA
      ARG=A*SQRT(Y)
      CALL BESSEL(X,FM,FN)
      FJZETA=ZETA*FM/(SQRT(Y)*FM)*(0.,1.)*2.*ZETA/(PI*A*Y*FM)
      GJZETA=SQRT(Y)*FN/FM*(0.,1.)*2./(PI*A*FM)
      C2FML1=C2FML1+(DZETA/DIVIDZ)*(A1+(0.,1.)*B1)*FJZETA*EZL1/(
      C2FML2=C2FML2+(DZETA/DIVIDZ)*(A2+(0.,1.)*B2)*FJZETA*EZL2/Y
      C2FPL1=C2FPL1+(DZETA/DIVIDZ)*(A1-(0.,1.)*B1)*FJZETA*EZL1/Y
      C2FPL2=C2FPL2+(DZETA/DIVIDZ)*(A2-(0.,1.)*B2)*FJZETA*EZL2/Y
      C2GML1=C2GML1+(DZETA/DIVIDZ)*(B1-(0.,1.)*A1)*GJZETA*EZL1/Y
      C2GML2=C2GML2+(DZETA/DIVIDZ)*(B2-(0.,1.)*A2)*GJZETA*EZL2/Y
      C2GPL1=C2GPL1+(DZETA/DIVIDZ)*(B1+(0.,1.)*A1)*GJZETA*EZL1/Y
      C2GPL2=C2GPL2+(DZETA/DIVIDZ)*(B2+(0.,1.)*A2)*GJZETA*EZL2/Y
```

```
03470 222 CONTINUE
03480 333 CONTINUE
03490 I1L1L2=-2.*I11*AIMAG(C2FML2+C2FML1-C2FPL2-C2FPL1)+(0.,1.)*
03500+REAL(C2FML2-C2FML1+C2FPL2-C2FPL1)
03510 I2L1L2=-2.*I21*AIMAG(C2GML2+C2GML1+C2GPL2+C2GPL1)+(0.,1.)*
03520+REAL(C2GML2-C2GML1-C2GPL2+C2GPL1)
03530 PARAXX=(0.,1.)*MPHI*I1L1L2/(8.*PI*PI*A)
03540 PARAXY=-M2*I2L1L2/(8.*PI*PI)
```

IF THE OBSERVATION POINT IS VERY CLOSE TO THE AXIS BUT NOT EXACTLY ON THE AXIS, THE SPHERICAL COMPONENTS OF THE PARAXIAL FIELD CAN BE FOUND IN TERMS OF ITS RECTANGULAR COMPONENTS AND THE TOTAL FIELD IN THESE DIRECTIONS CAN BE OBTAINED BY ADDING WEDGE DIFFRACTED FIELD TO THESE VALUES.

```
03550 ETETA=PARAXX*COS(PHI)*COS(TETA)+PARAXY*SIN(PHI)*COS(TETA)
03560+*EWTET
03570 EPHI=-PARAXX*SIN(PHI)+PARAXY*COS(PHI)+EWFI
03580 PRINT 866,PARAXX,PARAXY
03590 866 FORMAT(5X,3HEX=,F8.4,F9.4,5X,3HEY=,F8.4,F9.4)
03600 PRINT*," TOTAL FIELD"
03610 PRINT300,ETETA,EPHI
03620 900 CONTINUE
03630 RETURN
03640 END
```

SUBROUTINE "BESSEL"

THIS SUBROUTINE COMPUTES THE EXPRESSIONS

$$FM = \frac{1}{J'^2_1(X) + Y'^2_1(X)} \quad , \quad FN = J_1(X)J'_1(X) + Y_1(X)Y'_1(X)$$

AS FUNCTIONS OF X, TO BE USED IN EQUATIONS (9.17) AND (9.19).

```
03650 SUBROUTINE BESSEL(X,FM,FN)
03660 PI=3.14159265 36
03670 IF(X.EQ.0.) X=0.0001
03680 IF(X.GT.3.) GO TO 20
03690 XT=X/3.0SXT2=XT*XTSXT4=XT2*XT2SXT6=XT4*XT2SXT8=XT4**(2)
03700 XT10=XT8*XT2
03710 BJ1=X*(0.5-.56249985*XT2+.21093573*XT4-.03954289*XT6+.0044
03720+3319*XT8-.00031761*XT10)
03730 DBJ1=0.5-3.*.56249985*XT2+5.*.21093573*XT4-7.*.03954289*
03740+XT6+9.*.00443319*XT8-11.*.00031761*XT10
03750 ELOGX=ALOG(X/2.)
03760 BY1=(2./(PI*1.0))*ELOGX*BJ1+(1./X)*(-.6366198+.2212091*
03770+XT2+2.168270*XT4-1.316486 7*XT6+.3123951*XT8-.0400976*XT10
03780+*.0027873*XT12*XT2)
03790 DBY1=.0000000000+0.000000000000+(2./(PI*X**1))*BJ1+(2./(PI*
03800+1.0))*ELOGX*DBJ1+(1./(X*X))*(.6366198+.2212091*XT2+3.*2.16
03810+8270 9*XT4-5.*1.3164827*XT6+7.*.3123951*XT8-9.*.0400976*
03820+XT10+11.*.0027873*XT10*XT2)
03830 FM=DBJ1**2+DBY1**2SFN=DBJ1*BJ1+DBY1*BY1
03840 RETURN
03850 20 IF(X.GT.20.) GO TO 30
03860 XE1=X.*XSXE2=XE1**2SXE3=XE2*XE1SXE4=XE3*(XE1)
03870 P1=1.+15./12.*XE2)-14175./(24.*XE4)
```

```
03880 Q1=3./XE1-315./(6.*XE3)
03890 R1=1.-57./(2.*XE2)
03900 S1=7./XE1+585./(6.*XE3)
03910 FM=(2./(PI*X))*(PI*R1+S1*SI)$FN=(2./(PI*X))*(Q1*R1-P1*S1)
03920 RETURN
03930 30 CONTINUE
03940 FM=(2./(PI*X))*(1.-0./(8.*X)**2)$FN=-1./(PI*X*X)
03950 RETURN
03960 END
```

FUNCTION SUBPROGRAMS

"FOCKV", "FOCKU", "DFOCKU", "DFOCKV"

THESE FUNCTION SUBPROGRAMS COMPUTE:

$$v(x),\ u(x),\ u'(x),\ v'(x)$$

```
03970 COMPLEX FUNCTION FOCKV(X)
03980 COMPLEX FV,TP
03990 DIMENSION ABSTP(10)
04000 DATA ABSTP/1.01879,3.24820,4.82010,6.16331,7.37218,8.48849
04010+,9.53545,10.52766,11.47506,12.38479/
04020 FV=0.
04030 PI=3.1415926536
04040 IF(X.LE.0.6) GO TO 20
04050 DO 10 N=1,10
04060 TP=ABSTP(N)*CEXP(-(0.,1.)*PI/3.)
04070 FV=FV+CEXP(-(0.,1.)*X*TP)/TP
04080 10 CONTINUE
04090 FOCKV=FV*SQRT(PI)*SQRT(X)*CEXP(-(0.,1.)*PI/4.)
04100 RETURN
04110 20 CONTINUE
04120 FOCKV=1.-SQRT(PI)*CEXP((0.,1.)*PI/4.)*X**(3./2.)/4.+(0.,7.
04130+)*X**3/60.+7.*SQRT(PI)*CEXP((0.,-1.)*PI/4.)*X**(4.5)/512.
04140+-0.004141*X**6
04150 RETURN
04160 END
04170 COMPLEX FUNCTION FOCKU(X)
04180 COMPLEX FU,TN
04190 DIMENSION ABST(10)
04200 DATA ABST/2.33811,4.08795,5.52056,6.78671,7.99417,9.02265,
04210+10.04017,11.00852,11.93602,12.82878/
04220 FU=0.
04230 PI=3.1415926536
04240 IF(X.LE.0.6) GO TO 20
04250 DO 10 N=1,10
04260 TN=ABST(N)*CEXP(-(0.,1.)*PI/3.)
04270 FU=FU+CEXP(-(0.,1.)*X*TN)
04280 10 CONTINUE
04290 FOCKU=FU*2.*SQRT(PI)*X**(3./2.)*CEXP((0.,1.)*PI/4.)
04300 RETURN
04310 20 FOCKU=1.-SQRT(PI)*CEXP((0.,1.)*PI/4.)*X**1.5/2.+(0.,5.)
04320+*X**5/12.+5.*SQRT(PI)*CEXP((0.,-1.)*PI/4.)*X**4.5/64.
04330+-0.03701*X**6
04340 RETURN
04350 END
04360 COMPLEX FUNCTION DFOCKV(X)
04370 COMPLEX DFV,TP
04380 DIMENSION ABSTP(10)
04390 DATA ABSTP/1.01879,3.24820,4.82010,6.16331,7.37218,8.48849
04400+,9.53545,10.52766,11.47506,12.38479/
04410 DFV=0.
04420 PI=3.1415926536
04430 IF(X.LE.0.6) GO TO 20
04440 DO 10 N=1,10
```

```
      TP=ABSTP(N)*CEXP(-(0.,1.)*PI/3.)
      DFV=DFV+(1.-(0.,1.)*2.*X*TP)*CEXP(-(0.,1.)*X*TP)/TP
   10 CONTINUE
      DFOCKV=DFV*CEXP(-(0.,1.)*PI/4.)*SQRT(PI)*X**(-1./2.)/2.
      RETURN
   20 DFOCKV=3.*SQRT(PI)*CEXP((0.,-3.)*PI/4.)*X**0.5/8.+(0.,7
     +.)*X**2/20.+63.*SQRT(PI)*CEXP((0.,-1.)*PI/4.)*X**3.5/1024.
     +-0.3248*X**5
      RETURN
      END
      COMPLEX FUNCTION DFOCKU(X)
      COMPLEX DFU,TN
      DIMENSION ABST(10)
      DATA ABST/2.33811,4.08795,5.52056,6.78671,7.99417,9.02265,
     +10.04017,11.00852,11.93602,12.82878/
      DFU=0.
      PI=3.1415926536
      IF(X.LE.0.6) GO TO 20
      DO 10 N=1,10
      TN=ABST(N)*CEXP(-(0.,1.)*PI/3.)
      DFU=DFU+(1.-(0.,1.)*(2./3.)*X*TN)*CEXP(-(0.,1.)*X*TN)
   10 CONTINUE
      DFOCKU=DFU*CEXP((0.,1.)*PI/4.)*3.*SQRT(PI)*X**(1./2.)
      RETURN
   20 DFOCKU=.75*SQRT(PI)*CEXP((0.,-.75)*PI)*X**0.5+(0.,.5.)*
     +X**2/4.+45.*SQRT(PI)*CEXP((0.,-1.)*PI/4.)*X**3.5/128.
     +-0.2221*X**5
      RETURN
      END
```

SUBROUTINE "WDGPT"

THIS SUBROUTINE LOCATES THE DIFFRACTION POINTS ON THE WEDGES BY SOLVING EQUATION (7.3) FOR "ROOTD" = ϕ_w AS A FUNCTION OF "HA" = ℓ_2/a, "TETA" = θ_o, "PHI" = ϕ_o.

```
      SUBROUTINE WDGPT(HA,TETA,PHI,NMAX,ROOTD,IROOT)
      DIMENSION  PHIDD(400),FUNCT(400),ROOT(20),ROOTD(20)
      FCT(PHID,HA,TETA,PHI)=1.00*PHID/SQRT(HA**2+PHID**2)
     +-SIN(TETA)*SIN(PHI-PHID)
      PI=3.1415
      DELFID=2.*PI/NMAX
      NMAX1=NMAX+1
      NRMAX=3
      DPHI=0.00001
      F1=FCT(-PI,HA,TETA,PHI)$FUNCT(1)=F1$X1=-PI$IROOT=0
  510 DO 200 IPHID=1,NMAX1
      PHID=-PI+(IPHID-1)*DELFID$FUNCT(IPHID)=FCT(PHID,HA,TETA,
     +PHI)$PHIDD(IPHID)=PHID*180./PI
      IF(FUNCT(IPHID)) 105,102,105
  102 IROOT=IROOT+1$ROOT(IROOT)=PHID$ROOTD(IROOT)=PHID*180./
     +PI
      PHID=PHID+DPHI$X1=PHID$F1=FCT(X1,HA,TETA,PHI)
      IF(F1) 200,102,200
  105 IF(F1*FUNCT(IPHID).LT.0.) GO TO 110
      X1=PHID$F1=FUNCT(IPHID)
      GO TO 200
  110 X2=PHID
      DO 115 J=1,NRMAX
      X=(X1+X2)/2.$FX=FCT(X,HA,TETA,PHI)
      IF(FX*F1) 113,112,114
  112 IROOT=IROOT+1$ROOT(IROOT)=X$ROOTD(IROOT)=X*180./PI
      PHID=X+DPHI$X1=PHID$F1=FCT(X1,HA,TETA,PHI)
      IF(F1) 200,112,200
  113 X2=X1$X1=X$F1=FX
      GO TO 115
```

```
05040 114 X1=X$F1=FX
05050 115 CONTINUE
05060 PHIO=((X2-X1)/(FCT(X2,MA,IETA,PHI)-FX))*(-FX)+X1
05070 DPHI1=DELPIO/2**(NRMAX-1)
05080 IROOT=IROOT+1$ROOT(IROOT)=PHIO$ROOTD(IROOT)=PHIO*180./PI
05090 X1=PHIO+DPHI1$F1=FCT(X1,MA,IETA,PHI)
05100 200 CONTINUE
05110 RETURN
05120 END
```

FUNCTION SUBPROGRAMS: "F0", "G0", "G1"

THESE SUBPROGRAMS CALCULATE:

$$f_0(x),\ g_0(x),\ g_1(x)$$

```
05130 COMPLEX FUNCTION G0(X)
05140 COMPLEX ZG0(100),ZGA(100),ZGB(100)
05150 DATA ZGA/(1.9998,0.0055),(1.9997,0.0059),(1.9997,0.00
05160+03),(1.9996,0.0067),(1.9996,0.0073),(1.9995,0.0078),(1.999
05170+4,.0084),(1.9994,.0090),(1.9992,0.0098),(1.9991,0.0106),
05180+(1.999,0.0115),(1.999,.012),(1.999,0.014),(1.998,0.015),
05190+(1.998,0.016),(1.998,0.018),(1.997,0.020),(1.996,0.022),
05200+(1.9996,0.024),(1.995,0.026),(1.993,0.029),(1.992,0.033),
05210+(1.99,.036),(1.988,0.040),(1.985,0.045),(1.981,0.050),(1.9
05220+77,.056),(1.971,0.062),(1.965,0.068),(1.956,0.075),(1.946,
05230+0.082),(1.933,0.090),(1.919,0.098),(1.901,0.105),(1.880,.1
05240+13),(1.857,.121),(1.829,.123),(1.798,.126),(1.762,.126),
05250+(1.722,.122),(1.678,.115),(1.63,.103),(1.578,.086),(1.522,
05260+.063),(1.462,.034),(1.399,0.0)/
05270 DATA ZGB/
05280+(1.333,.040),(1.263,0.003),(1.19,-.127),(1.115,-.169),(1.038
05290+,.209),(0.96,-.244),(.883,-.274),(.806,-.299),(.732,-.317),(.
05300+66,.331),(.59,-.339),(.527,-.345),(.467,-.342),(.411,-.338)
05310+,(.36,-.33),(.313,-.32),(.27,-.309),(.232,-.296),(.197,-.281),(
05320+.167,-.267),(.14,-.252),(.116,-.237),(.095,-.222),(.076,-.208),
05330+(.0596,-.1936),(.0453,-.1797),(.033,-.1664),(.0224,-.1536),(-.0
05340+133,-.1414),(-.0055,-.1299),(-.0010,-.119),(-.0065,-.1081),(-.0
05350+11,-.0991),(-.0147,-.0901),(-.0176,-.0817),(-.0199,-.0739),(-.
05360+0210,-.0666),(-.0224,-.0596),(-.0237,-.0537),(-.0242,-.048),(-.0
05370+244,-.0428),(-.0243,-.038),(-.0240,-.0336),(-.0235,-.0296),(-.02
05380+28,-.026)/
05390P700
05400 100 FORMAT(6(F9.4,F7.4))
05410 IF(X.GT.4.5) GO TO 30
05420 IF(X.LT.-4.5) GO TO 40
05430 DO 10 I=1,46
05440 10 ZG0(I)=ZGA(I)
05450 DO 20 I=47,91
05460 ZG0(I)=CONJG(ZGB(I-46))
05470 20 CONTINUE
05480 ZG0(92)=ZG0(91)
05490 IX=10.*X$IX1=46+IX
05500 IF (X.LT.0.0) GO TO 25
05510 G0=ZG0(IX1)+(10.*X-IX)*(ZG0(IX1+1)-ZG0(IX1))
05520 RETURN
05530 25 INDIC=1$ IF(IX1.EQ.1) INDIC=0
05540 G0=(ZG0(IX1)+(10.*X-IX)*(ZG0(IX1)-ZG0(IX1-INDIC)))*CEXP((0
05550+.,1.)*X**3/3.)
05560 RETURN
05570 30 G0=CEXP(1.01879*X*(-.866025-(0.,.5)))/.545725-CEXP(3.24
05580+62*X*(-.866025-(0.,0.5)))/1.591061
05590 RETURN
05600 40 G0=2.*CEXP((0.,1.)*X**3/3.)*(1.-(0.,1.)/(4.*X**3)-1./X*
05610+*6)
05620 RETURN
05630 END
```

```
06330 20 DGXA=(1./(12.*DX))*(G0(XAM2)*EP(XAM2)-8.*G0(XAM1)*EP(X
06340+AM1)+8.*G0(XAP1)*EP(XAP1)-G0(XAP2)*EP(XAP2))
06350 DGXB=(1./(12.*DX))*(G0(XBM2)*EP(XBM2)-8.*G0(XBM1)*EP(XB
06360+M1)+8.*G0(XBP1)*EP(XBP1)-G0(XBP2)*EP(XBP2))
06370 G1=(DGXA+(X-XA)*(DGXB-DGXA)*IS/DX)/EP(X)+(0.,1.)*
06380+X**2*G0(X)
06390 RETURN
06400 10 G1=-CEXP((0.,1.)*PI/6.)*(CEXP(1.01879*X*(-.866025-(0.,0
06410+.5)))/.53566-CEXP(3.2482*X*(-.866025-(0.,0.5)))/.41902)
06420 RETURN
06430 30 G1=2.*CEXP((0.,1.)*X**3/3.)*((0.,1.)*X**2+1./(4.*X)-(0.
06440+,1.)/(4.*X**4)+6./X**7)
06450 RETURN
06460 END
```

FUNCTION SUBPROGRAM "UFUNC"

$$\text{UFUNC}(X) = \begin{cases} 0 & , \quad X < 0 \\ 0.5 & , \quad X = 0 \\ 1.0 & , \quad X > 0 \end{cases}$$

```
06470 REAL FUNCTION UFUNC(X)
06480 IF(X.EQ.0.) GO TO 10
06490 UFUNC=(SIGN(1.,X)+1.)/2.
06500 RETURN
06510 10 UFUNC=0.5
06520 RETURN
06530 END
```

FUNCTION SUBPROGRAM "WFUNC"

WFUNC(X) = W(X) , DEFINED IN (8.30)

```
06540 COMPLEX FUNCTION WFUNC(X)
06550 PI=3.1415926536
06560 IF(X.EQ.0.) GO TO 10
06570 Y=2.*ABS(X)/SQRT(PI)
06580 FOY=(1.+0.926*Y)/(2.+1.792*Y+3.104*Y*Y)
06590 GOY=1./(2.+3.142*Y+3.492*Y*Y+2.67*Y**3)
06600 WFUNC=SQRT(PI)*SIGN(1.,X)*((0.,1.)*FOY-GOY)
06610+*CEXP((0.,0.25)*PI)/SQRT(2.)
06620 RETURN
06630 10 WFUNC=0.
06640 RETURN
06650 END
06660 COMPLEX FUNCTION PHIDEL(T,R,S)
06670 COMPLEX IO,I1,PHIDEL
06680 PI=3.1415926536
06690 GAMMA3=2.6789585347
06700 U=0.050
06710 XMAX=U
06720 XMIN=-U
06730 NX=400
06740 DX=(XMAX-XMIN)/NX
06750 IO=0.
06760 DO 200 N=1,NX
06770 X=XMIN+(N-1)*DX
06780 DIVID=1.5IF((N.EQ.1).OR.(N.EQ.NX)) DIVID=2.
06790 IO=IO+(DX/DIVID)*CEXP((0.,1.)*(T*X*X+R*X**3+S*X**4))
06800 200 CONTINUE
06810 PHIDEL=IO$RETURN
06820 END
```

REFERENCES

[1] J. J. Bowman, T. B. A. Senior and P. L. E. Uslenghi, Electromagnetic and Acoustic Scattering by Simple Shapes, NorthHolland Publishing Co., Amsterdam (1969).

[2] P. L. E. Uslenghi, Lectures on High-Frequency Scattering Methods, Sorrento, Italy. September 58, (1972).

[3] R. G. Kouyoumjian, "Asymptotic high-frequency methods", Proc. IEEE, 53, 1965, pp. 864-876.

[4] G. N. Watson, "The diffraction of electric waves by the earth", Proc. Roy. Soc., A95, pp. 83-99, 1918.

[5] E. Pflumm, "Expansion problems arising from the Watson transformation", Research Report No. BR35, New York University, New York (1960).

[6] E. Fischer, "On the Watson Transformation", Comm. Pure Appl. Math., 19, pp. 287-297 (1966).

[7] D. S. Cohen, "New eigenfunction expansions and alternative representations for the reduced wave equations", J. Math. Mech., 14, pp. 403-412 (1965).

[8] J. W. Crispin, Jr. and A. L. Maffett, "Radar cross-section estimation for simple shapes", Proc. IEEE, 53, pp. 833-843 (1965).

[9] K. M. Siegel, "Far field scattering from bodies of revolution", Appl. Sci. Res., B7, pp. 293-328, (1958).

[10] K. M. Siegel, R. F. Goodrich and V. H. Weston, "Comments on far field scattering from bodies of revolution", Appl. Sci. Res., B8, pp. 8-12, (1959).

[11] R. K. Luneburg, Mathematical Theory of Optics, Brown University Notes, Providence, 1944.

[12] M. Kline and I. Kay, Electromagnetic Theory and Geometrical Optics, Interscience Publishers, New York, 1965.

[13] V. A. Fock, "The distribution of currents induced by a plane wave on the surface of a conductor", J. Phys. USSR, 10, pp. 130-136, 1946.

[14] V. A. Fock, "The field of a plane wave near the surface of a conducting body", J. Phys. USSR, 10, pp. 399-409, 1946.

[15] R. F. Goodrich, "Fock theory--an appraisal and Exposition", IRE Trans. Antennas Propagation, AP-7, Special supplement, pp. 2836, 1959.

[16] V. A. Fock, "Diffraction of radio waves around the earth's surface", J. Phys., 9, pp. 225-266, 1945.

[17] N. A. Logan, K. S. Yee, "A mathematical model for diffraction by convex surfaces", Electromagnetic Waves, edited by R. E. Langer, The University of Wisconsin Press, Madison, pp. 139180, 1962.

[18] J. A. Cullen, "Surface Current Induced by Short-Wavelength Radiation", Phys. Rev., 2nd series, 9, No. 6, pp. 1863-1867, 1958.

[19] S. Hong, "Asymptotic Theory of Electromagnetic and Acoustic Diffraction by Smooth Convex Surfaces of Variable Curvature", J. Math. Phys., 8, No. 6, 1967, pp. 12231232.

[20] B. R. Levy and J. B. Keller, "Diffraction by a Smooth Object", Comm. Pure Appl. Math., XII, pp. 159-209, 1959.

[21] S. W. Lee and S. Safavi-Naini, "Asymptotic solution of surface field due to a magnetic dipole on a cylinder", Electromagnetics Laboratory Technical Report No. 76-11, University of Illinois at Urbana-Champaign, November 1976.

[22] S. W. Lee and S. Safavi-Naini, "Asymptotic solution of surface field due to a magnetic dipole on a cylinder", IEEE Trans. on Antennas and Propagation, AP-26, No. 4, pp. 593598, 1978.

[23] J. B. Keller, "Diffraction by a convex cylinder", IRE Trans., AP-4, pp. 312-321, 1956.

[24] J. B. Keller, "Diffraction by an aperture I, II", J. Appl. Phys., 28, pp. 426-444 and 570-579, 1957.

[25] R. G. Kouyoumjian, "The GTD and its application", chapter 6 of Numerical and Asymptotic Techniques in Electromagnetics, edited by R. Mittra, Springer-Verlag, 1975.

[26] P. H. Pathak and R. G. Kouyoumjian, "The radiation from apertures in curved surfaces", Electro-Science Lab, Department of Electrical Engineering, Ohio State University. Report 3001-2, December 1972.

[27] J. B. Keller and B. R. Levy, "Decay exponents and diffraction coefficients for surface waves on surfaces of nonconstant curvature", IRE Trans. Antennas Propagation, AP-7, pp. S52-S61, 1959.

[28] W. Franz and K. Klante, "Diffraction by surfaces of variable curvature", IRE Trans. Antennas Propagation, AP-7, pp. S68-S70, 1959.

[29] D. R. Voltmer, "Diffraction by doubly curved convex surfaces", Ph.D. dissertation, Ohio State University, Columbus, Ohio, 1970.

[30] P. H. Pathak and R. G. Kouyoumjian, "An analysis of the radiation from apertures in curved surfaces", Proc. IEEE, 62, pp. 1438-1447, 1974.

[31] Yu. A. Kravtsov, "A modification of the geometrical optics method", Radiofizika, 7, pp. 664-673, 1964.

[32] D. Ludwig, "Uniform asymptotic expansions at a caustic", Comm. Pure App. Math., 19, pp. 215-250, 1966.

[33] E. Zauderer, "Uniform asymptotic solutions of the reduced wave equation", J. Math. Anal. Appl., 30, pp. 157-171, 1970.

[34] R. E. Langer, "Turning Point in Linear Asymptotic Theory", Res. Report No. 127, University of Wisconsin, 1960.

[35] F. W. J. Olver, "Asymptotic solution of linear differential equation of second order in a domain containing one transition point", Phil. Trans. Roy. Soc. London, Ser. A, 249, p. 65, 1956.

[36] R. M. Lewis, N. Bleistein and D. Ludwig, "Uniform asymptotic theory of creeping waves", Comm. Pure and Appl. Math., XX, pp. 295-328, 1967.

[37] V. H. Weston, "The effect of a discontinuity in curvature in high frequency", IRE Trans. Antennas Propagation, AP-10, pp. 775-780, 1962.

[38] J. B. Keller and Kaminetzky, "Diffraction coefficients for higher order edges and vertices", SIAM J. Appl. Math., 22, pp. 109-134, 1972.

[39] Thompson, "Radio propagation over a sectionally cylindrical surface", Proc. Roy. Soc., Ser. A, 267, pp. 183-196, 1962.

[40] P. L. Christiensen, "Diffraction of creeping wave by discontinuity in the surface impedance of a smooth body", URSI spring meeting, Washington, D. C., USA, 1966.

[41] N. Chr. Albertsen, "Diffraction of creeping waves", Tech. Rept., Technical University of Denmark, Lyngby, December 1974.

[42] R. F. Goodrich, R. E. Kleinman, A. L. Maffett, C. E. Schonsted, K. M. Siegel, M. G. Chernin, H. E. Shank and R. E. Plummers, "Radiation from slot arrays and cones", IRE Trans. Antennas Propagation, pp. 213-222, 1959.

[43] R. N. Buchal and J. B. Keller, "Boundary Layer Problems in diffraction theory", Comm. Pure Appl. Math., 13, pp. 85-114, 1960.

[44] Z. W. Chang, L. B. Felsen and A. Hessel, "Surface ray methods for mutual coupling in conformal arrays on cylindrical surfaces", Final Report, Department of Electrical Engineering and Electrophysics, Polytechnic Insitute of New York, February 1976.

[45] K. K. Chan, L. B. Felsen, A. Hessel and J. Shmoys, "Creeping waves on a perfectly conducting cone", IEEE Trans. Antennas Propagation, AP-25, No. 5, pp. 661-671, 1977.

[46] S. W. Lee and R. Mittra, "Mutual admittance between slots on a cylinder or cone", Tech. Rept. No. 77-24, Electromagnetic Laboratory, Department of Electrical Engineering, University of Illinois at Urbana-Champaign, 1977.

[47] V. A. Fock, "The field from a vertical and a horizontal dipole raised above the earth's surface", J. Expt. and Theor. Phys. (JETP), 19, No. 10, p. 916, 1949 (in Russian). English translation can be found in Electromagnetic Diffraction and Propagation Problems, Pergamon Press, 1965.

[48] N. Chako, "Asymptotic expansion of double and multiple integrals occuring in diffraction theory", J. Inst. Math. Applic., Vol. 1, pp. 372-422, 1965.

[49] D. S. Jones and M. Kline, "Asymptotic expansion of multiple integrals and the method of stationary phase", J. Math. Physc., 37, pp. 7-28, 1958.

[50] J. W. Nicholson, "On the bending of electric waves around the earth", Phil. Mag., 18, pp. 757-760, 1910.

[51] B. Van der Pol, "On the propagation of electromagnetic waves around the earth", Phil. Mag., 38, pp. 365-380, 1919.

[52] B. Van der Pol and H. Bremmer, "Diffraction of electromagnetic waves from an electrical point source around a finitely conducting sphere with applications to radio-telegraphy and the theory of the rainbow", Part I: Phil. Mag., 24, pp. 141-176, 1937; Part II: Phil. Mag., 24, pp. 825-864, 1937.

[53] M. H. L. Pryce, "The diffraction of radiowave by the curvature of the earth", Advance in Physics, 2, pp. 67-95, 1953.

[54] V. A. Fock, Tables of the Airy Function, Moscow, 1946.

[55] J. R. Wait and A. M. Conda, "Diffraction of electromagnetic waves by smooth obstacles for grazing angles", Journal of Research NBS D. Radio Propagation, 63D, 1959.

[56] J. R. Wait, Electromagnetic Radiation from Cylindrical Structures, Pergamon Press, New York, 1959.

[57] M. G. Belkina, Tables to Calculate the Electromagnetic Field in the Shadow Region for Various Soils, Soviet RAdio Press, Moscow, 1949 (translated by M. D. Friedman, ASTIA Document No. AD110298, 1956).

[58] A. S. Goriainov, "An asymptotic solution of the problem of diffraction of a plane wave by a conducting cylinder", Radiotekh i Elektron., 3, pp. 603-614, 1958.

[59] V. A. Fock, L. A. Vainshtein and M. G. Belkina, Diffraction of Electromagnetic Waves by Certain Bodies of Revolution, Soviet Radio Press, 1949.

[60] S. O. Rice, "Diffraction of plane radio waves by a parabolic cylinder--Calculation of shadows behind the hills", Bell System J., 33, pp. 417-504, March 1954.

[61] N. A. Logan, General Research on Diffraction Theory, 1 and 2, Lockheed Missiles and Space Division Technical Reports LMSD-288087 and LMSD-288088 (ASTlA Nos. AD241228 and AD243182), Synnyvale, California, 1959.

[62] M. Abramowitz and I. A. Stegun, Handbook of Mathematical Functions, Chapter 9, Dover Pub., Inc., New YOrk, 1970.

[63] P. C. Bargeliotes, A. T. Villeneuve and W. H. Kummer, "Pattern Synthesis of Conformal Arrays", prepared for Department of the Navy, Washington, D. C. by Radar Microwave Laboratory, Aerospace groups, Hughes Aircraft Company - Culver City, California, January 1975.

[64] T. B. A. Senior, "Impedance boundary conditions for imperfectly conducting surfaces", Appl. Sci. Res., Dec. B, 8, pp. 418-436, 1960.

[65] V. A. Fock, Electromangetic Diffraction and Propagation Problems, Pergamon Press, 1965.

[66] M. A. Leontovich, Investigations of Propagation of Radiowaves, Part II, Moscow, 1948.

[67] F. K. Oshiro, K. M. Mitzner, and R. W. Cross, "Scattering from finite cylinders by source distribution techniques", presented at the 2nd GISAT Symp., Bedford, Mass., 1967.

[68] J. Goldhirsh, D. L. Knepp, and R. J. Doviak, "Radiation from a dipole near a conducting cylinder of finite length", IEEE Trans. on Electromagnetic Compatibility, ENC-12, No. 3, pp. 96-105, 1970.

[69] A. H. Cherin, and J. Goldhirsh, "Impedance and farfield characteristics of a linear antenna near a conducting cylinder", IEEE Trans. on Electromagnetic Compatibility, EMC-15, No. 3, p. 110, 1973.

[70] C. C. Kao, "Three-dimensional electromagnetic scattering from a circular tube of finite length", Journal of Applied Physics, 10, No. 12, pp. 4732-4740, 1969.

[71] C. C. Kao, "Measurements of surface currents on a finite circular tube illuminated by electromagnetic wave.", IEEE Trans. on Antennas and Propagation, pp. 569573, 1970.

[72] J. Meixner, "The radiation pattern and induced current in a circular antenna with an annular slit", IRE Trans. on Antennas and Propagation, AP-4, pp. 408-411, 1956.

[73] H. H. Kuehl, "Radiation from a radial electric dipole near a long finite circular cylinder", IRE Trans. on Antennas and Propagation, pp. 546-553, 1961.

[74] C. W. Harrison, and R. W. P. King, "Excitation of a coaxial line through a transverse slot.", IEEE Trans. on Electromagnetic Compatibility, EMC-14, No. 4, pp. 107-112, 1972.

[75] R. W. P. King and C. W. Harrison, "Transmission line coupled to a cylinder in an incident field.", IEEE Trans. on Electromagnetic Compatibility, ENC-14, No. 3, pp. 97-105, 1972.

[76] R. B. Kieburtz, "Scattering by a finite cylinder", Proceedings of Electromagnetic Wave Theory Symp., London, pp. 145-157, 1966.

[77] P. Ia. Ufimtsev, "Approximate computation of the diffraction of plane electromagnetic waves at certain metal bodies," parts (I) and (II), Soviet Physics, 2, pp. 1708-1718 and pp. 2386-2369, 1958.

[78] H. Bach, K. Pontoppidan, L. Solymar, and N. E. Jensen, "High frequency radiation pattern prediction for satellite antennas", ESTEC-contract No. 1821/72 HP Final Report, The Technical University of Denmark, Lyngby, Denmark, 1973.

[79] F. Molinet, L. Saltiel, and N. E. Jensen, "High frequency radiation Pattern prediction for satellite antennas", ESTEC contract no. 1820/72 HP, final report, Laboratoire Central de telecommunications (LCT), Velizy-Villacoublay, France, 1973.

[80] N. C. Albertsen, H. Bach, F. Jensen, K. Pontoppidan, P. Balling, and L. Solymar, "A study on radiation pattern prediction for high frequency satellite antennas", Contract No. ESTEC 2069/73 HP, Interim Report, Electromagnetic Institute, Technical University of Denmark, Lyngby, Denmark, Report No. D220, 1974.

[81] W. E. Burnside, C. L. Yu, and R. J. Marhefka, "A technique to combine the geometrical theory of diffraction and the moment method", IEEE Trans. on Antennas and Propagation, pp. 551-558, 1975.

[82] R. Mittra, Y. Rahmat-Samii, and W. L. Ko, "Spectral theory of diffraction", Journal of Applied Physics, 10, pp. 1-13, 1976.

[83] R. Mittra, Y. Rahmat-Samii, and W. L. Ko, "Solution of Electromagnetic scattering and radiation problems using a spectral domain approach; a review" (to appear in Wave Motion Journal).

[84] W. L. Ko, and R. Mittra, "A new approach based on a combination of integral equation and asymptotic technique for solving electromagnetic problems", IEEE Trans. on Antennas and Propagation, AP-25, No. 2, pp. 187-197.

[85] S. Safavi-Naini and R. Mittra, "Source radiation in the presence of smooth convex bodies", Technical Report No. 78-3, Electromagnetic Laboratory, Department of Electrical Engineering, University of Illinois, Urbana, Illinois, 1978 (Supported by contract No. N00019-78-C-0069)

[86] G. E. Stewart, and K. E. Golden, "Mutual admittance for axial rectangular slots in a large conducting cylinder", IEEE Trans. on Antennas and Propagation, AP-19, pp. 120-122, 1971.

[87] K. E. Golden, G. E. Stewart, and D. C. Pridmore-Brown, "Approximation techniques for the mutual admittance of slot antennas on metallic cones", IEEE Trans. on Antennas and Propagations, AP-22, pp. 43-48, 1974.

[88] Y. Hwang, and R. G. Kouyoumjian, "The mutual coupling between slots in a perfectly conducting circular cylinder by the GTD," Electro-Science Laboratory, Department of Electrical Engineering, The Ohio State University, Semi-annual Report 2902-21, under Grant NGL 36-003-138, 1975.

[89] P. H. Pathak, "Analysis of a conformal receiving array of slots in a perfectly conducting circular cylinder by the GTD," Electro-Science Laboratory, Department of Electrical Engineering, The Ohio State University, Technical Report ESL 3735-2, prepared under contract N00140-74-C-6017, 1975.

[90] P. H. Pathak, and N. N. Wang, "An analysis of the matual coupling between antennas on a smooth convex surface", Electro-Science Lab., Department of Electrical Engineering, The Ohio State University, Final Report 784583-7, prepared under contract No. N62269-76-C-0554, 1978.

[91] Z. W. Chang, L. B. Felsen, A. Hessel and J. Shmoys, "Surface ray method in the analysis of conformal arrays", Digest of 1976 APS International Symposium held at University of Massachusetts at Amherst, 1976, pp. 366-369.

[92] J. Boersma, and S. W. Lee, "Surface field due to a magnetic dipole on a cylinder: Asymptotic expansion of exact solution", Technical Report No. 78-17, Electromagnetics Laboratory, Department of Electrical Engineering, University of Illinois, Urbana, Illinois, 1978 (Supported by contract No. N00019-78-C-0064).

[93] R. G. Kouyoumjian, and W. D. Burnside, "The diffraction by a cylinder-tipped half-plane", IEEE Trans. on Antennas and Propagation, AP-18, pp. 424-426, 1970.

[94] L. Peters, Jr., and C. E. Ryan Jr., "Empirical formulas for E-plane creeping waves on general smooth conducting bodies" IEEE Trans. on Antennas and Propagation, AP-18, pp. 432-434, 1970.

[95] C. E. Ryan Jr., "Analysis of antennas on finite circular cylinders with conical or disk and caps", IEEE Trans. on Antennas and Propagation, AP-20, pp. 474-476, 1972.

[96] E. F. Knott, T. B. A. Senior and P. L. E. Uslenghi, "High frequency e e electromagnetic scattering from a finite circular cylinder", URSI Symposium on Electromagnetic Wave Theory, London, England, Symposium Digest, pp. 112-113, 1974.

[97] N. C. Albertsen and P. L. Christiensen, "Diffraction of creeping wave by an edge", URSI Symposium on Electromagnetic Wave Theory, London, England, Symposium Digest, pp. 114-116, 1974.

[98] S. W. Lee, "Uniform asymptotic theory of electromagnetic edge diffraction: A review", Technical Report No. 77-1, Electromagnetics Laboratory, Department of Electrical Engineering, University of Illinois, Urbana, Illinois, 1977 (Supported by Grant No. NSF-ENG-73-08218).

[99] J. B. Keller, "Geometrical theory of diffraction", Journal of optical Society of America, 52, pp. 116-130, 1962.

[100] R. M. Lewis, and J. Boersma, "Uniform asymptotic theory of edge diffraction", J. Math. Phys., 1o, pp. 2291-2305, 1969.

[101] R. G. Kouyoumjian and P. H. Pathak, "A uniform geometrical theory of diffraction for an edge in a perfectly conducting surface", Proc. IEEE, 62, pp. 1448-1461, 1974.

[102] G. A. Deschamps, "Ray techniques in electromagnetics", Proc. IEEE, 60, pp. 1022-1035, 1972 (A minus sign is missing in the definition of χ.)

[103] S. W. Lee, "Differential geometry for GTD application", Report No. 77-21, Electromagnetic Laboratory, Department of Electrical Engineering, University of Illinois, Urbana, Illinois, (Supported by Grant No. NSF-ENG-73-08218, 1977).

[104] J. J. Stoker, Differential Geometry, Chapter IV, Wiley Interscience, New York, 1969.

[105] C. E. Ryan Jr., and L. Peters Jr., "Evaluation of edge-diffracted fields including equivalent currents for the caustic regions," IEEE Trans. on Antennas and Propagation, AP-17, No. 3, pp. 292-299, May 1969.

[106] C. E. Ryan Jr., and L. Peters Jr., "Correction to 'Evaluation of edge diffracted fields including equivalent currents for the caustic regions'", IEEE Trans. on Antennas and Propagation, AP-18, No. 2, pp. 275, 1970.

[107] M. E. Bechtel, "Vertically polarized radar back scattering from the rear of a cone or cylinder", IEEE Trans. Antennas and Propagation, AP-17, pp. 244-246, 1969.

[108] L. B. Felsen, and N. Marcuvitz, Radiation and Scattering of waves, Englewood Cliffs, New Jersey, Prentice Hall, 1975.

[109] R. H. Duncan, "Theory of the infinite cylindrical antenna including the feed point singularity in antenna current," Journal of Research of the National Bureau of Standards-D Radio Propagation, 66D, pp. 181-188, 1962.

[110] R. Mittra, and M. Tew, "Accuracy test for high-frequency asymptotic solutions", IEEE Trans. on Antennas and Propagation, AP-27, No. 1, pp. 62-68, January 1979.